STUDY ON THE INTERFACE BEHAVIOR BETWEEN UNSATURATED SOIL AND STEEL SURFACE

LALIT BORANA

Ph.D

The Hong Kong Polytechnic University

2014

The Hong Kong Polytechnic University

Department of Civil and Environmental Engineering

Study on the Interface Behavior between Unsaturated Soil and Steel Surface

Lalit BORANA

A Thesis Submitted in Partial Fulfillment of the Requirements for the Degree of Doctor of Philosophy

November 2013

CERTIFICATE OF ORIGINALITY

I hereby declare that this thesis entitled "STUDY ON THE INTERFACE BEHAVIOR BETWEEN UNSATURATED SOIL AND STEEL SURFACE" is my own work and at, to the best of my knowledge and belief, it reproduces no material previously published or written, nor material that has been accepted for the award of any other degree or diploma, except where due acknowledgement has been made in the text.

Signature:_____.

Name: Lalit Borana

Abstract of thesis entitled

STUDY ON THE INTERFACE BEHAVIOR BETWEEN UNSATURATED SOIL AND STEEL SURFACE

An interface formed between a structural material and an unsaturated soil is common in numerous civil engineering projects. The ultimate shear strength at the interface is an important parameter for the design and safety assessment of the structures in the soils and is also a key factor in the design and analysis of the structural interfacial interactions with soil. Matric suction has a predominant effect on the shear strength and volume change behavior of the soil and soil-steel interfaces, thereby proper characterization of interface behavior is important for its accurate performance predictions. The experimental study of the interface behavior plays an important role in advancing the understanding of the complex behavior of soil-steel interfaces. It is believed that the critical interface plane which possesses the minimum shear strength exists on the surface of the structural material (counterface). Also, no definite criterion for the selection of interface thickness (i.e., the layer which possesses the minimum shear strength) for different soil-structure interfaces is readily available. The main focus of this study is to investigate the behavior of the interface between a compacted completely decomposed granite (CDG) soil and steel counterfaces at (a) different shearing planes (b) and different counterface roughness under the influence of different matric suctions and net stresses. Considering the main focus of the study in view, an effort has been made to examine the variation of shear strength for pure soil and soil-steel interface by employing a modified direct shear testing device.

Firstly, to investigate the elementary behavior of the soil-steel interface (rough) sheared at different shearing levels and compare the interface shear behavior with the soil shear behavior, a number of single-staged consolidated drained direct shear tests were carried out on interface and pure CDG soil specimens, under different matric suctions and net normal stresses. The results confirm that the suction and net normal stress significantly influences the shear behavior of pure soil and soil-steel interfaces sheared at different shearing planes. The behavior of stress-displacement curves of soil-steel interface tests is similar to those of soil tests. The suction envelopes were noted to be nonlinear. The degree of dilatancy contributes to the gain in shear strength and is dependent of both matric suction and net normal stress. It is noted that the matric suction plays an important role in evaluating the critical shear strength, as it directly affects the volume change behavior. It is found that the critical failure plane is dependent on the matric suction and an increase in suction reduces the critical interface layer thickness thereby gradually shifting the critical shear plane from the soil towards the counterface. The experimental results compare well with shear strength model proposed by Hossain (2010), which considers the influence of suction and dilation.

Secondly, to examine the elementary interface behavior with different counterface roughness values and compare it with the behavior of pure CDG soil, a series of interface direct shear tests were performed between the CDG soil and a steel plate with different counterface roughness values under the same matric suctions and net normal stresses. The test results show that the counterface roughness, matric suction and net

normal stress have significant influence on the hardening-softening and contractive-dilative interface behavior. An increase in the value of the net normal stress results in a partial stick-slip behavior during the shearing of soil-steel interfaces. The suction envelopes for different counterface roughness were observed to be non-linear and the apparent interface friction angle increases with matric suction. The experimental shear strength data are compared with an analytical model, that considers the influence of suction and dilation on apparent interface friction angle, and it is noted that the analytical model works well for rough interfaces under all the applied stress-state variables.

Finally, a series of model pile pullout test were performed under different unsaturated conditions to evaluate the influence of surface roughness and water content on the elementary interface behavior. To measure the axial strain along the model pile during pullout, the model piles were installed with fibre bragg grating (FBG) sensors. The pullout test results are in good agreement with the observation from direct shear tests. The pullout forces are noted to be directly proportional to the surface roughness and decreases with increase in water content of the soil. The axial strain value along the model pile obtained from FBG sensors reveal that the strain at the top of the model pile is notably greater than that at the base. It is opined that it is worth to employ FBG sensors for examining the interface behavior of piles in unsaturated soil. Further studies are recommended to ascertain the performance of FBG sensors in unsaturated soil and testify the non-linearity of axial strain, shear stress and skin friction of pile.

To summarize, this study attempts to investigate the interface behavior formed between CDG soil-steel counterfaces under different stress state variables. Different types of test suction as (a) suction controlled direct shear test to study the several key factors (such as matric suction, net normal stress and counterface roughness) that influences the interface shear behavior (b) FBG sensor based model pile pullout test were conducted to study several aspects of soil-steel interface behavior such as pullout behavior, axial strain, and skin friction of pile. The results show that the critical interface shear plane is greatly influenced by the soil suction and the critical interface layer thickness reduces as soil suction increases. The gain or loss interface shear strength is a function of particle grain size and counterface roughness. Variation in counterface roughness influences the interface shear strength non-linearly. However, further studies are required to investigate and identify the optimum counterface roughness for unsaturated soil-steel interface. Furthermore, this study also demonstrates successful implementation of FBG sensors in determining the axial strain and skin friction of pile in unsaturated soil. The axial strain induced in the pile is significantly influenced by the counterface roughness and the degree of soil saturation. The axial force along the length of the pile is noted be greater at upper end of model piles as compared to the lower end. Also, the variation of skin friction is non linear throughout the length of the pile. Summary and important findings from this study are presented in Chapters 5 to 7. Chapter 8 presents the major conclusions from this research along with the recommendation for further research work related to this research topic area.

LIST OF PUBLICATIONS

Journal Papers

[1] **Borana, L.,** Yin, J.H., Singh. D.N., and Shukla S.K. (2013). A modified suction controlled direct shear device for testing unsaturated soil and steel plate interface. Marine Georesources & Geotechnology. DOI:10.1080/1064119X.2013.843045

[2] **Borana, L.,** Yin, J.H., Singh. D.N., and Shukla S.K. (2013). Behavior from suction-controlled direct shear tests on soil-steel interfaces sheared at different planes. Canadian Geotechnical Journal. (submitted)

[3] Xu, D.S., **Borana, L.,** Yin J. H. (2013). Measurement of small strain behavior of a local soil by fiber Bragg grating based local displacement transducers. Acta Geotechnica. DOI 10.1007/s11440-013-0267-y.

[4] Yin, J.H., Pei, H. F., **Borana, L.,** and Chiu C.Y., (2013. Experimental investigations into the skin friction of pile-soil interface behavior using fiber bragg grating sensors. Smart Structures and Systems. (under review)

Conference Papers

[1] **Borana,L.,** Xu, D.S., and Yin, J.H. (2012). A study on measurement of local small strain by FBG sensor, Proceedings of 65th Canadian Geotechnical Conference, GeoManitoba , Manitoba, Canada, Paper No. 414

[2] **Borana,L.,** Xu, D.S., and Yin, J.H. (2011). Study on the interface between unsaturated soil and rough steel plate from suction controlled direct shear tests. Proceedings of 14th Asian Regional Conference, Hong Kong, Paper No. 446

[3] **Borana,L.,** and Yin, J.H. Shear behavior of an unsaturated soil-steel interface from direct shear test. Proceedings of 3rd Int. Postgraduate Conf. 2011, Hong Kong, Vol. 2, pp. 124-128

ACKNOWLEDGEMENTS

I would like to express my deepest gratitude to my chief supervisor, Professor Jian-Hua Yin for his encouragement and guidance throughout the study. His supports and experienced guidance that have made this work possible are highly acknowledged. I would also like to thank my co-supervisor Professor D.N. Singh and Dr. S.K Shukla for their willingness to supervise me and advising me from time to time. The privilege of working with all of them has remarkably influenced my professional development and perspectives.

Financial supports from The Hong Kong Polytechnic University (G-YJ99, G-U960, 5-ZJE2, 5-ZJE9) for my study are gratefully acknowledged.

I would like to express my thanks to Mr. Xu Dong-sheng, Dr. Hossain, Dr. Pei, Dr. Hong, Dr. Tong, Dr. Zhou, Mr. Fei Wei-qiang and the technicians of Soil Mechanics Laboratory and Concrete Laboratory of Department of Civil and Environmental Engineering, The Hong Kong Polytechnic University for their co-operation in manufacturing different parts of the testing apparatus, test setup, and installing the computer program.

Finally, I would like to express my sincere thanks to my dear parents, my wife, family members, teachers, colleagues, and friends whose encouragement, love and friendship over the past years have enabled me to reach a new level in my life and overcome the challenges throughout my study period.

TABLE OF CONTENTS

LIST OF TABLES

LIST OF FIGURES

Appendix

Chapter 1

INTRODUCTION

1.1 GENERAL

The load-carrying capacity of the soil and rock is commonly defined by the shear strength (τ), which is an important state variable. The shear strength can be measured by performing different conventional laboratory tests such as direct shear test, triaxial test, ring shear test and true triaxial tests. The shear strength τ is a better representation of strength properties of the porous media. In view of this, several researchers have tried to correlate values of τ with different properties of unsaturated porous media (Fredlund and Rahardjo 1993).

The presence of air in the soil can be observed in the significant areas of earth surface which could consist of arid, semi arid or extremely arid regions, having low or very low water content and thus rendering the soil to be unsaturated. Many researchers have pointed out that the behavior of a soil in unsaturated condition is very different from that of a fully saturated soil (Aitchison and Donald 1956; Bishop et al. 1960; Burland and Ridley 1996; Bao et al. 1998; Su et al. 2007). Fredlund and Morgenstern (1977) established that the unsaturated soil consists of more than two phases i.e., solids, fluid (water/oil), air and air water interface or contractile skin. It is recognized that the behavior of an unsaturated soil is significantly affected by the soil suction; properties like seepage, volume change, and shear strength and are all greatly influenced by the

variation of moisture content in the soil (Elzeftawy and Cartwright 1981; Ng and Menzies 2007).

Construction of geotechnical engineering structures in soil has increased significantly worldwide and specially in developing countries. The unsaturated soil when comes in contact with material like steel, iron, concrete, ply vinyl chloride (PVC), cement, wood, etc., forms an interface layer between them (Yoshimi and Kishida 1981; Uesugi et al. 1990; Rao et al. 2000; Zhan and Ng 2006), also referred as unsaturated soil interface and is common to many geotechnical engineering structures e.g., buried pipelines, soil nail, retaining walls, shallow foundations and pile foundations, etc. For instance in USA, on average more than 850,000 m^2 of mechanical stabilized earth walls and 190,000 m^2 of reinforced soil slopes are constructed annually. One of the most important parameters for the design and safety assessment of these structures in the soil is the ultimate shear strength at the interface between the structural surface and the surrounding soil surface.

In the last few decades, the construction of infrastructural projects has received a significant boom across the globe. The pile foundations have been increasingly adopted for the geotechnical structures in mainland China and Hong Kong (Bai et al. 2006) and the axial response of the pile foundation is largely affected by the soil-pile interfacial interaction (Noorany 1985; Mroueh and Shahrour 2012). Piles can be divided into friction piles (more than 90% contributed by friction), end bearing piles (more than 90% contributed by end bearing friction), and piles in between. For piles used to resist uplift, the uplift capability of the piles is all contributed by the side friction of the piles. The skin friction of the pile is greatly dependent on the behavior of the interface. Over the past few decades, researchers focused on the total bearing capacity of the friction pile

foundation but not the distribution of skin friction along the pile under vertical pullout loading. The properties and behavior of the interface between a structure and the soil are needed for understanding the performance of the structures and their analysis and design.

There are limited efforts by researchers to study the behavior of interfaces in unsaturated soils. It has also been realized that there is a dearth of literature on behavior of unsaturated interfaces in coarse grained soil. Furthermore, it is assumed that the critical interface layer, which possesses the minimum shear strength, exists on the counterface surface (surface of the structural material in contact) and no definite criterion for selecting the thickness of the interface layer for different soil-structure interfaces is readily available. With this in view, the present study entitled as "Study on the Interface Behavior between Unsaturated Soil and Steel Surface" has been conducted to (a) investigate the elementary interface behavior of the soil– rough steel interface at different shearing planes, (b) study the elementary interface behavior of the soil–steel interface under different stress state variables and counterface roughness, and (c) examine the distribution of axial strain and skin friction on rough and smooth model piles in a soil mass at different water contents.

1.2 OBJECTIVE OF THE RESEARCH

There is a lack of literature about the interface shear strength behavior between an unsaturated soil and construction material. Keeping in view the above mentioned engineering background, the main motivation for this work is to investigate and understand interface behavior between a local completely decomposed granitic (CDG) soil and a steel plate with various roughnesses. Not much literature is available about the interface strength behavior between an unsaturated soil and a steel interface. The primary focus of this study is to have a better understanding of the variation interface

thickness and interface strength of an unsaturated CDG soil and a steel plate counterfaces under different net normal stresses and matric suctions. The main objectives of the current research are as follows:

(a) To investigate the variation of interface thickness formed between CDG soil and rough steel counterfaces in saturated and unsaturated condition with net normal stress. Based on laboratory test results the variation of interface shear strength will be verified with an existing unsaturated shear strength model that includes the effect of soil dilation.

(b) To have a better understanding of the soil-steel interface behavior, the shear strength and dilatancy characteristics of the pure CDG soil are to be investigated at both saturated and unsaturated conditions under different net normal stresses and matric suctions.

(c) The shear strength and dilatancy behaviors of the interface between the compacted CDG soil and three different steel counterfaces are to be examined under different net normal stresses and matric suctions. The test results are to be testified, with an existing unsaturated shear strength model that includes the effect of soil dilation and to evaluate the suitability of the model for predicting unsaturated shear strength of soil-steel interface.

(d) The interface shear strength of the soil will be compared with the interface test results and to provide a general conclusion about the performance of soil-steel interfaces at different matric suction.

(e) The influence of counterface roughness and degree of saturation is investigated to provide general conclusion about the variation of skin friction at different soil water content and surface roughness of the pile. To study the distribution of axial strain and skin friction on rough and smooth model piles in a soil mass, pullout behavior of the model piles is investigated using fiber Bragg grating (FBG) sensors.

(f) The performance evaluation of FBG sensors for estimating the axial stress distribution along the model piles is to be done by the stain data collected by FBG sensors.

1.3 ORGANIZATION OF THE THEISIS

This thesis is divided into eight chapters as follows:

Chapter 1. Introduction: This chapter presents briefly the background of research, the objectives and specific issues to be investigated, and the organization of the thesis.

Chapter 2. Literature review: This chapter describes about the existing literatures related to the unsaturated soil shear tests, components and effects of suction on soil characteristics, soil-water characteristic curve (swcc), unsaturated shear strength models, interface shear tests between soil and different construction materials, pullout interface behavior and fibre optic sensing technology in geotechnical application. Lastly, the research gaps in the existing literatures are identified and it is attempted to fill up these gaps.

Chapter 3. Experimental technique and testing apparatus: This chapter includes the description of the suction controlling techniques used in the present study, different

features of the testing apparatus employed in the present study, and calibration of accessories of the apparatus.

Chapter 4. Testing materials, specimen preparation and test procedure: This chapter presents the basic properties of the soil and steel counterfaces, initial preparatory work for test apparatus, specimen preparation procedure adopted for soil and interface direct shear specimen, and procedure of conducting direct shear tests and model pile pullout tests.

Chapter 5. Interface shearing at different shearing planes: This chapter describes the test results of soil and three interface specimens sheared at three different shear planes of 0 mm (INT-0), 1 mm (INT-1) and 2 mm (INT-2) from the counterface plane. Furthermore, it includes the load-displacement and volume change behavior during shearing, influence of matric suction on the failure envelopes, and comparison of experimental results with existing shear strength model.

Chapter 6. Influence of counterface roughness on interface behavior: This chapter presents the test results of soil and three types of soil-steel interface specimens with different counterface roughness. It also includes the load-displacement and volume change behavior during shearing, influence of matric suction on the failure envelopes, and comparison of experimental results with existing shear strength model.

Chapter 7. Pullout test results and interpretations: This chapter illustrates the pullout test results and its interpretations, the influence of water content on the pullout resistance of smooth and rough piles, influence of surface roughness on the axial strain of the model piles and the comparisons of average shear stresses obtained from FBG sensors.

Chapter 8 : This chapter deals with the main findings and conclusions obtained from the present study and recommendation for future studies in this topic area.

Chapter 2

Literature Review

2.1 INTRODUCTION

Estimating the shear strength of unsaturated soil is important in many geotechnical engineering applications. The interface shear strength between compacted soil and structure is a key factor in assessing the reliability and stability of the structure. To study the behavior of soil-structure interfaces, a variety of tests are conducted. It is recognized that unsaturated soils are common in nature, and soil suction affects the engineering behavior of an unsaturated soil (Boulon 1989; Mashhour et al. 1996). It is believed that the interface shear strength depends upon the surface roughness of the counterface. For instance, in a soil-steel interface, rough steel counterface may exhibit more shearing resistance compared to smooth steel counterface. Furthermore, it is also believed that the critical interface layer which possesses the minimum shear strength exists on the counterface surface and no definite criterion for selection of interface layer thickness for different soil-structure interfaces is readily available.

This chapter aims to review the existing literatures related to the unsaturated soil shear tests, different unsaturated shear strength models, effect of suction on soil characteristics and behavior of interface shear tests between soil and different construction materials.

2.2 SOIL SUCTION AND SUCTION COMPONENTS

Schofield (1935) has firstly used the term 'soil suction' to represent the 'pressure deficiency' in the pore water of any soil in saturated and unsaturated state. Soil suction plays a key role in unsaturated soil mechanics (Sivakumar 1993; Oloo and Fredlund 1996) and is frequently referred as the free energy state of soil water, which can be measured in terms of its partial vapor pressure. From thermodynamic perspective the total suction in soil can be described using Kelvin's equation:

$$\psi = -\frac{RT}{v_{w0}\omega_v}\ln\left(\frac{u_v}{u_{v0}}\right) \qquad 2.1$$

where ψ is total suction (kPa); R is the universal gas constant $[J/(mol \cdot K)]$; v_{w0} is the specific volume of water or the inverse of the density of water (m^3/kg); u_v is the partial pressure of pore-water vapour (kPa); ω_v is the molecular mass of water vapour (g/mol); T is the absolute temperature (K); u_{v0} is the saturation pressure of water vapour over a flat surface of pure water at the same temperature (kPa), and (u_v / u_{v0}) represents the relative humidity, RH (%).

The total soil suction consists of two components i.e., (a) matric component and (b) osmotic component. Any variation of relative humidity in the soil normally results in a change of total suction. Relative humidity in soil can be reduced due to the occurrence of a curved water surface as a result of capillary phenomenon, that is, contractile skin (Fredlund and Rahardjo 1993). The change in the radius of curvature of the curved water surface is dependent on the air pressure (u_a) and water pressure present (u_w) in the soil fabric. The radius of curvature is noted to be inversely proportional to the difference between u_a and u_w diagonally to the surface, i.e., $u_a - u_w$, and is termed as

matric suction. Variation in relative humidity due to the presence of dissolved salts in pore water is referred to as osmotic suction. The concentration of dissolved salts in the pore fluid of the soil directly influences the osmotic suction and is measured in terms of pressure.

Matric suction significantly influences the flow of water and mechanical behavior of unsaturated soils. Nevertheless, it is difficult to identify the effect of osmotic suction on mechanical behavior of unsaturated soil (Hossain 2010) and has been controversial (Alonso et al. 1987). As this study involves variation of matric suction, the subsequent discussions shall focus on matric suction.

2.3 MECHANICAL BEHAVIOR OF SOIL WATER

The water present in unsaturated soil fabric can be divided into three major components (Wheeler and Karube 1996) such as, (a) adsorbed water, (b) bulk water and (c) meniscus water. Firstly, the adsorbed water is firmly bonded to soil grain and can be considered as an integral part of the soil skeleton. Secondly, the bulk water occupies the void spaces in the soil skeleton that are fully saturated. Finally, the menisci water is the water that surrounds the particle contact points in all the void spaces which are not filled up by bulk water, as observed Fig. 2.1. In a state of hydraulic equilibrium all the components of water, i.e., bulk water, meniscus water and adsorbed water, are at the identical pressure. The pores which are not filled completely with soil water, develops a curved menisci at the particle contact points between individual soil grains or between aggregations of soil particles (Gens and Alonso 1992; Kayadelen et al. 2005). The surface tension of the pore fluid in menisci causes the capillary effects. The value of matric suctions is a function of surface tension (T_s) and the radius of curvature of the

menisci characterized by radii R_1 and R_2 (refer to Fig. 2.2) and is defined by Kelvin's law as follows:

$$s = u_a - u_w \approx T_s = \left(\frac{1}{R_1} + \frac{1}{R_2} \right) \qquad 2.2$$

where u_a and u_w are the gas and fluid pressures, respectively, acting on both sides of the fluid surface. As the water content reduces, the menisci withdraw into smaller pore spaces and the menisci radius of curvature also reduces, and hence matric suction increases. Clayey soil possesses a smaller pore sizes, as a result higher matric suctions can be developed in it as compared to coarse granular soils.

Wheeler et al. (2003) have studied the influence of suction on inter-particle forces and pointed out that matric suction within bulk water and within meniscus water produces different inter-particle contact forces transmitted through the soil skeleton. The results show that the variation of matric suction within bulk water affects both normal and tangential forces acting on the contact point between the soil particles. Any increase in suction tends to reduce the probability of slippage at the particle contacts. On the contrary, any decrease in suction value to the unsaturated soils causes a reduction in the normal stress at particle contacts and resulting in inter-particle slippage.

Sharma (1998) studied the mechanical behavior of unsaturated highly expansive clays and analyzed contribution of meniscus water to inter-particle contact stress. For millimeter-sized (or sand-sized) particles, the induced inter-particle contact stress by meniscus water is small and likely to be insignificant as compared with those caused by external loading. On the contrary, for micron-sized particles, much larger values of contact stress can be achieved and may be considerable as compared to those caused by external loading.

2.4 EFFECT OF SUCTION ON SOIL CHARACTERISTICS

Soil characteristics including mechanical and hydraulics behavior are significantly influenced the suction (Fredlund and Rahardjo 1993). Many researchers have studied the effects of suction on yielding and compressibility. The increase of suction stiffens the unsaturated soil against the external loading and thus resulting in an increase of apparent pre-consolidation pressure (yielding stress). The yielding surfaces are enlarged with increased suction resulting in a gradual suction-hardening effect. By contrast, the compressibility of an unsaturated soil increases with a reduction in suction value (Alonso et al. 1990). However, Wheeler and Sivakumar (1995) and Chiu and Ng (2003) have conducted extensive experimentation and have demonstrated that the compressibility under saturated conditions is smaller than that under unsaturated conditions. Peterson (1988) and Estabragh et al. (2004) showed that the compressibility of silty soil does not change monotonically with suction. The degree of specimen compaction plays an important role in influencing the compressibility at a given suction: a denser specimen has a lesser compressibility. The compressibility in an unsaturated soil is dependent on suction, compaction conditions and wetting-induced change of the fabric. The volumetric response of unsaturated soils is highly dependent on the stress path due to the irreversibility.

The shear strength in an unsaturated soil increases with an increase in suction, and may sometimes result in an increase in apparent cohesion while maintaining constant friction angle ϕ' (Hossain and Yin 2010a). Nevertheless, the gain in shear strength with respect to increase in suction cannot persist for an indefinite period. Largely the experimental observation shows that the relationship between shear strength with soil suction is nonlinear (Fredlund et al. 1987; Gan and Fredlund 1996). The experimental findings of

Mancuso et al. (2002) and Ng and Yung (2007) showed that the suction increases elastic shear modulus. Furthermore, suction increases the dilatancy and brittleness of an unsaturated soil (Cui and Delage 1996; Ng and Zhou 2005; Hossain and Yin 2010b; Borana et al. 2013).

The permeability of an unsaturated soil is dependent on the degree of saturation which is an important factor. The relationship between degree of saturation and soil suction can be described using the soil-water characteristic curve (SWCC). The coefficient of permeability for unsaturated soil can be estimated from the SWCC, because soil suction bears a relationship with SWCC. The saturated permeability of coarse grained or sandy soil is greater than fine grained clayey soil. Nevertheless, the unsaturated permeability of sandy soil reduces more rapidly with an increase in suction and eventually turns out to be lower than that of clayey soil. It is due to the greater desaturation rate of sandy soil, which is reflected by a steep slope in the SWCC.

2.5 SOIL-WATER CHARACTERISTIC CURVE

The soil-water characteristic curve (SWCC) for a soil is defined as the relationship between matric suction and water content or degree of saturation. SWCC is also sometimes referred as soil water retention curve and is generally presented in terms of volumetric water content, gravimetric water content and degree of saturation. This curve plays an important role in predicting and evaluating unsaturated soil properties (Fredlund 1998; Thakur et al. 2005). Therefore, the SWCC is normally used to examine different behavior of unsaturated soils such as shear strength, permeability, etc (Rahadjo and Leong 1997; Barbour 1998). Fig. 2.3 depicts an ideal SWCC with distinctive features which includes the hysteresis between the desorption and adsorption curves, air-entry value, residual water content and desorption. Fig. 2.4 presents the typical

SWCC for different types of soils. Some of the major factors that significantly influences on the SWCC includes grain size distribution, plasticity, dry density and stress state of the soil.

There are several empirical equations proposed in the literature to represent the soil-water characteristic curve (Brooks and Corey 1964; McKee and Bumb 1987; Van Genutchen 1980). These equations have often been restricted to certain types of soils or to SWCCs of a particular shape or to a limited range of suction values (Thakur et al. 2005). Among others, Fredlund and Xing (1994) have proposed a relationship (Eq. 2.3) based on the pore-size distribution curve of the soil matrix as follows:

$$\theta = C(u_a - u_w)\frac{\theta_s}{\left\{\ln\left[e + \left(\frac{(u_a - u_w)}{a}\right)^n\right]\right\}^m} \qquad 2.3$$

where θ is the volumetric water content (defined as ratio of volume of water to the total volume) at unsaturated state; θ_s is the volumetric water content at saturation; a, n and m are fitting parameters; $(u_a - u_w)$ is the matric suction; e is the natural number ($\approx$ 2.71828); and $C(u_a - u_w)$ is a correction factor function that can be determined by Eq. (2.4).

$$C(u_a - u_w) = 1 - \frac{\ln\left[1 + \frac{(u_a - u_w)}{(u_a - u_w)_r}\right]}{\ln\left[1 + \frac{1000000}{(u_a - u_w)_r}\right]} \qquad 0 \le (u_a - u_w) \le 10^6 \text{ kPa} \qquad 2.4$$

where $(u_a - u_w)_r$ is the virtual matric suction corresponding to the residual water content and varies in the range of 1500 to 3000 kPa. Eq.(2.3) has often been used because of its practical applicability (Leong and Rahardjo 1997; Sillers and Fredlund 2001) and can be rewritten as follows (Vanapalli et al. 1996):

$$\Theta = C(u_a - u_w)\left[\frac{1}{\ln\left(e + \left(\frac{(u_a - u_w)}{a}\right)^n\right)}\right]^m \qquad 2.5$$

where Θ is the normalized volumetric water content function and $\Theta = \theta/\theta_s$. Equations (2.2) to (2.4) can be used to best-fit soil-water retention curve data of any soil for the entire suction range of $0 \le (u_a - u_w) \le 10^6$ kPa.

2.6 STUDIES ON SHEAR BEHAVIOR OF UNSATURATED SOILS

It is well recognized that most of the subsurface soils are typically in an unsaturated state and the soil suction affects their engineering behavior including the shear behavior. The ultimate shear strength of a soil is normally associated with stress state variable of the soil. Generally, the stress state variables used for an unsaturated soil are the net normal stress and matric suction (Fredlund and Rahardjo 1993; Vanapalli 1994; Zhang and Lytton 2006). From early 1950s researchers have conducted numerous investigations to understand the principles of unsaturated soil mechanics (Donald 1956; Potyondy 1961; Kishida and Uesugi 1987; Rao et al. 2000; Gallipoli et al. 2003; Wang et al. 2007). Several studies have been performed on unsaturated soils using different testing devices viz., direct shear, torsional shear and annular shear tests (Bishop and

Henkel 1962; Brumund and Leonards 1973; Gulhati 1975 ; Yoshimi and Kishida 1981; Potyondy 1961; Gan 1986; Frost and Han 1999). Sometimes the matric suction was measured only at the beginning of the test, while in some cases it was monitored and maintained consistent throughout the testing period (Escario 1980; Gan and Fredlund 1992; Fakharian and Evgin 1996; Sharma et al. 2007). The results obtained from the shear strength tests on unsaturated soils acts as a qualitative indicator of the soil shear strength, as the actual stress state variables at failure are not known. Therefore, the interpretation of these shear test results is ambiguous (Vinayagam 2004; Hossain 2010). Donald (1956) examined shear behavior of unsaturated fine sand and coarse silt by conducting several direct shear tests using a modified direct shear box apparatus. The results revealed that as the matric suction increases, the shear strength increases until it reaches peak value and thereafter it remains approximately steady.

Hilf (1956) proposed the use of axis translation technique for the indirect measurement of pore-water pressure especially when higher matric suction values were required. Bishop and Blight (1963) examined the application of axis translation technique in evaluating the shear strength testing of unsaturated clay. The results obtained in the presence and absence of axis translation was compared and it was noted that the curves of shear stress versus strain closely matches with each other. Gulhati (1975) conducted a series of consolidated drained tests on two types unsaturated soil by maintaining the pore pressure in a modified triaxial apparatus of two unsaturated.

In late 1970's. Fredlund and Morgenstern (1977) and Fredlund et al. (1978) carried out extensive research in the unsaturated soil shear behavior and proposed the use of net normal stress and suction as independent stress state variables and derived a new shear strength equation for unsaturated soils. Ho and Fredlund (1982) examined the

unsaturated shear behavior of decomposed rhyolite and decomposed granite by conducting a series of consolidated drained multistage triaxial tests (with pore-air and pore-water pressure control during shear). The desired matric suction in the specimen was obtained by controlling the pore-air and pore-water pressure using axis translation technique.

Gan and Fredlund (1996) examined the shear behavior of unsaturated completely decomposed granite (CDG) soil from Hong Kong, by conducting a series of direct shear and triaxial tests. The experimental results revealed that stiffness and shear strength increase with an increase in matric suction. Lee et al. (2005) have employed modified triaxial apparatus to evaluate the effect of stress state on unsaturated shear strength of Korean residual soil. The results showed that the SWCC and shear strength of the soil are greatly influenced by the change of net normal stresses. Therefore, it is necessary to consider the effect of net normal stress in the unsaturated shear strength model. Ying et al. (2006) have verified the findings of Campos and Carrillo (1995) and Feuerharmel et al. (2006) that net normal stress and matric suction have a predominant influence on the shear strength of unsaturated soil. Zhan and Ng (2006) demonstrated that the shear strength and dilatancy of the expansive clayey soil is directly proportional to the applied matric suction. Wang and Leung (2008) performed several triaxial tests and compared the experimental results with the numerical simulations on using the discrete element method (DEM) to explore the underlying mechanisms of the unique behavior of artificially cemented sands. The results showed that the particles in the bonding region jointly share the shear loading. As compared with uncemented sand, much stronger force–chain complex is formed in cemented sand resulting in higher strength. The bonded clusters help to stabilize the particle and maintain the volumetric dilation. It is also noted that the gain of apparent friction angle with an increase in matric suction may

be credited to the increase of dilation angle (Hossain and Yin 2010a; Hossain and Yin 2013).

Generally while testing unsaturated soils, it is mostly anticipated to control the total suction or matric suction throughout the course of testing. The most popular and widely employed technique is for testing unsaturated soil is axis-translation technique. This study aims to investigate the effect of matric suction on the shear strength, dilatancy and deformation characteristics of an unsaturated recompacted completely decomposed granite (CDG) soil, using suction controlled direct shear apparatus. The soil used in the present study was obtained from Tai Wai, Hong Kong. The testing of CDG soil was done so that the test results of unsaturated CDG soil could be compared with the test results of soil-steel interface. Subsequent sections will discuss the study related to the interfaces in unsaturated soil.

2.7 MODELING OF SHEAR STRENGTH IN UNSATURATED SOIL

Earlier researchers have formulated shear strength equations (Bishop 1959; Fredlund and Morgenstern 1977; Lamborn 1986; Gan et al. 1988; Fredlund et al. 1996; Vanapalli et al. 1996; Khalili et al. 1998; Hamid and Miller 2008) based on different stress state variables, namely, net normal stress and matric suction.

Bishop (1959) proposed a relationship in Eq. (2.6) for determining the unsaturated shear strength of the soil:

$$\tau_f = c' + [\sigma_n - u_a + \chi(u_a - u_w)]\tan\phi' \quad 2.6$$

where τ_f is shear strength, c' is effective cohesion, ϕ' is effective friction angle, σ_n is total stress, χ is a coefficient (ranging from 0 to 1), u_a is pore air pressure and u_w is the porewater pressure. Bishop's equation fails to explain the collapse potential of some soil on wetting and also has difficulties in predicting values of χ (Alonso *et al.* 1990; Bernier *et al.* 1997; Lee *et al.* 2005).

Fredlund et al. (1978) proposed Eq. (2.7), which considers the influence of two independent stress state variables (i.e., net normal stress and matric suction) and also the limitation associated with Eq (2.6):

$$\tau_f = c' + (\sigma_{nf} - u_{af})\tan\phi' + (u_a - u_w)_f \tan\phi^b \quad 2.7$$

where $(\sigma_{nf} - u_{af})$ is net normal stress on the failure plane, u_{af} is pore pressure at failure, $(u_a - u_w)_f$ is the matric suction at failure, ϕ^b is angle of internal friction with respect to matric suction. Theoretically it is believed that the net normal stress $(\sigma_{nf} - u_{af})$ and matric suction $(u_a - u_w)_f$ are not dependent of each other, but several researchers including Escario and Saez (1986), Vanapalli *et al.* (1999), Rassam and Williams (1999), Ng and Pang (2000) and Lee *et al.* (2005) have showed that the net normal stress can affect matric suction and shear strength.

Lamborn (1986) proposed a shear strength equation for unsaturated soils by extending a micromechanics model and is as follows:

$$\tau = c' + (\sigma - u_a)\tan\phi' + (u_a - u_w)\theta_w \tan\phi' \quad 2.8$$

where, θ_w is the volumetric water content (VWC) and is defined as the ratio of the volume of water to the total volume of the soil. The volumetric water content decreases

as matric suction increases, and it is a nonlinear function of matric suction. However, it must be noted that unless the volumetric water content is equal to 1, the friction angle associated with matric suction does not become equal to $\phi^{'}$.

A simple and practical model based on the soil water characteristic curve (SWCC) to determine the shear strength of the soil was proposed by Vanapalli et al. (1996) as shown below,

$$\tau_f = c^{'} + (\sigma_n - u_a)\tan\phi^{'} + (u_a - u_w)_f(\Theta^k)\tan\phi^b \qquad 2.9$$

where, (Θ^k) is the normalized water content obtained from SWCC, k is a soil parameter (ranging from 1.0 to 3.0)

Zhan and Ng (2006) have modified the equation (2.9) by incorporating the volume change behavior on the shear strength and the equation is rewritten as,

$$\tau_f = c' + (\sigma_{nf} - u_{af})\tan(\phi' + \psi) + (u_a - u_w)_f \tan\phi^b \qquad 2.10$$

where, ψ is the dilation angle.

Hossain (2010) have further modified the unsaturated shear strength model, proposed by Vanapalli et al. (1996) by considering the matric suction induced soil dilatancy, as follows:

$$\tau_f = c^{'} + (\sigma_n - u_a)\tan(\phi^{'} + \psi) + (u_a - u_w)_f(\Theta^k)\tan(\phi^{'} + \psi) \qquad 2.11$$

In addition to the above mentioned equations, some more equations have been proposed by researchers including Satija (1978), Karube (1988), and Toll (1990). The shear strength equations for unsaturated soils in the literature are mostly observed to be either linear or bilinear.

2.8 STUDIES ON SOIL STRUCTURE INTERFACE BEHAVIOR

An interface formed between a structural material (e.g., steel, concrete, rock, cement, geotextiles and wood) and an unsaturated soil (Yoshimi and Kishida 1981; Zhan and Ng 2006; Sharma et al. 2007; Khoury et al. 2010, Hossain and Yin 2012; Borana et al. 2013) is common in various civil engineering projects. Soil-structure interface behavior has been one of the most interesting and challenging topic for the researchers worldwide. One of the most important parameters for the design and safety assessment of the structures in the soils is the ultimate shear strength at the interface (Potyondy 1961; Jewell and Wroth 1987; Liu et al. 2007a). In other words, the behavior of the unsaturated interface governs the design and analysis of these interfacial interactions (Hamid 2005). The mechanics of interface behavior are complicated and it is difficult to mathematically model the interface behavior because of its complex nature (Boulon et al. 1995; Shibuya et al. 1997). Thus, experimental observations of interface behavior play a crucial role in advancing understanding of this complex behavior. The interface behavior depends on several factors and boundary conditions. One of the major factors that influence the mechanical behavior of the interface is the moisture content of the soil (matric suction). Nonetheless, a large number of the interface studies in the existing literatures are related either to completely saturated or completely dried condition. It is noted that very little attention was given to examine the unsaturated soil-interface behavior.

2.8.1 INTERFACE SHEAR TESTS AT COMPLETELY SATURATED OR COMPLETELY DRIED CONDITION

Researchers have investigated various aspects, such as the effect of skin friction, grain size and over consolidation ratio, of soil interface behavior by using different testing

devices (Potyondy 1961; Yoshima and Kishida 1981; Noorany1985; Kim and O' Neil 1998; Rao et al. 2000). Generally, to study the behavior of soil-structure interfaces, different type of tests viz., direct shear, torsional shear, triaxial, annular shear and pullout tests are conducted (Brumund and Leonards 1973; Kishida and Uesugi 1987; Tsubakihara et al. 1993; Fakharian and Evgin 1996; Frost and Han 1999; Rao et al. 2000; Giuseppe et al. 2007). Furthermore, Panchanathan and Ramaswamy (1964) and Kulhawy and Peterson (1979) examined interface shear behavior between soil and different construction materials using direct shear device and showed that the counterface roughness of the construction materials plays a key role in determining the ultimate interface shear strength. It has also been pointed out that the effect of normal stress and soil density on the counterface roughness is insignificant (Acar et al. 1982).

Noorany (1985) examined the interface behavior and effect of side friction (skin friction) of piles in calcareous sands with special focus on the effects of grain between sand-steel interfaces. The result revealed that skin friction is a function of the stresses present at the interface. In other words, lower skin friction of steel piles driven in sands (non-cemented calcareous) is caused by lower effective soil-pile interface stresses. Uesugi et al. (1990) performed several direct shear test on coarse grained dry sandy soil and concrete, with special emphasis on surface roughness (concrete). The results indicated that the maximum coefficient of sand-concrete friction not only depends on the surface roughness of concrete but also on the mean grain size diameter of sandy soil. Yin et al. (1995) investigated the relative slip displacements along the soil-concrete interface by conducting a series of direct shear test. The results indicated that the relative displacement distribution is irregular. The conventional method of deriving the shear stiffness or shear modulus from curves of shear stress versus relative displacement is unreasonable. For more realistic simulation, a rigid- plastic model for interface

deformation was proposed which considers interface element thickness. Chu and Yin (2006) and Hossain and Yin (2013) investigated the interface behavior between completely decomposed granite (CDG) soil and a cement grout by employing direct shear apparatus. It has been concluded that the interface shear strength of the CDG and cement grout material primarily depends on the normal stress level, soil suction (water content) and the interface surface roughness.

2.8.2 INTERFACE SHEAR TESTS AT UNSATURATED CONDITION

Researchers have reported that matric suction plays a predominant effect on the shear strength of the soil structure interfaces (Khoury et al. 2005, Sharma et al. 2007; Hossain and Yin 2013). However, there are very limited efforts by researchers to study the behavior of interfaces in unsaturated soils.

Khoury et al. (2005) have studied the effect of soil suction on the mechanical behavior of unsaturated soil-geotextile interfaces, by conducting numerous suction controlled laboratory tests using a modified direct shear apparatus. The reported experimental results show nonlinear increase in peak shear strength of the soil-geotextile interface with increase in soil suction. On the contrary, there was negligible effect of suction on the post-peak shear strength of the interface. Fleming et al. (2006) have performed Interface shear tests on non-textured geomembrane–soil interfaces using a special direct shear device. The pore-water pressure in the vicinity of the interface was measured using a pore pressure transducer. These researchers reported that the shear strength of a geomembrane–soil interface in terms of effective stresses could be predicted using the concepts of unsaturated soil mechanics at low normal stresses. However, at high normal stresses, the failure mechanism changed resulting into higher shear strength at the

geomembrane–soil interface. The mobilization of high shear strength interface was attributed to plowing failure mechanism.

Sharma et al. (2007) have investigated the soil– geomembrane interface shear strength by conducting a series of laboratory tests, with a special provision for continuous measurement of suction at the soil geomembrane interface using miniature pore pressure transducers (during the shearing process). To achieve this, direct shear testing device was modified and miniature pore-pressure transducer (PPT) installed adjacent to the surface of the geomembrane. The authors have demonstrated an effective use of PPT in evaluating shear behavior at the interface between a geomembrane and an unsaturated soil at low matric suction values. It is reported that the soil suction contributes to shearing resistance at low normal stress values. However, at higher normal stresses, the interface shear behavior appears to be governed only by the magnitude of net normal stress.

Hamid and Miller (2009) have examined the shearing behavior of unsaturated soil-steel interfaces by conducting a series of interface direct shear tests on a low-plasticity fine-grained soil. The results indicate that the matric suction significantly contributes to the peak shear strength of unsaturated interfaces; whereas, no variation was observed for the post peak shear strength with changes in matric suction. The results also show that the variations in net normal stress affected both peak and post peak shear strengths and are in agreement with the results reported by Miller and Hamid (2007).

Hossain (2010) carried out a series of suction-controlled direct shear tests on the interface between completely decomposed granitic soil and cement grout with and without grouting pressure using suction controlled direct shear device. The results

established that apart from the two stress state variables, i.e., matric suction and net normal stress, the interface shear strength, dilation angle and apparent cohesion are considerably influenced by the applied grouting pressure.

The reviewed literature suggests that there have been very limited efforts by researchers to study the shear behavior of soil-steel interfaces in unsaturated soils. It has been realized that there is a dearth of literature on behavior of interfaces in unsaturated coarse-grained soils. Furthermore, it is believed that the critical interface layer which possesses the minimum shear strength exists on the counterface surface and no definite criterion for selection or identification of the interface layer thickness for different soil-structure interfaces is readily available.

2.8.3 INTERFACE SHEAR STRENGTH EQUATION AT SATURATED AND UNSATURATED CONDITIONS

The relationship between interface shear resistance and displacement can be represented by a linear-elastic-perfectly-plastic formulation. For saturated case, the interface shear strength is governed by the Mohr-Coulomb failure criteria. Potyondy (1961) modified the Mohr-Coulomb's equation, to establish the ratio between interface friction and shearing stress, see Eq (2.11), by introducing the coefficient f_a (for the reduction of cohesion) and a coefficient f_ϕ (for the reduction of the internal soil friction angle in the interface model).

$$\tau_f = f_a c' + \sigma'_{nf} \tan(f_\phi \phi') \qquad 2.12$$

where τ_f is the interface shear strength at failure; $f_a = \frac{c'_a}{c'}$; $f_\phi = \frac{\delta'}{\phi'}$; σ'_{nf} is the effective normal stress at failure; c'_a is the effective soil adhesion; δ' is the effective

interface friction angle; c' is the effective cohesion of soil; and ϕ' is the effective angle of internal friction of soil.

Chandler (1968) established that relationship described in Eq. (2.13) can be used to model the shear strength of an interface in a saturated soil:

$$\tau_f = c_a^{'} + \sigma_n \tan\delta^{'} \qquad 2.13$$

Table 2.1 presents the comparison of different modes of shearing on interfaces friction angle.

For unsaturated case, Miller and Hamid (2007) modified Fredlund et al. (1978) shear strength equation (see Eq. 2.7), to consider the interface between unsaturated silty soil-stainless steel, as follows:

$$\tau_f = c_a' + (\sigma_{nf} - u_{af}) \tan\delta' + (u_a - u_w)_f \tan\delta^b \qquad 2.14$$

where $(\sigma_{nf} - u_{af})$ is the net normal stress variable on the failure plane at failure; u_{af} is the pore-air pressure at failure; $(u_a - u_w)_f$ is the matric suction at failure; and δ^b is the angle indicating the rate of increase in interface shear strength relative to matric suction $(u_a - u_w)_f$.

Sharma et al. (2007) modified Bishop's (1959) effective stress equation for unsaturated soil to consider the interface between silty sand and geomembrane, as follows:

$$\tau = \alpha + [(\sigma - u_a) + \chi(u_a - u_w)] \tan\delta \qquad 2.15$$

where τ is the interface strength; α is the adhesion; σ is the total normal stress; u_a is the pore-air pressure; u_w is the pore-water pressure; δ is the angle of shearing resistance at the soil-geomembrane interface; and χ is a parameter whose value ranges

from 0 to 1. It is noteworthy mentioning here that Sharma et al. (2007) have opined that Eq. (2.15) predicts the measured shear strength inaccurately and its performance is highly dependent on the applied normal stress.

The shear strength equation for unsaturated soils proposed by Vanapalli et al. (1996) was modified by Hamid and Miller (2009) as follows to predict the shear strength of unsaturated silty soil-steel interface:

$$\tau_f = c'_a + (\sigma_{nf} - u_{af}) \tan\delta' + (u_{af} - u_{wf}) \tan\delta' \left(\frac{\theta - \theta_r}{\theta_s - \theta_r} \right) \quad 2.16$$

where θ is the current volumetric water content; θ_r is the residual volumetric water content and θ_s is the saturated volumetric water content from a SWRC.

Hossain and Yin (2010a) modified Eq. (2.14) to consider dilatancy induced by matric suction and have proposed Eq. (2.17) for predicting the interface shear strength between unsaturated decomposed granitic soil and cement grout:

$$\tau_f = c_a + (\sigma_n - u_a)_f \tan(\delta' + \psi_i) \quad 2.17$$

where c_a is the adhesion intercept, and can be defined as $c_a = c'_a + (u_a - u_w)_f \tan\delta^b$, δ' is the effective interface friction angle at saturated condition; ψ_i is the interface dilation angle; and $(\delta' + \psi_i) = \delta_{\max}$ is the apparent interface friction angle. It must be noted that Eq 2.17 has been used to predict the shear strength of soil-cement grout interface. However, so far its validity has not been explored for soil-steel interfaces.

2.9 STUDIES ON PULLOUT INTERFACE BEHAVIOR

Pullout tests are commonly used to study the performance and behavior of the interface between a soil and a pile (or soil nail) subjected to tension. As is well known, the surface roughness of a pile is a key parameter affecting the shear strength of the soil-structure interface (Chan et al. 1993; Su 2006; Zhou 2008). With the progress of urbanization, considerable high-rise buildings have been constructed every year in Hong Kong and Chinese Mainland. Pile foundations can take large vertical, lateral and even uplift loads in comparison with conventional shallow foundations. Piles can be divided into friction piles (more than 90% contributed by friction), end bearing piles (more than 90% contributed by end bearing friction), and piles in between. For piles used to resist uplift, the uplift capability of the piles are all contributed by the friction of the piles. Examples of piles used to resist uplift are (a) piles installed underneath basement concrete slab to stabilize the slab against the buoyancy, (b) the tension pile in a pile group subjected to lateral loading, and (c) a pile acting as an anchorage, to name a few. In this literature study, particular focus is given to the friction behavior of a tension pile and soil nail.

2.9.1 INTERFACE BEHAVIOR BY PULLOUT TESTS

Earlier several researchers have performed some investigations to understand the interface shear strength of piles and soil nails. For instance, Juran et al. (1982) and Junaideen et al. (2004) presented the results of theoretical and experimental studies, on the mechanism of interaction between the soil and reinforcing elements during a direct shearing of a nailed soil mass and discussed the influence of different parameters on the efficiency of the reinforcement. Palmeira and Milligan (1989) investigated the pullout behavior of grids buried in sand and concluded that pullout test results can be influenced

by numerous factors, such as the properties of soil, the roughness and stiffness of the pile (or nail), and boundary condition of tests. Heyman *et al.* (1992) performed pullout test and demonstrated the importance of soil dilatancy in the prediction of soil nail pullout resistance. Also, they established a correlation between pullout resistance of a soil nail and basic soil parameters (obtained from routine laboratory and field tests). Kim and O' Neil (1998) have conducted field testing programs on a shaft in expansive clay, and proposed an empirical correlation for the change in upward shear stresses resulting from the variation in matric suction. Milligan and Tei (1998) performed a set of pullout tests, direct shear tests of sand and interface tests between three different type of sands and nails. The test results showed that the apparent coefficient of friction between the stiff rough nails and soils is dependent on (a) the friction angle of the soil, the rate of soil dilation during shear, (b) the stiffness of the soil and (c) the diameter of the nail in relation to the mean particle grain size of the soil.

Pradhan (2003) illustrated that the interface strength of the grouted soil nails at natural moisture contents obtained using pullout test, is very similar to the interface strength determined using the direct shear test. Chu and Yin (2005) and Yin and Zhou (2009) conducted several pullout tests on cement grouted nail in a completely decomposed granite (CDG) soil by employing a new pullout testing apparatus. The results showed that the interface strength depends on factors such as the normal stress, the soil degree of saturation, the surface roughness of the nail and grouting pressure.

2.9.2 EQUATION FOR PULLOUT SHEAR RESISTANCE

The mean pullout shear stress of a tension pile or soil nail can be calculated from a measured pullout load by using the following equation:

$$\tau_s = \frac{F}{A} = \frac{F}{(\pi D)L_s} \qquad 2.18$$

where τ_s is the pullout shear stress; F is the pullout load; A is the active nail surface area which can be calculated by multiplying the embedded length L_s (in m) of the nail in contact with the surrounding soil with the perimeter of the pulled-out nail πD (in m).

Schlosser and Guilloux (1981) estimated the pullout force of the soil nail by using the following equation:

$$T_{ult} = \pi D c'_a + 2D\sigma'_v \mu' \qquad 2.19$$

where T_{ult} is the pullout force per lineal meter; c'_a is the effective adhesion of the soil-nail interface; D is the nail diameter; σ'_v is the vertical stress at the mid-depth of the soil nail; and μ' is the coefficient of apparent friction of the soil-nail interface.

Wong (1995) proposed the Eq. (2.19) for the estimation of a soil nail pullout capacity per linear meter:

$$T = (\pi D c' + 2D\sigma'_v \tan\phi') \qquad 2.20$$

where T is the pullout capacity per linear meter, and $T = F/L_s$; D is the diameter of the soil nail; c' is the soil cohesion; and ϕ' is the internal angle of friction of soil. Eq (2.19) was initially proposed for driven nails and has been adopted by the practicing engineers due to its simplicity.

2.10 FIBRE OPTIC SENSING TECHNOLOGY IN GEOTECHNICAL APPLICATION

In recent years, advanced optical fiber sensors have been developed rapidly for health monitoring of numerous geotechnical engineering structures including pile foundation,

soil nails and anchors. In comparison with conventional transducers, fiber optic sensors have several apparent advantages such as immunity to EMI, insensitivity to corrosion, high precision and tiny size. The different types of fibre optic sensing technology includes Fiber Bragg gratings (FBG), low-coherence interferometry (LCI), optical time domain reflectometry (OTDR) and Fabry-Perot interferometry (FPI) and Brillouin scattering (Inaudi 1999). The present study mainly emphasises on the FBG technology as it is widely popular due to its adherent advantages. One of the main advantages of this technique is that FBG can measure multiple parameters, such as temperature and strain. Also, it offers excellent range of measurement and great measuring resolution with absolute measurement and modest cost per channel. Moreover, as the FBG are passive sensors, they can be either time- or wavelength-multiplexed, which allows for distributed sensing - a key advantage for geotechnical monitoring (Zhu 2009).

2.10.1 WORKING PRINCIPLE OF FIBER BRAGG GRATING SENSOR

Fig 2.5 depicts the schematic diagram of the functional principle of FBG sensor. According to Bragg's law, when a broadband source of light has been injected into the fiber, FBG reflects a narrow spectral part of light at certain wavelength, which is dependent on the grating period and the refractive index of fiber (Meltz et al. 1989 ; Morey et al. 1989). In the reflected spectrum of an FBG sensor, the wavelength at which the reflectivity peaks is called the Bragg wavelength λ_B and can be expressed by

$$\lambda_B = 2n_{eff}\Lambda \qquad 2.21$$

where n_{eff} is the effective core index of refraction, Λ is the periodicity of the index modulation.

For a standard single mode silica fiber, the relationship between the Bragg wavelength change $\Delta\lambda_B$, strain change $\Delta\varepsilon$, and temperature change ΔT can be simplified as (Kersey et al. 1997; Othonos and Kalli 1999):

$$\frac{\Delta\lambda_B}{\lambda_B} = \mathrm{c}_\varepsilon \Delta\varepsilon + \mathrm{c}_\mathrm{T} \Delta T \qquad 2.22$$

where λ_B is the original Bragg wavelength under strain free and $0\,^{\circ}\mathrm{C}$ condition, and c_ε and c_T are the calibration coefficients for strain and temperature.

In order to measure strains on model piles resulting from pullout force, temperature compensation of FBG sensors is required. Once the temperature is measured, the mechanical strain can be expressed by

$$\Delta\varepsilon = \frac{1}{\mathrm{c}_\varepsilon}\left(\frac{\Delta\lambda_B}{\lambda_B} - \mathrm{c}_\mathrm{T}\Delta T\right) \qquad 2.23$$

Using Eq.(2.23), the mechanical strains along the fiber fixed along the model pile can be obtained.

2.10.2 FBG BASED GEOTECHNICAL APPLICATION

In 1978, Hill et al. (1978) discovered photosensitivity in optical fiber and fabricated the first FBG with a visible laser beam propagating along the fiber core. Since then, FBG sensors are by far the most commonly used in civil engineering, accounting for over 50% of the fiber optic sensors in structural health monitoring, as well as in fiber-optic communication as the optical filter. Optical fiber sensors have been used to perform strain monitoring of cast-in-place piles during axial compression, pull-out and flexure tests, small strain measurement in soil (Zhu et al. 2007; Borana et al. 2012; Zhu et al. 2012). Glisic et al. (2002) performed laboratory and field tests to investigate the suitability of FBG based multiplexed sensor system in the instrumentation of piles. The

results obtained from FBG sensors when compared with conventional strain gauges indicated that the measured strains, the distributions of axial load in three model piles and a field test pile were similar in terms of magnitude and trend. Borana et al. (2012) evaluated the suitability of the FBG sensors for measuring the small strain stiffness of soil by modifying conventional triaxial apparatus. The major modifications include addition of piezoceramic sensors (bender elements) for measuring the maximum shear modulus and fiber Bragg grating (FBG) sensor-based local displacement transducers (FBG–LDTs) for measuring the stress–strain behavior at small strains. The comparison of results obtained using the FBG–LTDs, and the external displacement transducer showed that, irrespective of confining pressure the FBG sensors are capable of measuring small strains with higher accuracy as compared to electrical circuit-based external LVDTs. Xu et al. (2013) utilized FBG sensors based LDT and conducted a series of triaxial test to measure small strain behavior of CDG soil. The results showed that it is more feasible to employ the FBG sensors based LDT for measuring small strain of a soil specimen as it outperforms the external LVDT in all the aspects, such as higher accuracy, light weight, system compatibility, and ease of handling.

Schmidt-Hattenberger et al. (2003) and Liu et al. (2007b) evaluated the field performance of FBG sensor network installed in a large diameter concrete pile and monitored its deformation throughout the quasi-static loading cycles. The comparison of results between the data obtained from FBG sensors and conventional strain gauges has displayed excellent agreement. Lee et al. (2006) evaluated the applicability of an FBG sensor system in the instrumentation of piles, by comparing laboratory and field tests data. The results indicated that FBG sensor system is an effective tool for the analysis of the axial load transfer in piles.

Yin et al. (2008) have successfully employed advanced FBG sensors for monitoring deformation in mat foundation. The results showed that the FBG sensors perform very well as compared to the conventional sensors. In recent times, FBG sensors have also been used to monitor deformation in laboratory scale model tests (Yoshida et al. 2002; Zhu et al. 2010a). For instance, Zhu et al. (2010b) have developed a sensing bar with surface adhered FBG sensors and successfully evaluated its performance, for monitoring and measuring internal displacements of laboratory scale model tests of a gravity dam and a cavern group.

2.11 CRITICAL APPRAISAL OF THE REVIEWED LITERATURE

The reviewed literature in the previous sections suggests that matric suction has significant influence on the engineering behavior of soils, and therefore it must be taken into consideration to understand the mechanical behavior of interface between soil and construction materials. Also, there are very limited efforts by researchers to study for the behavior of interfaces in unsaturated soils. It has also been realized that there is a dearth of literature on behavior of unsaturated steel interfaces in coarse-grained soils. Though, it is assumed that the unsaturated interface shear failure plane, which posses the minimum shear resistance, exists on counterface surface but there is no such literature in the references regarding the soil-steel interface shear tests. Also, no definite criterion for selection of interface layer thickness for different unsaturated soil-structure interfaces is readily available. To fill up the above-mentioned gaps, in existing literature, the present study is aimed to conduct a series of suction controlled direct shear tests under a combination of different matric suctions, net normal stresses for soil and steel plates with different counterface roughness. Direct shear tests on the interface are basic elemental tests and measure the shear strength behavior directly. However, pullout tests are not elementary tests; the data obtained from the test is indirect and need

careful considerations. In this study, both direct shear tests for unsaturated CDG soil and pullout tests will be conducted to examine the unsaturated interface behavior.

2.12 SUMMARY

This chapter illustrates the literature review about the soil suction and its components, mechanical behavior of soil water, effects of suction on soil behavior, soil-water characteristic curve, the review of the literatures regarding the shear behavior of unsaturated soils and interface, existing analytical equations for unsaturated soil and interface, pullout test and, fiber optic sensors in geotechnical applications. The next chapter will discuss the experimental technique and testing apparatus used for unsaturated soil tests, interface tests and pullout test.

Table 2.1 Comparison of different modes of shearing on interface friction angle (after Chu 2003)

Author	**Type of testing apparatus**	**Results of investigation**
Potyondy (1961)	Direct shear test apparatus (Type B model)	(δ/ϕ) values for sand, cohesionless silt, cohesive granular soil and clay with smooth or rough steel, wood and concrete. $\delta = \phi$ in rough materials surfaces
Panchanathan *et al.* (1964)	Direct shear test apparatus (Type B model)	(δ/ϕ) values for sand with smooth or rough steel, cast iron, wood, brick and concrete. The ratio δ/ϕ is obtained between 0.60 to 0.75 for smooth materials and for rough materials 0.90 to 1.00
Kulhawy *et al.* (1979)	Direct shear test apparatus (Type B model)	(δ/ϕ) values for sand with different roughness of concrete surface. δ/ϕ is 0.99 in rough concrete surface and δ/ϕ is 0.89 in smooth concrete surface
Yoshimi and Kishida (1981)	Ring torsion apparatus (Type A model)	δ_{max} depends on surface roughness but does not depend on properties of sand and material type. $\delta_{lim} = \phi_{cv}$ for smooth surface material
Acar *et al.* (1982)	Direct shear test apparatus (Type B model)	δ_{max} increases with density of sand and roughness of steel, wood and concrete materials
Levacher and Sieffert (1984)	Direct shear test apparatus (Type B model)	δ_{max} increases with soil density
Desai *et al.*(1985)	Translational test box (Type B model)	δ_{max} for concrete material depends on density of sand
Noorany (1985)	Direct shear test apparatus (Type A model)	δ_{max} is independent of soil density
Bosscher *et al.* (1987)	Direct shear test apparatus (Type B model)	$\delta = \phi$ in rough concrete and sandstone, δ is lower in granite
Uesugi *et al.* (1990)	Simple shear apparatus (Type A model)	δ_{max} depends on sand density and concrete surface roughness
Subba Rao *et al.* (1998)	Direct shear apparatus (Type A and B models)	δ in Model B depends on sand density while in Model A is independent of density.

*Type A model: Construction materials are placed on the free surface of prepared soil.
*Type B model: Soil is placed against the material surface which functions as a confined boundary.

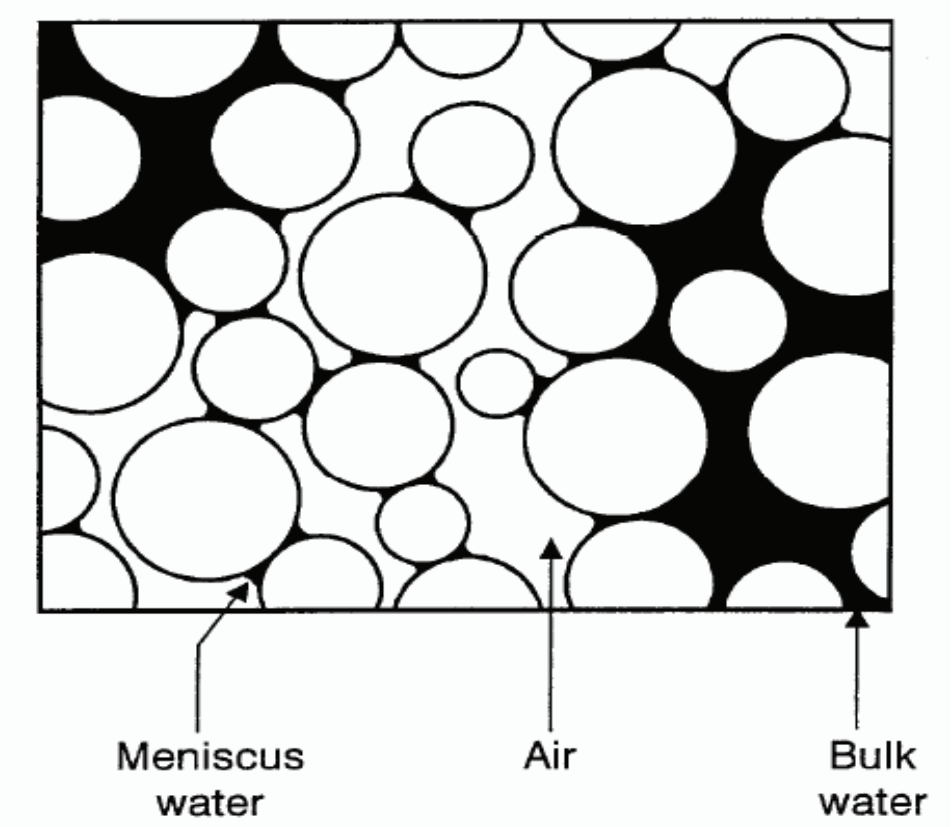

Figure 2.1 Schematic diagram of bulk water and meniscus water in an unsaturated soil (after Wheeler and Karube 1996)

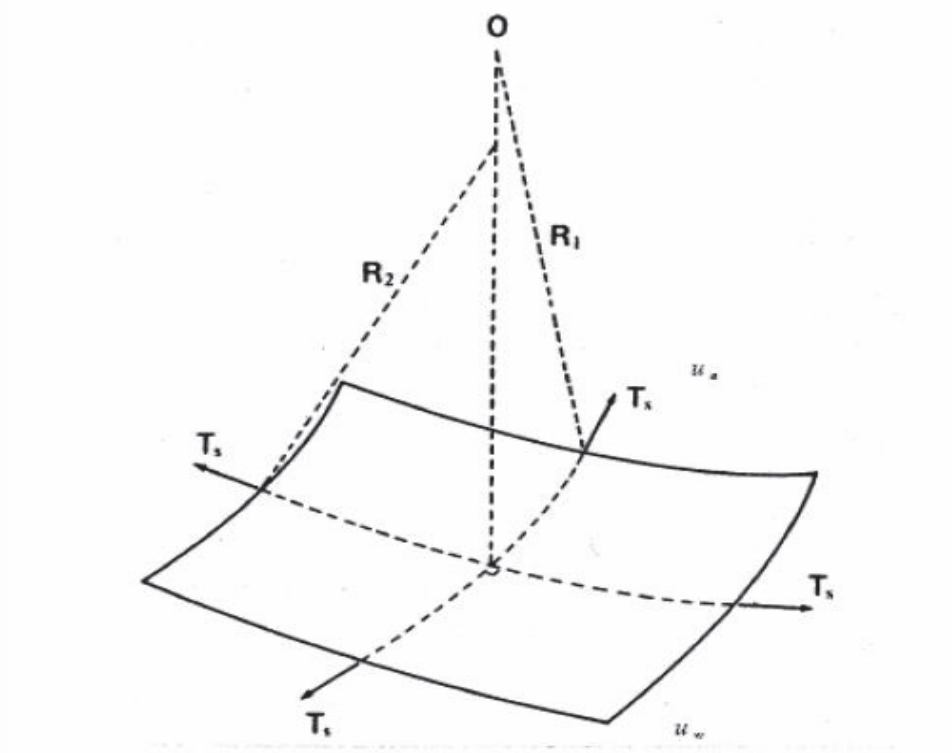

Figure 2.2 Surface tension on a warped membrane (after Fredlund and Rahardjo 1993)

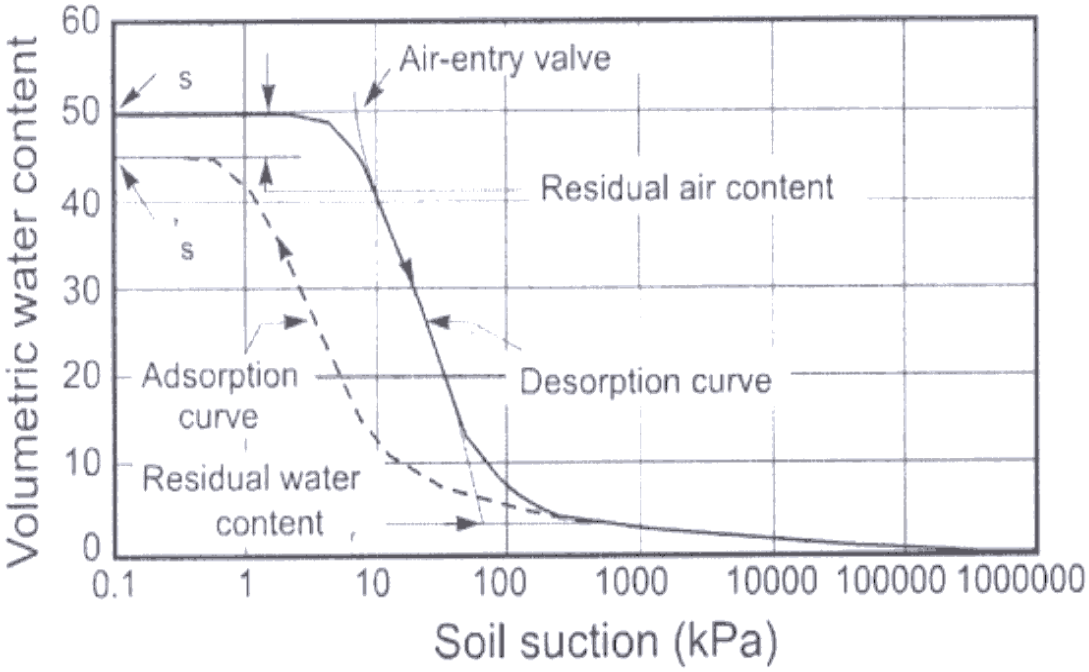

Figure 2.3 Soil-water characteristic curves for a silty soil (after Fredlund and Xing 1994)

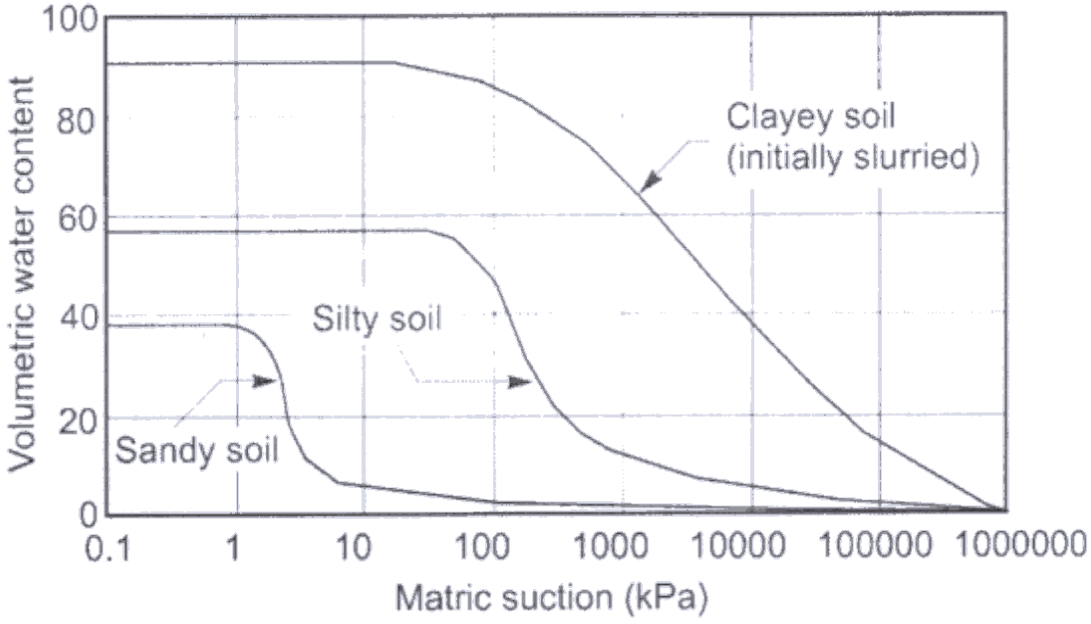

Figure 2.4 Typical soil-water characteristic curves for a sandy, silty, and clayey soil (after Fredlund and Xing 1994)

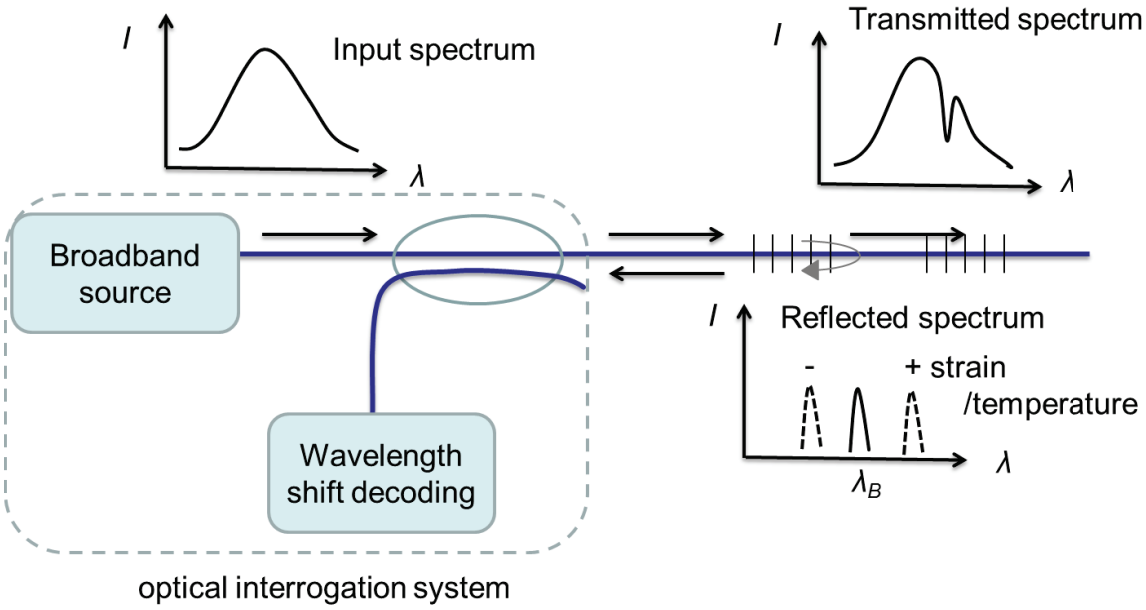

Figure 2.5 Schematic diagram of the functional principle of FBG sensors (after Xu et al. 2013)

Chapter 3

EXPERIMENTAL TECHNIQUE AND TESTING APPARATUS

3.1 GENERAL

Suction control in the soil mass is a key concern for experimental study on unsaturated soil and interfaces. The most popular technique for controlling suction is axis-translation technique (Hilf 1956), followed by osmotic technique (Zur 1966) and humidity control technique (Esteban and Saez 1988). This chapter presents the working principle and concise overview of the suction controlled direct shear testing device and the pull out test apparatus employed in the present study.

3.2 SUCTION CONTROLLED DIRECT SHEAR APPARATUS

3.2.1 SUCTION CONTROL TECHNIQUE USED IN THE PRESENT STUDY

Axis-translation technique was used in this study to control the matric suction for both the soil tests and soil-steel interface tests. This technique was initially proposed by Hilf (1956) and thereon has become one of the most commonly used technique for controlling suction in soil. Axis-translation is accomplished by separating air and water phases in a soil through porous ceramic disk with high air-entry value. This technique requires the control of pore air pressure (u_a) and pore water pressure (u_w) in a manner to avoid cavitations in the drainage water system. The total stress (σ) is elevated with

u_a at the same amount to maintain the net stress $(\sigma - u_a)$ unchanged. Due to the ease of measurement and control of suction, this technique has been cited to be one of the most preferred methods for unsaturated soil testing (Bishop and Blight 1963; Fredlund and Morgenstern 1977; Hamid and Miller 2009; Hossain 2010). However, one limitation of the axis-translation technique relates to the maximum suction value that could be applied on the specimen is restricted to the air entry value of the porous ceramic disk and ultimate capacity of cell pressure. As a result this technique is commonly employed for controlling suction in the range of several hundred kPa.

In the present study in-order to control the matric suction, water pressure (5 kPa) was applied in the water chamber on top of (below for soil tests) the high air entry porous disk (HAEPD) followed by application of necessary air pressure in the air pressure chamber. The desired matric suction is the difference between the applied air pressure and water pressure. A lower water pressure was applied for two reasons (a) to prevent the desaturation of HAEPD in water chamber (b) prevent the possible cracking or damage to HAEPD (as HAEPD is brittle material it is likely that higher pressure can induce cracks in the disk).

3.2.2 TESTING APPARATUS

In laboratory, the unsaturated soil shear behavior can be investigated by either conducting direct shear test or triaxial test. In the past, some studies performed using triaxial device indicates that, (a) for conducting one experiment in unsaturated soils, triaxial tests require a relatively longer time and may hinder in solving the in-situ problem that needs to be treated within shorter time duration, (b) due to the increase of net mean stress increases with deviator stress during shearing the soil dilation affinity might not be observed clearly. The specimen tends to contract with the increase of net

mean stress and thereby shrouding the effect of suction on the dilation (Zhan and Ng 2006). As a result researchers have been recommending employing the suction controlled direct shear testing device (Donald 1956; Escario 1980; Escario and Saez 1986; Gan et al. 1988).

Usually, to study the behavior of soil-structure interfaces a variety of instruments have been employed and every device has its own advantages and limitation. To understand the interface behavior it is important to acutely examine the load-displacement behavior, mode of deformation, and extent of dilatancy. The direct shear testing apparatus can be employed effectively to examine the elementary interface behavior and overcome the limitations presented above. With this in view, a suction controlled direct shear testing apparatus was employed and suitably modified to conduct soil-soil direct shear tests and soil-steel interface tests. The different features of the testing device are presented and discussed in the following section.

3.2.3 MODIFIED DIRECT SHEAR APPARATUS (MDSA)

In the Soil Mechanics Laboratory at The Hong Kong Polytechnic University the modified direct shear apparatus (MDSA) was fabricated, installed and employed. Fig. 3.1 and Fig. 3.2 depicts the schematic diagram and photographical view of the MDSA. The Fig. 3.3 and Fig. 3.4 shows the schematic diagrams of test cell /shear box used for pure soil and soil-steel interface direct shear tests respectively. The MDSA consists of an air pressure chamber, HAEPD, DAVI, a pressure/volume controller (used to drain out and measure all the air bubbles from the connecting tubes), measuring /monitoring devices eg; two LVDTs (Linear Variable Differential Transformer) for monitoring horizontal and vertical displacements, a pore-water pressure transducer, load cell, and a auto volume meter (AVC) device.

The MDSA used in this study is similar in principle to that of Gan and Fredlund (1988). The major difference of MDSA used in present study with the conventional apparatus, used for unsaturated soil testing, is the provision of a detachable high air entry value porous ceramic disks (HAEPD) assembly that can be easily be replaced depending on the maximum target suction values. The HAEPD is embedded in the steel plate and installed over the water chamber with the help of screws and rubber O-ring. Fig. 3.5(a) and Fig. 3.5(b) shows the AVC device (after Wykeham Farrance Engineering Ltd.) and diffused air volume indicator (DAVI) device (after Geotechnical Consulting & Testing System) respectively. One end of water chamber is connected the AVC (to monitor the flow of water from or into the specimen), while the other end of water chamber is connected to DAVI (to measure the total volume of diffused air). To flush out the air bubbles from the drainage lines and water chamber, a GDS pressure/volume controller (after Geotechnical Digital System) as shown in Fig. 3.6(a) was employed. High pressure polyvinylidene fluoride tubes of 3 mm diameter are used as drainage lines, to transmit the water from the AVC to the soil specimen through the HAEPD with an air entry value of 5 bars, and flushing diffused air from the base of the HAEPD. The air pressure and water pressure in the MDSA is controlled and monitored using pressure regulators (as shown in Fig. 3.6(b)) and pressure gauge of 1kPa resolution. The load cell as shown in Fig. 3.7(a) was used for measuring the horizontal shear load and has a maximum capacity of 20kN.

For soil-steel interface testing, modifications were made in test cell/shear box of MDSA as compared to the test cell/shear box used for unsaturated soil testing. This includes the construction of water chamber inside the top steel platen, (see Fig. 3.7(b)). The HAEPD

was installed at a same level in the top steel platen located below the water chamber. The major features of the MDSA are presented in the following sections.

3.2.3.1 Shear box base

The shear box consists of two parts- upper half and lower half as shown in Fig. 3.8(a). Both the parts of the shear box are made of stainless steel having a thickness of 15mm and an internal dimension of 100.05 mm x 100.05 mm for soil testing and 100.06 mm x100.06 mm for soil-steel interface testing. A stainless steel mould, of dimension of 100.05 mm x 100.05 mm x 50 mm was utilized for compacting the soil specimen (see in Fig. 3.8(b)). Specimen shearing is initiated by applying the shear load on the lower half of the shear box with the help of a digital motor, having a minimum displacing capacity of 0.001 mm/min and maximum of 2 mm/min. The horizontal resisting shear load is measured on upper half of the shear box as the shear resistance is measured via upper part of shear box. The lower half of the shear box may not offer any resistance to movement with the base as a result of provision friction resistance rollers and thereby might not introduce errors to the measured resisting shear load (Hossain 2010).

Fig. 3.9 (a) and Fig. 3.9 (b) show the photographic view of the shear box base used for soil and interface testing respectively. The presence of water chamber in the shear box base (for soil) facilitates the circulation of water from entry port to the exit port and thereby ensuring a proper flushing and removal of air bubbles from the drainage lines. However as mentioned earlier the water chamber for interface shear box is located in the top steel platen, and is mounted on the compacted sample specimen. The base of the lower halves of both the shear box base is rests on the stainless steel rollers present in the chamber base (can be seen in Fig. 3.1).

3.2.3.2 Air pressure chamber

The shear box is placed inside the air pressure chamber in order to apply and maintain the target air pressure in and around the specimen. The air pressure chamber is made up of stainless steel and consists of three main components viz., (a) the chamber body (b) the chamber cap, , and (c) the chamber base. The air pressure chamber, as shown in Fig. 3.10 (a), is cylindrical in shape and can withstand a maximum pressure of 1000 kPa. It has a uniform thickness of 8 mm with an internal diameter of 300 mm and height of 400mm. The chamber cap, as shown in Fig. 3.10 (a), consists of air inlet valve, an air outlet valve, and an axial loading ram and is held to the chamber body by using six steel cap screws. The air tightness of the chamber is ensured, as all the holes in this chamber are lined on the inside with an airtight Teflon seal. Two diametrically opposite holes that offer the necessary movement for the pistons to apply the shearing force to the shear box are also lined in with airtight Teflon seal.

3.2.3.3 High air entry porous disk

The high air entry porous disk (HAEPD) is the key element for controlling and measuring the pore-water pressure; it is 7.14 mm thick and has a diameter of 79.38 mm. The HAEPD behaves as a semi-permeable membrane that does not to allow the passage of free air and also separates the air and water phases. However, the dissolved air (in water) can sometimes diffuse through passage water. The air entry value of the HAEPD plays a key role in achieving the proper separation of the air and water phases. It must be noted that the air entry value of the disk needs to be greater than the desired maximum matric suction of the soil. The air entry value of the HAEPD is mainly based on the maximum pore size in the disc and, refers to the limit of maximum matric suction that the HAEPD can be applied prior to the passage of free air through the disk.

Therefore, while testing an unsaturated soil the selection of a HAEPD must be based on the highest expected matric suction that might occur at some stage in the test. It is noteworthy mentioning that the permeability and the thickness of the HAEPD directly influences the total time required for the testing of unsaturated soil and thus needs to be considered while selecting the disk.

In this study for soil testing a circular HAEPD, as shown in Fig. 3.11(a), was installed at the centre of a square steel plate with dimension of 100mm, using super glue (araldite). To ensure proper installation of disk, to the 2 mm gap between the steel plate and HAEPD was filled with super glue, along with another groove of 2 mm x 2 mm which was made on the centre of the perimeter of HAEPD and inside the steel plate. Whereas, for interface testing the HAEPD is mounted in the top platen (see Fig. 3.11(b)). Perspex cells as shown in Fig. 3.12 (a) were used to apply the water pressure in the water chamber (below the disk for soil testing and top of the disk for interface testing), and the pressure was controlled by valves in pressure control panel.

3.3 CALIBRATION OF MDSA COMPONENTS

The data logging of the shear test was done using two mini-scanner data loggers (supplied by VJ Technology, UK), as shown in Fig. 3.12 (b). The data was transferred from the data loggers to the computer using 'LabVIEW' program. All the pore-water pressure transducers (used to measure the applied air and water pressure) were calibrated by using the pressure/volume controller. The AVC device that measures the movement of water from or into the sample specimen was calibrated within the range of 0 to 100 ml with the help of pressure/volume controller. Fig. 1 & Fig. 2 in the Appendix demonstrate the calibration curve for the pore pressure transducer and AVC device respectively. The DAVI device used to measure the total volume of diffused air while

flushing was calibrated, as shown in Fig. 3 (Appendix) within a range up to 10 ml. The load cell used for measuring shear load was calibrated, as shown in Fig. 4 (Appendix), by applying compressive load of 0 to 15 kN through a universal testing machine. The horizontal and vertical LVDT that had a maximum displacement capacities 50 mm and 25 mm respectively were calibrated (see Fig. 5 and Fig. 6 in the Appendix) by a slidecaliperse. The increase of air pressure in the pressure chamber induces additional load on the load cell and thereby necessary corrections are required for controlling or computing the net normal stress and shear load for different air pressure. Fig. 7 in the Appendix shows the correction required on load cell reading due to application of air pressure in the pressure chamber. The corrections obtained from Fig. 7 (Appendix) were considered while calculating the net horizontal shear resisting load. The bottom of the upper half of the shear box was provided with a groove of 2mm (wide) and 3mm (deep) and this gap between the two halves of the shear box was filled with grease thereby the frictional resistance between upper and lower halves of shear box was almost negligible.

Tables 3.2 presents the additional load required for the correction of net normal stress due to different air pressure applied in the chamber. The additional load is applied to the hanger which has a load factor ratio of 1: 20. The frictional resistances of vertical and horizontal loading rams were noted to be very negligible, and were neglected during computation.

3.4 PULL OUT TEST APPARATUS

For a friction pile, one of the most important parameters is the skin friction between the pile and the surrounding soil. Over the past few decades, researchers focused on the total bearing capacity of the friction pile foundation but not the distribution of skin friction along the pile under vertical pullout loading. The main objectives of the current

research are to (a) measure axial strain of the model pile and the friction behavior between the pile and the surrounding soil with different degrees of saturation and (b) the model piles with different roughness using FBG sensor technology. Pullout tests are commonly used to study the performance and behavior of the interface between a soil and a pile subjected to tension. As described in previous chapter, the surface roughness of a pile is a key parameter affecting the shear strength of the soil-structure interface (Palmeira and Milligan1989; Chu and Yin 2005).

3.4.1 PULLOUT TESTS FOR MODEL PILES

In this study, two series of pullout tests have been conducted to study the distribution of axial strain and skin friction on rough and smooth model piles in a soil mass at different water contents. In these test series, the changes of skin friction and axial strain can be calculated from strain values measured by the fiber Bragg grating (FBG) sensors. The test set up for the pull out model pile test is explained in the subsequent sections.

3.4.1.1 FBG based model pile

In this study, FBG strain sensors are used to determine the skin friction and axial strain for the model pile in group of pullout tests. Three pairs of FBG strain sensors are used for a model pile. Fig. 3.13 depicts the schematic view of the FBG installed on the model pile. The installation consists of total six FBG sensors on two diametrically opposite sides of the model pile using two cables. Considering the fact that the pairs of sensors are installed at the sides diametrically opposite to each other, it facilitates the measurement of bending moment occurred in the model pile during the pullout test.

3.4.1.2 Test Setup

Fig. 3.14 shows the schematic diagram of the model pile pullout test in this study. The setup mainly consists of a cylindrical container (having a diameter of 30cm and height of 68cm), hydraulic jack (for pullout force during the test), a steel reaction frame (used to provide reaction force), tensiometer (for suction measurement), a load cell (to measure the pullout force during the test), and LVDT (to measure the horizontal displacement of the model pile during the pullout). Fig. 3.15 and Fig. 3.16 show the photographic view of the tensiometer and test set setup used for pull out test. A data acquisition system for FBG sensors commonly known as an interrogator (Supplied by Micron Optics Inc, USA), and having a frequency of 1000 Hz, was employed to capture the real-time wavelengths of all six FBG strain sensors during the pullout test. Also, a conventional data logger (refer Fig. 3.16a) was also used to record the data from the LVDT and the load cell. The calibration curves for the load cell and LVDT are presented in Fig. 8 and Fig. 9 (Appendix) respectively.

3.5 SUMMARY

This chapter presents the brief overview of the axis translation technique that is used in the present study to control or gauge the matric suction. The target matric suction is achieved by applying and controlling the pore-air (i.e., by applying air pressure in pressure chamber) and pore-water pressure in the specimen (i.e., by applying water pressure in water chamber). The details of the modified suction controlled direct shear device, the FBG sensor based model pile and pullout test apparatus employed in the present study are described and discussed. Furthermore, the calibration curves of different components of the testing device are presented. The next chapter presents a detailed description of testing materials, sample specimen preparation for soil tests, soil-steel interface direct shear tests and pullout tests along with the test procedure adopted for the present study.

Table 3.1 Supplementary hanger load applied for the correction of net normal stress due to different air pressure applied inside the chamber

Air pressure (kPa)	Additional hanger load (N)
100	1.54
200	3.08
300	4.62
400	6.16
500	7.7

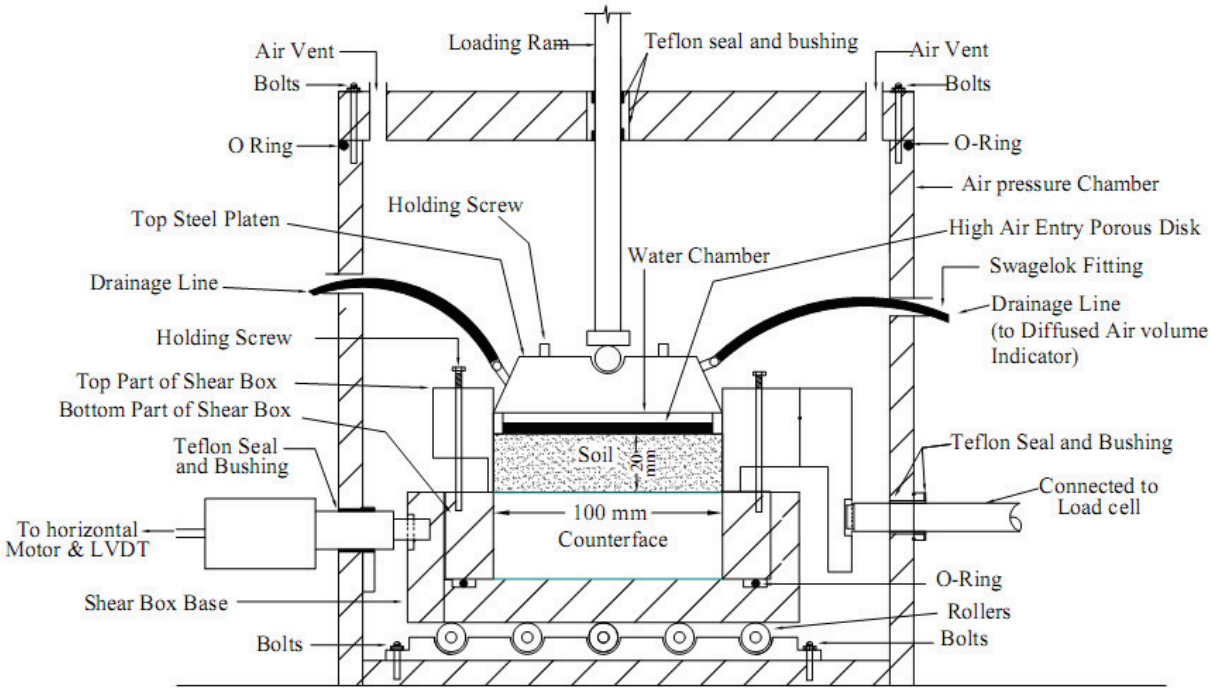

Figure 3.1 Schematic diagram of the Modified Direct Shear Apparatus for testing a soil-steel interface (not to scale)

1. DAVI
2. Hanger
3. Vertical LVDT
4. Air entry valve
5. Chamber cap screw
6. Horizontal LVDT
7. Air pressure chamber
8. Pore water pressure transducer
9. Motor control panel
10. Moment arm
11. Mini scanner

Figure 3.2 A photograph of the modified direct shear apparatus used in the present study

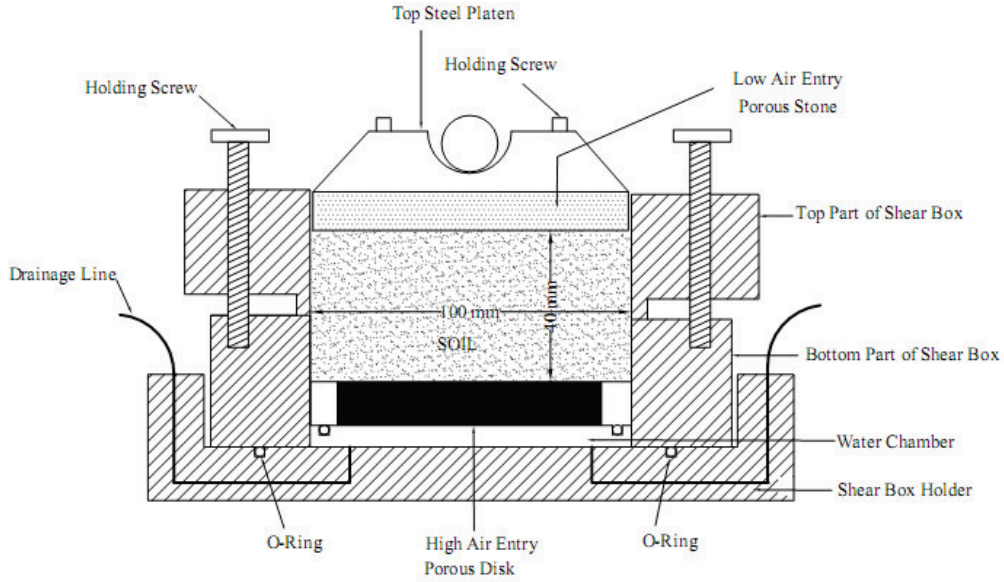

Figure 3.3 Schematic diagram of modified direct shear apparatus used for soil-soil direct shear test

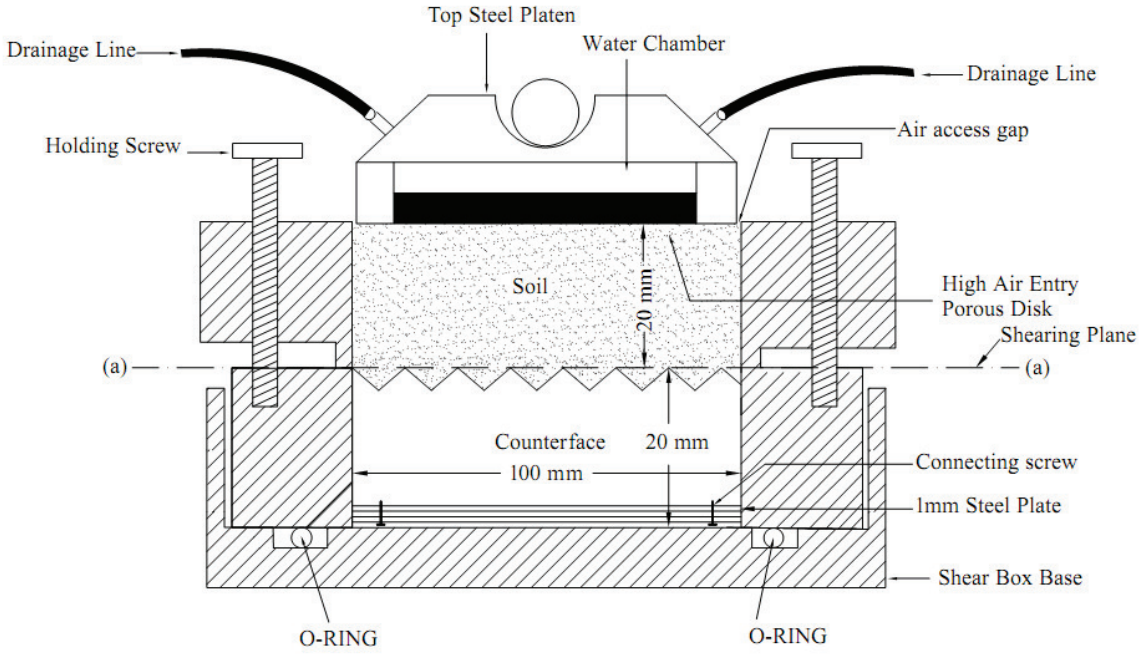

Figure 3.4 Schematic diagram of modified direct shear apparatus used for soil-cement grout interface test

(a) Auto volume change device

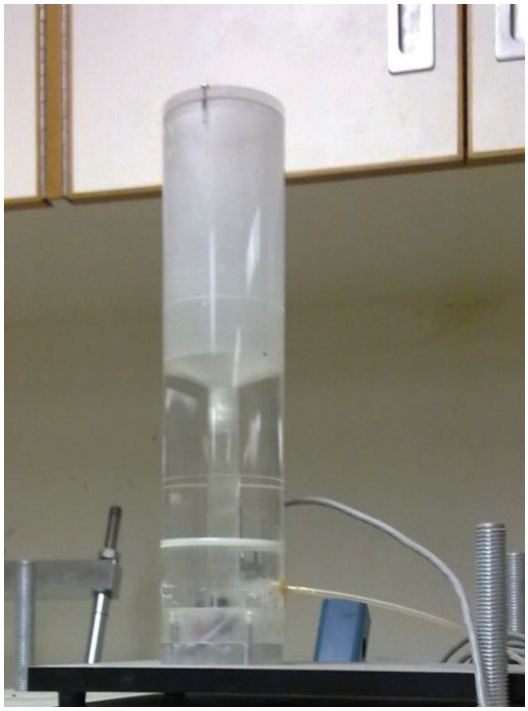

(b) diffused air flushing device

Figure 3.5 Devices used for measuring the volume change of water and diffused air

(a) GDS pressure/volume controller

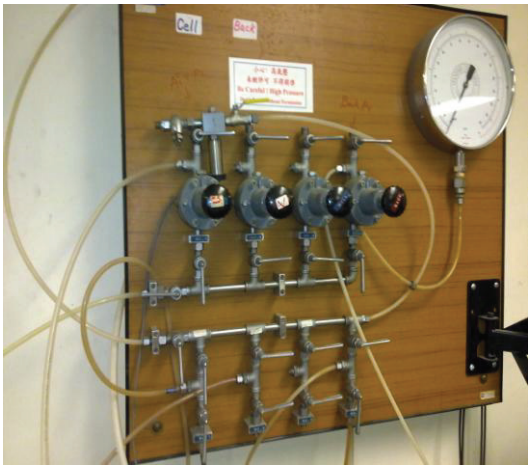

(b) air and water pressure regulator panel

Figure 3.6 Air and water pressure applying and controlling devices

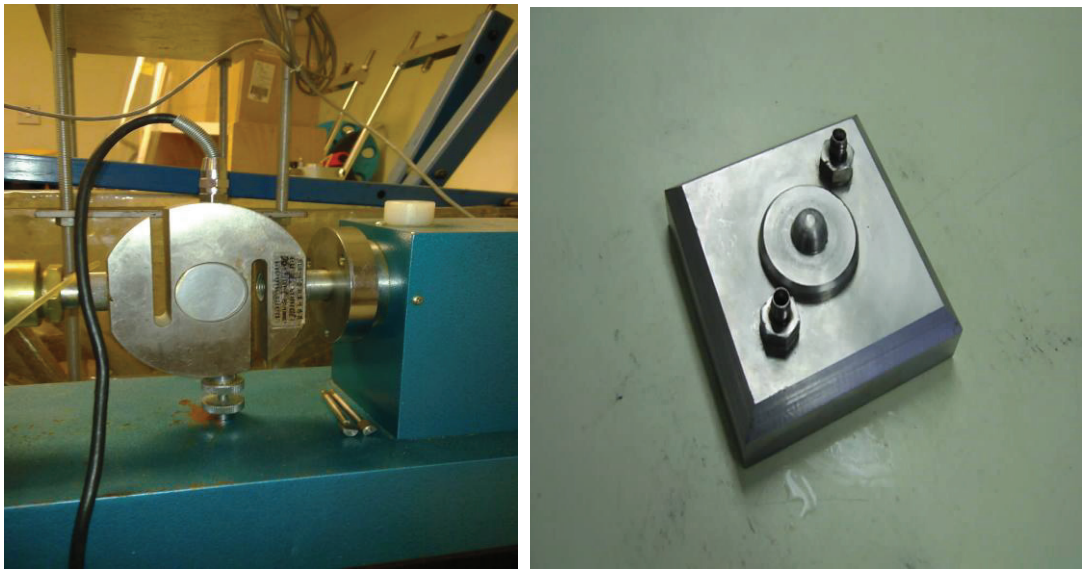

(a) load cell (b) top platen

Figure 3.7 Load cell, and top platen for soil steel -interface tests

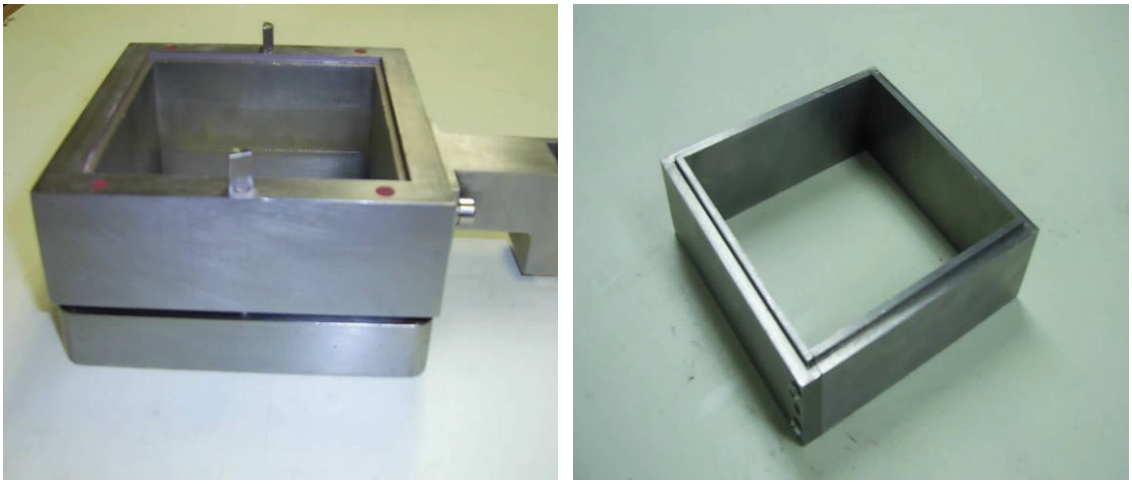

(a) shear box (a) steel mould

Figure 3.8 Shear box, and steel mould used for compaction of soil

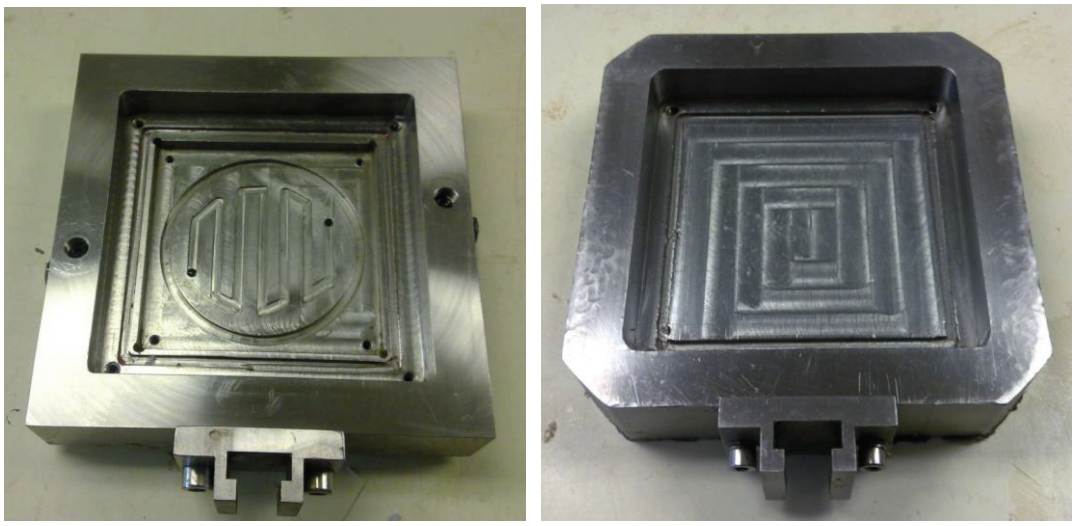

(a) for unsaturated soil tests (b) for unsaturated interface tests

Figure 3.9 Shear box bases used for unsaturated soil and interface tests

(a) pressure chamber (b) chamber cap

Figure 3.10 Air pressure chamber and chamber cap of MDSA

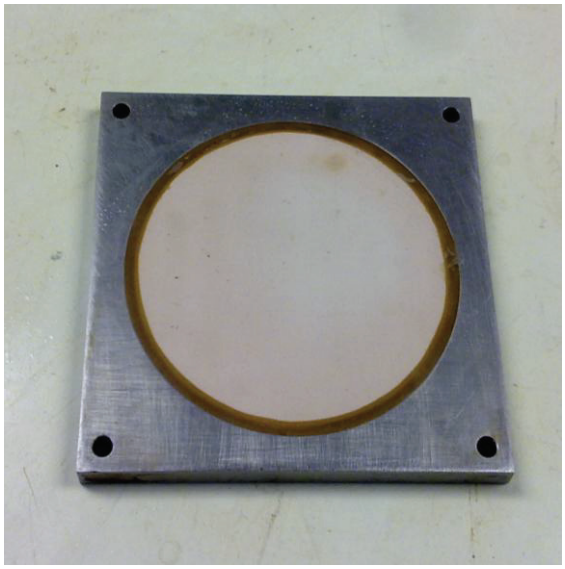

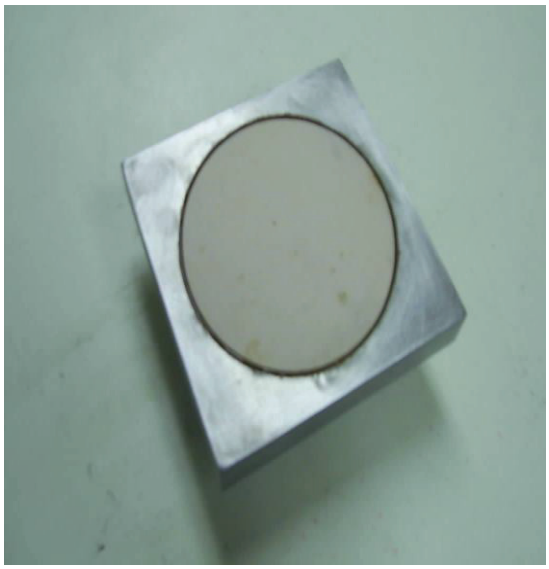

(a) steel plate with HAEPD (b) top platen with HAEPD

Figure 3.11 HAEPD installed in steel plate and top platen

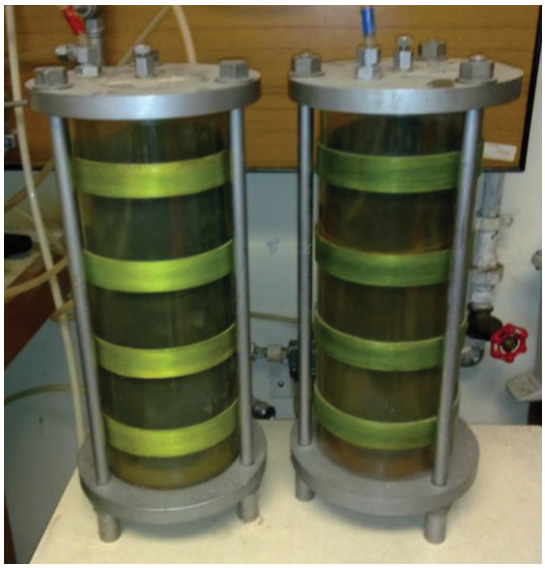

(a) Perspex cell (b) miniscanners

Figure 3.12 Air-water interface perspex cell, and shear test data logging device

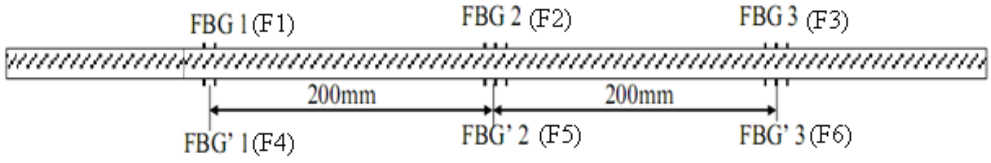

Figure 3.13 Schematic diagram of the FBGs instrumented model pile

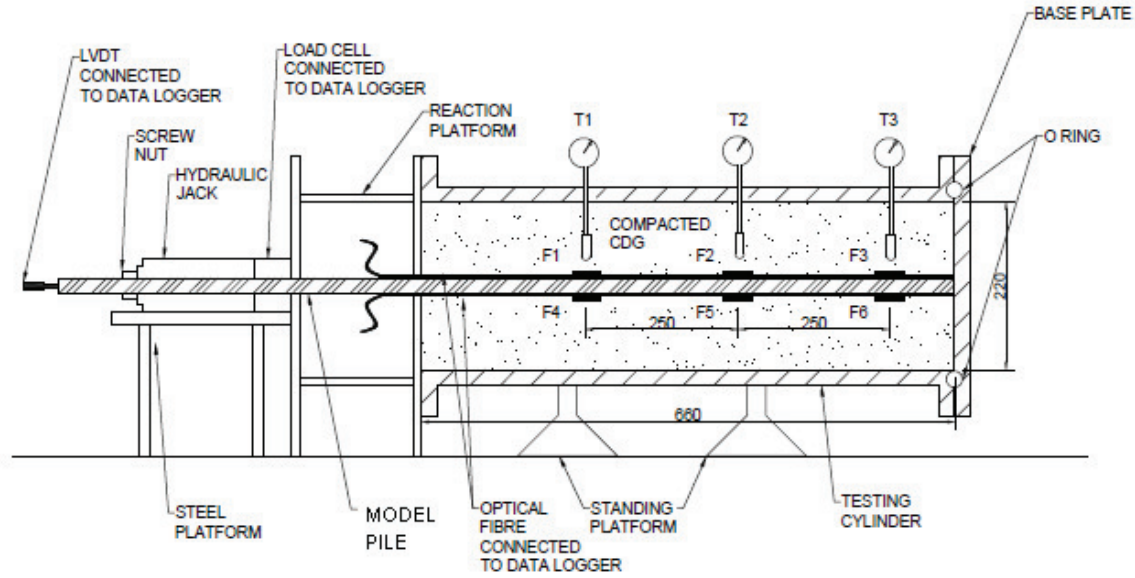

Figure 3.14 Schematic diagram of the model pile pullout test set up

Figure 3.15 Tensiometer employed for suction measurement

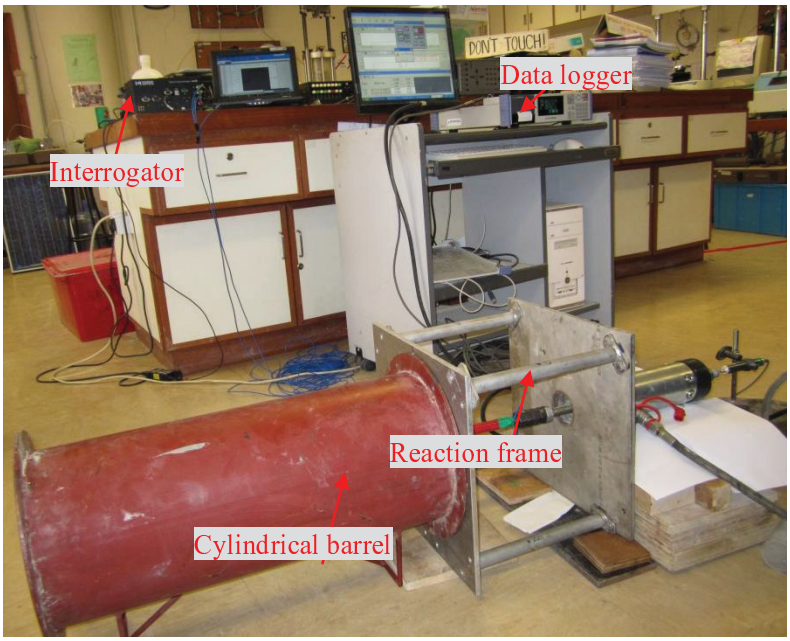

(a)

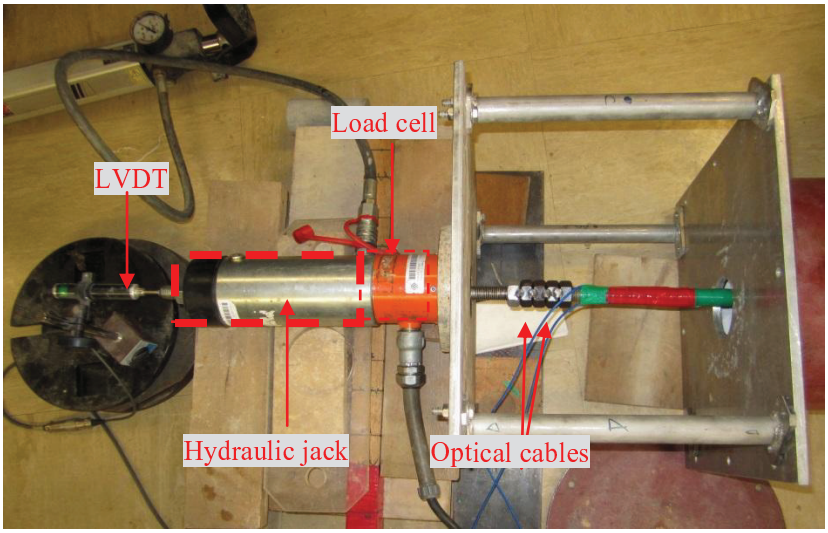

(b)

Figure 3.16 Photographic view of the of the model pile pullout test set up.

Chapter 4

TESTING MATERIALS, SPECIMEN PREPARATION AND TEST PROCEDURES

4.1 INTRODUCTION

The aim of this study was to examine the interface direct shear behavior between compacted soil and steel plate under different suctions, net normal stresses, shear planes and counterface roughness. The soil-steel interface direct shear tests were performed using the suction controlled direct shear apparatus as described earlier in chapter 3. For the sake of comparison, pure soil was also tested in similar condition. The soil used for present study was physically and geotechnically characterized prior to the main testing program. This chapter presents details of the material properties, sample specimen preparation and tests procedure adopted to achieve the objective of the study.

4.2 MATERIAL PROPERTIES

4.2.1 SOIL

The Completely Decomposed Granite (CDG) soil (typical insitu soil in Hong Kong) was used in this study. This soil is widely used as a fill material locally and its characterization is of great interests to engineers and scholars. The CDG soil used in the study was taken from a construction site at Tai Wai, Hong Kong.

4.2.1.1 Physical characterization

The CDG soil was physically characterized for its specific gravity, liquid limit and plastic limit, grain size distribution and maximum dry density by using relevant BS codes (e.g., BS-1337, 1990; BS-5930, 1999). The specific gravity of the soil was determined with the help of density bottles and noted to be 2.59. The particle grain size distribution curve the soil is presented in Fig. 4.1. The consistency limits of the soil samples were determined and the results obtained for liquid limit ($w_{L)}$ plastic limit (w_P) and plasticity index (I_p) are listed in Table 4.1 along with the details of percentage size fractions.

4.2.1.2 Geotechnical characterization

Standard proctor test was performed for CDG soil to establish its compaction characteristics by following the BS guidelines (BS-1337, 1990). The compaction is done using a rammer of weight 2.5 kg with a free fall of 310 mm. Fig. 4.2 depicts the compaction characteristics curve of the soil along with the zero air void line. Table 4.2 lists the value maximum dry unit weight, γ_{dmax}, the optimum moisture content (OMC). The hydraulic conductivity of the soil was determined by conducting the falling-head permeability test and the result shows that the permeability (k_{20}) of the soil is 2.29×10^{-8} m/s.

4.2.2 STEEL COUNTERFACE

Three different square stainless steel plate of dimension of 100 mm x 100 mm x 20 mm and different counterface surface roughness were employed for this study. The surface roughness of the counterface was defined based on the roughness profile. The counterfaces were designated as rough (INT-R), medium (INT-M) and smooth (INT-S),

as shown in Fig. 4.3-Fig. 4.5 respectively, based on the maximum peak to depression height ($R_{max)}$. The normalized surface roughness (R_n) of the counterface is based on roughness profile proposed by Kishida and Usegi (1987) in Eq. (4.1).

$$R_n = R_{\max} / D_{50} \qquad 4.1$$

where, $R_{\max}$ is the maximum peak to valley height and D_{50} is the grain size (diameter) corresponding to 50% finer. The $R_{\max}$ for INT-S, INT-M and INT-R was measured to be 0.0031mm, 0.48mm and 0.75 mm reflecting the corresponding R_n to be 0.04, 5 and 10 respectively.

A rough square stainless steel plate (employed as the counterface material), as shown in Fig. 4.6, was specially fabricated for testing the interface behavior at different shearing planes. This counterface plate was manufactured in a manner that the height of the counterface could be adjusted depending on the target shearing plane. It can be noted that the maximum height of the counterface is 20 mm and its base consists of four plates of 1 mm thickness. For example, refer. Fig. 4.6, to perform interface testing for "1 mm interface thickness" the counterface plane(b-b) position must be 1mm below the shearing plane (i.e. a-a). In other words the counterface height(x) must be adjusted 19 mm and can be done by removing a 1 mm plate from the base of the counterface. In this study, the interface direct shear testing for a rough counterface (INT-R) was conducted by shearing the soil-steel interface at 0mm, 1mm and 2mm above the counterface plane and designated as INT-0, INT-1 and INT-2, respectively.

4.3 PRELIMINARY PREPARATION OF DIRECT SHEAR TEST APPARATUS

The modified direct shear apparatus (MDSA) is primarily inspected and prepared before initiating the direct shear testing program; the preliminary preparation includes saturating the HAEPD and inspecting leakages (Padilla et al. 2006; Hossain 2010). After ensuring that HAEPD is completely saturated, and there is no leakage in HAEPD and pressure chamber, the testing program was started. The procedure adopted for saturating the HAEPD and inspection of leakages is presented in the following sections.

4.3.1 SATURATION OF HIGH AIR ENTRY POROUS DISK

One of the most important tasks for the preliminary preparation of the MDSA is to saturate the HAEPD with distilled water. In this study, the saturation of HAEPD was achieved by following the guidelines proposed by Fredlund and Rahardjo (1993). Briefly, it includes removal of air from water chamber through flushing device and subsequently flooding shear box base with distilled water and applying pressure. The chamber cap is placed on the air chamber of the MDSA (containing the shear box base flooded with distilled water) and tightened by the cap screws. It must be noted that both the valves connecting the water chamber are turned off while applying air pressure as a result the diffused present air in the HAEPD is accumulated in the water chamber. Initially an air pressure of 100 kPa is applied in the air pressure chamber for 1hr, which forces the flooded water through the HAEPD. The application of air pressure on flooded water diffuses the accumulated air bubbles in the water chamber. The entrapped diffused air in the water chamber is then flushed by the GDS flushing device (during flushing both the valves of water chamber are kept open). This process is repeated with an increment of 100 kPa air pressure and up to a maximum 500 kPa air pressure. A similar procedure was adopted to saturate the HAEPD for interface testing. As

mentioned earlier, for interface testing the HAEPD is located in the top steel platen, thereby the top steel platen was placed in the shear box base filled with distilled water.

4.3.2 INSPECTING LEAKAGES

There are two types of possible leakages in MDSA (i.e., leakage in HAEPD and leakages in air pressure chamber) and are discussed in the following section.

4.3.2.1 Leakages from high air entry porous disk

The inspection of leakage in HAEPD is very important in order to apply and maintain the target matric suction. After saturating the HAEPD, it is necessary to inspect any detectable leaks or cracks in the disk. This is achieved by applying stepwise sequential air pressure on the shear box base containing HAEPD. Initially, constant air pressure of 100 kPa was applied on the HAEPD for 1 hr. The water chamber was then flushed to check the presence of any diffused air bubbles. The air pressure was increased by a stepwise with an increment of 100 kPa up to the air entry value of the HAEPD and flushed. Negligible amount of presence of air bubbles while flushing the water chamber indicates no leakages of the disk. After inspecting the leakages of the HAEPD, it was again saturated by the procedure described in earlier section.

4.3.2.2 Leakages from pressure chamber

The air tightness of the air pressure chamber is essential as air leakage could hinder the matric suction during testing. Also, leakages in pressure chamber could result in continuous possible loss of moisture from the system. Inspection of leakages in air pressure chamber was accomplished by applying soap solution on all the joints, vents and sealed areas. After applying the soap solution the air pressure chamber was tightened by the chamber cap and a stepwise sequential air pressure (of 100 kPa) was

applied up to a maximum 500 kPa. The presence of leakages is reflected by the bubbling of the soap foam (from the vents and sealed areas) and no solution coming out indicates leakage free air pressure chamber.

4.4 PREPARATION OF DIRECT SHEAR TEST SPECIMEN

In this study three different types of specimens were prepared for the testing which includes direct shear specimens prepared for pure-soil testing, rough interface testing under different shearing planes, interface testing under different counterface roughness. However, the procedure adopted for both types interface specimen preparation is exactly similar. The preparation of direct shear specimens generally includes: pretreatment of the disturbed soil, mixing with water, and compaction of soil. The subsequent sections presents the procedure adopted for preparing different specimens for direct shear testing.

4.4.1 PREPARATION OF PURE-SOIL DIRECT SHEAR TEST SPECIMEN

4.4.1.1 Pretreatment of disturbed soil

The virgin soil was oven dried for 24 hrs at a temperature of 104 °C. After drying, the large particles were broken into small particles, using a rubber hammer to ensure that the gravel particles in the soil do not get broken. Then, the smaller particles were transferred into a crucible and were broken down to sizes smaller than 2 mm with the help of a rubber pestle. Subsequently, the broken particles were sieved by 2 mm BS sieve and the gravel content retained on 2 mm sieve was discarded. Whereas, the soil portion passing through the 2 mm sieve was collected, mixed thoroughly and kept in the oven for three days.

4.4.1.2 Mixing with water (Treated wet soil)

To prepare the treated wet soil, the pretreated oven dry soil (i.e, passing through 2 mm BS sieve) was taken in a mixing bowl and adequate amount (i.e, about 18% to 20%) of distilled water was poured into the bowl (i.e. to flood the soil). It is necessary to ensure that the lumps are not formed and the soil exhibits uniform water content. This is achieved by following the guidelines presented by Hossain (2010). It includes continuous weight monitoring of the mixing bowl (containing wet soil) onto the weight balance (of accuracy 0.0001g) until the target water content was achieved (i.e, optimum moisture content : 13.4 %). In, case if the water content is dropped below the target water content additional water is sprayed in to the bowl. As the target moisture content is reached the soil was mixed properly using a spatula. It is noteworthy here that the target water content is achieved by natural evaporation process and at a constant room temperature of 18℃.

4.4.1.3 Compaction of soil

A square steel mould, having a dimension of 100.05 mm and 80 mm high, was used for compaction of the soil. The interior side walls of the mould were polished uniformly with the lubricating oil, to reduce the friction between the soil and the side walls of the mould. The gap between the two halves of the shear box is filled with grease. The treated wet soil was compacted inside the mould in four layers (i.e, 10 mm thickness for each layer) to produce a 40 mm thick specimen. The required mass of the pretreated wet soil for every layer was placed in the mould. Then, every layer was compacted (at the optimum moisture content 13.4 %) to achieve a controlled dry density of 1.75 Mg /m^3 (i.e, 95% of the maximum dry density of 1.84 Mg /m^3). After completing the compaction, the weight of specimen was recorded and the change in weight of specimen was noted to be negligible. Subsequently, the mould with the specimen was turned

upside down and placed over the shear box. The soil specimen was pushed gently inside the shear box until it set properly over the HAEPD. As the dimension of the specimen and the dimension of the shear box are precisely the same, the disturbance caused to the specimen while pushing into the shear box is negligible.

4.4.2 PREPARATION OF SOIL-STEEL INTERFACE SPECIMEN

The pretreatment of the CDG soil and specimen preparation procedures for pure soil was comprehensively discussed in the previous sections (4.5.1). The procedure adopted for preparing all types of soil-steel interface specimen is described in the followings.

Prior to the compaction of soil in the shear box, both the halves of shear box were fastened together using screws. The gap between the two part of shear box was filled with grease and the interior side walls were polished with lubricating oil. The square steel counterface was placed in the lower half of the of the shear box. It should be noted that the maximum height of the counterface was 20 mm. The pretreated soil was then compacted over the counterface in two layers (each of 10 mm thickness), at optimum moisture content of 13.4% and dry density of 1.75 Mg/m^3. After compacting the first layer of soil, its top layer was scratched to ensure proper bonding between the two layers. After completing the compaction, the shear box was weighed and the loss in moisture content during the compaction was found to be negligible. Subsequently, the shear box placed inside the pressure chamber. It is worth mentioning here that the soil-steel interface specimens were prepared inside the shear box, which ensures that there is no disturbance of soil-steel interface before testing.

4.5 TEST PROCEDURE

4.5.1 SOIL WATER CHARACTERISTIC CURVE FOR CDG SOIL

In this study, the SWCC curve for CDG soil was determined using MDSA under zero net normal stress. The specimen for determining the SWCC curve was prepared in a similar manner to that of pure soil test as described in previous section. After compacting the soil and transferring it to the shear box, a porous disk was placed on top of the specimen and flooded with ample amount of water. The shear box was placed in the pressure chamber for about 24 hrs to attain saturation under gravity. After attaining saturation excess water on top of the porous disk was removed and the chamber cap was closed using cap screws to initiate the testing. It is noteworthy that no detectable volume change or swelling was observed after the saturation of specimen.

The air pressure inside the pressure chamber was raised stepwise during the testing to increase the matric suction. A constant suction was maintained until the equilibration of specimen was attained. The equilibration of specimen was considered to be achieved, when the flow of water from the specimen to the AVC was nearly ceases or sample attains less than 1% of degree of saturation. The continuous data recorded by the data-logger pertaining to the AVC shows that the CDG soil takes about 24 hrs to attain the equilibration for a each suction value. After completion of the final suction, the AVC valve was closed and the air pressure from the pressure chamber was gradually released. Subsequently, the sample specimen quickly was taken out from the shear box and kept in the oven for the final water content determination. The water content corresponding to each suction value is obtained by back calculating the flow of water from specimen and the final gravimetric water content. Lastly, to determine the SWCC curve of the CDS soil, the equilibration suction versus the water content variation at

different stages was plotted as shown in Fig. 4.7 and the fitting parameters are tabulated in Table 4.3.

4.5.2 DIRECT SHEAR TESTING

In the present study, a series of single staged consolidated drained direct shear test were conducted to examine the behavior of pure soil and soil-steel interfaces having different counterface roughness under same stress state variables. The test procedure for both soil and interface test consist of three stages which includes saturation, equilibration at constant net normal stress and suction and drained shearing at constant suction and net normal stress and will be elaborated in the following sections.

From the existing literature, it is noted that no definite criterion is available for identification or selection of the interface layer thickness for soil-structure interfaces. It has been noted that the major factors influencing the interface layer thickness includes counterface surface roughness and asperity angle of the counterface, void ratio and soil moisture. Kulhawy and Peterson (1979) observed that the shear surface of the rough interface between concrete and compacted soil is located away from the soil surface. Desai et al. (1985) pointed out that the interface action for soil-structure interfaces take place in a thin zone in close proximity to the counterface. Kishida and Uesugi (1987) have considered the interface thickness as zero while examining the behavior of soil-steel interface in saturated condition. Hamid and Miller (2009) have investigated the interface behavior of fine grained silty soil and smooth steel by considering the interface thickness as zero. Hossain (2010) have considered the interface thickness of 2mm while examining the rough interface between cement grout and soil. It has been realized that there is lack of literature in selecting or identifying the interface layer thickness in unsaturated soils. With this in mind, the variation of interface shear strength

of rough interface has been examined by using a modified suction controlled direct shear testing apparatus at different shearing planes.

4.5.2.1 Loading path of direct shear test

The loading path adopted for the pure soil and all soil-steel interface tests is shown in Fig. 4.8, where point 'I' marks the initial condition of the soil specimen before achieving the saturation and path 'IO' shows the phase of saturation. Path 'OA' presents the phase of equilibration under the influence of target net normal stress, whereas, path 'AB' represents the equilibration phase under matric suction. Point 'B' indicates the conclusion of equilibration phase as well as start of the shearing phase. Lastly, the path 'BC' shows the progression of shearing phase under target net normal stress and matric suction.

4.5.2.2 Saturation of specimen

Saturation of the specimen is the first stage of the unsaturated direct shear testing. After compacting and placing the sample specimen inside the shear box, a porous disk plate was placed over the specimen and sufficient amount of water was poured on it. The sample was allowed to soak water for 26-28hrs as advocated by Gan and Fredlund (1994) and heights of the specimen, before and after soaking, were recorded. Several pilot tests were conducted to verify the degree of saturation under gravity and the results revealed that the most of the specimen reached a saturation level of nearly 100% in 18 -20 hrs. After achieving the saturation (almost 100%), the porous plate and excess water on it were removed (For interface specimen, after achieving saturation the excess water and the disk were removed and the top steel platen was mounted). The final height of the specimen was noted, and no detectable changes in the initial and final height were observed.

4.5.2.3 Equilibration of specimen

After the specimen is saturated it is to be equilibrated under the target stress state variables and this marks the second stage of the testing. A pre-determined axial load, air pressure and water pressure were applied (by opening the valve of AVC) sequentially to the sample specimens, to attain the equilibration of desired matric suction. The valves connected to the DAVI and GDS pressure controller were kept closed. As described earlier, axis translation technique was used to achieve target matric suction and lower water pressure of 5 kPa was applied in the water chamber in order to ensure that the HAEPD is not subjected to greater pressures. Perhaps it is possible that there might be formation of small cracks in the HAEPD if subjected to higher pressure. During the equilibration process, vertical deformation and water movement were monitored using data loggers and recorded in the computer. Equilibration of the specimen was noted to be achieved when the vertical deformation was constant and flow of water essentially ceased ($\leq$ 1% of degree of saturation per day). Generally, the time duration of the equilibration phase is noticed to be about 24 – 30 hrs depending on the specimen, as in the present study the soil specimen was 40mm thick and interface specimen was 20mm.

4.5.2.4 Shearing at constant suction and net stress

After attaining the equilibration, the sample specimen was sheared under drained condition. The vertical displacement, horizontal displacement and flow of water from/into the specimen were recorded by employing the data-logger. It is noted that shearing rate plays an important role while testing unsaturated soils. Gan and Fredlund (1994) performed modified direct shear test on CDG soil using the shearing rate of 0.005mm/min. Han (1997) has investigated the shearing rate effect on a residual soil, and reported that the shear strength remains constant below the shearing rate of

0.004mm/min. In this study, a constant shearing rate of shearing 0.004mm/min was adopted, which is lower than the shearing rate suggested by Gan and Fredlund (1994). All the sample specimens were sheared until the horizontal displacement of 15mm was reached. After completion of the shearing stage, the sample was quickly taken out from the shear box for water content determination. During the shearing stage, a constant suction was maintained in the specimen and all the data were recorded automatically in a computer with an interval of two minutes. After the completion of the shearing stage, the specimen was dismantled from the apparatus and quickly taken out for water content determination.

4.5.3 PULLOUT TEST

4.5.3.1 Preparation of FBG based pile

In this study, two different FBG based model piles (i.e., rough and smooth) were used to perform the pullout test. Two set of optical fiber cable were fabricated in the soil laboratory at the Hong Kong Polytechnic University, each consisting of three FBG sensors connected in series. As described in earlier (refer section 3.4.1.1), each cable was installed in diametrically opposite side to each other using a thin layer of super glue (AB glue). It is noteworthy before installing the FBG sensored cable on the model pile, the surface of the pile was cleaned using Ethyl alcohol. This is done to ensure dust free and clean base surface for the optical fiber. To install FBG sensor based optical cable on the rough model pile, a groove of 2.5 mm width was provided for the total length of rough pile. This is provision facilitates the measurement capacity of FBG sensors and considerably reduces the risk of the FBG sensors being damaged during pullout.

4.5.3.2 Roughness of FBG based pile

The model piles used in this study consisted of mild steel material. The roughness of the model piles is measured by a roughness tester as shown in Fig. 4.9 (supplied by Mitutoyo Corporation, Japan). The R_n value is obtained using Eq.(4.2). The basic properties of the model pile are listed in Table 4.4. It was found that the average $R_{\max}$ value of the rough model pile was 0.95 mm and 0.019mm for the smooth model pile.

$$\overline{R}_n = \frac{1}{i}\sum R_i \qquad 4.2$$

where i is the number of data.

4.5.3.3 Compaction of soil and pullout test

Before conducting the compaction, the CDG soil pretreated as described in previous section (see section 4.5.1.1 and 4.5.1.2). The model pile was placed and clamped at the centre of the cylindrical container. After pre-treating and maturing the soil at desired target water content the soil was compacted in the cylindrical container. The soil was compacted to achieve the dry density of 95% of MDD (maximum dry density) for each layer of 5cm thickens using a standard 4.5 kg (ASTM) rammer. After compacting each layer, the surface of the soil was scratched using spatula to ensure proper bonding between soil layers. During the compaction process the verticality of the pile was checked by using leveling tool. After completing compaction the surface of the soil was sealed and the soil-pile interface was allowed to cure for about 24 hrs.

After the completion of curing, all the devices and equipments such as LVDT, load cell, data logger, interrogators and hydraulic jack were assembled as described in chapter 3 (refer Fig. 3.23). The data logger and interrogator were then connected to the computer

and continuous data were logged. The pullout force was applied to the model pile using hydraulic jack, at the rate of about 0.05mm/min, until the horizontal displacement of model pile reached 10 mm. The gravimetric water content of the soil before curing and after pullout was determined and the loss of water content was noted to be in the range of 0.1% to 0.2%.

4.6 SUMMARY

This chapter presents the properties of CDG soil and steel counterface. It describes the preliminary preparation required before starting the testing program, which includes saturating the HAEPD and inspecting leakages in air pressure chamber. Also, it illustrates the loading path adopted for direct shear testing along with the test procedure, and presents the details of the FBG sensor based model pile for pullout test. Furthermore, the procedure of specimen preparation for soil direct shear test, soil-steel interface tests and pullout test are discussed in detail. The next chapter will present the direct shear test results of soil test and rough interface test sheared at different planes.

Table 4.1 Basic properties of completely decomposed granite (CDG) soil

Soil Property	Unit	Value
Specific gravity (G_s)	-	2.59
Clay	%	12
Silt	%	38
Sand	%	50
Plastic limit (w_p)	%	21
Liquid limit (w_L)	%	31
Plasticity index (I_P)	%	10

Table 4.2 Details of compaction characteristics

Soil Property	Unit	Value
Maximum dry density ($\rho_{d(\max)}$)	Mg/m^3	1.84
Optimum moisture content (w_{opt})	%	13.4

Table 4.3. Fitting parameter for the SWCC of the CDG soil

Preload stress (kPa)	a	n	m	κ	$(u_a-u_w)_r$ (kPa)
0	16	2.5	0.26	2.2	3000

Table 4.4 Properties of the model pile

Model Pile	Pile 1	Pile 2
Type of texture	Smooth	Rough (screwed surface)
Roughness (mm)	0.019	0.95
Type of material	Mild steel	Mild steel
Diameter	20mm	20mm
Total embedded depth to soil (mm)	650	650
Elastic modulus (GPa)	205	205

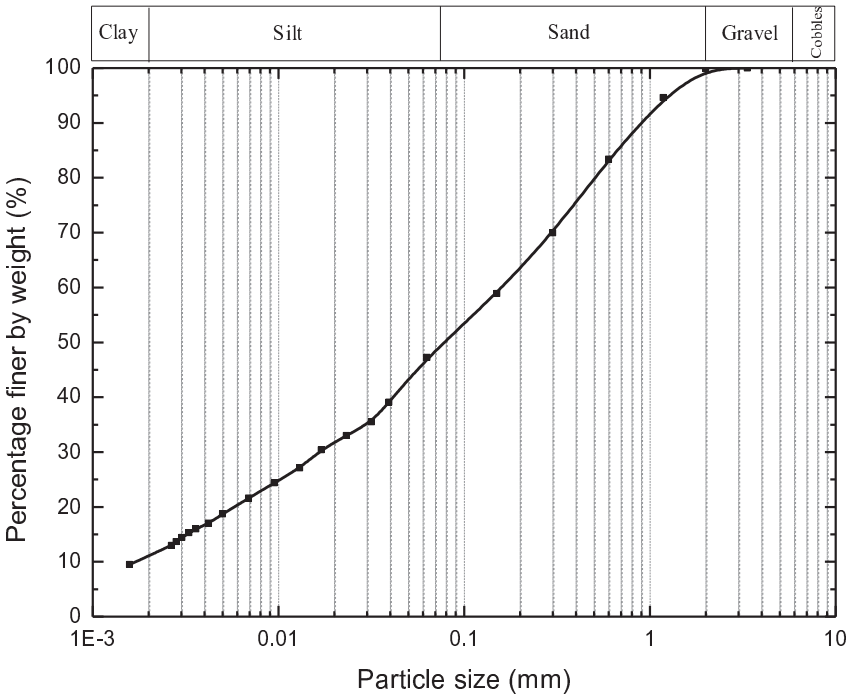

Figure 4.1 Particle size distribution of completely decomposed granite

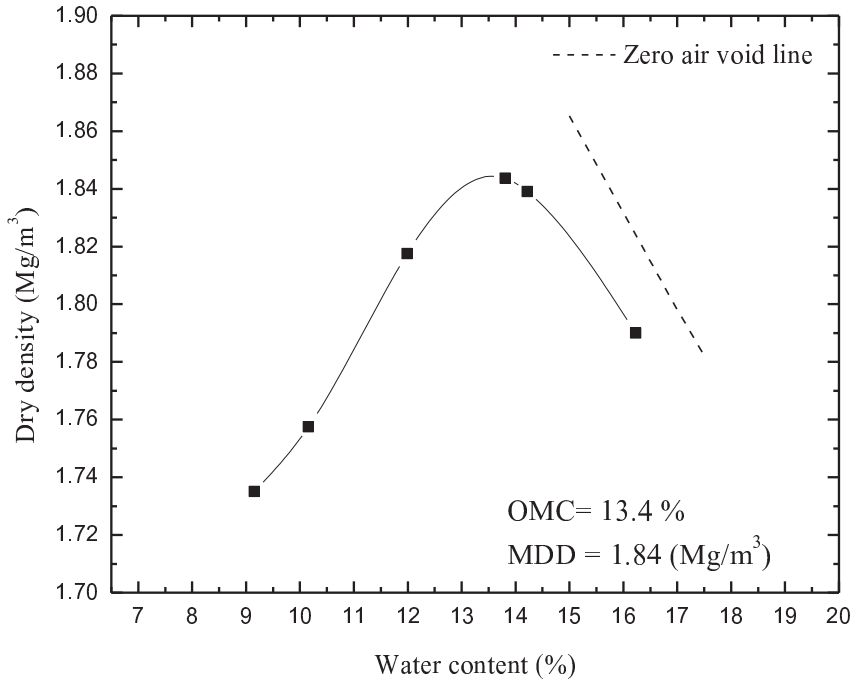

Figure 4.2 Variation of dry density with moisture content for CDG soil

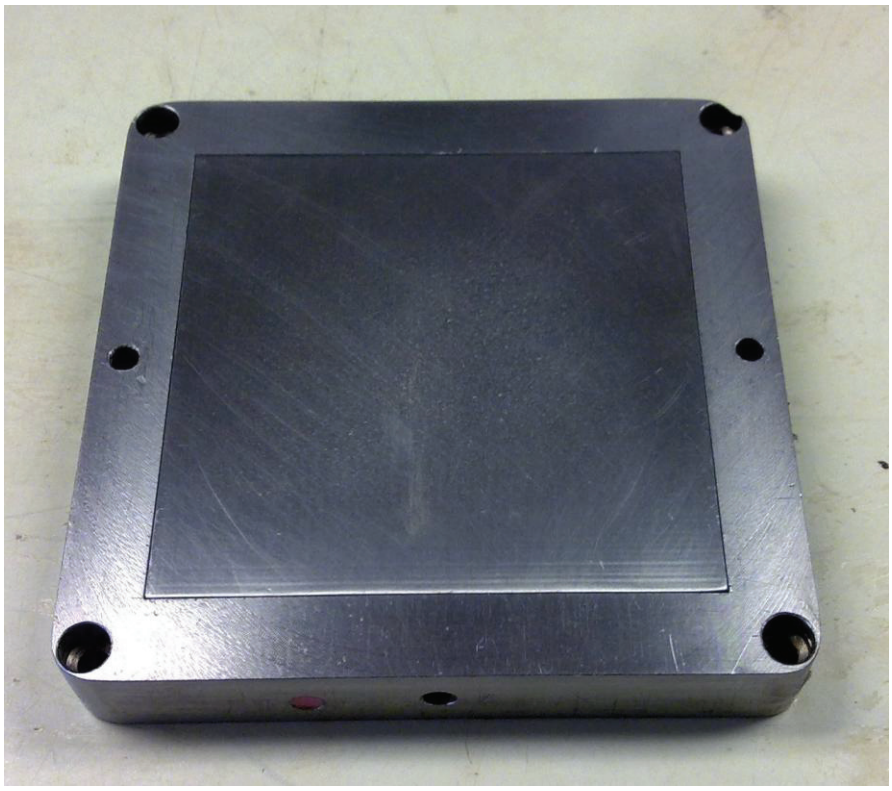

Figure 4.3 Photograph of INT-S counterface for direct shear test

Figure 4.4 Photograph of INT-M counterface for direct shear test

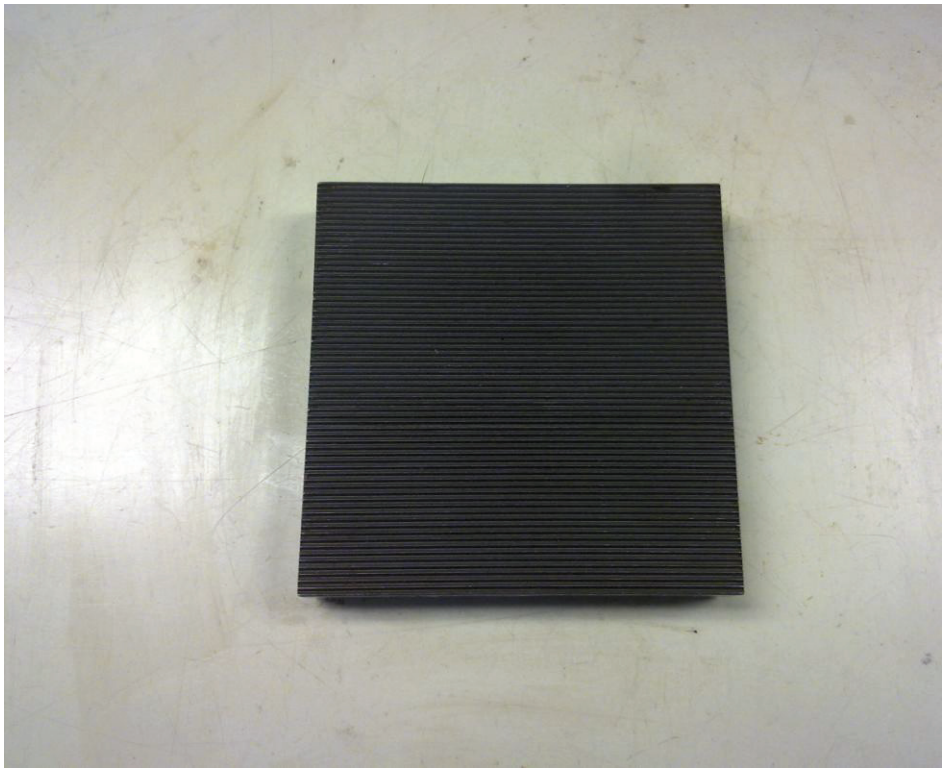

Figure 4.5 Photograph of INT-R counterface for direct shear test

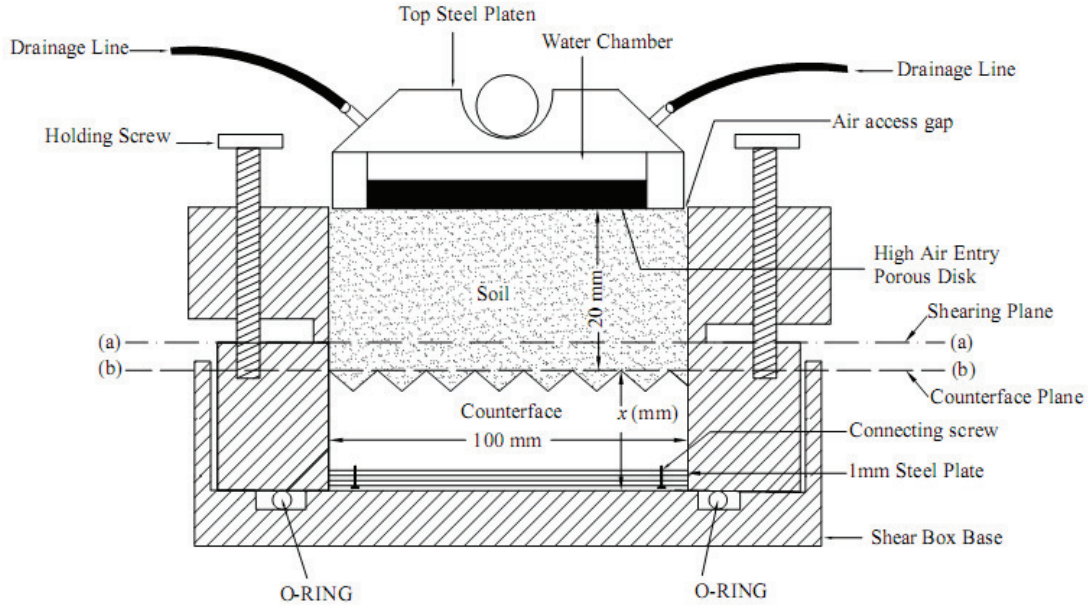

Figure 4.6. Schematic diagram of the modified shear box used for soil- rough steel plate interface testing (not to scale)

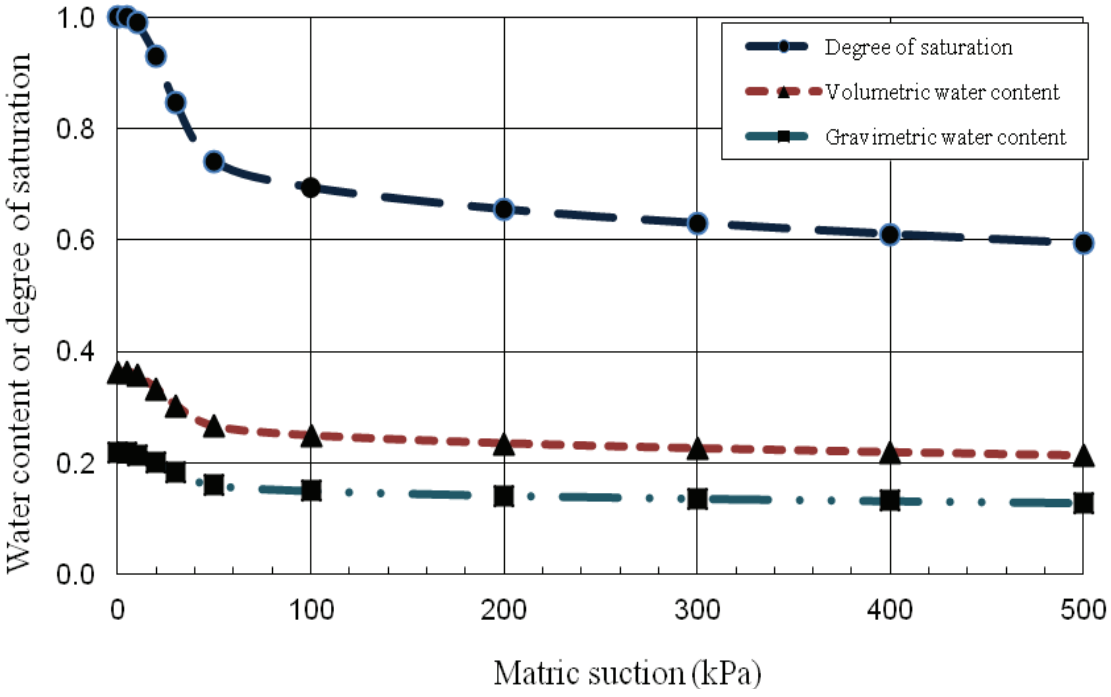

Figure 4.7. SWCC - variation of the normalized water content with the matric suction for soil at zero net normal stress

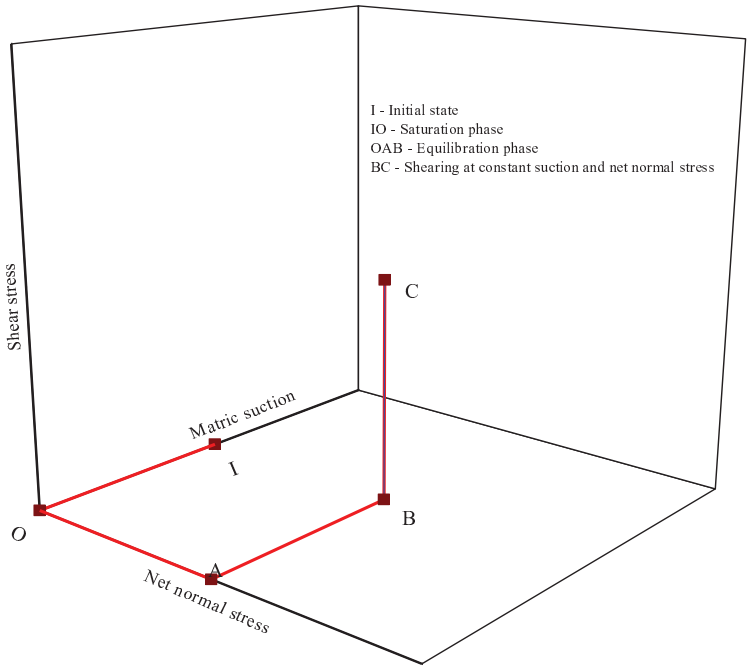

Figure 4.8 The sketch of the loading path employed for the suction controlled direct shear tests

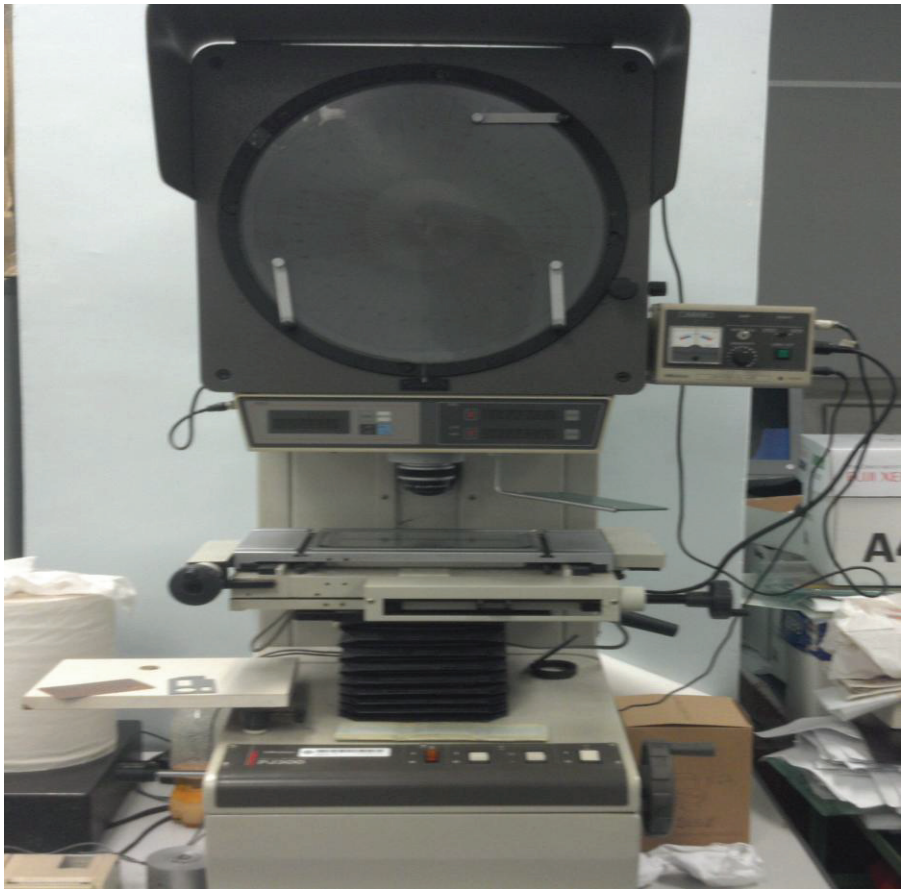

Figure 4.9 Roughness testing machine (supplied by Mitutoya Corporation, Japan)

Chapter 5

INTERFACE SHEARING AT DIFFERENT SHEARING PLANES

5.1 INTRODUCTION

One of the important factors affecting the interface behavior is the way of its formation such as (a) pre-cast interface (i.e., the soil is compacted over the structure/counterface material) and (b) cast in-situ interface (i.e, structure/counterface materials is placed or applied over a treated soil surface). The pre-cast interface is common to many geotechnical projects such as (i) driven piles and (ii) soil nails. To examine the influence of different stress state variables on the behavior of a pre-cast interface created between the CDG soil and rough steel plate, a series of suction controlled direct shear tests were conducted under consolidated drained condition. As described in previous chapters, in this study axis-translation technique was effectively employed to control the matric suction. This chapter focuses on the results of interface direct shear tests sheared at different shearing planes and soil, their interpretations, and discussion. The impact of interface dilation angle on the apparent friction angle and on shear strength was examined, and considered to determine the shear strength of soil-steel interface. To establish the influence of dilation angle on apparent interface friction angle and shear strength, the experimental results are compared with modified interface shear strength model is proposed by Hossain (2010).

A series single-staged consolidated drained direct shear tests were conducted on CDG soil and soil–steel plate interface under different matric suctions of 0, 50 and 200 kPa with a net normal stresses of 50, 150 and 300 kPa, at a temperature of 18^0C. The results and important observations of the shear tests are discussed in the following sections

5.2 EXPERIMENTAL RESULTS AND INTERPRETATIONS

To study the variation of interface shear strength at different shearing plane from the counterface surface, a series of direct shear tests were performed on soil-steel interface specimens, sheared at three different shearing levels of 0 mm (INT-0), 1 mm (INT-1) and 2 mm (INT-2) from the counterface plane under different values of suction and net normal stress. Also, for the sake of assessment, direct shear testing of pure soil specimens was performed under the same stress state condition. The typical results from the pure soil tests and interface tests are presented and discussed in the followings.

5.2.1 LOAD-DISPLACEMENT AND VOLUME CHANGE BEHAVIOR DURING SHEARING

Fig. 5.1- Fig. 5.9 compare the relationship between (a) shear stress and horizontal displacement, (b) volumetric strain (v/H_0, where v is the vertical displacement and H_0 the initial specimen height) during shearing, and (c) change in water content with horizontal displacement for INT-0, INT-, INT-2 and soil at a different net normal stress of 50, 150, and 300 kPa and matric suction of 0, 50, 200 kPa. Several important observations noted from the test results are discussed in the following:

(1) During the shearing of all interfaces at three different shearing planes and the pure soil at zero suction, the curves of shear stress versus horizontal displacement for INT-0, INT1, INT-2 and the soil show a gentle hardening behavior at all the applied net normal stresses. As compared to soil, the interfaces are noted to gain greater shear strength through dilation.

(2) For suction of 50 kPa, the curves of shear stress and horizontal displacement show a slight hardening behavior for lower net not normal stress of 50 kPa. The differences in peak shear stress and the post peak shear stress are modest. For INT-2 and the pure soil, a peak shear stress is achieved and followed by a reduction and increase in the post peak shear stress. In other words, a gradual hardening-softening behavior is observed only for the soil and INT-2 at lower suction and lower net normal stress. However, as the net normal stress increases (150 and 300kPa), fairly identical and gradual hardening behavior is observed for all the three interfaces and the pure soil. This change in shear behavior may be credited to the lower net normal stress, as at a higher net normal stress of 300 kPa, fairly identical and gradual hardening behavior is observed for both INT-0 and the pure soil.

(3) The curves for suction 200 kPa, show that the net normal stress has a significant effect on the post peak shear strength. At a suction of 200kPa and net normal stress of 50kPa, considerable reduction in post peak shear strength is observed for all interfaces, while partial hardening stick-slip behavior is evidenced at higher net normal stress of 150 and 300 kPa. Interestingly, it is observed that regardless of the net normal stress, the soil gains higher peak shear strength value through dilation as compared to interface. This reaffirms that net normal

stress and matric suction significantly influences the shear behavior, however the effect of specific matric suction is noted to be suppressed with an increase in net normal stress.

(4) For lower net normal stress of 50 kPa, the peak shear strength increases with the matric suction for all three interfaces and the soil. The post peak shear strength of INT-0 and INT-1 for matric suction of 50 kPa appears to be little affected by the suction as compared to INT-2 and the soil. It shows that for a lower suction and lower net normal stress, the shear behavior of INT-2 and the soil are fairly identical. Likewise, the shear behavior of INT-0 and INT-1 are also comparable. However, the shear behavior of all the interfaces and the soil is nearly similar at a higher matric suction of 200 kPa.

(5) For net normal stress of 150 and 300 kPa, the curves of shear stress versus horizontal displacement for three interfaces and soil indicate a gradual hardening behavior at zero and 50 kPa matric suctions. However, for a higher matric suction of 200 kPa, a partial hardening stick-slip behavior is evidenced for all the interfaces and is in contrast to the gradual hardening behavior for the soil. The occurrence of stick-slip behavior is directly related to the amount of dilation and net normal stress. In other words, greater net normal stress yields lesser dilation and thereby resulting in a stick-slip behavior for the interface.

(6) It is also noted that, at higher suction and regardless of the net normal stress, the soil has a higher peak shear strength compared to the three interfaces in which INT-0 has the least shear strength. In contrast, for saturated condition or zero suction, it is found that the interfaces have approximately similar peak shear

strength values which are noticeably higher than that of the pure soil. As the suction increases, the shear strength of INT-0 reduces noticeably as compared to INT-1, INT-2 and the soil. This probably shows the shift of a critical shear failure plane towards the counterface surface as the matric suction increases. It is inferred that the critical shearing plane is dependent on the matric suction and gradually moves towards the counterface surface.

(7) Generally, a similar total volume change behavior for the three interfaces and the soil, is evidenced from the curves of v/H_0 versus horizontal displacement. The total volume change is noted to be influenced by both net normal stress and matric suction. Overall, it is observed that a small compression is followed by dilation, until the peak shear stress is attained. The degree of compression is directly proportional to the net normal stress, and the degree of dilation is inversely proportional to the net normal stress. On the contrary, a reverse effect is noticed for an increase in matric suction.

(8) Among all the three interfaces, it is observed that INT-2 has a greater degree of dilatancy in unsaturated condition, while INT-0 has the least. During shearing, the rearrangement of particle grains takes place at the shearing plane resulting in volume change. The difference in the total volume change for the three interfaces is likely due to the dissimilarity in the typical boundary conditions prevailing at the shearing plane of different interface specimens.

(9) During shearing, water drained out of the specimen; the change in water content was in the range on 0.25% to 0.95%. Among the interfaces, the amount of drainage was the greatest for INT-2 and the least for INT-0. Based on the

observations, it is inferred that, due to rearrangement and sliding of soil grains during the shearing, disruption and probably rupture are likely to be caused to the menisci between soil grains and steel plates, This disruption may probably result in increase in the pore water pressure and thereby water drains out from the specimen causing a reduction in water content. This is typical of laboratory shearing along interfaces (Hamid and Miller 2009).

5.2.2 FAILURE ENVELOPES FOR THE INTERFACES AND THE SOIL

Figs. 5.10-5.12 show the variation of the peak shear stress τ_f versus net normal stress $(\sigma_{nf} - u_{af})$, for three interface tests and the pure soil tests, under different matric suction values $(u_a - u_w)_f$ of 0, 50 and 200 kPa, respectively. It is worth mentioning that area correction for direct shear tests is applied to calculate the shear stress. Based on the raw test data, the failure criterion was considered as the point at which the shear load starts decreasing or remain reasonably constant than the peak shear load. The shear strength envelopes of shear stress against net normal stress at a given matric suction for interface and soil are approximately linear. The declivity of the envelopes represents the apparent interface friction angle $\delta_{\max}$ (in saturated condition, $\delta_{\max} = \delta'$). The apparent interface friction angle $\delta_{\max}$ and adhesion intercept c_a increases with matric suction. The variation of the apparent friction angle is probably due to the change in dilation angle with matric suction. This observation is in agreement with previously published observations (Zhan and Ng 2006; Hossain and Yin 2010). The change of adhesion intercept is due to change of suction and δ^b angle. Table 5.1 presents the values of $\phi_{\max} = \phi' + \psi$, $\delta_{\max} = \delta' + \psi$ and adhesion (c_a) or cohesion intercepts c' for different suction values as defined from in Eq. (5.1) and Eq. (5.2):

$$\tau_f = c_a + (\sigma_n - u_a)_f \tan(\delta' + \psi_i) \quad 5.1$$

where, ψ_i is the interface dilation , δ' is the effective interface friction angle with respect to net normal stress and

$$c_a = c'_a + (u_a - u_w)_f \tan \delta^b \quad 5.2$$

where, c'_a is the adhesion at saturated condition; $(u_a - u_w)_f$ is the matric suction at failure; and δ^b is the angle indicating the rate of increase in interface shear strength relative to matric suction $(u_a - u_w)_f$.

Fig. 5.13 – 5.16 show the variation of interface shear strength τ_f with different matric suction $(u_a - u_w)_f$ (suction envelope) for different net stresses $(\sigma_{nf} - u_{af})$ for INT-0, INT-1, INT-2 and soil. Both the interface and soil shear strengths exhibits a nonlinear relationship with suction, indicating that the δ^b parameter in Eq.(5.2) is not constant (Vannapalli *et al.* 1996, Hamid and Miller 2009). Table 5.2-5.5 lists the values of δ^b obtained from Eq.(5.2) for INT-0, INT-1, INT-2 and soil under different matric suctions. The interface dilation angle ψ_i under different net normal stresses and suctions can be calculated from the curves of normalized vertical displacement versus horizontal displacement as shown in Fig. 5.1(b)–5.9(b), by equation Eq. (5.3):

$$\tan \psi_i = -\frac{\delta v}{\delta h} \quad 5.3$$

where δv and δh are the incremental vertical displacement and horizontal displacements (expansion '-' and contraction '+') respectively. The average interface dilation is determined by taking the positive algebraic mean value of the net normal

stress for constant matric suction. Tables 5.6-5.9 summarizes the analytical values of interface dilation angles and apparent for different matric suction obtained from volume change behavior curves The vertical displacement values used for computing the angle of dilation are based on $\pm$ 2mm (maximum particle size) corresponding to the horizontal displacement. It is evident that the average dilation angle increases with matric suction for all the three interfaces and soil.

5.3 COMPARISON OF EXPERIMENTAL RESULTS WITH EXISTING SHEAR STRENGTH MODEL

The shear strength equation for unsaturated soil proposed by Fredlund *et al.* (1978) was modified by Miller and Hamid (2007) to consider for interaction between Minco silt and stainless steel. Following the same theory, Hossain (2010) has further amended the modified model proposed by Miller and Hamid (2007), by including the effect of interface dilation angle on apparent interface friction angle(see Eq. 5.1), for predicting the interface shear strength between CDG soil and cement grout. However, this model has not been used to testify or verify the shear strength between soil-steel interfaces.

In this chapter, the shear strength model proposed by Hossain (2010) has been used to obtain a better correlation between experimental soil-steel interface shear strength data and analytical results. Figure 5.17-5.20 show the comparison between experimental shear strength data for the soil-steel interfaces and analytical results (obtained from Eq. 5.1) using effective interface shear strength parameters (c'_a and δ') of soil-steel interface at saturated condition, and analytical values of interface dilation angle, ψ_i and δ^b angles under different suctions (refer to Tables 5.6-5.9). It is obvious from the

results that interface shear strength predicted from the proposed modified model agrees well with the experimental shear strength data for soil as well as interfaces (INT-0, INT-1 and INT-2) under different net normal stresses and matric suctions. This implies that interface dilation has noteworthy influence on apparent friction angle and the analytical model can very well predict the interface shear strength. However, it would be interesting to testify the suitability of the model for predicting the interface shear strength having different counterface roughness and the same has been discussed in the next chapter.

5.4 SUMMARY

This chapter presents the direct shear test results of soil and soil-steel interfaces sheared at different shearing planes under different matric suction and net normal stress, their interpretations and discussion focusing on the influences of stress state variables on the behavior of critical interface plane. Rough counterface having different interface thickness was tested under different net normal stresses and matric suction. The typical test results obtained from the soil and interface tests have been presented and discussed. To testify and validate an existing analytical model (that considers the influence of suction and interface dilation angle on apparent interface friction angle), the experimental test results have been compared with the analytical model. The next chapter will discuss about the test results and interpretations for influence of counterface roughness on interface behavior under different net normal stress and matric suction.

Table 5.1. Variation of the peak shear strength parameters of the failure envelopes with matric suction

Matric suction (kPa)	INT-0			INT-1			INT-2			Soil		
	$c_a^{'}$ (kPa)	$\delta^{'}+\psi$ (^{o})	r^2	$c_a^{'}$ (kPa)	$\delta^{'}+\psi$ (^{o})	r^2	$c_a^{'}$ (kPa)	$\delta^{'}+\psi$ (^{o})	r^2	$c^{'}$ (kPa)	$\phi^{'}+\psi$ (^{o})	r^2
0	38.8	36.3	.9971	40.9	34.2	.9994	41.6	32.1	.9998	0	35.9	.9734
50	39.1	39.9	.9991	42.3	40.9	.9998	53.2	42.9	.9994	34.8	41.3	.9998
200	51.5	40.2	.9998	62.6	40.1	.9994	70	42.7	.9999	97.1	44.0	.9997

Table 5.2 Variation of δ^b angle with matric suction for INT-0

Matric suction (kPa)	0	50	200
δ^b (deg)	36.3	0.34	3.6

Table 5.3 Variation of δ^b angle with matric suction for INT-1

Matric suction (kPa)	0	50	200
δ^b (deg)	34.2	1.6	6.2

Table 5.4 Variation of δ^b angle with matric suction for INT-2

Matric suction (kPa)	0	50	200
δ^b (deg)	32.1	13.1	8.1

Table 5.5 Variation of δ^b angle with matric suction for Soil

Matric suction (kPa)	0	50	200
δ^b (deg)	35.9	34.8	24.2

Table 5.6 Values of dilation angle and apparent friction angle for different matric suctions obtained from volume change behavior curves for INT-0

Matric suction (kPa)	Net normal stress (kPa)	Interface dilation angle (°)	Average dilation angle ψ_i (°)	Effective adhesion c'_a (kPa)	Effective interface friction angle δ' (°)	Apparent interface friction angle $\delta_{max} = (\delta' + \psi_i)$ (°)
0	50	2.6	0.9	38.8	35.4	36.3
	150	0.1				
	300	0				
50	50	3.6	2.4	38.8	35.4	37.8
	150	1.9				
	300	1.7				
200	50	10.7	7.9	38.8	35.4	43.3
	150	8.3				
	300	4.6				

Table 5.7 Values of dilation angle and apparent friction angle for different matric suctions obtained from volume change behavior curves for INT-1

Matric suction (kPa)	Net normal stress (kPa)	Interface dilation angle (°)	Average dilation angle ψ_i (°)	Effective adhesion c'_a (kPa)	Effective interface friction angle δ' (°)	Apparent interface friction angle $\delta_{max} = (\delta' + \psi_i)$ (°)
0	50	3.0	1	40.9	33.2	34.2
	150	0				
	300	0				
50	50	5.2	3.2	40.9	33.2	36.4
	150	3.5				
	300	0.9				
200	50	11.1	7.9	40.9	33.2	41.1
	150	7.3				
	300	5.5				

Table 5.8 Values of dilation angle and apparent friction angle for different matric suctions obtained from volume change behavior curves for INT-2

Matric suction (kPa)	Net normal stress (kPa)	Interface dilation angle (°)	Average dilation angle ψ_i (°)	Effective adhesion c'_a (kPa)	Effective interface friction angle δ' (°)	Apparent interface friction angle $\delta_{max} = (\delta' + \psi_i)$ (°)
0	50	1.1	0.4	41.6	31.7	32.1
	150	0				
	300	0				
50	50	6.7	4.8	41.6	31.7	36.6
	150	5.0				
	300	3				
200	50	8.3	7.6	41.6	31.7	39.4
	150	7.7				
	300	6.8				

Table 5.9 Values of dilation angle and apparent friction angle for different matric suctions obtained from volume change behavior curves for Soil

Matric suction (kPa)	Net normal stress (kPa)	Interface dilation angle (°)	Average dilation angle ψ_i (°)	Effective adhesion c'_a (kPa)	Effective friction angle δ' (°)	Apparent interface friction angle $\delta_{max} = (\delta' + \psi_i)$ (°)
0	50	0	0.0	0	35.9	35.9
	150	0				
	300	0				
50	50	8.7	5.0	0	35.9	40.9
	150	5.5				
	300	0.8				
200	50	14.1	9.5	0	35.9	45.4
	150	9.8				
	300	4.8				

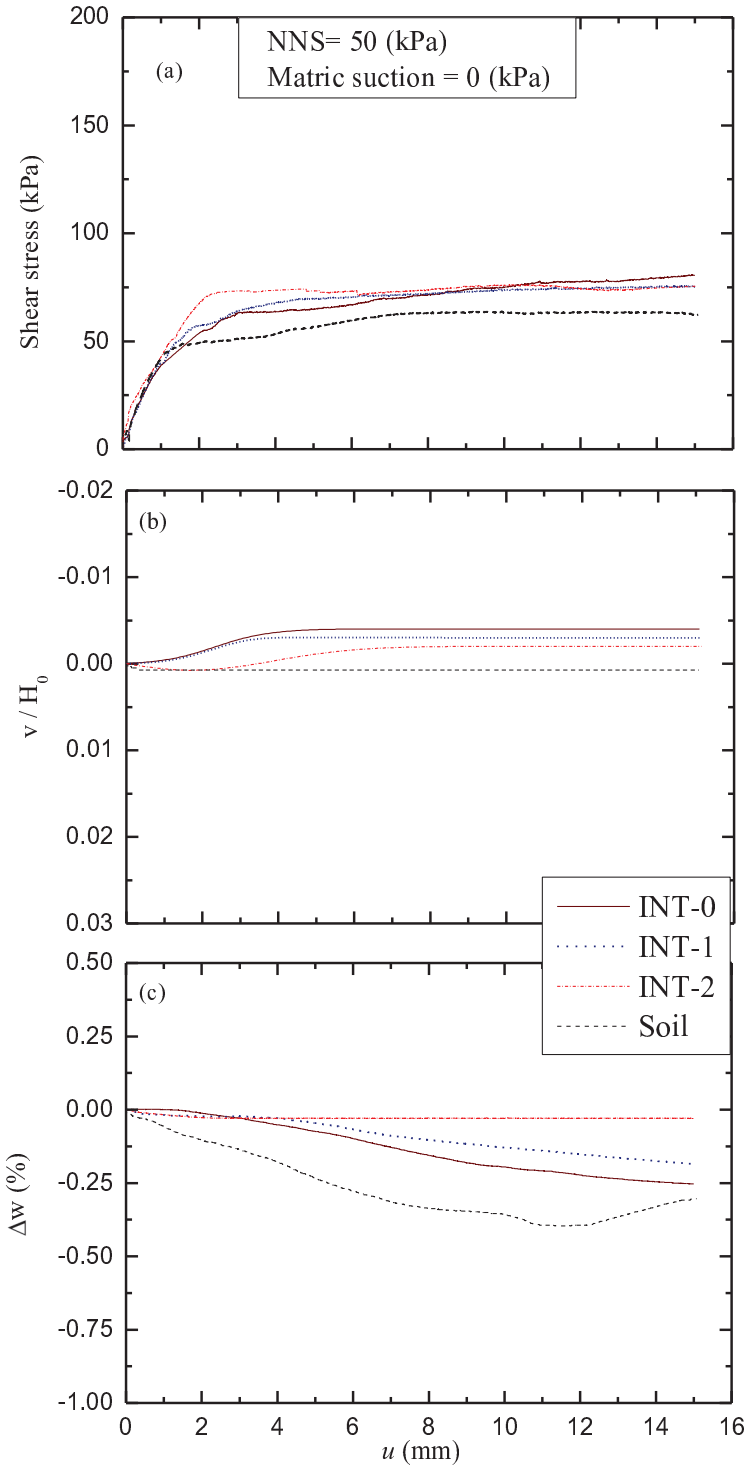

Figure 5.1 Variation of (a) shear stress versus horizontal displacement; (b) normalized vertical displacement versus horizontal displacement (c) migration of water content with horizontal displacement of INT-0, INT-1, INT-2 and Soil under net normal stresses of 50 kPa and matric suction of 0 kPa (saturated condition).

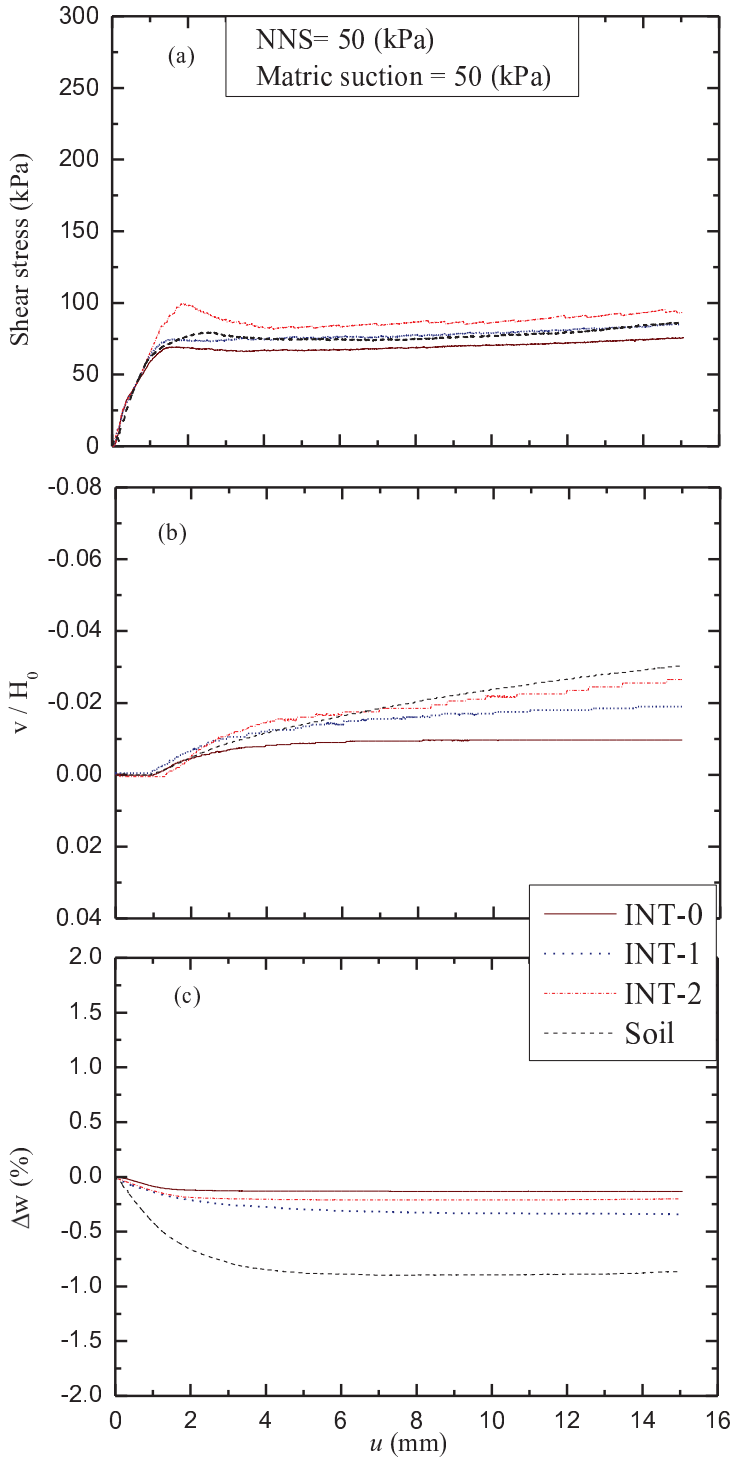

Figure 5.2 Variation of (a) shear stress versus horizontal displacement; (b) normalized vertical displacement versus horizontal displacement (c) migration of water content with horizontal displacement of INT-0, INT-1, INT-2 and Soil under net normal stresses of 50 kPa and matric suction of 50 kPa.

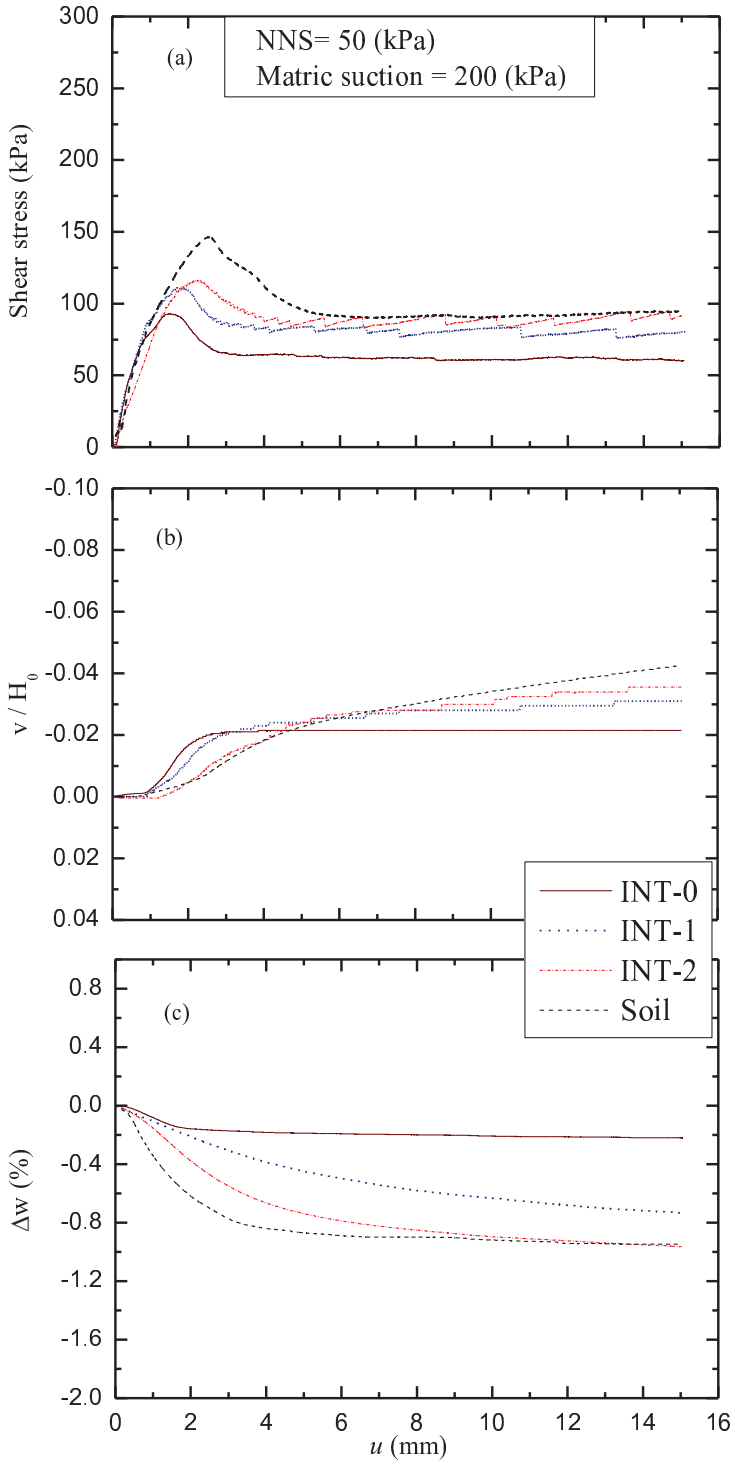

Figure 5.3 Variation of (a) shear stress versus horizontal displacement; (b) normalized vertical displacement versus horizontal displacement (c) migration of water content with horizontal displacement of INT-0, INT-1, INT-2 and Soil under net normal stresses of 50 kPa and matric suction of 200 kPa.

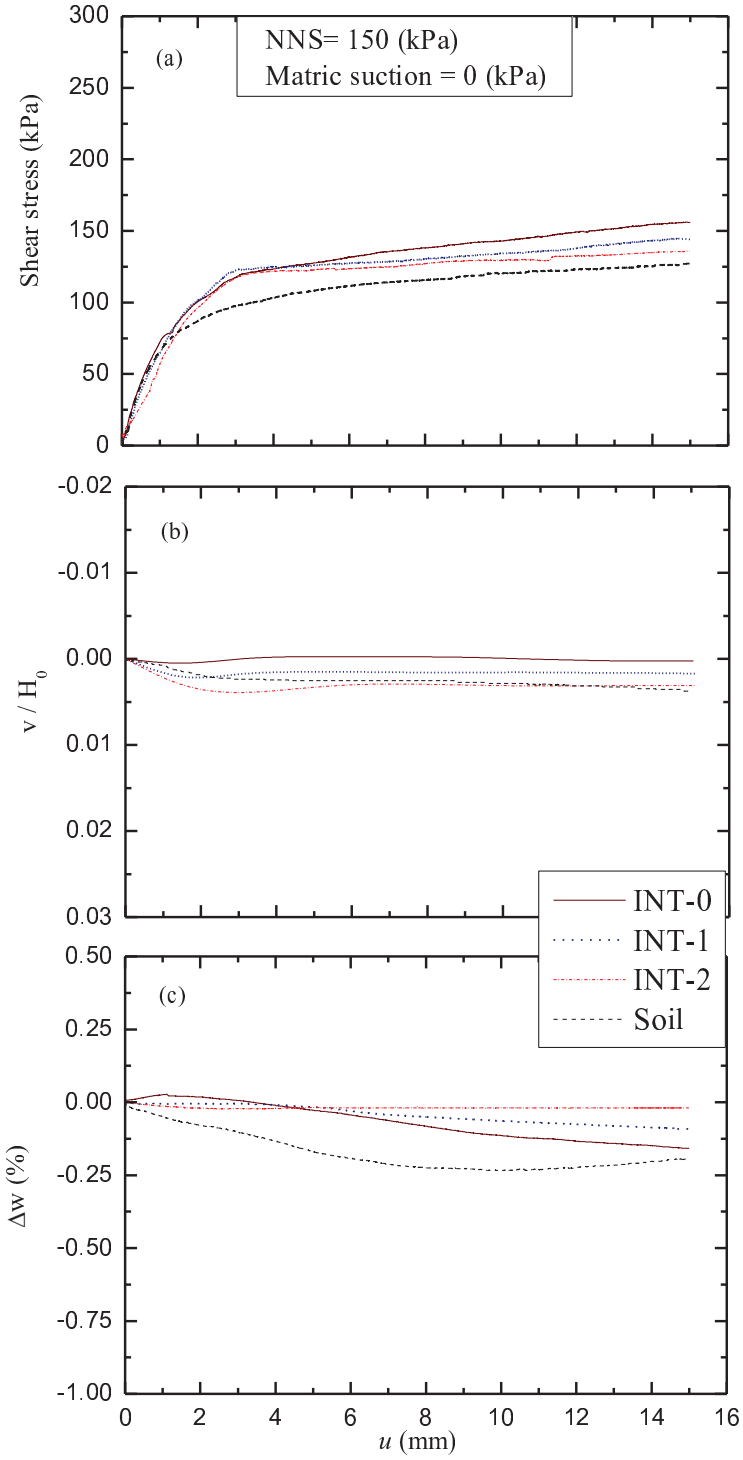

Figure 5.4 Variation of (a) shear stress versus horizontal displacement; (b) normalized vertical displacement versus horizontal displacement (c) migration of water content with horizontal displacement of INT-0, INT-1, INT-2 and Soil under net normal stresses of 150 kPa and matric suction of 0 kPa (saturated condition).

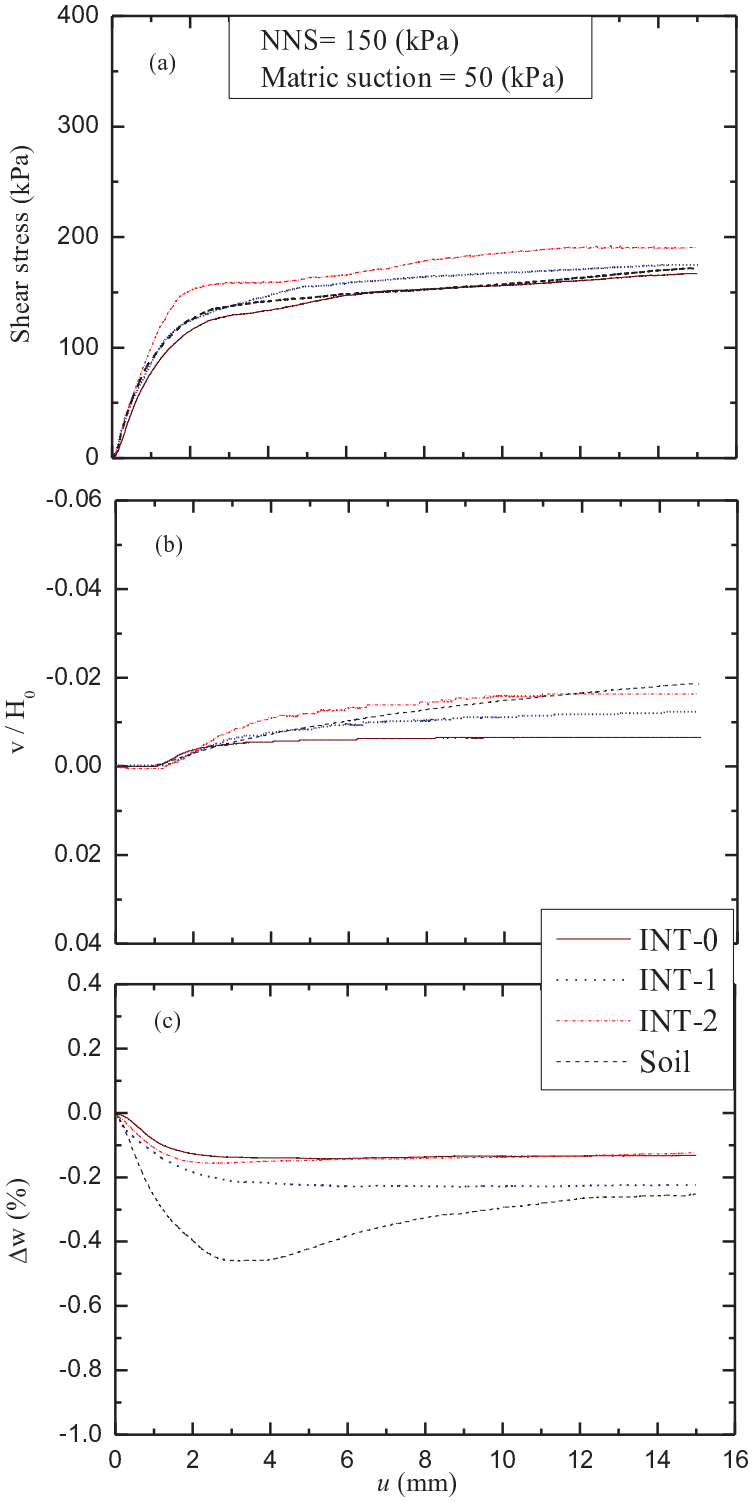

Figure 5.5 Variation of (a) shear stress versus horizontal displacement; (b) normalized vertical displacement versus horizontal displacement (c) migration of water content with horizontal displacement of INT-0, INT-1, INT-2 and Soil under net normal stresses of 150 kPa and matric suction of 50 kPa.

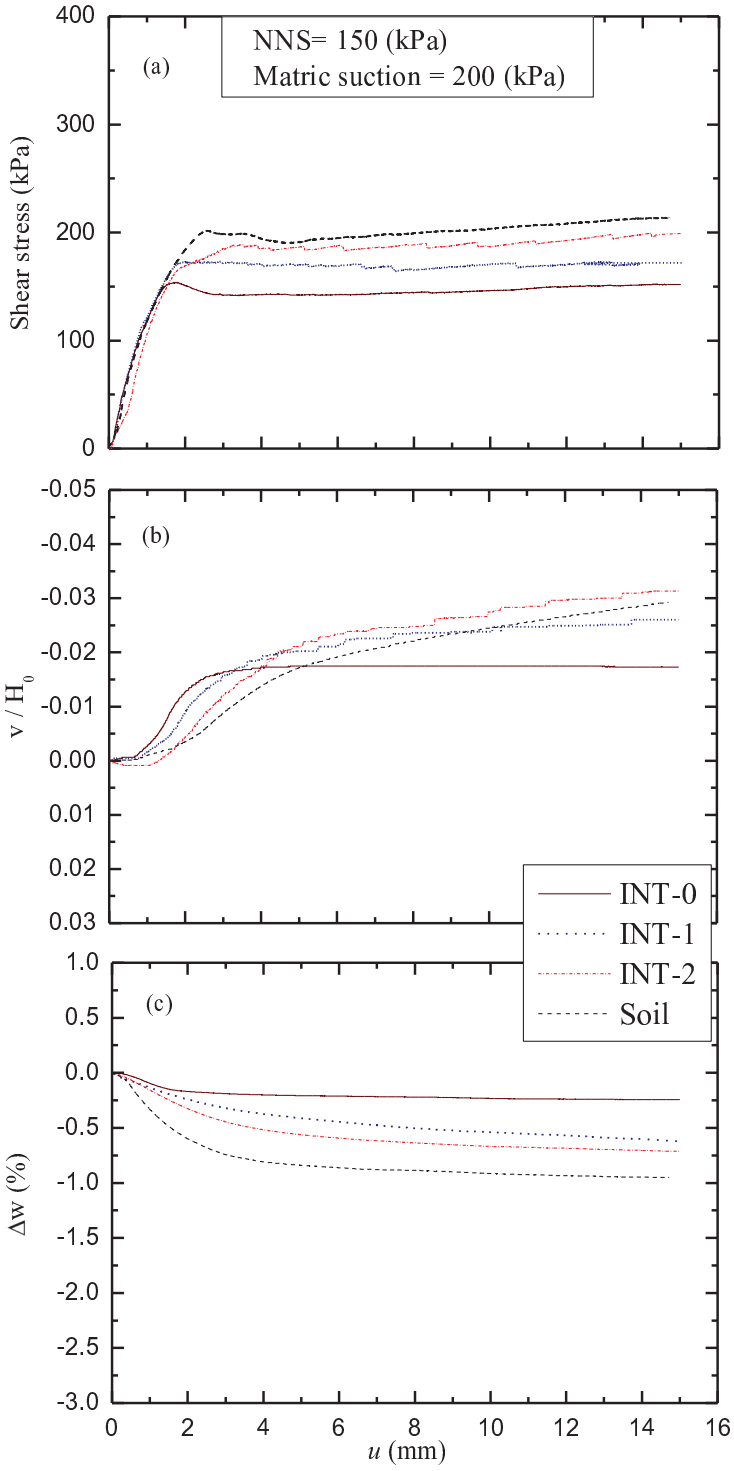

Figure 5.6 Variation of (a) shear stress versus horizontal displacement; (b) normalized vertical displacement versus horizontal displacement (c) migration of water content with horizontal displacement of INT-0, INT-1, INT-2 and Soil under net normal stresses of 150 kPa and matric suction of 200 kPa.

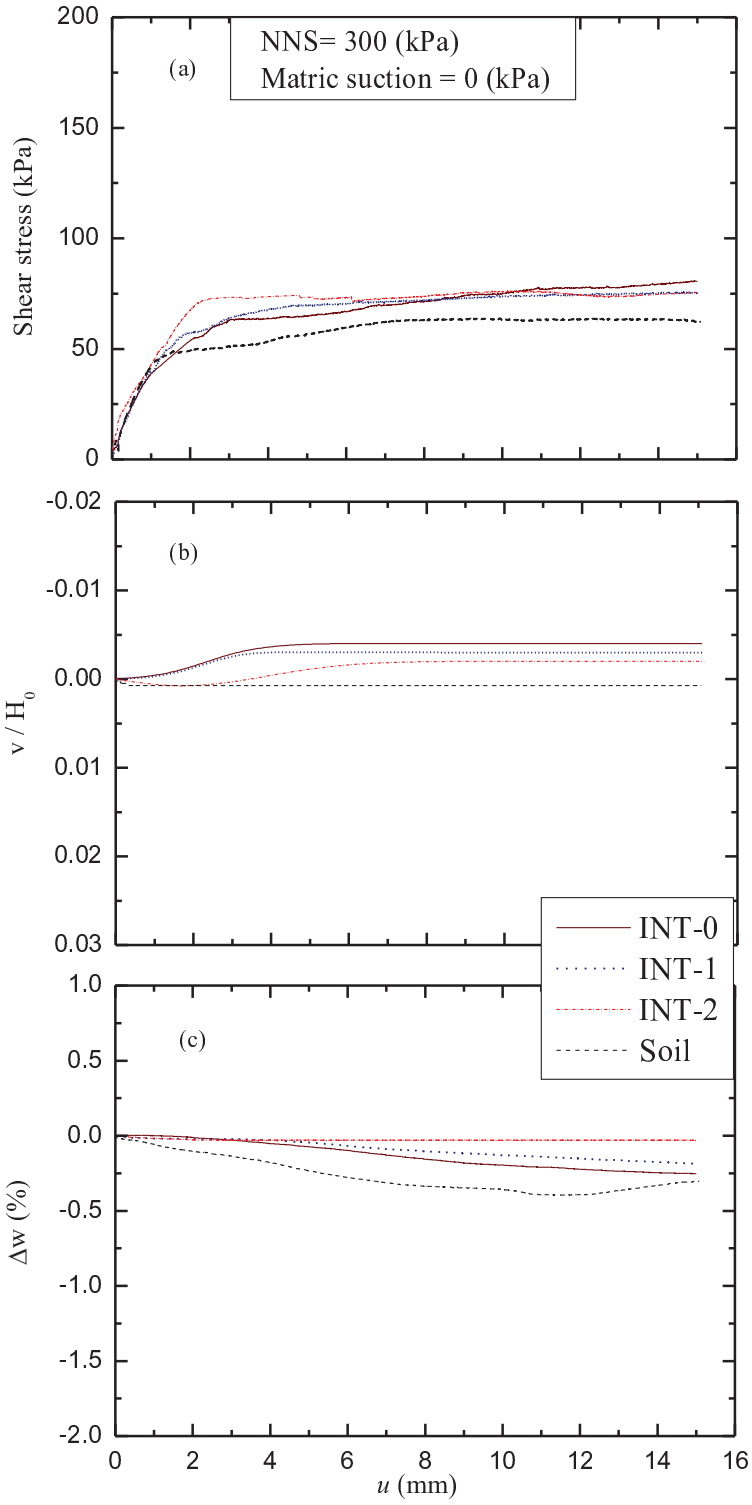

Figure 5.7 Variation of (a) shear stress versus horizontal displacement; (b) normalized vertical displacement versus horizontal displacement (c) migration of water content with horizontal displacement of INT-0, INT-1, INT-2 and Soil under net normal stresses of 300 kPa and matric suction of 0 kPa (saturated condition).

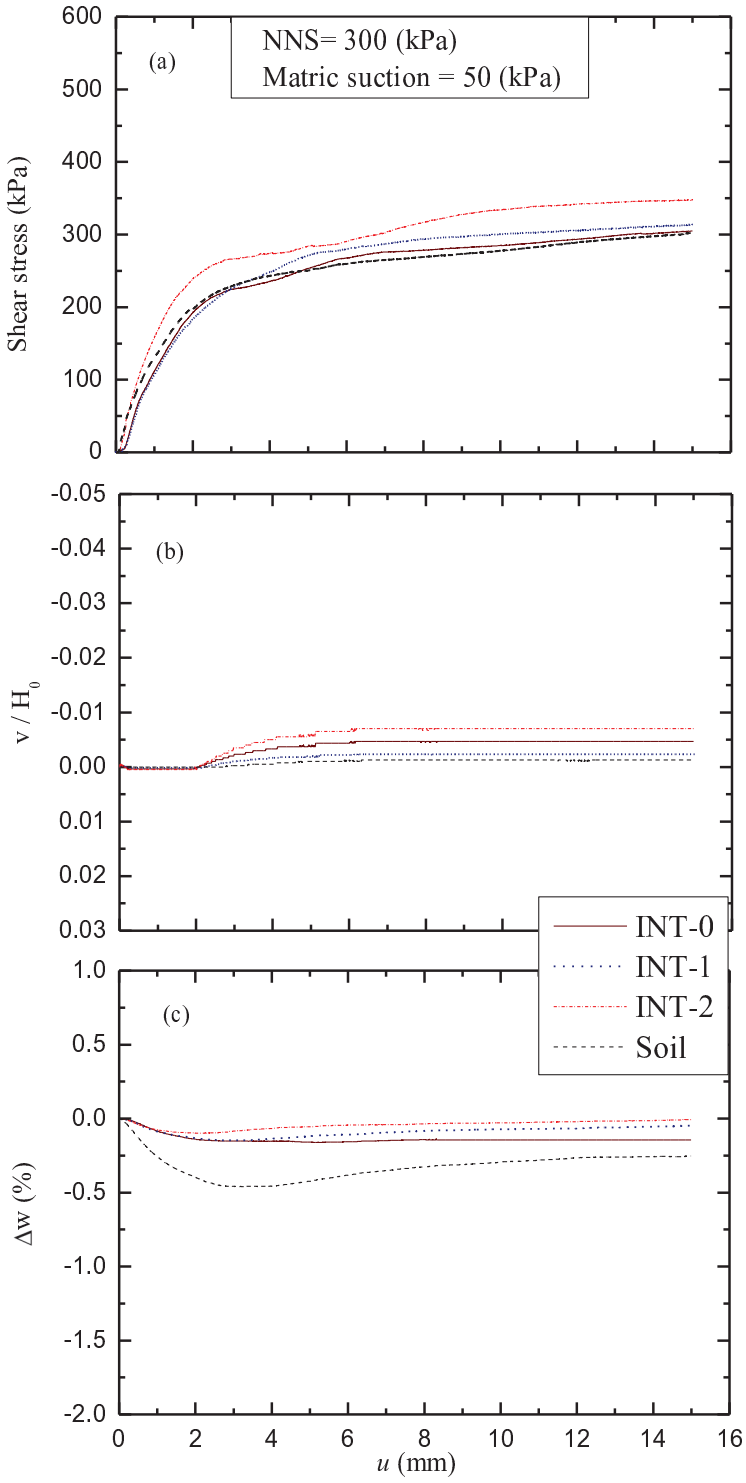

Figure 5.8 Variation of (a) shear stress versus horizontal displacement; (b) normalized vertical displacement versus horizontal displacement (c) migration of water content with horizontal displacement of INT-0, INT-1, INT-2 and Soil under net normal stresses of 300 kPa and matric suction of 50 kPa

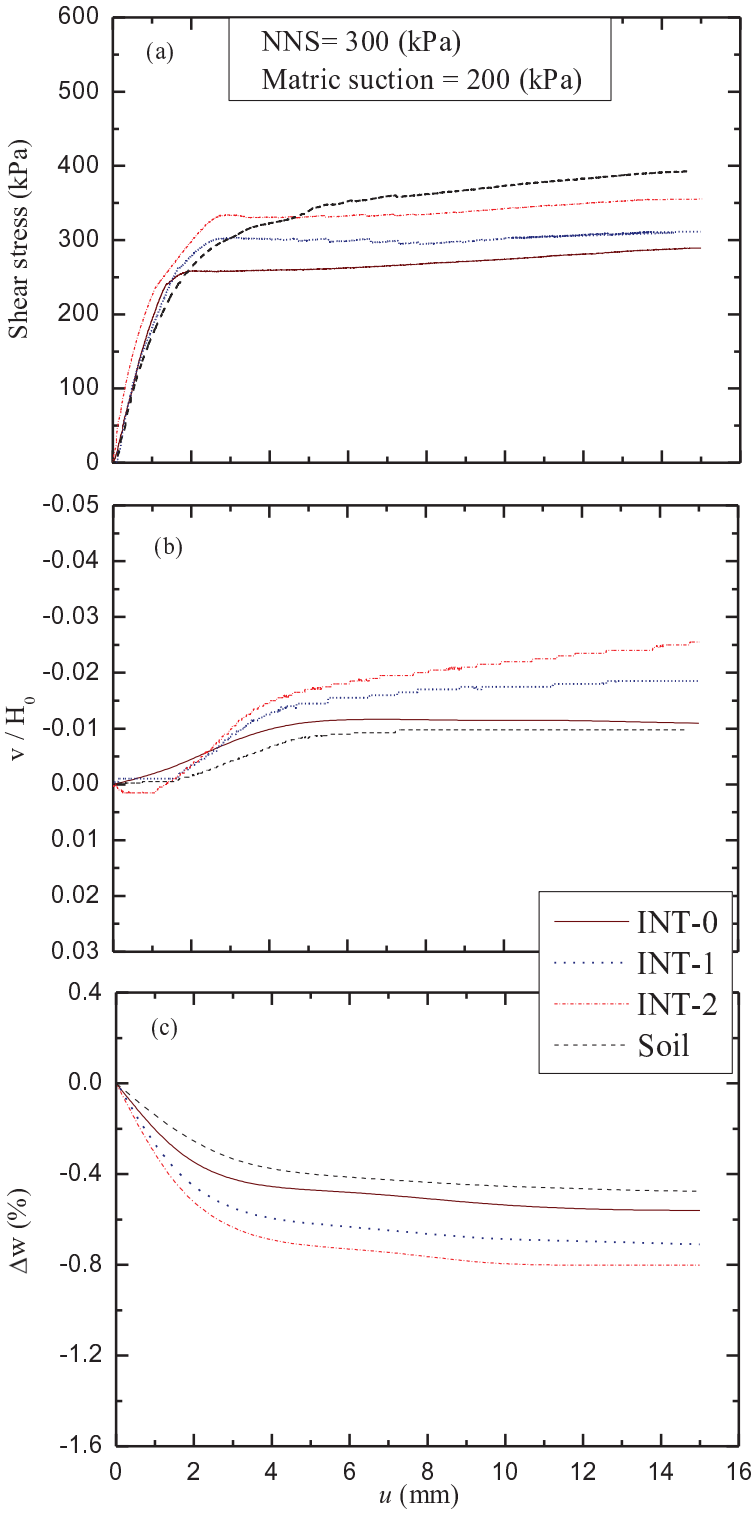

Figure 5.9 Variation of (a) shear stress versus horizontal displacement; (b) normalized vertical displacement versus horizontal displacement (c) migration of water content with horizontal displacement of INT-0, INT-1, INT-2 and Soil under net normal stresses of 300 kPa and matric suction of 200 kPa

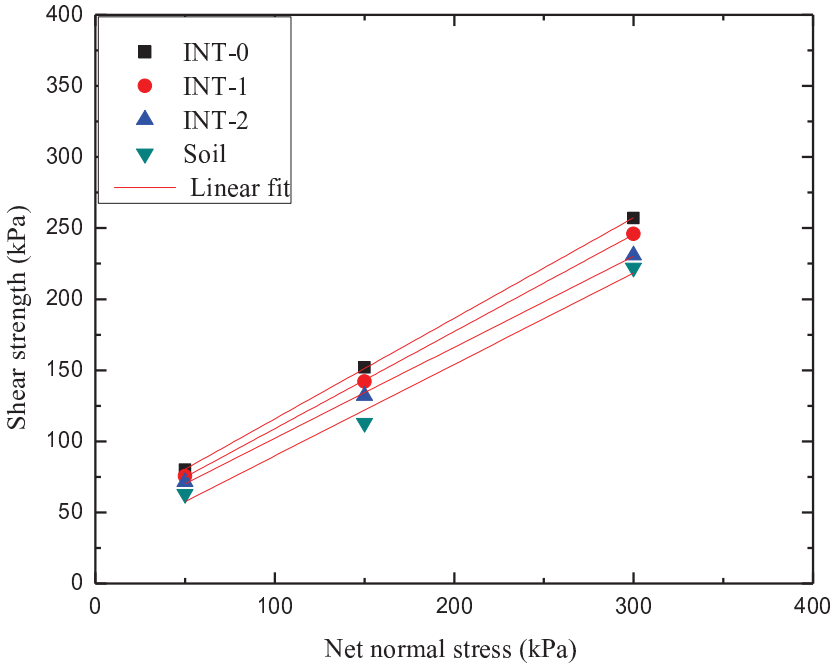

Figure 5.10 Relationships between shear strength and net normal stress from direct shear tests on interface tests and pure soil at 0 kPa matric suction

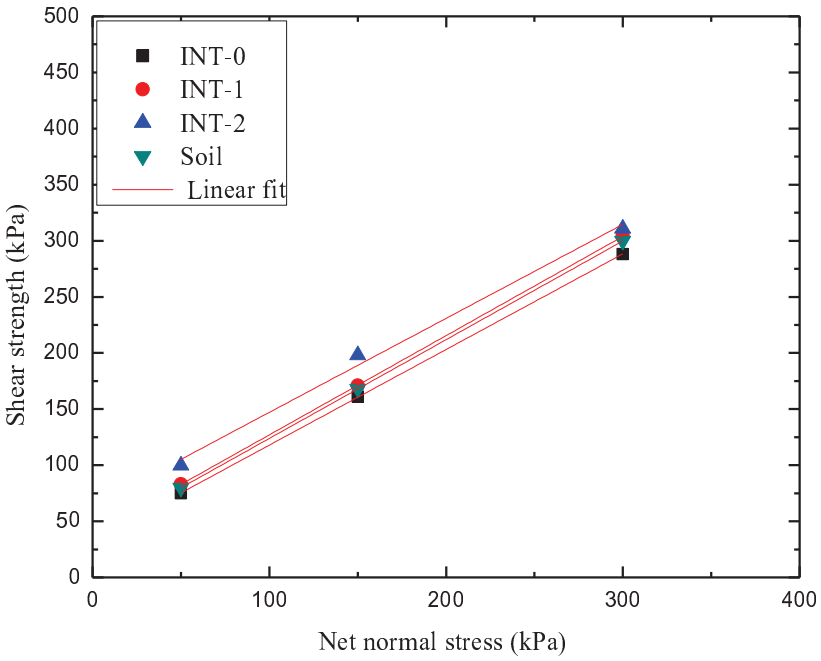

Figure 5.11 Relationships between shear strength and net normal stress from direct shear tests on interface tests and pure soil at 50 kPa matric suction

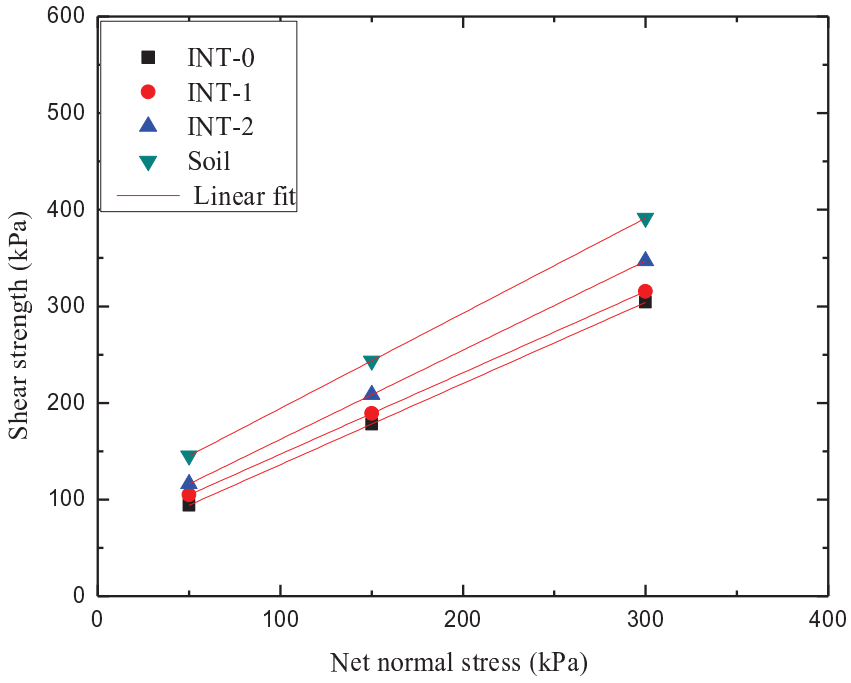

Figure 5.12 Relationships between shear strength and net normal stress from direct shear tests on interface tests and pure soil at 200 kPa matric suction

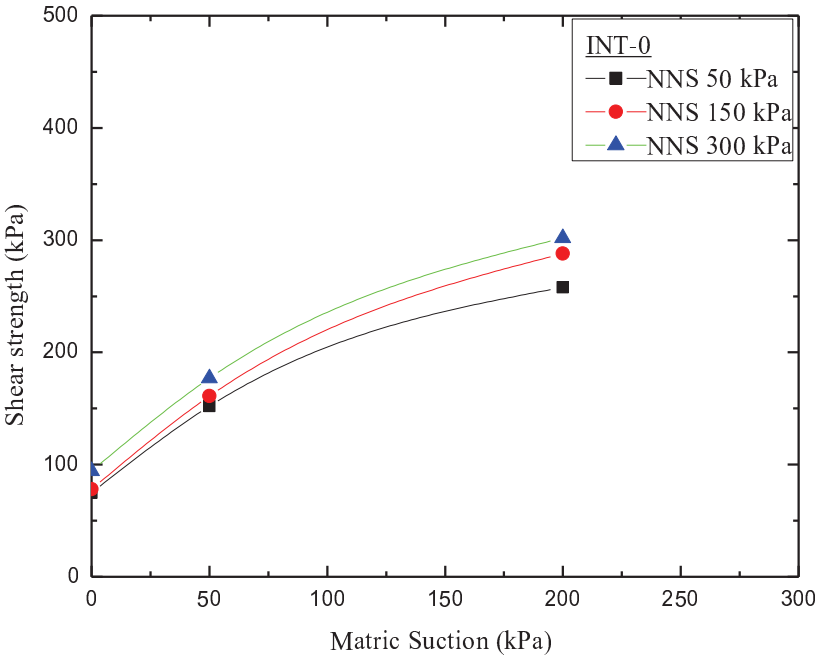

Figure 5.13 Relationship between shear strength and matric suction from direct shear tests on INT-0 for different net normal stresses

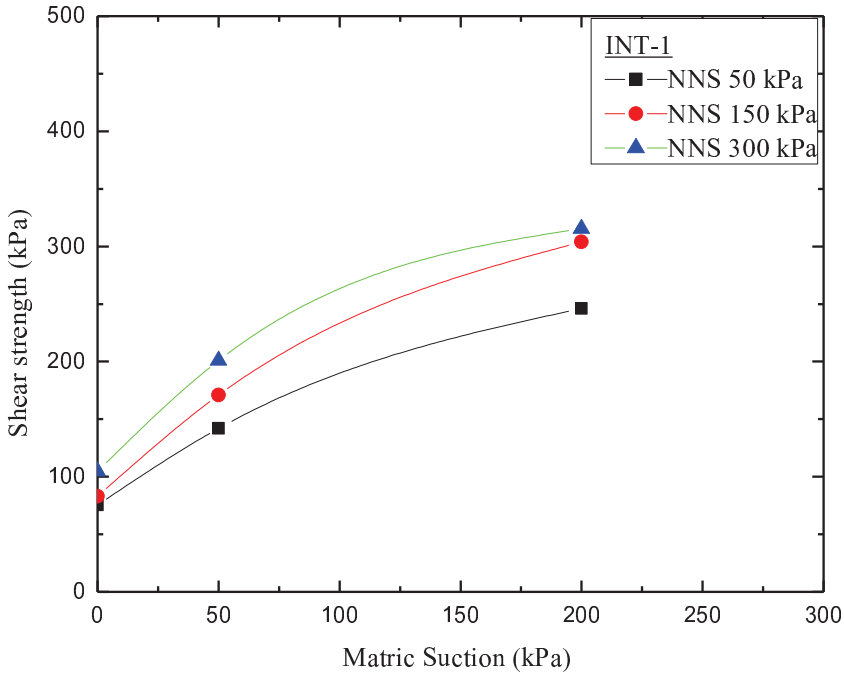

Figure 5.14 Relationship between shear strength and matric suction from direct shear tests on INT-1 for different net normal stresses

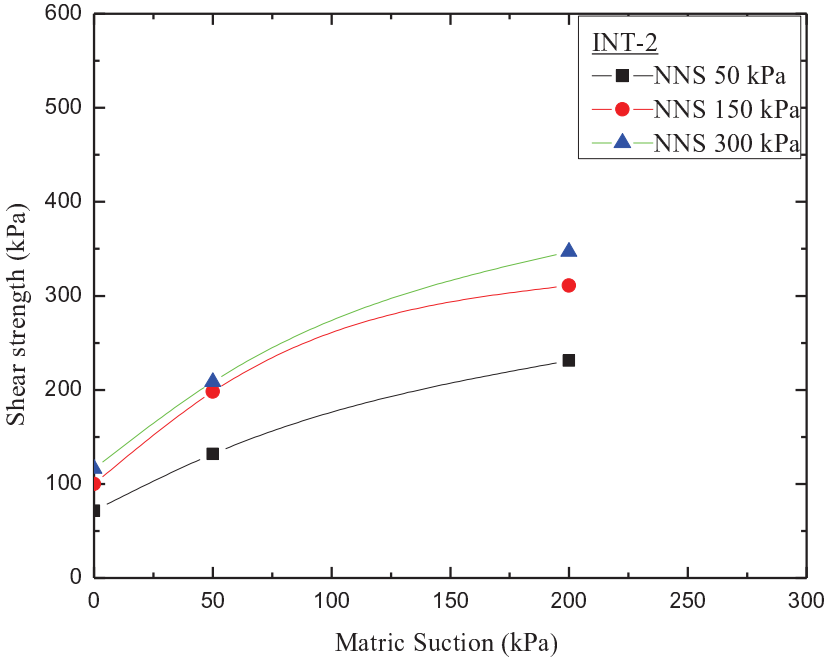

Figure 5.15 Relationship between shear strength and matric suction from direct shear tests on INT-2 for different net normal stresses

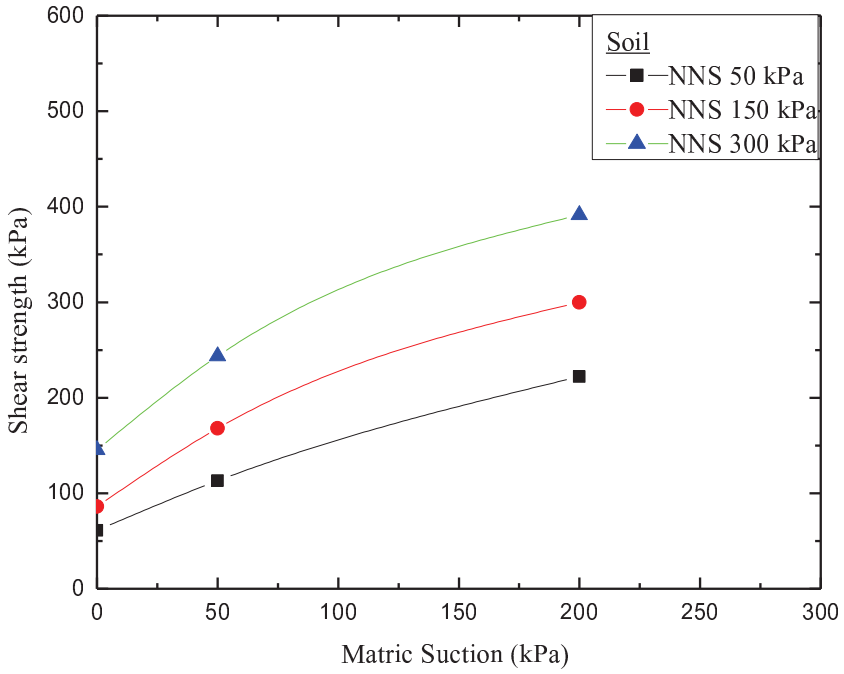

Figure 5.16 Relationship between shear strength and matric suction from direct shear tests on soil for different net normal stresses

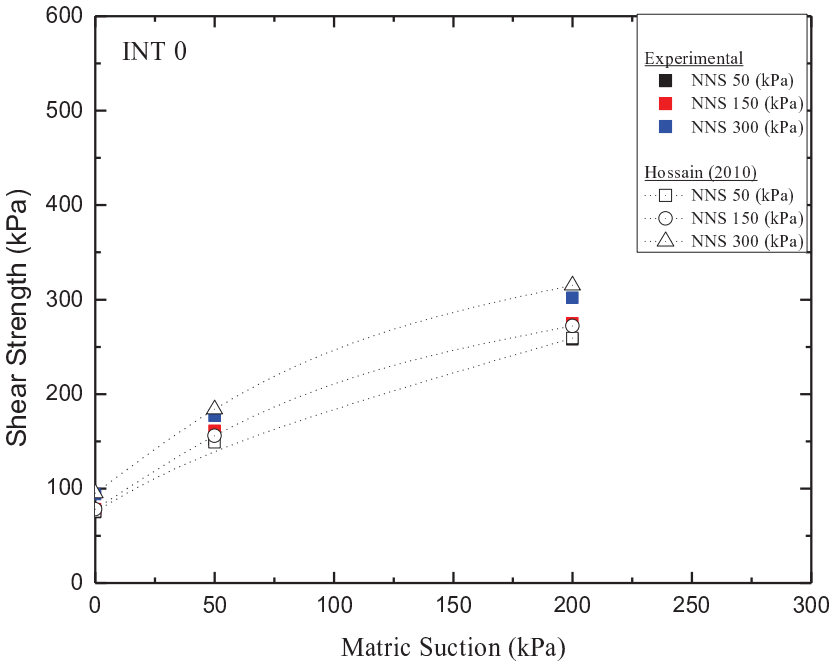

Figure 5.17 Comparison between experimental interface shear strength data for INT-0 and analytical results obtained from the Hossain (2010) model.

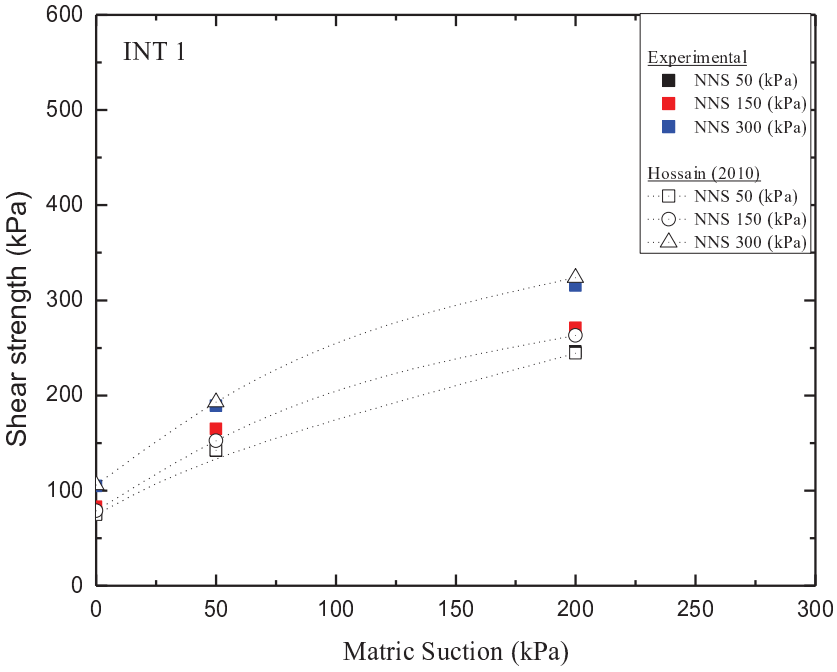

Figure 5.18 Comparison between experimental interface shear strength data for INT-1 and analytical results obtained from the Hossain (2010) model.

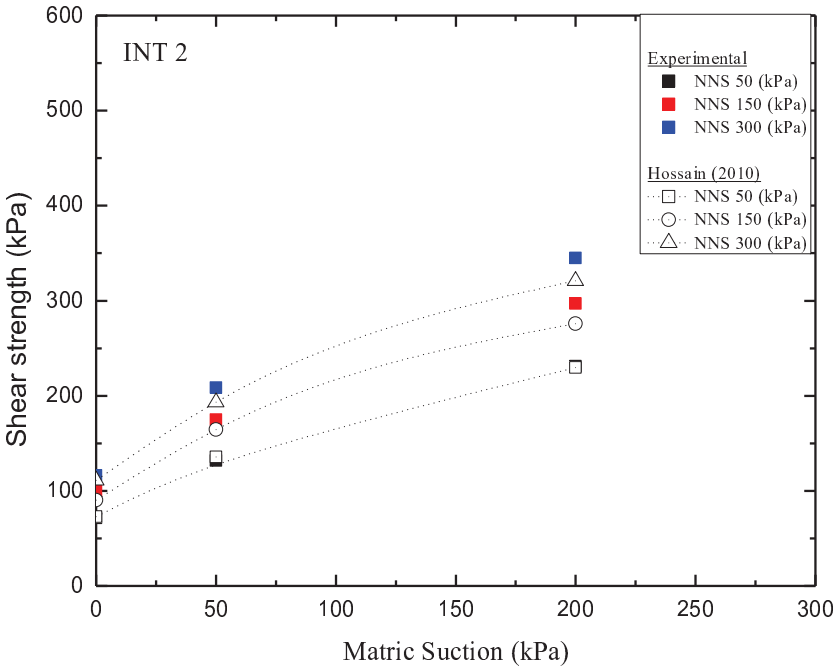

Figure 5.19 Comparison between experimental interface shear strength data for INT-2 and analytical results obtained from the Hossain (2010) model.

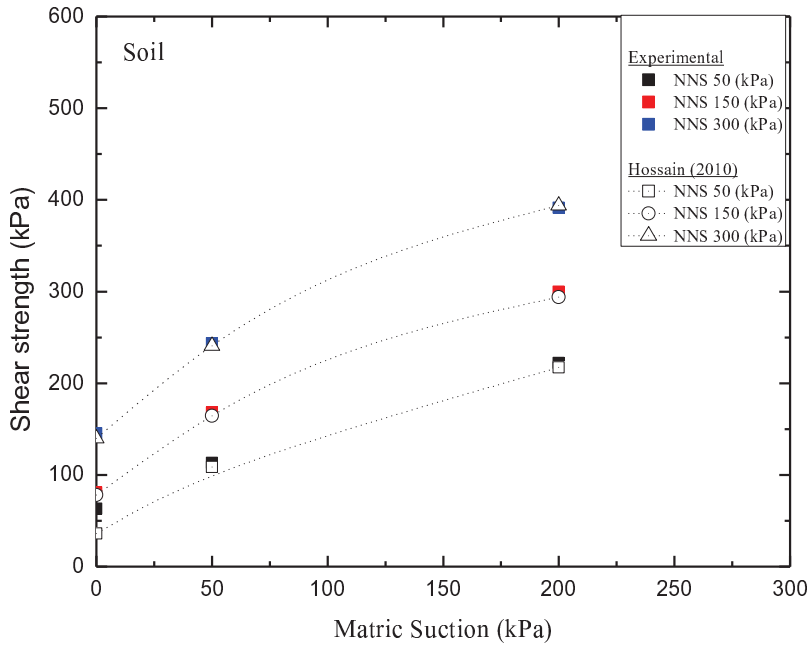

Figure 5.20 Comparison between experimental interface shear strength data for soil and analytical results obtained from the Hossain (2010) model.

Chapter 6

INFLUENCE OF COUNTERFACE ROUGHNESS ON INTERFACE BEHAVIOR

6.1 INTRODUCTION

It is understood from the reviewed literature that the unsaturated interface shear behavior is primarily governed by many factors, including matric suction, net normal stress and the surface roughness of the counterface material. However there have been no attempts to study the interface behavior unsaturated coarse grained soil and construction material. To examine the influence of matric suction and net normal stress on the behavior of a pre-cast interface created between the CDG soil and steel plate of different surface roughness, a series of suction controlled direct shear tests were conducted under consolidated drained condition. As described earlier, to control the matric suction axis-translation technique was effectively employed in this study. This chapter presents results of the direct shear tests on soil and soil-steel interface, their interpretations, and discussion. The impact of interface dilation angle on the apparent friction angle and on shear strength has been examined, and considered to determine the shear strength of soil-steel interface. To establish the influence of dilation angle on apparent interface friction angle and shear strength, the experimental results are compared with interface shear strength model that incorporates the influence of dilatancy induced by matric suction (Hossain 2010). It can be noted that the interface

thickness while shearing the interface specimens was zero mm. However, from the previous chapter it was noted that the critical interface thickness is directly related to the matric suction and shifts towards from the counterface as the matric suction increases. Hence, further study can be conducted to ascertain the impact of counterface roughness on the critical interface thickness.

A series single-staged consolidated drained interface direct shear tests were conducted on CDG soil and soil–steel plate with different counterface roughness under different matric suctions of 0, 50 and 200 kPa with a net normal stresses of 50, 150 and 300 kPa, at a constant laboratory temperature of about 18^0C. The results and important observations of the shear tests are discussed in the following sections

6.2 EXPERIMENTAL RESULTS AND INTERPRETATIONS

To study the influence of counterface roughness on the interface shear, a series of direct shear test were conducted soil and interface specimens shear using three counterface steel plates of different normalized roughness (Rn) under different stress state variables. The interface specimens are designated as INT-R (Rn=10), INT-M (Rn=5), and INT-S (Rn=0.041). The typical results from the interface tests and soil are presented and discussed in the following sections.

6.2.1 LOAD-DISPLACEMENT AND VOLUME CHANGE BEHAVIOR DURING SHEARING

The influence of net normal stress on the interface shear strength can be examined from the curves of shear stress-horizontal displacement at a constant value of matric suction. Figs. 6.1- 6.12 compare the relationship between (a) shear stress and horizontal

displacement, (b) volumetric strain (v/H_0) during shearing, and (c) change in water content with horizontal displacement for INT-R, INT-M, INT-S and soil at a different net normal stress of 50, 150, and 300 kPa and constant matric suction of 0, 50, 200 kPa.

Similarly, the influence of matric suction on the interface shear strength can be examined from the curves of shear stress-horizontal displacement at a constant value of net normal stress. Figs. 6.13- 6.24 compare the relationship between (a) shear stress and horizontal displacement, (b) volumetric strain (v/H_0) during shearing, and (c) change in water content with horizontal displacement for INT-R, INT-M, INT-S and soil at different matric suction of 0, 50, 200 kPa and constant net normal stress of 50, 150, and 300 kPa. Several important observations noted from the test results are discussed in the following:

(1) For zero suction, the curves of shear stress versus horizontal displacement for INT-R, INT-M, INT-S and the soil show a gentle hardening behavior for all the applied net normal stresses. However, at higher net normal stresses the curves for INT-S shows a stick slip hardening behavior. INT-R has higher peak shear strength value among all the three interfaces and INT-S has the least shear strength value. The shear compression is observed to increase with net normal stress for all the curves of interfaces and soil.

(2) For suction of 50 kPa, a slight hardening behavior is observed from the curves of shear stress and horizontal displacement for all the interfaces and soil at lower net normal stress. At a higher net normal stress a well defined hardening behavior is observed for both the rough interfaces and soil. While stick slip behavior is evidenced for the curves of INT-S. Rough interfaces especially

INT-R gains a higher peak shear strength value due to greater extent of soil dilation whereas INT-S gains less due to stick–slip phenomenon.

(3) For suction 200 kPa, the curves of INT-R, INT-M, INT-S and soil show that the net normal stress has a noteworthy influence on the post peak shear strength. At lower net normal stress, notable reduction in post peak shear strength is observed for rough interfaces and soil, whereas stick-slip behavior is observed for smooth interface. Interestingly at higher net normal stress, a hardening stick slip behavior is observed for the rough interfaces. It shows that the shear behavior of rough interfaces at higher net normal stresses is similar to that of smooth interface. Also, soil gains more shear strength as compared to the all the interfaces due to rearrangement of the soil grains at the shearing plane. Shear dilation is observed at lower net normal stresses while shear compression is observed under higher net normal stresses.

(4) For net normal stress 50 kPa, the peak shear strength increases with the matric suction for all three interfaces and the soil. The post peak shear strength of rough interfaces (INT-R and INT-M) is not affected much at lower matric suction, whereas the notable influence is observed for INT-S and the soil at all the applied matric suctions. However, at a higher matric suction of 200 kPa, strain softening behavior is evidenced for rough interfaces (INT-R and INT-M). At lower net normal stresses shear behavior of rough interfaces in nearly similar, this shows that the contribution counterface roughness to the interface shear depends on the lower net normal stresses. Also, shear dilation for rough interfaces and soil increases with suction and contributes to the gain in shear

strength. For the smooth interface almost no dilation is observed due to the stick–slip phenomenon.

(5) For net normal stress of 150, the curves of shear stress versus horizontal displacement for rough interfaces and soil indicate gradual hardening behavior lower suctions and partial hardening softening behavior at higher suction. In contrast hardening stick slip behavior is observed for smooth interface. The effect of suction on rough interfaces is noted to be more profound at lower and intermediate net normal stresses. With an increase in net normal stresses, the change in the difference of the shear strength value for INT-R and INT-M increases as compared to lower net normal stress. Shear dilation is directly proportional to the matric suction and inversely to the net normal stress.

(6) For net normal stress of 300, gentle hardening behavior is observed from the curves of shear stress versus horizontal displacement for all the interfaces and soil at lower suctions and partial hardening stick slip behavior at higher suction. It is noted that at higher suction partial hardening stick slip behavior is evidenced for all the interfaces, but gradual hardening of the soil is observed. One of the reasons for this difference in shear behavior could be attributed to the differences in the boundary conditions at the failure planes for interfaces and soil. The presence of counterface in interface test results in the sliding of the soil grain particles at higher net normal stresses and suction, whereas for soil tests, the soil to soil interaction leads to rearrangement of the grain particles, which results in greater shear strength.

(7) The increment in the shear interface shear strength based on the normalized counterface roughness is found vary nonlinearly with change in stress state variables. In other words, for a specific constant net normal stress and matric suction, the increment in the value of interface shear stress with respect to the counterface roughness is nonlinear.

(8) The total volume change behavior for the three interfaces is noted to be significantly influenced by the counterface roughness. Generally, shear dilation mainly occurs in the interfaces having a rough counterface, whereas, stick slip behavior is predominant for interfaces having smooth counterface. The volume change behavior varies none linearly with the change in counterface roughness. In other words, for a specific constant net normal stress and matric suction, the increment in the value of shear dilation (or shear compression) with respect to the counterface roughness is nonlinear. The overall degree of dilation (or compression) is directly influenced by the stress state variables.

(9) Water drained out from the specimen during shearing phase, for rough (INT- R and INT-M) and smooth interfaces, was in the range of 0.12-0.46% and 0.02-0.19%. It is obvious that the amount of drainage is greater for rough interfaces and soil as compared to the smooth interfaces due to greater dilation and rearrangement of particles on the counterface planes. The rearrangement of the particles caused by rolling over of the soil particles on the counterface probably causes a failure in the air-water menisci and thereby draining out more amount of water from the specimen. However, stick slip phenomenon was evidenced while shearing INT-S causes sliding of soil particles and the possibility of rearrangement of the soil particles is little.

6.2.2 FAILURE ENVELOPES FOR THE INTERFACES AND THE SOIL

The relationship between the peak shear stress τ_f versus net normal stress $(\sigma_{nf} - u_{af})$ corresponding to under different matric suction values $(u_a - u_w)_f$, for three interface tests and the pure soil tests, are shown in Figs. 6.25- 6.27. As described in previous chapter, the shear stress is calculated by considering the area correction for direct shear tests. Based on the raw test data, the failure criterion was considered as the point at which the shear load starts decreasing or remains reasonably constant than the peak shear load. The shear strength envelopes of shear stress against net normal stress, at a given matric suction for the three interface and soil are approximately linear. The declivity of the envelopes represents the apparent interface friction angle $\delta_{\max}$ (in saturated condition, $\delta_{\max} = \delta'$). The apparent interface friction angle $\delta_{\max}$ and adhesion intercept c_a increases with matric suction. The variation of the apparent friction angle is probably due to the change in dilation angle with matric suction. This observation is in agreement with previously published observations (Hossain and Yin 2010a). The change of adhesion intercept is due to change of suction and δ^b angle. The values of $\phi_{\max} = \phi' + \psi$, $\delta_{\max} = \delta' + \psi$ and adhesion (c_a) or cohesion intercepts c', as defined by Eq. (5.1) and Eq.(5.2), for different suction values of interfaces and pure soil are presented in Table 6.1.

Figs. 6.28 – 6.30 show the variation of interface shear strength τ_f with different matric suction $(u_a - u_w)_f$ (suction envelope) for different net stresses $(\sigma_{nf} - u_{af})$ for INT-R, INT-M and INT-S. The δ^b parameter for the interface shear test, irrespective of the counterface roughness exhibits a nonlinear relationship with suction (Vannapalli

et al. 1996; Hamid and Miller 2009). The values of δ^b for INT-R, INT-M, INT-S obtained from Eq. [5.2] under different matric suctions are presented in Table 6.2-6.4. The analytical values of interface dilation angles and apparent for different matric suction obtained from volume change behavior curves are summarized in Table 6.5-6.7. The relationship between the normalized counterface roughness versus matric suction values $(u_a - u_w)_f$ versus interface dilation angle (ψ) for three interface test is shown in Fig. 6.31, whereas Fig- 6.32- 6.34 shows the variation of interface shear strength with respect to matric suction and normalized counterface roughness at different net normal stresses. As observed in previous chapter, it is reaffirmed that the average dilation angle increases with matric suction for all the three interfaces irrespective of the counterface roughness. It is noted that, for a specific suction, the interface dilation angle increases non-linearly for the normalized surface values used in this study. Nonetheless, it would be interesting to study the variation interface dilation angle and shear strength with respect to suction for a normalized counterface roughness value above 10. Also, it is evident from the results that, at a specific matric suction and net normal stress, the interface shear strength increases non-linearly with normalized counterface roughness. It is obvious from Table 6.8 that the δ_{max} under different suction for interface test are varies when compared to the apparent friction angle for soil ϕ_{max} under the same suctions (ratio of δ_{max}/ϕ_{max} varies from 0.33 to 1.02). At saturated condition, the ratio of δ_{max}/ϕ_{max} for the rough interfaces (INTR and INT-M) is greater as compared to unsaturated state and vice versa for the smooth interface. This implies that unlike smooth interfaces, the rough interface behaves in a manner similar to that of soil at lower suctions and gradually looses strength as suction increases.

6.3 COMPARISON OF EXPERIMENTAL RESULTS WITH EXISTING SHEAR STRENGTH MODEL

Hossain (2010) have proposed modified model for predicting the interface shear strength between CDG soils and cement grout by considering the effect of interface dilation angle on apparent interface friction angle. As described earlier, this model has not been tested or verified, to consider the shear strength between soil-steel interfaces especially with different counterface roughness.

Figs. 6.35- 6.37 shows the comparison between experimental shear strength data for the soil-steel interfaces and analytical results obtained from Eq [5.1] using effective interface shear strength parameters (c'_a and δ') of soil-steel interface at saturated condition, and analytical values of interface dilation angle, ψ_i and δ^b angles under different suctions (refer to Tables 6.5-6.7). From the results it is evident that the interface shear strength predicted from Hossain's (2010) modified model agrees well with the experimental shear strength data for rough interfaces (INT-R and INT-M) under different net normal stresses and matric suctions. However, the analytical model agrees partially for smooth interface. In other words, the model agrees well only under lower net normal stress. This indicates that interface dilation especially in rough interfaces has significant influence on apparent friction angle, and thereby on interface shear strength. Therefore it is important to consider the interface dilation while designing and assessing safety of different soil-structure interactions.

6.4 SUMMARY

A series of suction controlled single stage consolidated drained direct shear test are performed on compacted soil and soil-steel interfaces with different counterface roughness to investigate the influences of both matric suction and net normal stress on the behavior of soil-steel interface. Three counterfaces having different normalized surface roughness were tested under net normal stresses of 50, 150 and 300 kPa and matric suction of 0, 50 and 200 kPa. The typical test results obtained from the study have been presented and discussed. The experimental results have been compared with an existing model that considers the influence of interface dilation angle on apparent interface friction angle. The prediction of the model is found to match well with the experimental results of rough interface. The next chapter will discuss about the pull out test results and their interpretations under different degree of saturation and counterface roughness.

Table 6.1 Variation of the peak shear strength parameters of the failure envelopes with matric suction

Matric suction (kPa)	INT-R			INT-M			INT-S			Soil		
	c_a' (kPa)	$\delta'+\psi$ (^{o})	r^2	c_a' (kPa)	$\delta'+\psi$ (^{o})	r^2	c_a' (kPa)	$\delta'+\psi$ (^{o})	r^2	c' (kPa)	$\phi'+\psi$ (^{o})	r^2
0	38.8	36.3	.9971	33.0	31.8	.9997	1.9	11.9	.9974	0	35.9	.9734
50	39.1	39.9	.9991	41.0	32.6	.9991	2.1	14.8	.9978	34.8	41.3	.9998
200	51.5	40.2	.9998	64.0	33.6	.9989	2.6	15.9	.9982	97.1	44.0	.9997

Table 6.2 Variation of δ^b angle with matric suction for INT-R

Matric suction (kPa)	0	50	200
δ^b (deg)	36.3	0.3	3.6

Table 6.3 Variation of δ^b angle with matric suction for INT-M

Matric suction (kPa)	0	50	200
δ^b (deg)	31.8	9.1	8.8

Table 6.4 Variation of δ^b angle with matric suction for INT-S

Matric suction (kPa)	0	50	200
δ^b (deg)	11.9	0.2	0.2

Table 6.5 Values of dilation angle and apparent friction angle for different matric suctions obtained from volume change behavior curves for INT-R

Matric suction (kPa)	Net normal stress (kPa)	Interface dilation angle (°)	Average dilation angle ψ_i (°)	Effective adhesion c'_a (kPa)	Effective interface friction angle δ' (°)	Apparent interface friction angle $\delta_{max} = (\delta' + \psi_i)$ (°)
0	50	2.7	0.9	38.8	35.4	36.3
	150	0				
	300	0				
50	50	3.7	2.4	38.8	35.4	37.8
	150	1.9				
	300	1.7				
200	50	10.7	7.9	38.8	35.4	43.3
	150	8.4				
	300	4.6				

Table 6.6 Values of dilation angle and apparent friction angle for different matric suctions obtained from volume change behavior curves for INT-M

Matric suction (kPa)	Net normal stress (kPa)	Interface dilation angle (°)	Average dilation angle ψ_i (°)	Effective adhesion c'_a (kPa)	Effective interface friction angle δ' (°)	Apparent interface friction angle $\delta_{max} = (\delta' + \psi_i)$ (°)
0	50	4.6	2.2	33.0	29.6	31.8
	150	2.1				
	300	0				
50	50	5.0	2.6	33.0	29.6	32.3
	150	2.5				
	300	0.3				
200	50	9.2	6.5	33.0	29.6	36.2
	150	6.7				
	300	3.6				

Table 6.7 Values of dilation angle and apparent friction angle for different matric suctions obtained from volume change behavior curves for INT S

Matric suction (kPa)	Net normal stress (kPa)	Interface dilation angle (°)	Average dilation angle ψ_i (°)	Effective adhesion c'_a (kPa)	Effective interface friction angle δ' (°)	Apparent interface friction angle $\delta_{max} = (\delta' + \psi_i)$ (°)
0	50	0	0.0	1.9	11.9	11.9
	150	0				
	300	0				
50	50	0	0.0	1.9	11.9	11.9
	150	0				
	300	0				
200	50	0.1	0.0	1.9	11.9	11.9
	150	0				
	300	0				

Table 6.8 Variation of δ_{max}/ϕ_{max}, c_a/c and δ^b/ϕ^b ratio with matric suction for interface tests

Matric suction (kPa)		0	50	200
INT-R	δ_{max}/ϕ_{max}	1.02	0.97	0.91
	c_a/c	-	1.12	0.53
	δ^b/ϕ^b	1.02	0.01	0.2
INT-M	δ_{max}/ϕ_{max}	0.88	0.78	0.76
	c_a/c	-	1.17	0.66
	δ^b/ϕ^b	0.88	0.26	0.36
INT-S	δ_{max}/ϕ_{max}	0.33	0.35	0.36
	c_a/c	-	0.06	0.03
	δ^b/ϕ^b	0.33	0.01	0.01

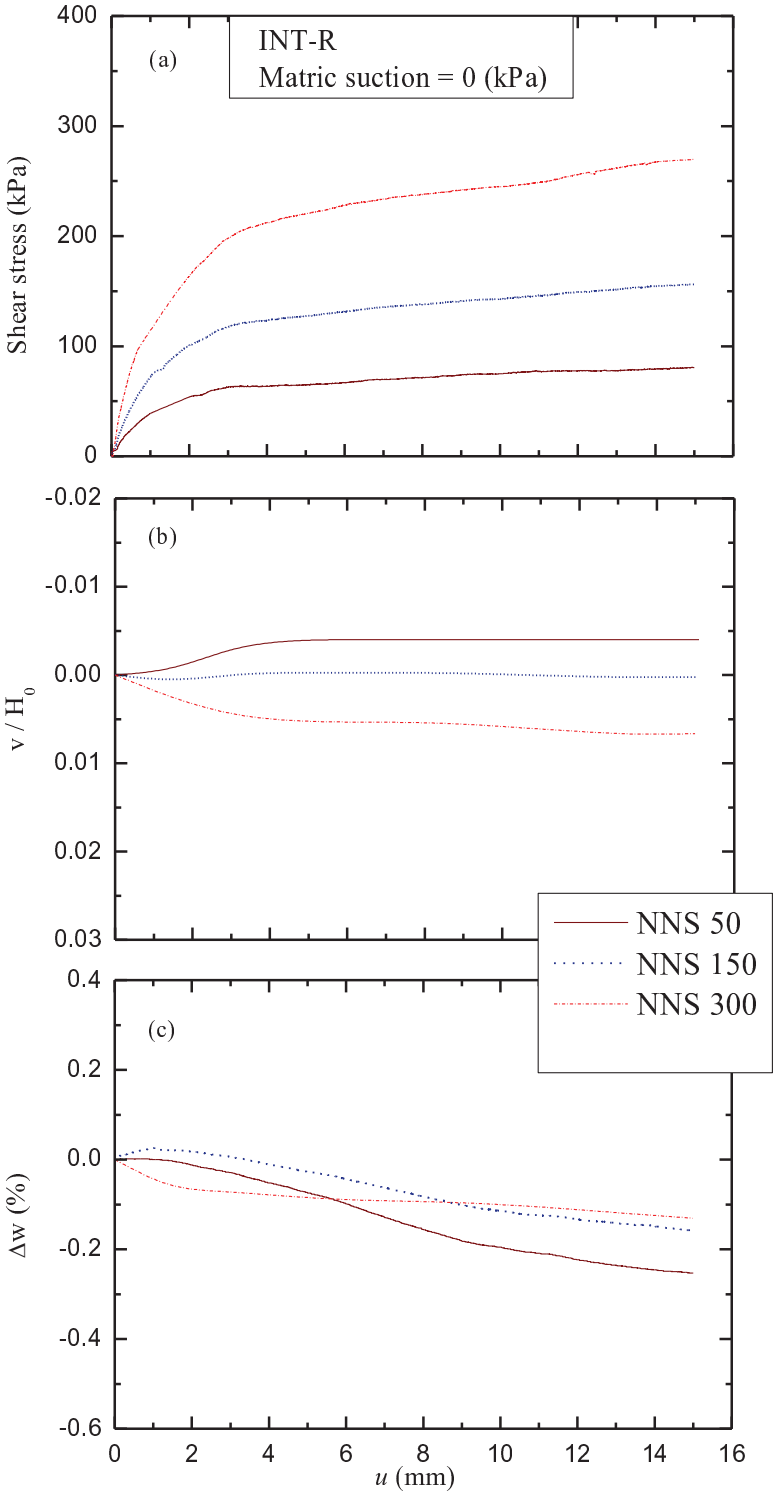

Figure 6.1 Variation of (a) shear stress versus horizontal displacement; (b) normalized vertical displacement versus horizontal displacement (c) migration of water content with horizontal displacement of INT-R at different net normal stress and constant matric suction of 0 kPa (saturated condition).

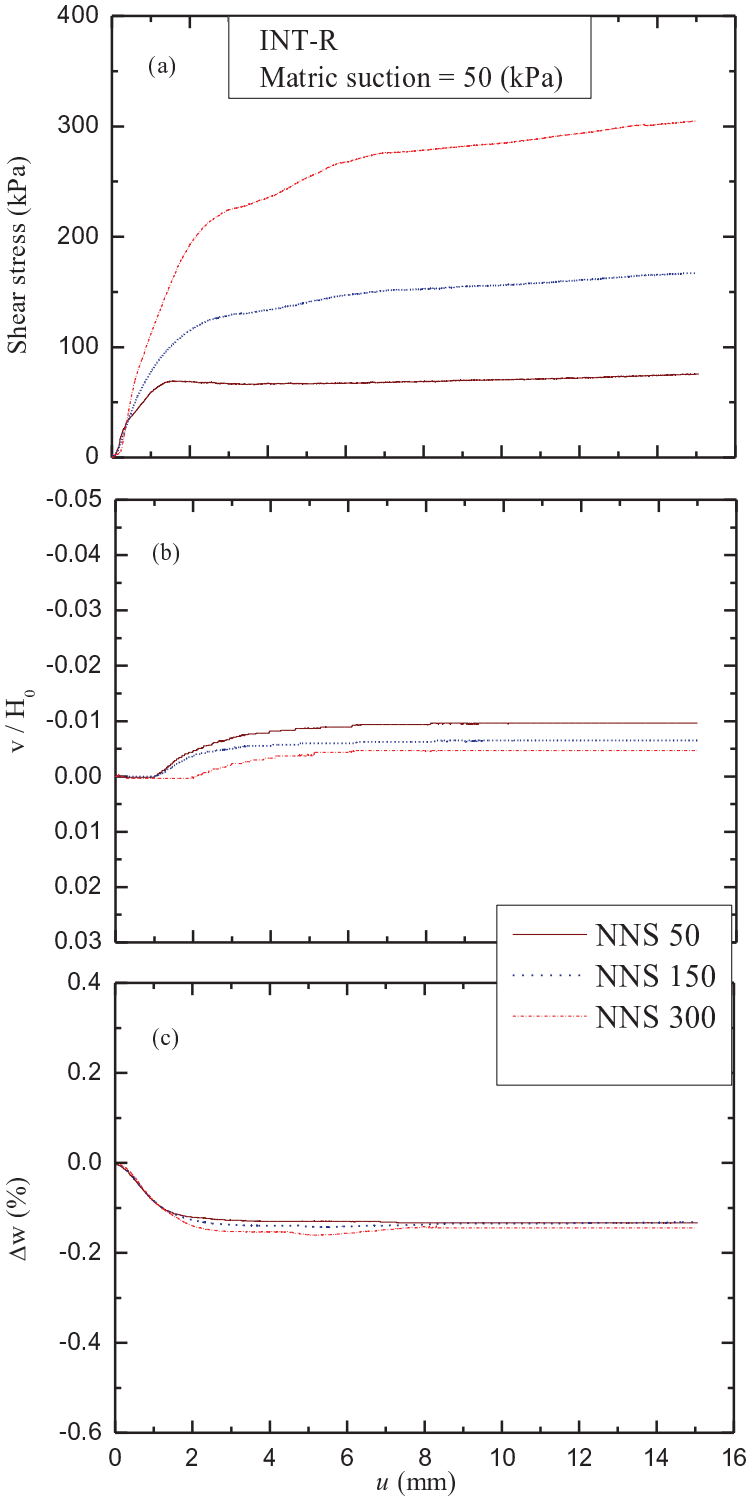

Figure 6.2 Variation of (a) shear stress versus horizontal displacement; (b) normalized vertical displacement versus horizontal displacement (c) migration of water content with horizontal displacement of INT-R at different net normal stress and constant matric suction of 50 kPa.

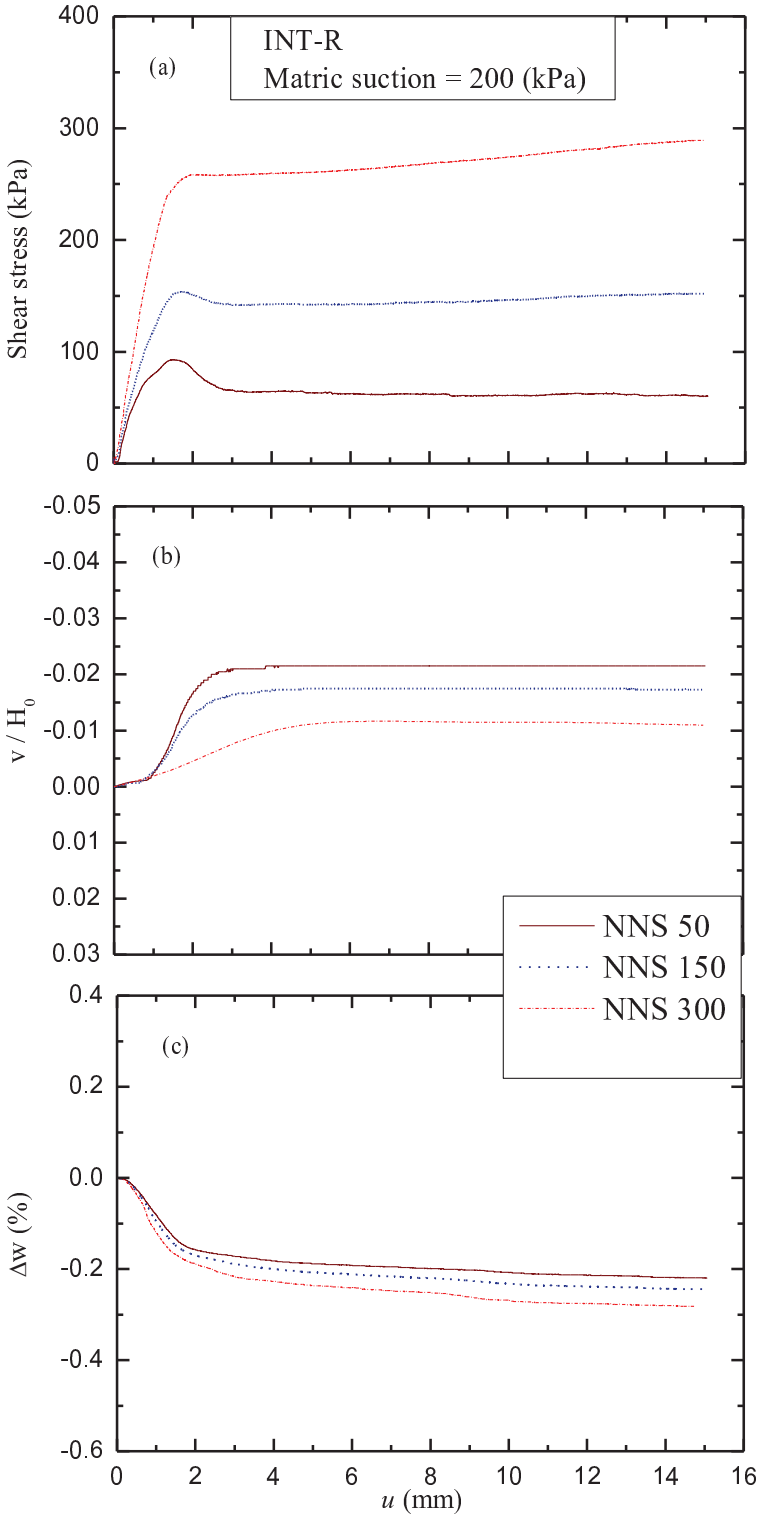

Figure 6.3 Variation of (a) shear stress versus horizontal displacement; (b) normalized vertical displacement versus horizontal displacement (c) migration of water content with horizontal displacement of INT-R at different net normal stress and constant matric suction of 200 kPa.

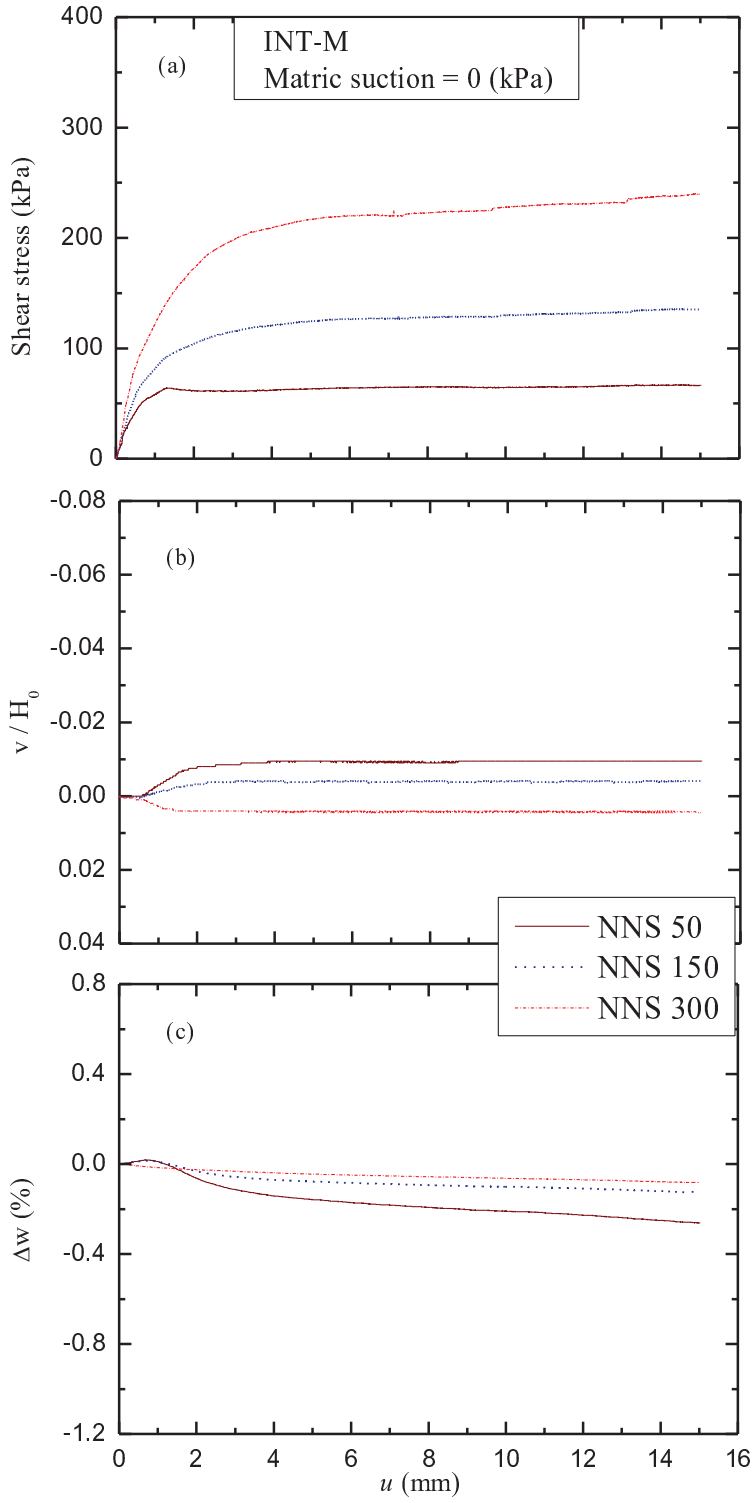

Figure 6.4 Variation of (a) shear stress versus horizontal displacement; (b) normalized vertical displacement versus horizontal displacement (c) migration of water content with horizontal displacement of INT-M at different net normal stress and constant matric suction of 0 kPa (saturated condition).

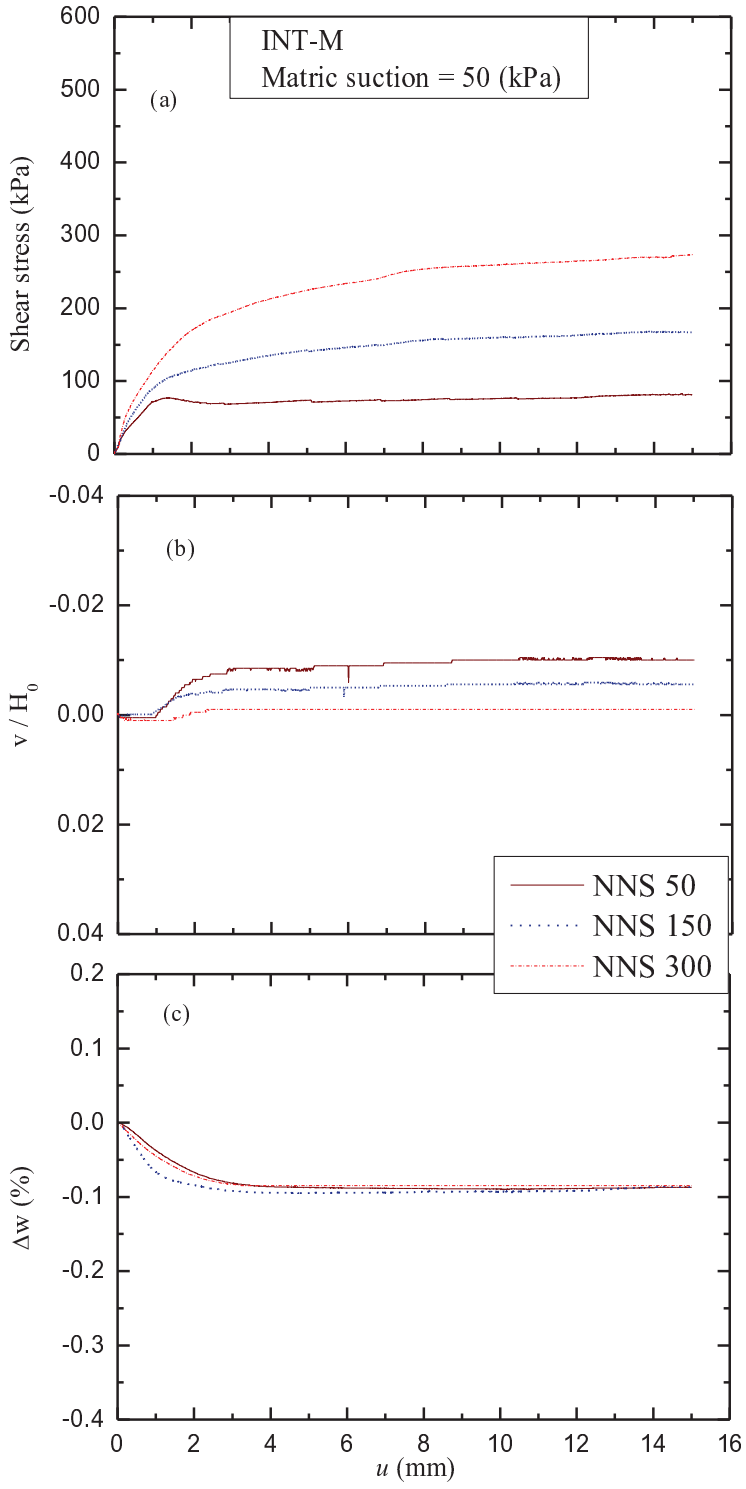

Figure 6.5 Variation of (a) shear stress versus horizontal displacement; (b) normalized vertical displacement versus horizontal displacement (c) migration of water content with horizontal displacement of INT-M at different net normal stress and constant matric suction of 50 kPa.

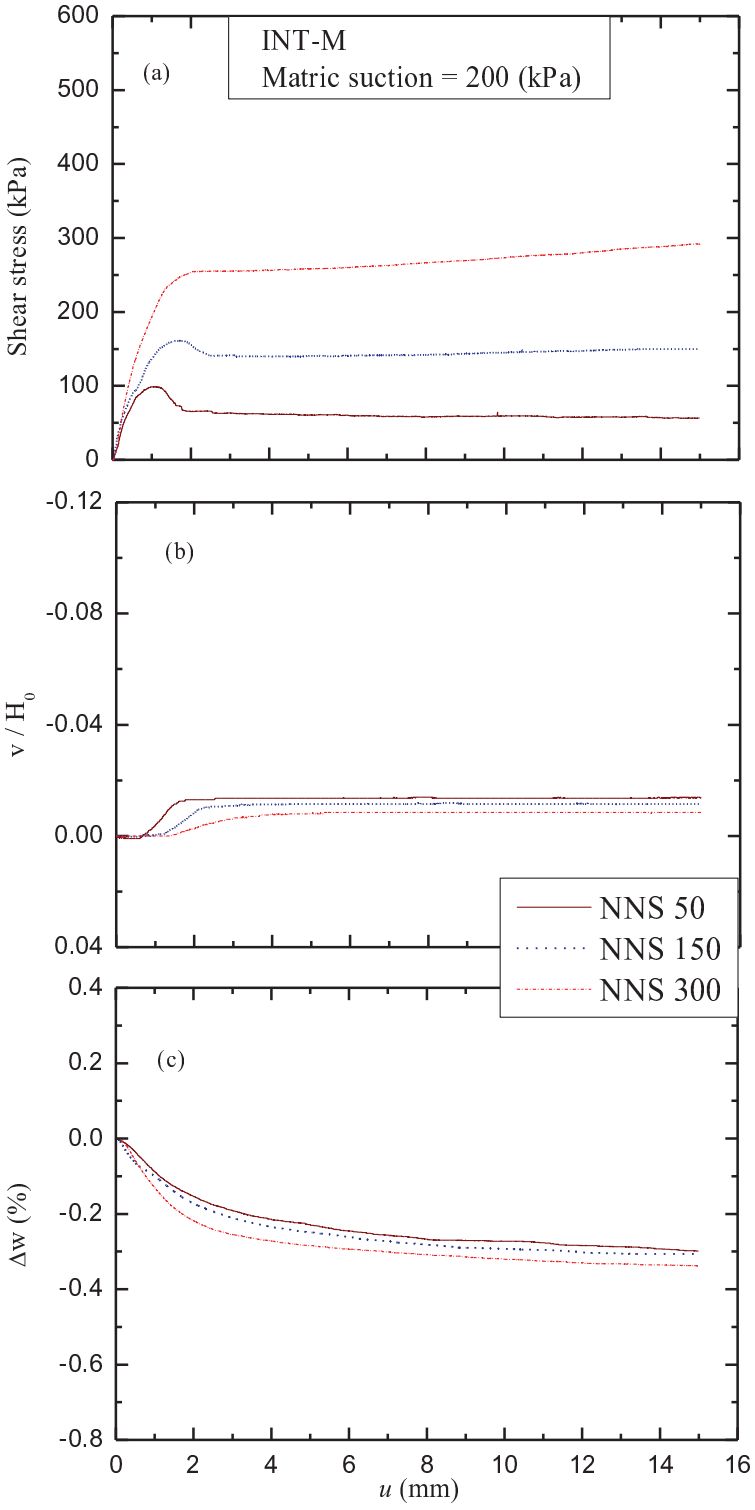

Figure 6.6 Variation of (a) shear stress versus horizontal displacement; (b) normalized vertical displacement versus horizontal displacement (c) migration of water content with horizontal displacement of INT-M at different net normal stress and constant matric suction of 200 kPa.

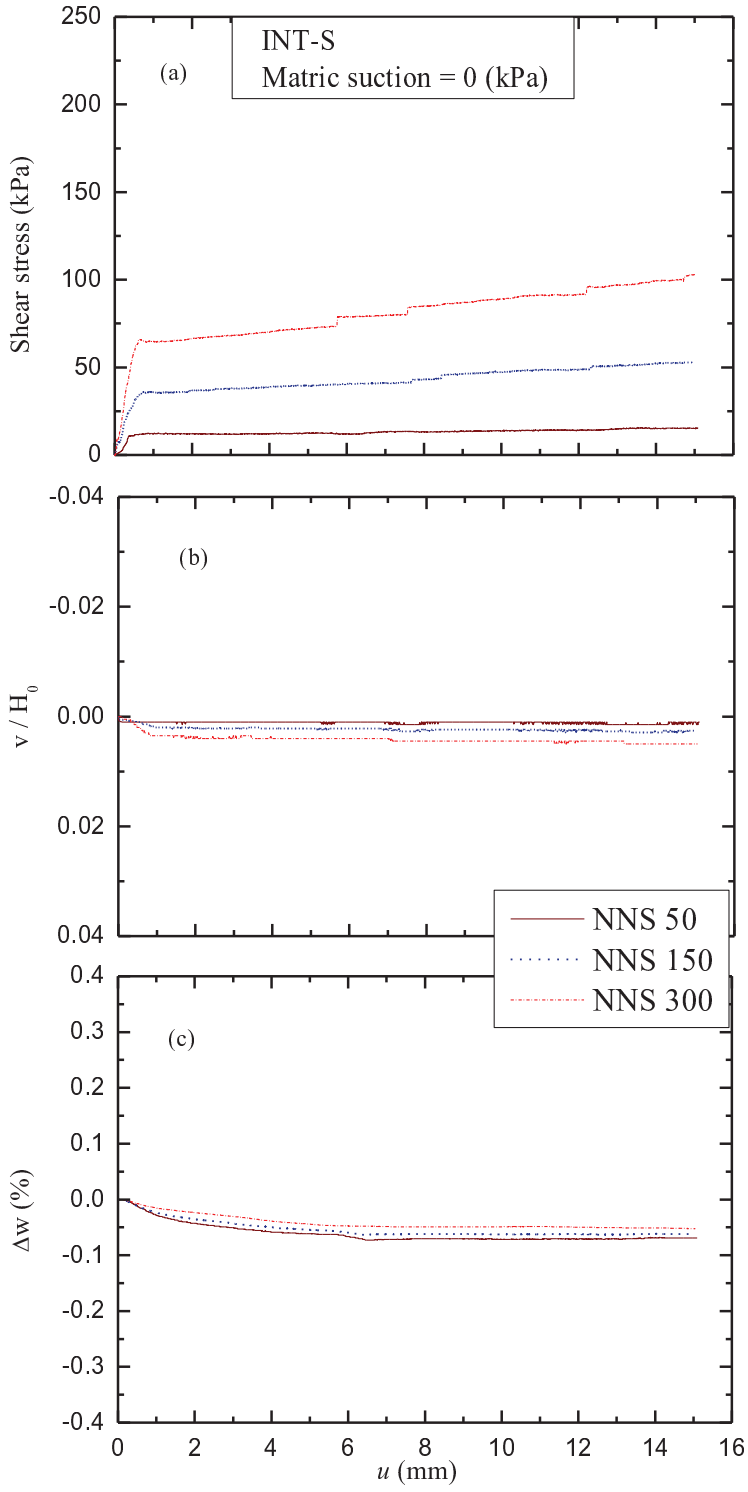

Figure 6.7 Variation of (a) shear stress versus horizontal displacement; (b) normalized vertical displacement versus horizontal displacement (c) migration of water content with horizontal displacement of INT-S at different net normal stress and constant matric suction of 0 kPa (saturated condition).

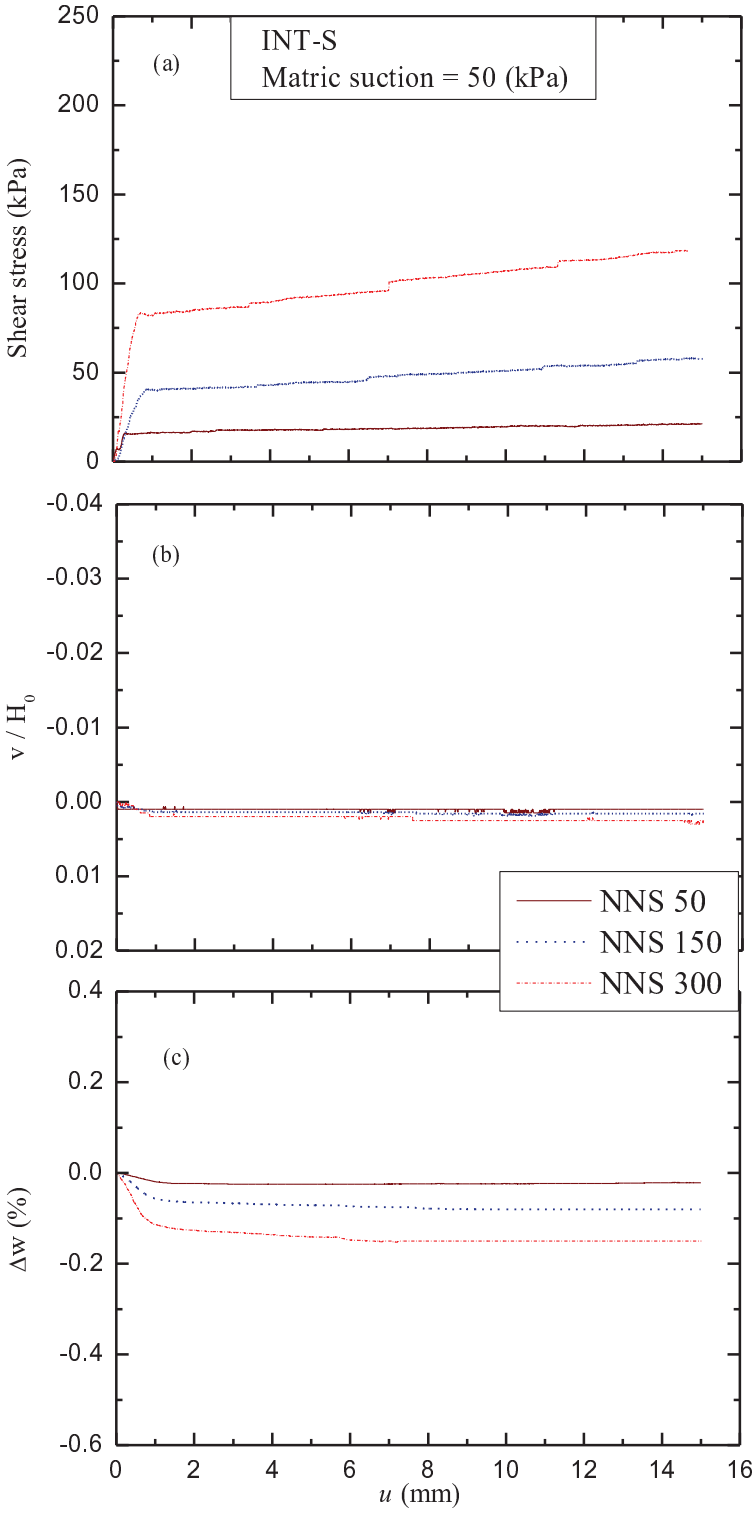

Figure 6.8 Variation of (a) shear stress versus horizontal displacement; (b) normalized vertical displacement versus horizontal displacement (c) migration of water content with horizontal displacement of INT-S at different net normal stress and constant matric suction of 50 kPa.

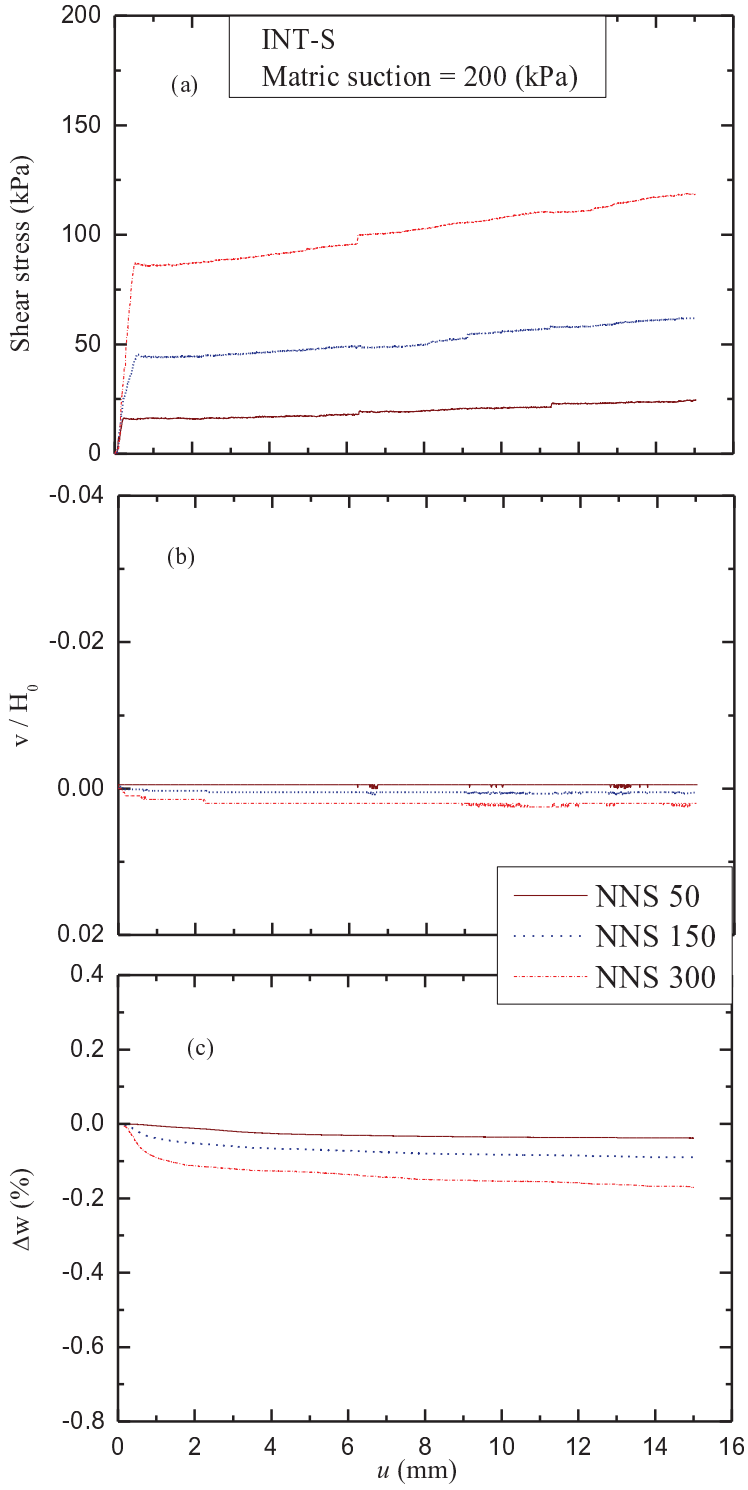

Figure 6.9 Variation of (a) shear stress versus horizontal displacement; (b) normalized vertical displacement versus horizontal displacement (c) migration of water content with horizontal displacement of INT-S at different net normal stress and constant matric suction of 200 kPa.

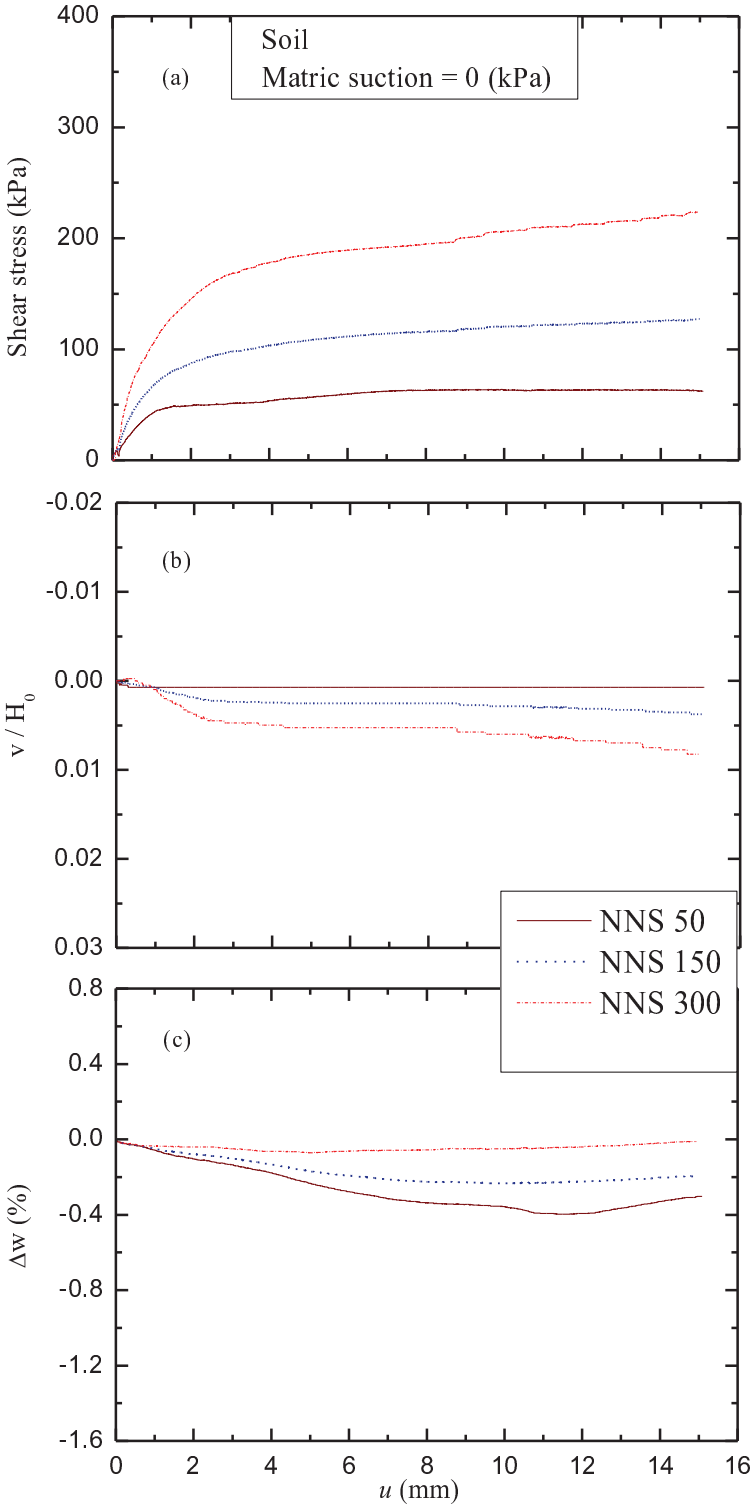

Figure 6.10 Variation of (a) shear stress versus horizontal displacement; (b) normalized vertical displacement versus horizontal displacement (c) migration of water content with horizontal displacement of soil at different net normal stress and constant matric suction of 0 kPa (saturated condition).

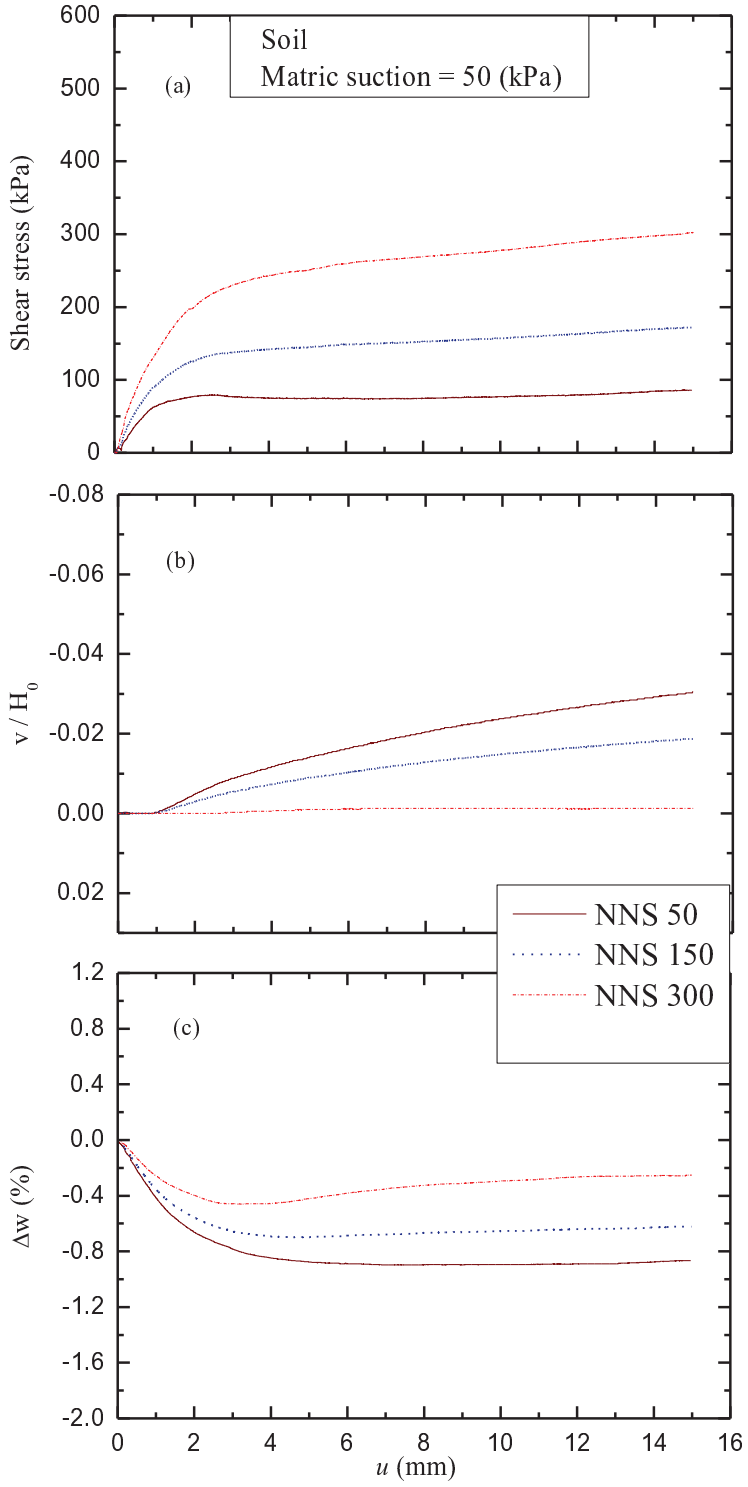

Figure 6.11 Variation of (a) shear stress versus horizontal displacement; (b) normalized vertical displacement versus horizontal displacement (c) migration of water content with horizontal displacement of soil at different net normal stress and constant matric suction of 50 kPa.

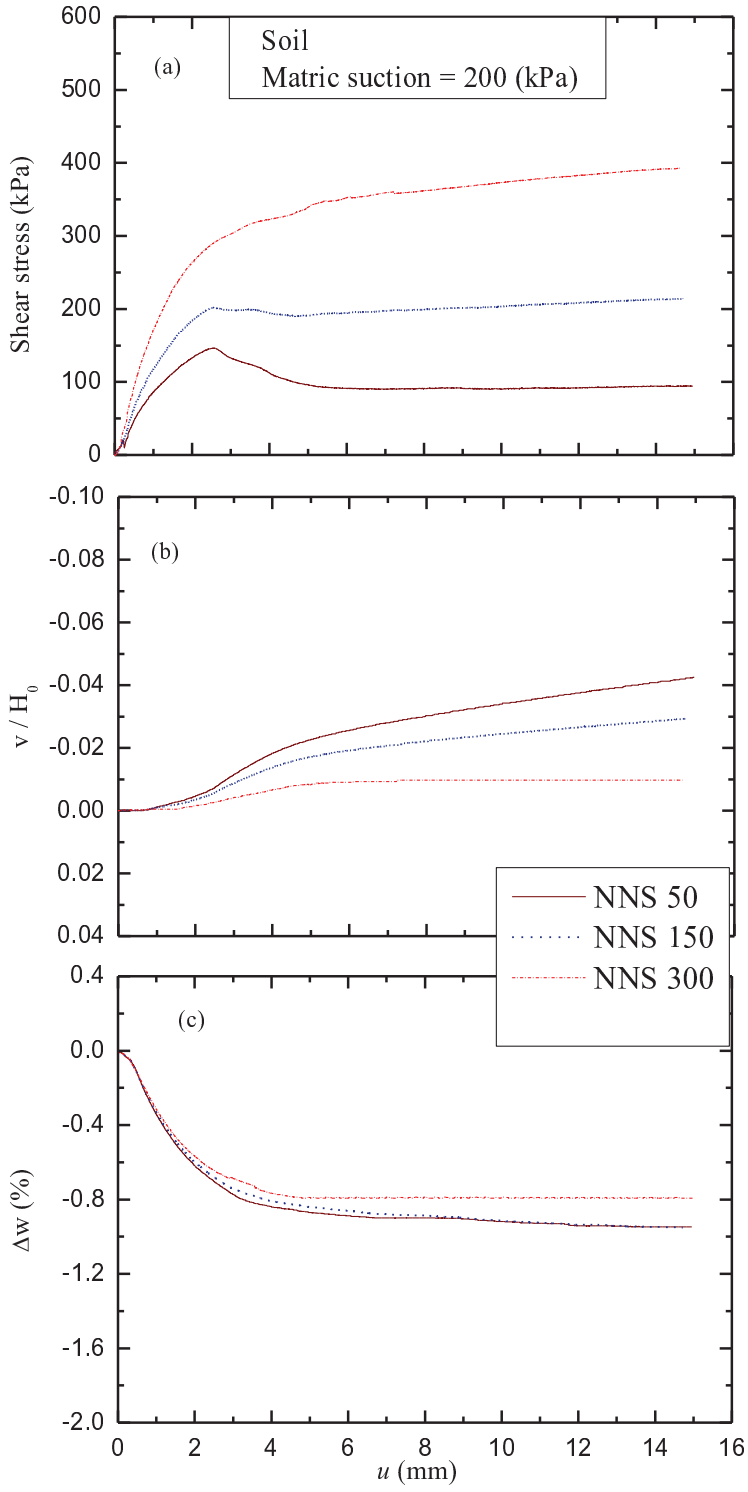

Figure 6.12 Variation of (a) shear stress versus horizontal displacement; (b) normalized vertical displacement versus horizontal displacement (c) migration of water content with horizontal displacement of soil at different net normal stress and constant matric suction of 200 kPa.

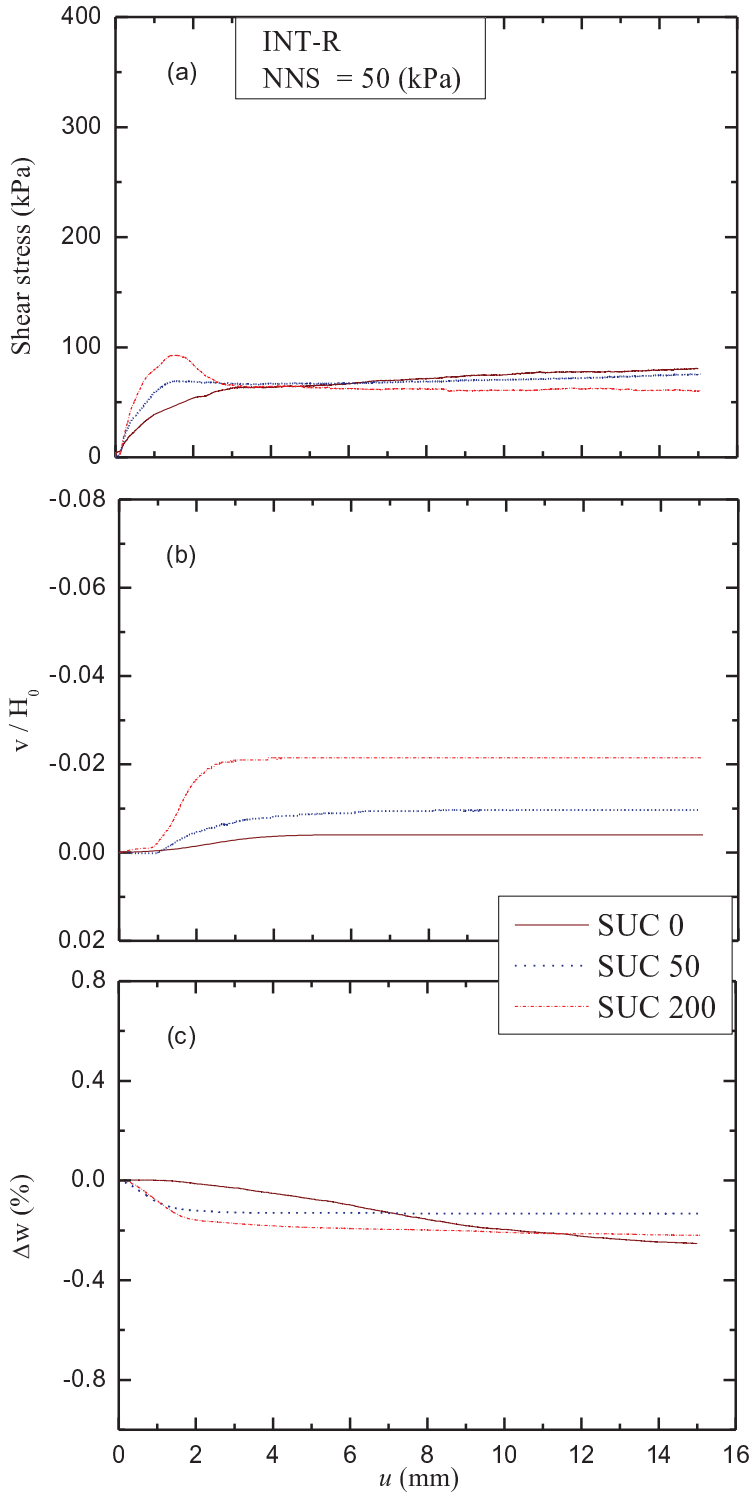

Figure 6.13 Variation of (a) shear stress versus horizontal displacement; (b) normalized vertical displacement versus horizontal displacement (c) migration of water content with horizontal displacement of INT-R at different matric suction and constant net normal stress of 50 kPa.

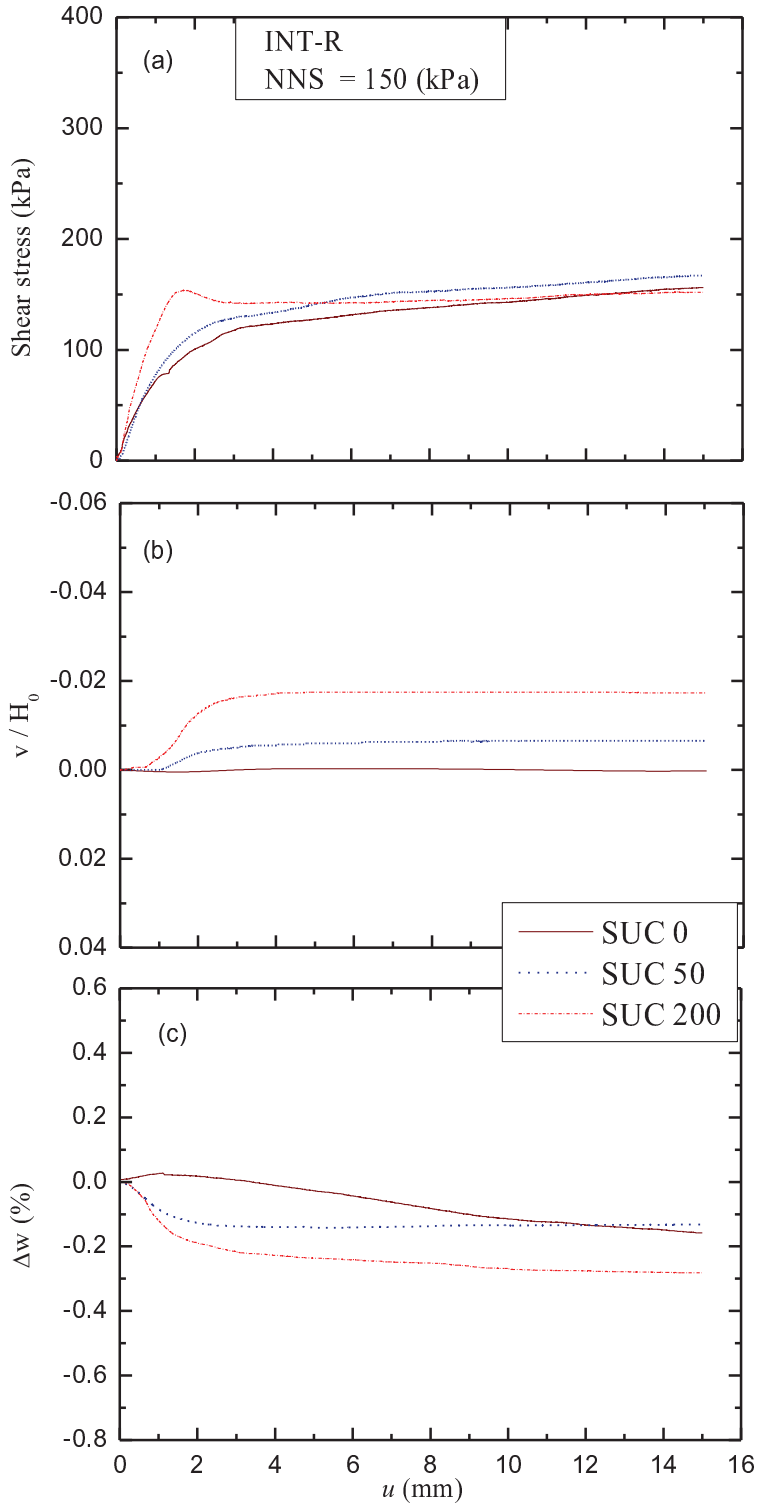

Figure 6.14 Variation of (a) shear stress versus horizontal displacement; (b) normalized vertical displacement versus horizontal displacement (c) migration of water content with horizontal displacement of INT-R at different matric suction and constant net normal stress of 150 kPa.

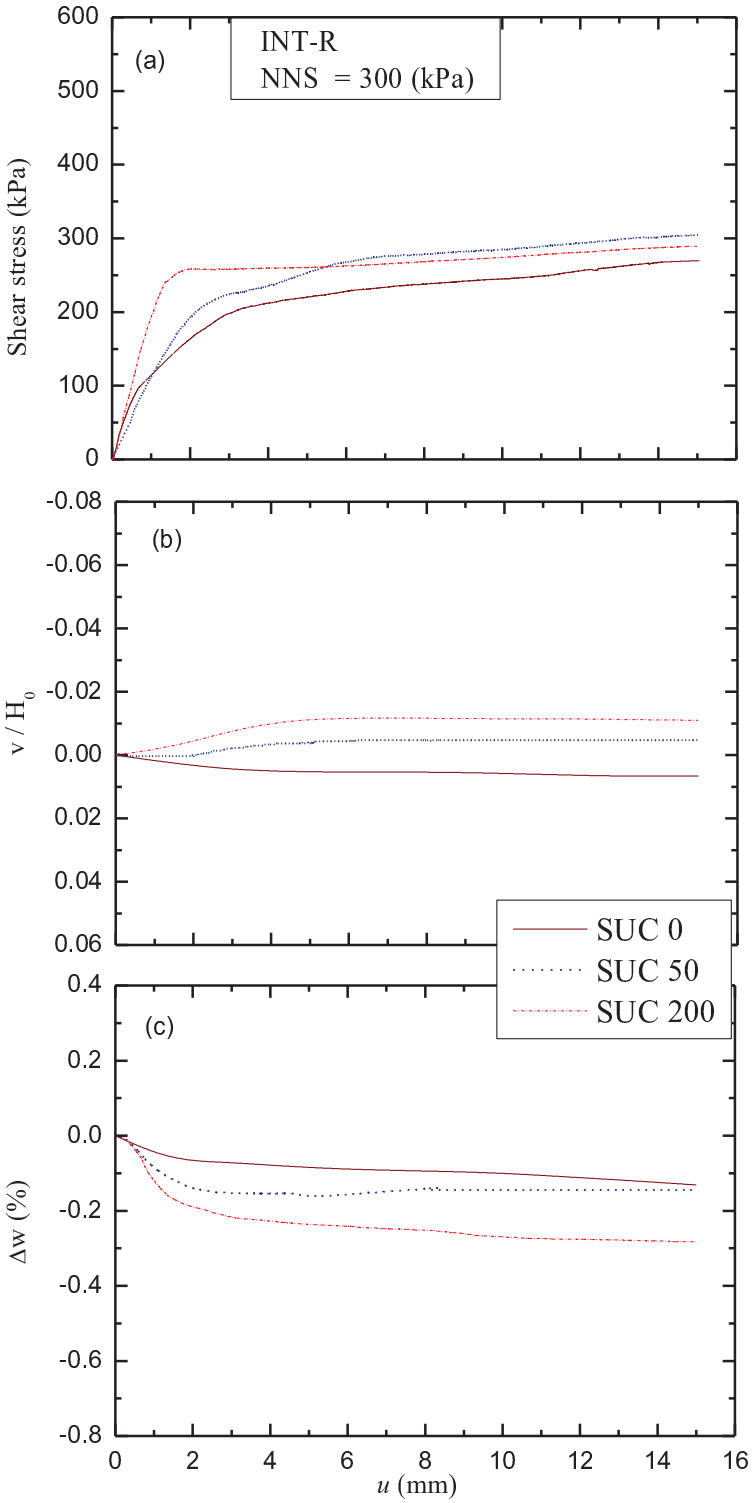

Figure 6.15 Variation of (a) shear stress versus horizontal displacement; (b) normalized vertical displacement versus horizontal displacement (c) migration of water content with horizontal displacement of INT-R at different matric suction and constant net normal stress of 300 kPa.

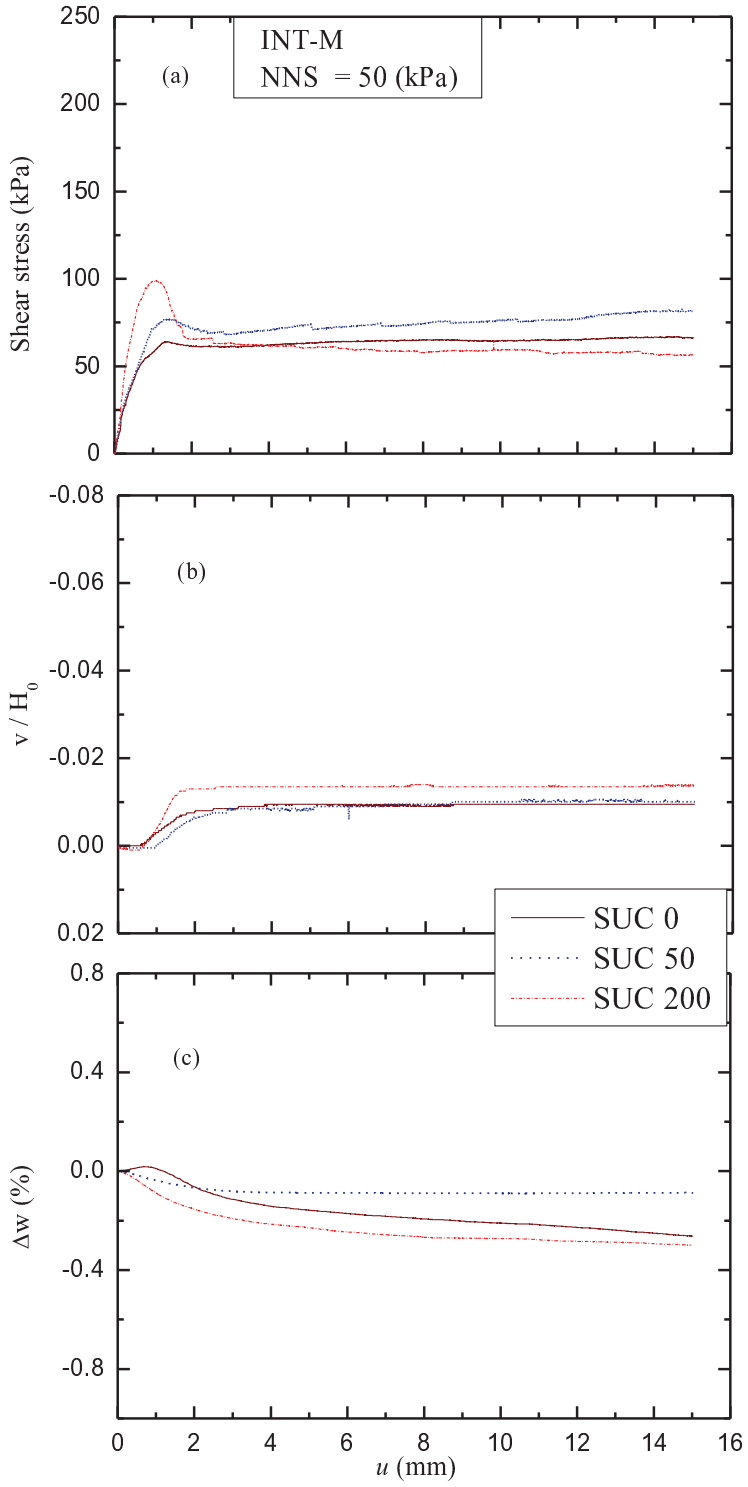

Figure 6.16 Variation of (a) shear stress versus horizontal displacement; (b) normalized vertical displacement versus horizontal displacement (c) migration of water content with horizontal displacement of INT-M at different matric suction and constant net normal stress of 50 kPa.

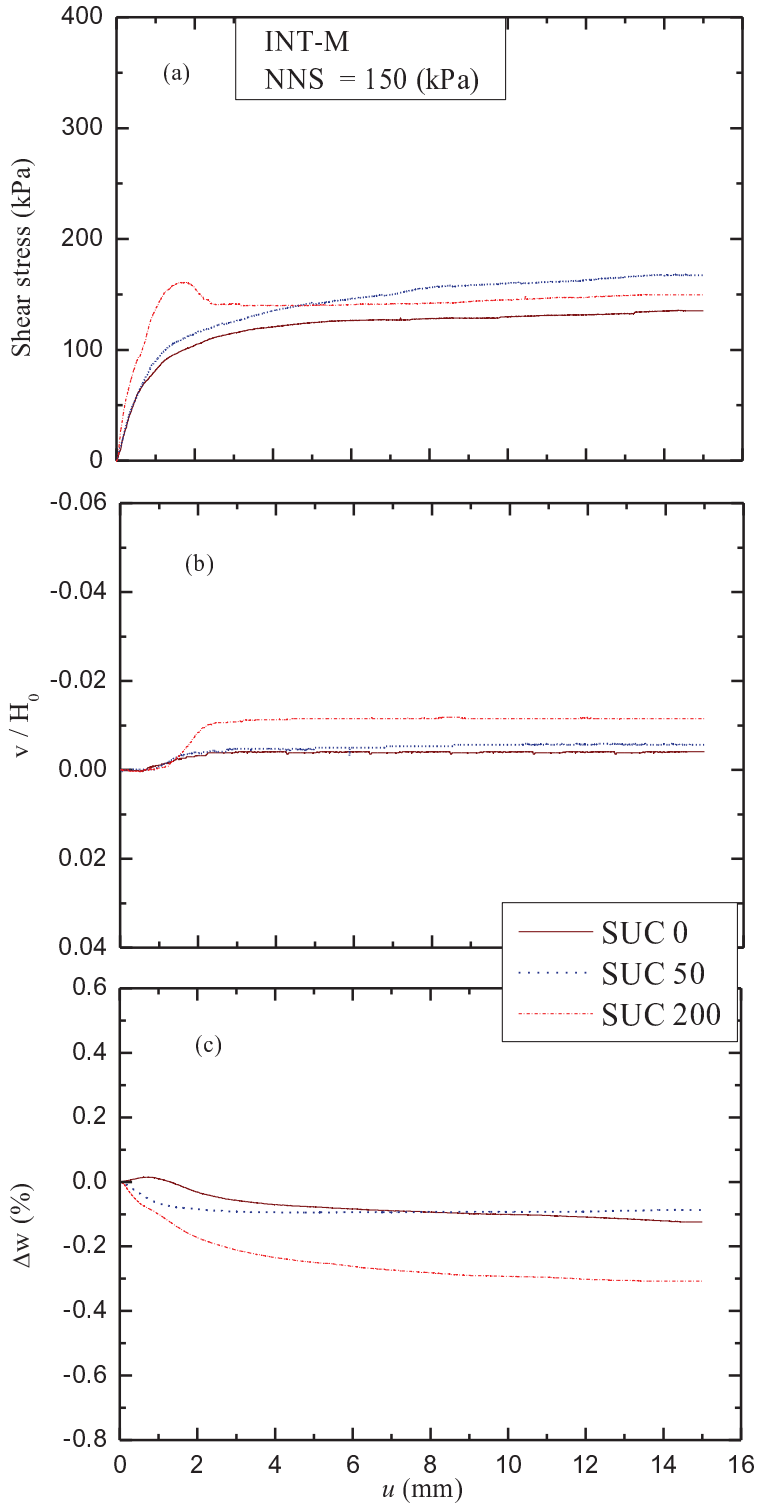

Figure 6.17 Variation of (a) shear stress versus horizontal displacement; (b) normalized vertical displacement versus horizontal displacement (c) migration of water content with horizontal displacement of INT-M at different matric suction and constant net normal stress of 150 kPa.

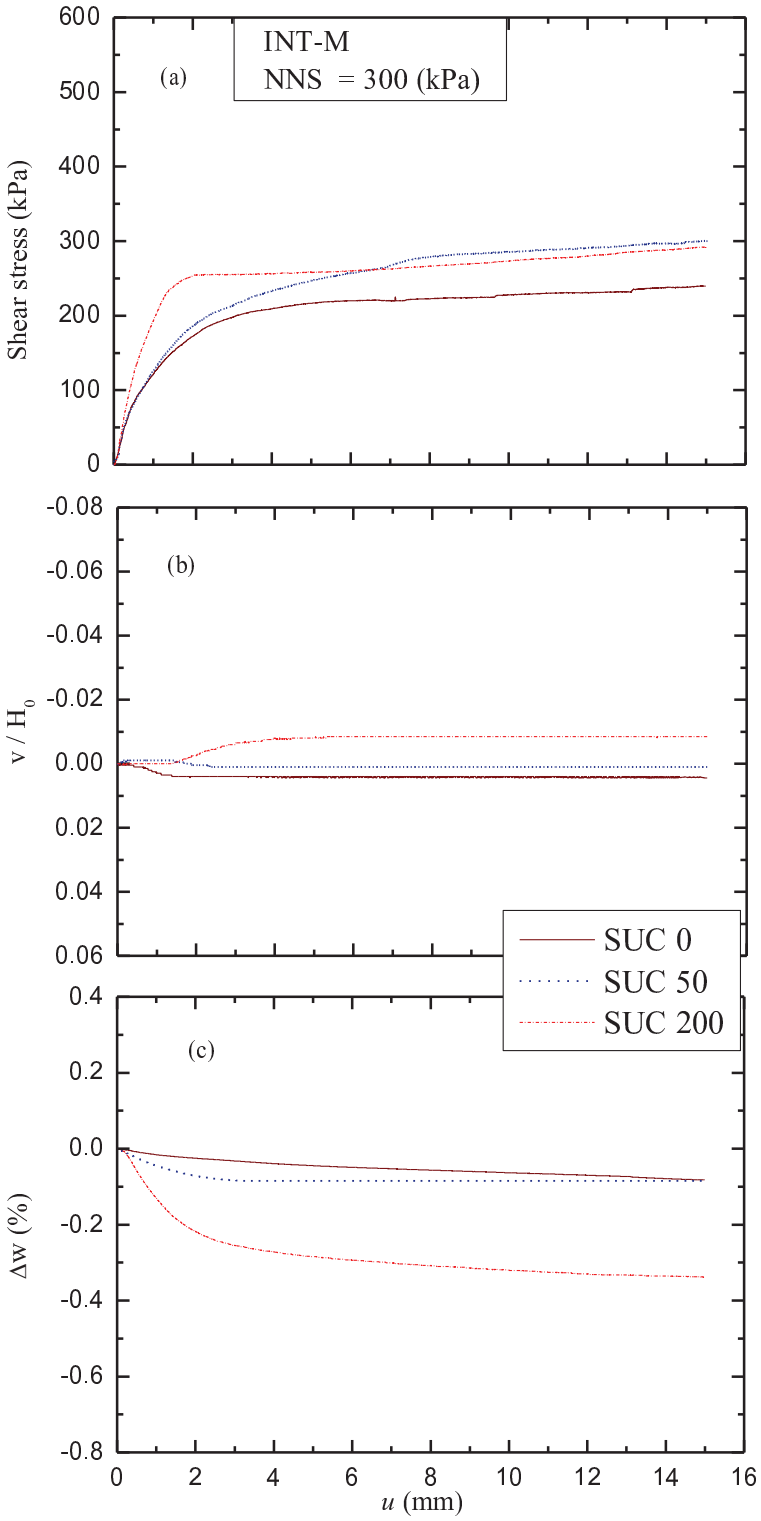

Figure 6.18 Variation of (a) shear stress versus horizontal displacement; (b) normalized vertical displacement versus horizontal displacement (c) migration of water content with horizontal displacement of INT-M at different matric suction and constant net normal stress of 300 kPa.

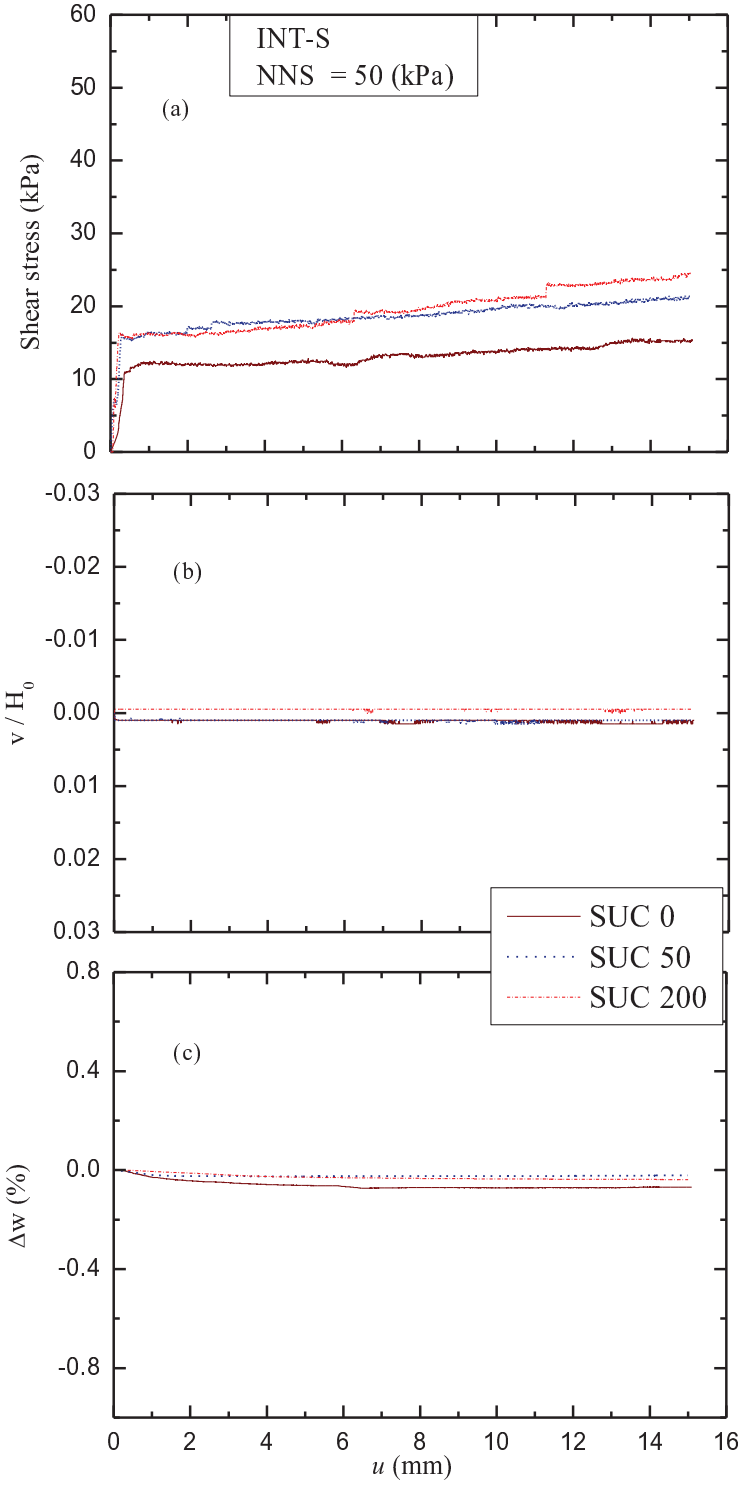

Figure 6.19 Variation of (a) shear stress versus horizontal displacement; (b) normalized vertical displacement versus horizontal displacement (c) migration of water content with horizontal displacement of INT-S at different matric suction and constant net normal stress of 50 kPa.

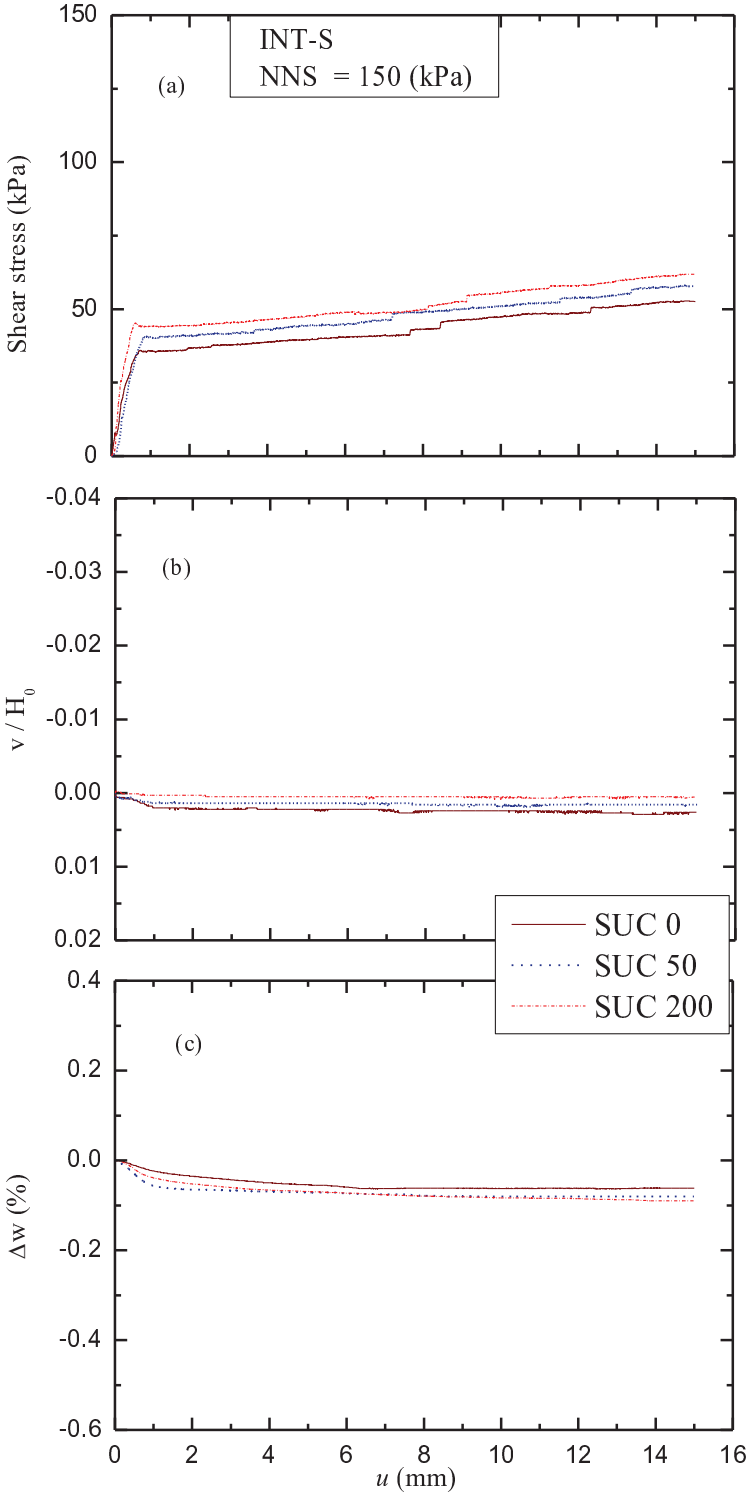

Figure 6.20 Variation of (a) shear stress versus horizontal displacement; (b) normalized vertical displacement versus horizontal displacement (c) migration of water content with horizontal displacement of INT-S at different matric suction and constant net normal stress of 150 kPa.

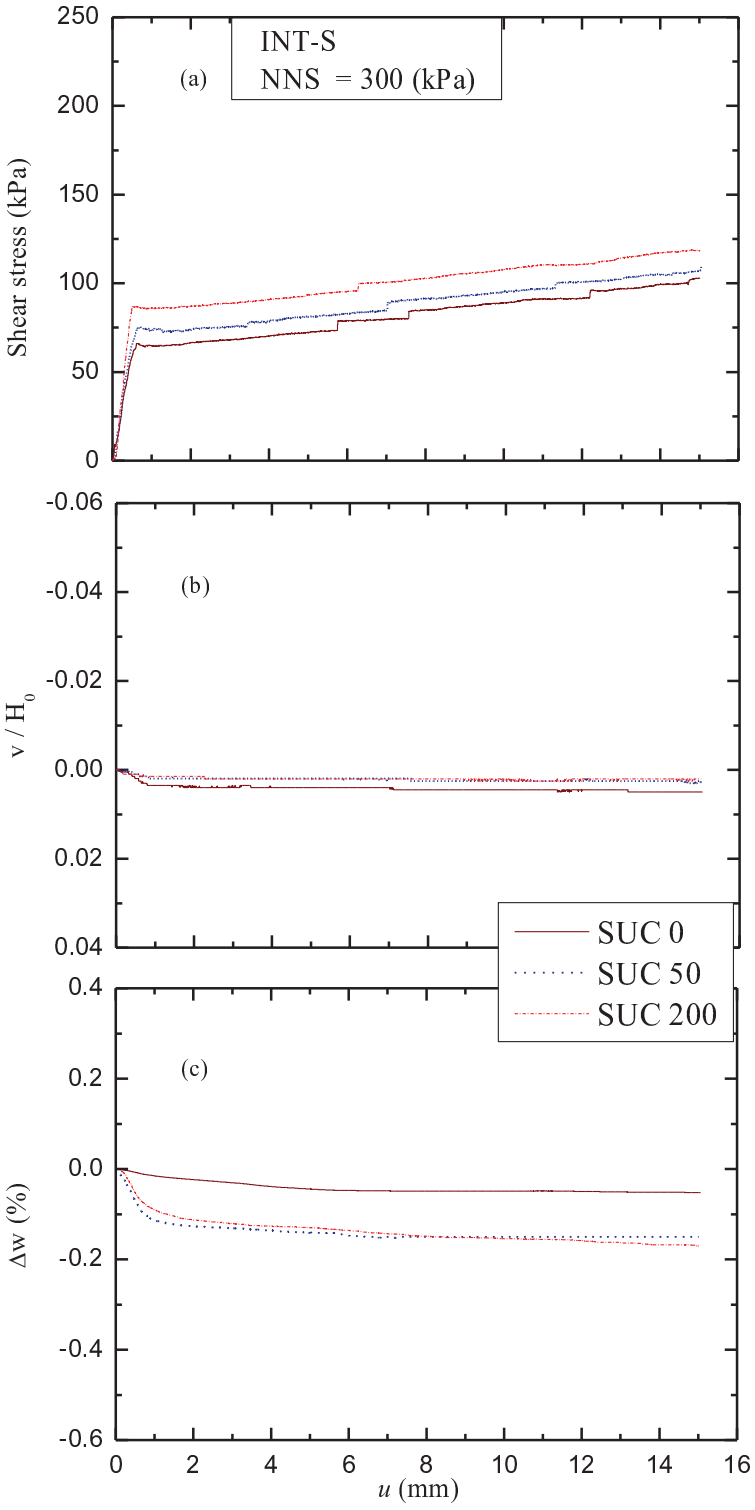

Figure 6.21 Variation of (a) shear stress versus horizontal displacement; (b) normalized vertical displacement versus horizontal displacement (c) migration of water content with horizontal displacement of INT-S at different matric suction and constant net normal stress of 300 kPa.

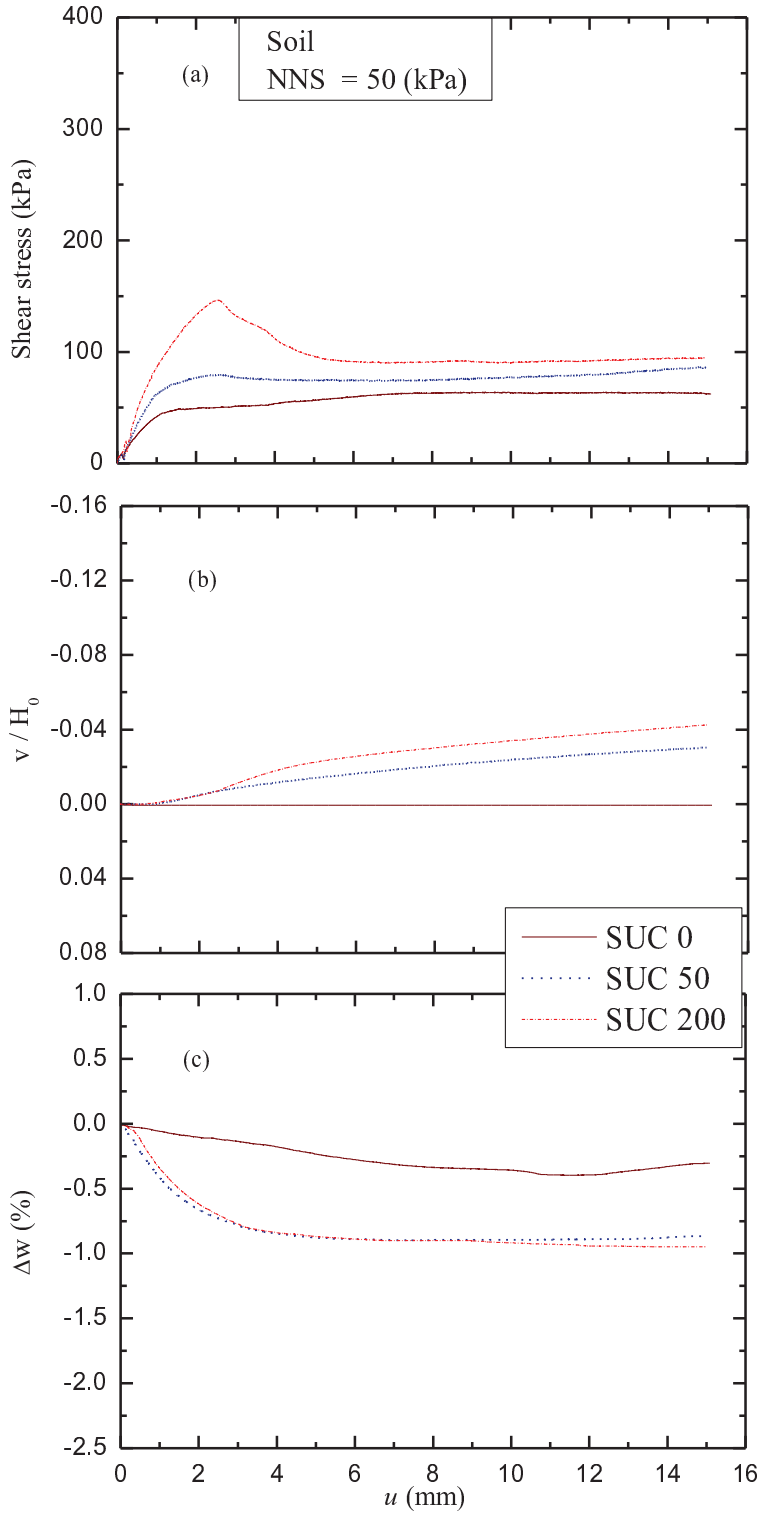

Figure 6.22 Variation of (a) shear stress versus horizontal displacement; (b) normalized vertical displacement versus horizontal displacement (c) migration of water content with horizontal displacement of soil at different matric suction and constant net normal stress of 50 kPa.

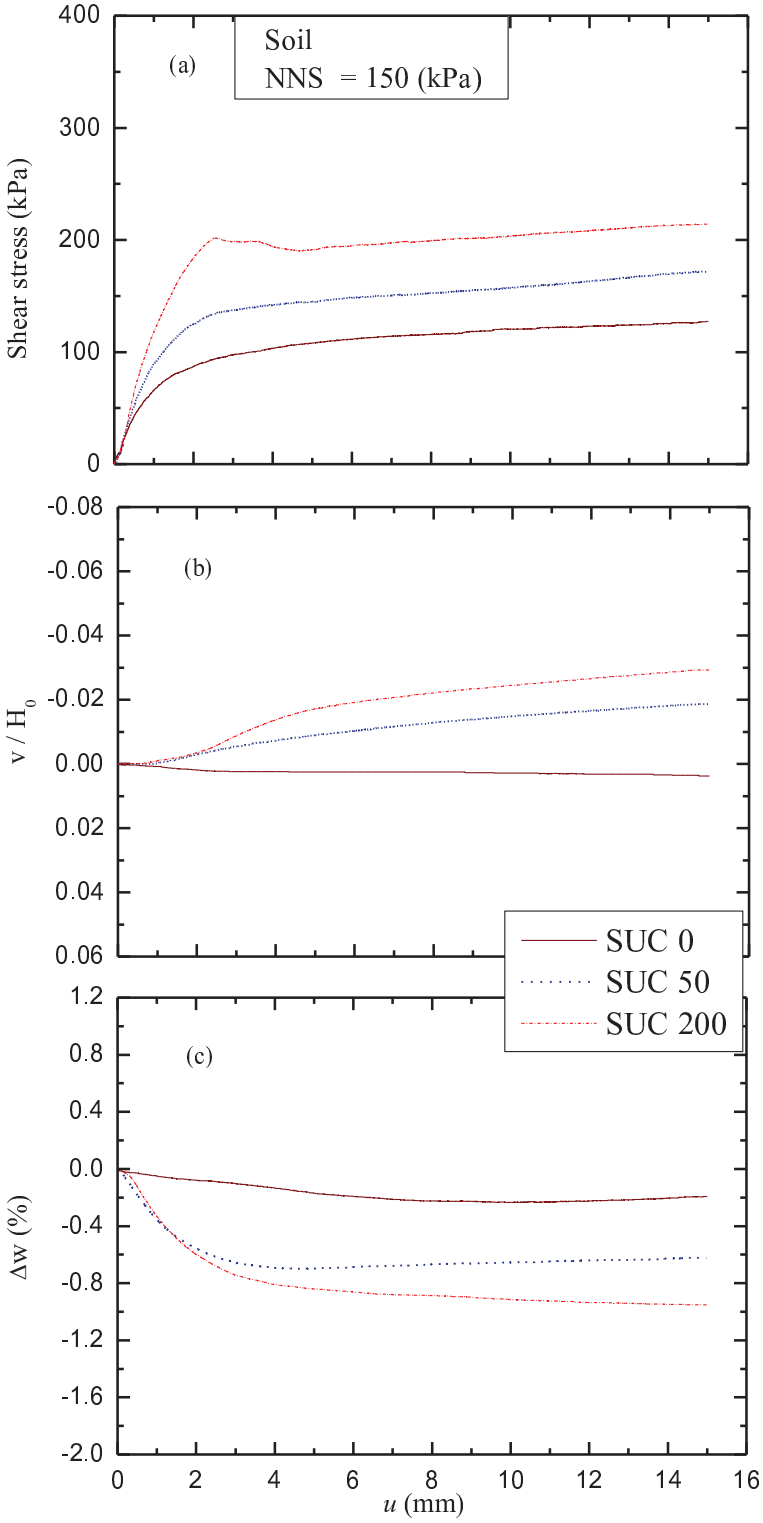

Figure 6.23 Variation of (a) shear stress versus horizontal displacement; (b) normalized vertical displacement versus horizontal displacement (c) migration of water content with horizontal displacement of soil at different matric suction and constant net normal stress of 150 kPa.

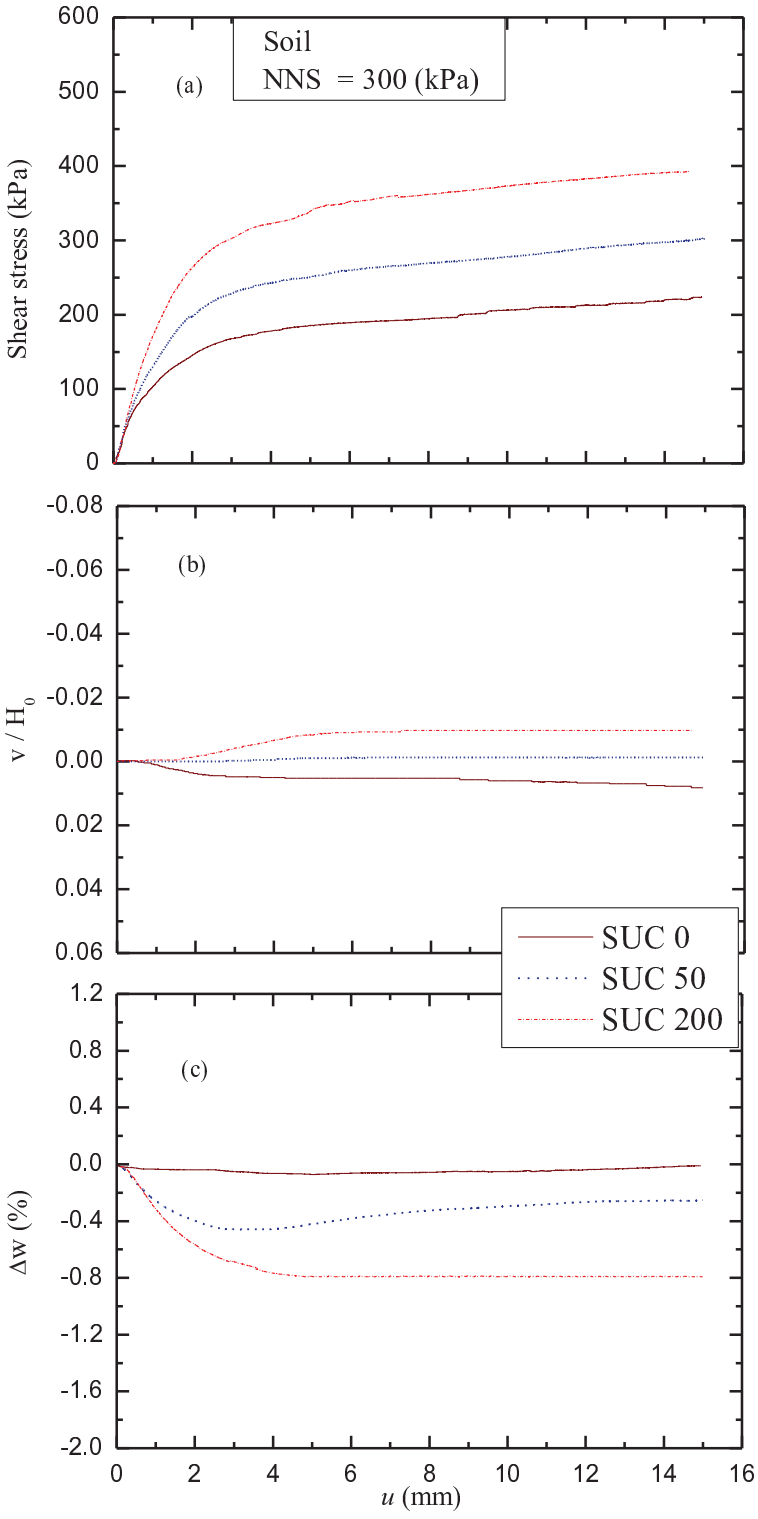

Figure 6.24 Variation of (a) shear stress versus horizontal displacement; (b) normalized vertical displacement versus horizontal displacement (c) migration of water content with horizontal displacement of soil at different matric suction and constant net normal stress of 300 kPa.

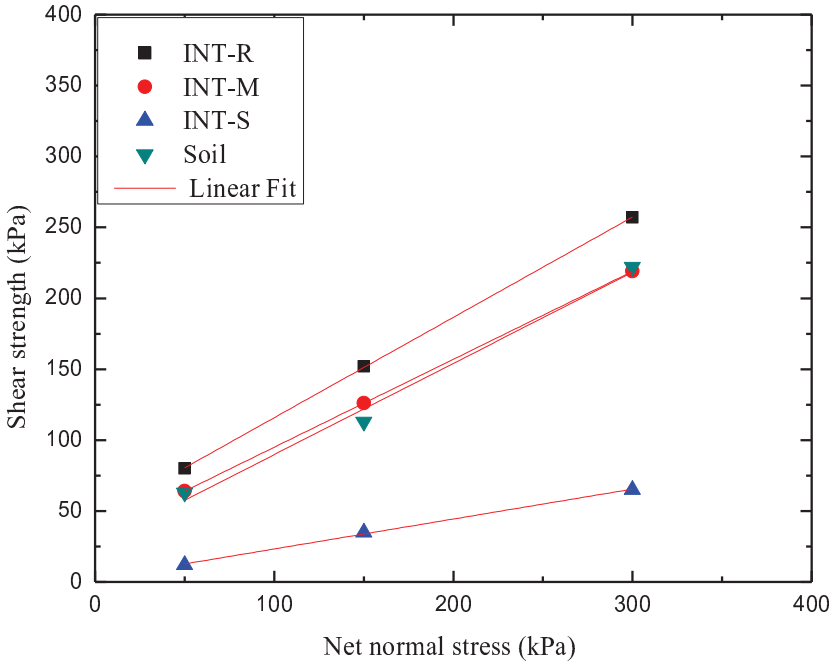

Figure 6.25 Relationships between shear strength and net normal stress from direct shear tests on interface tests and pure soil at 0 kPa matric suction

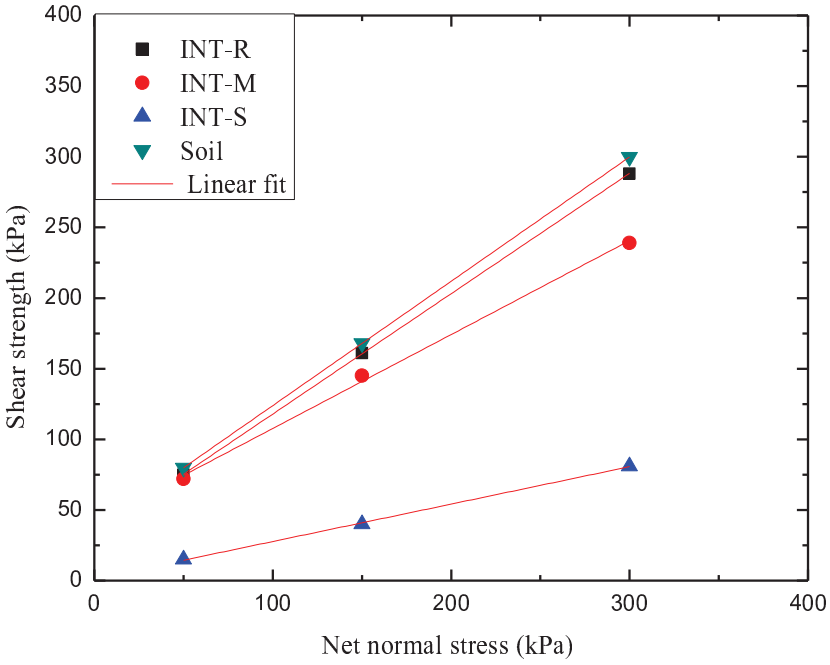

Figure 6.26 Relationships between shear strength and net normal stress from direct shear tests on interface tests and pure soil at 50 kPa matric suction

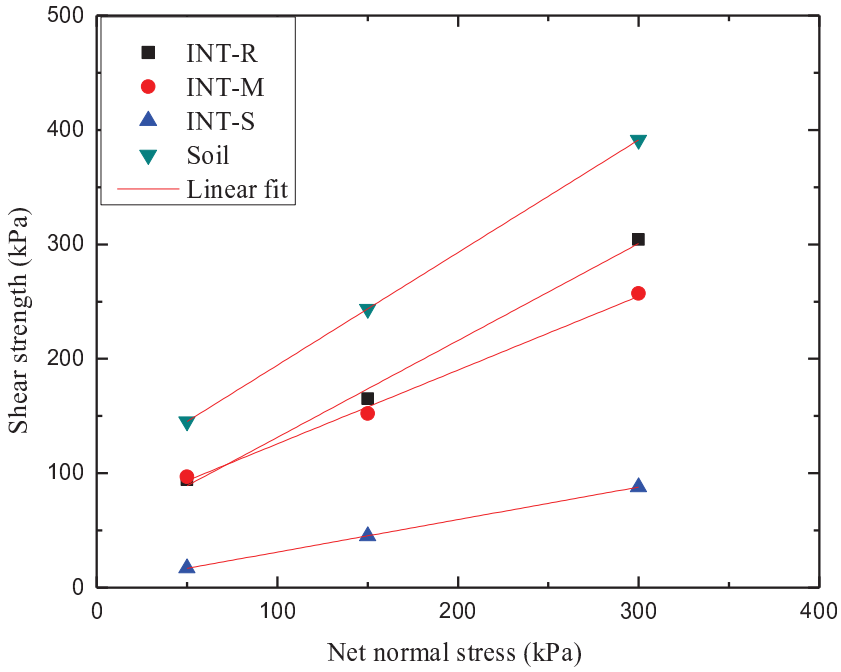

Figure 6.27. Relationships between shear strength and net normal stress from direct shear tests on interface tests and pure soil at 200 kPa matric suction

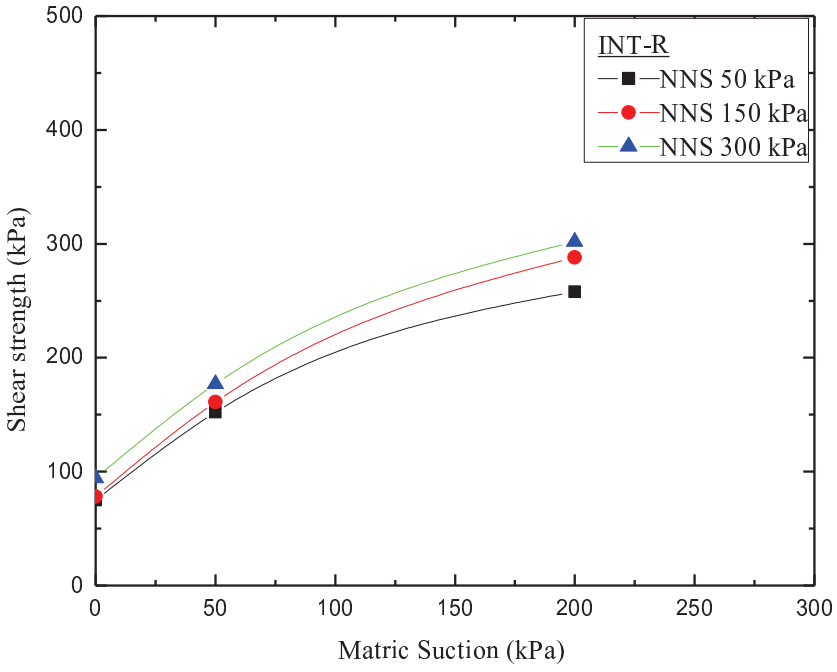

Figure 6.28 Relationship between shear strength and matric suction from direct shear tests on INT-R for different net normal stresses

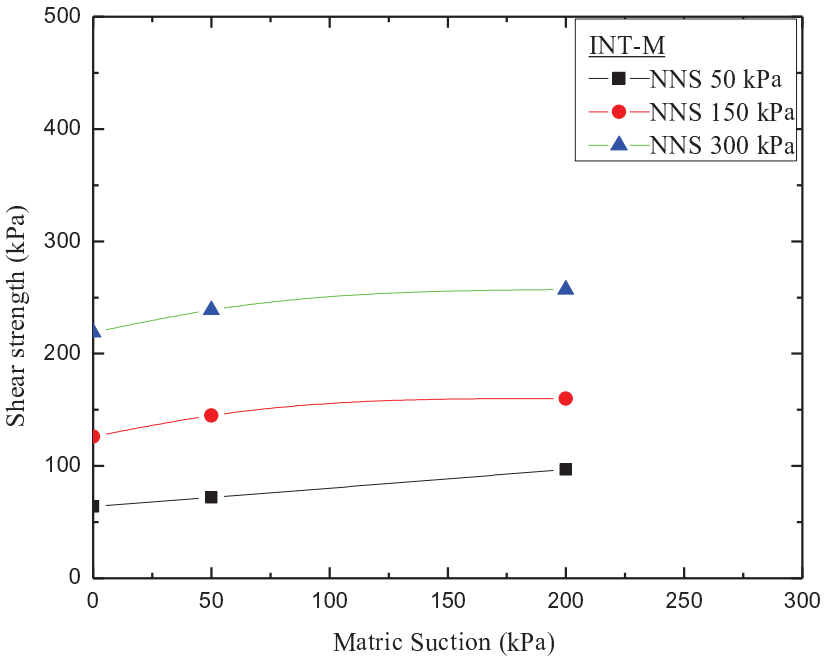

Figure 6.29 Relationship between shear strength and matric suction from direct shear tests on INT-M for different net normal stresses

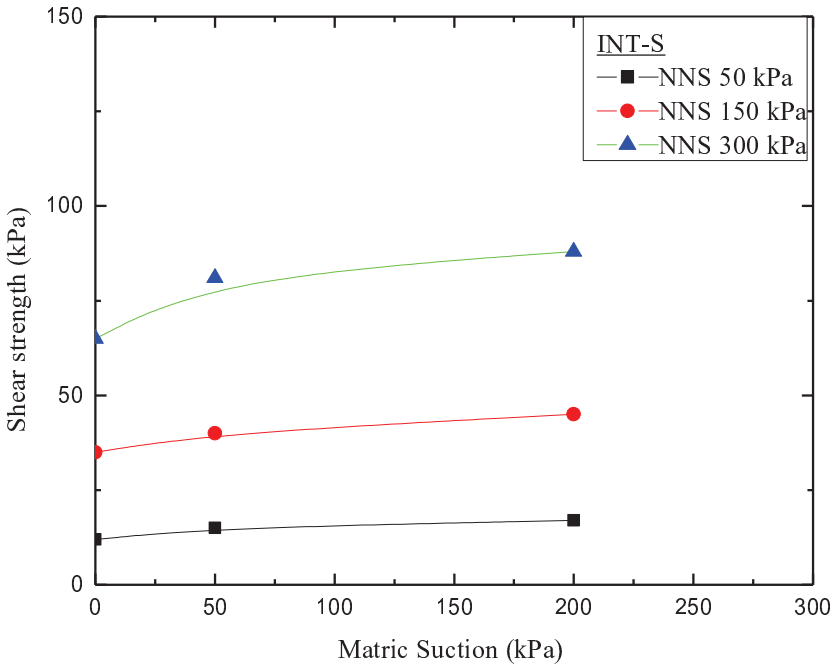

Figure 6.30 Relationship between shear strength and matric suction from direct shear tests on INT-S for different net normal stresses

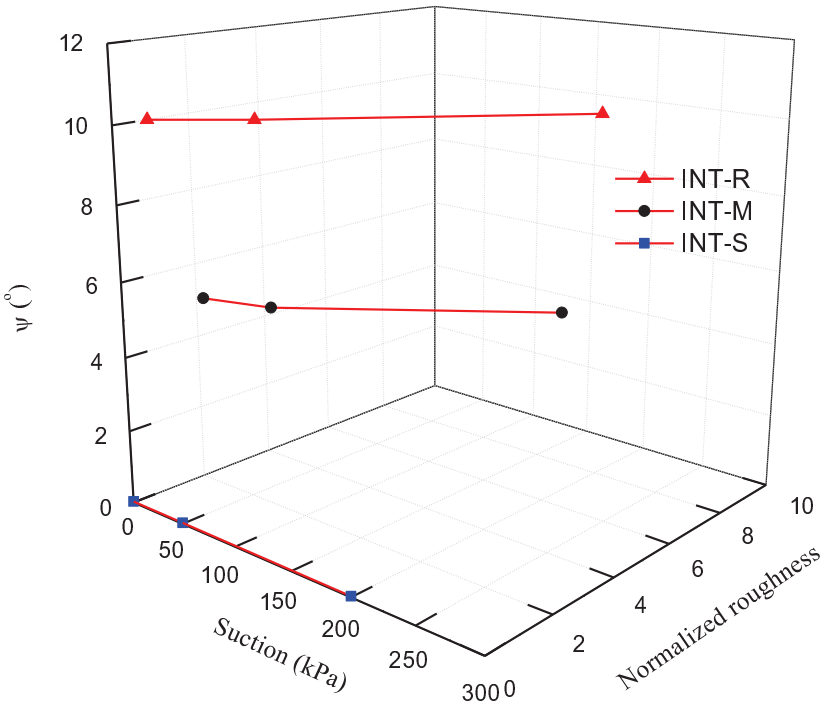

Figure 6.31 Variation of interface dilation angle with respect to matric suction and normalized surface roughness of the steel counterface.

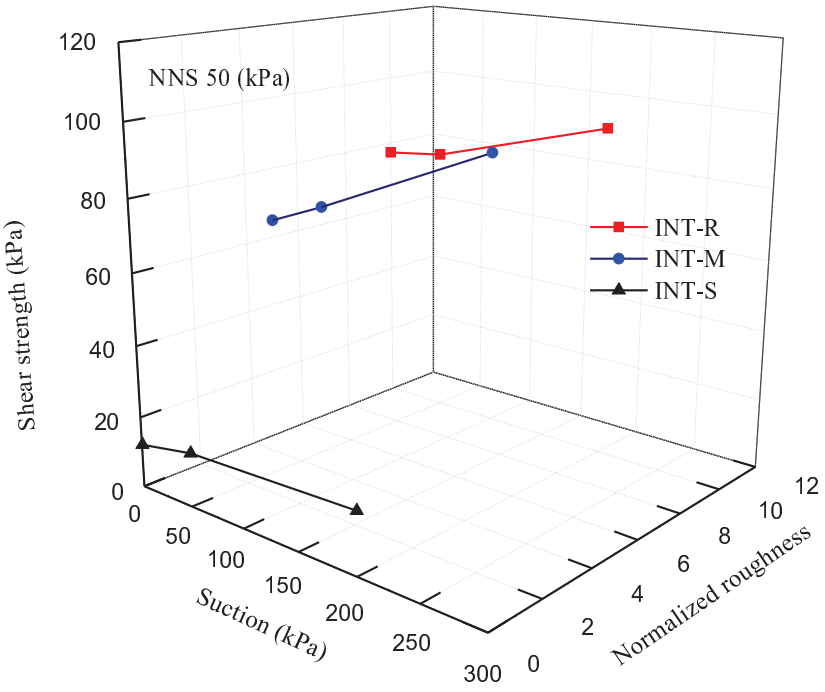

Figure 6.32 Variation of interface shear strength with respect to matric suction and normalized counterface roughness at constant net normal stress of 50 kPa.

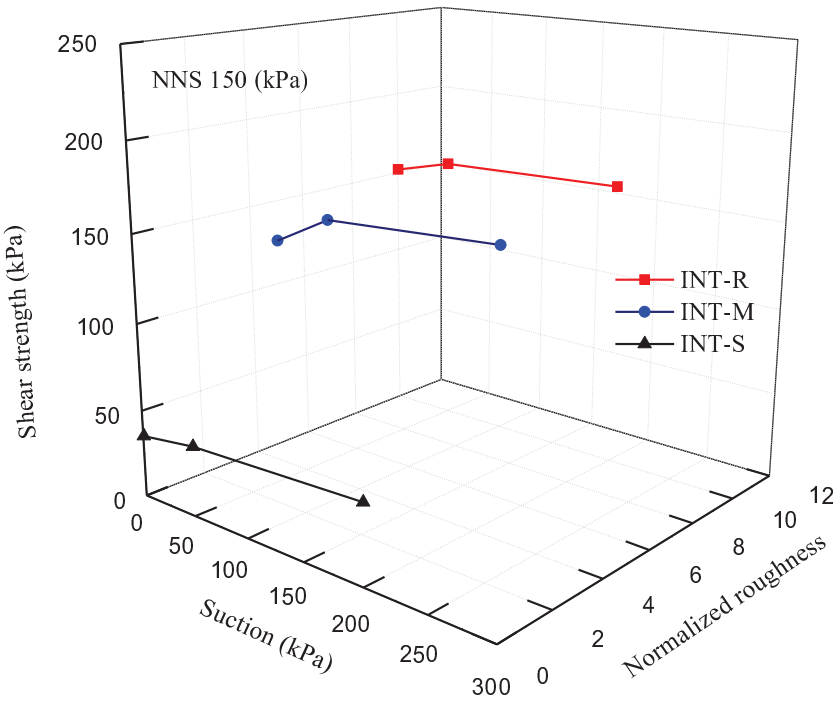

Figure 6.33 Variation of interface shear strength with respect to matric suction and normalized counterface roughness at constant net normal stress of 150 kPa.

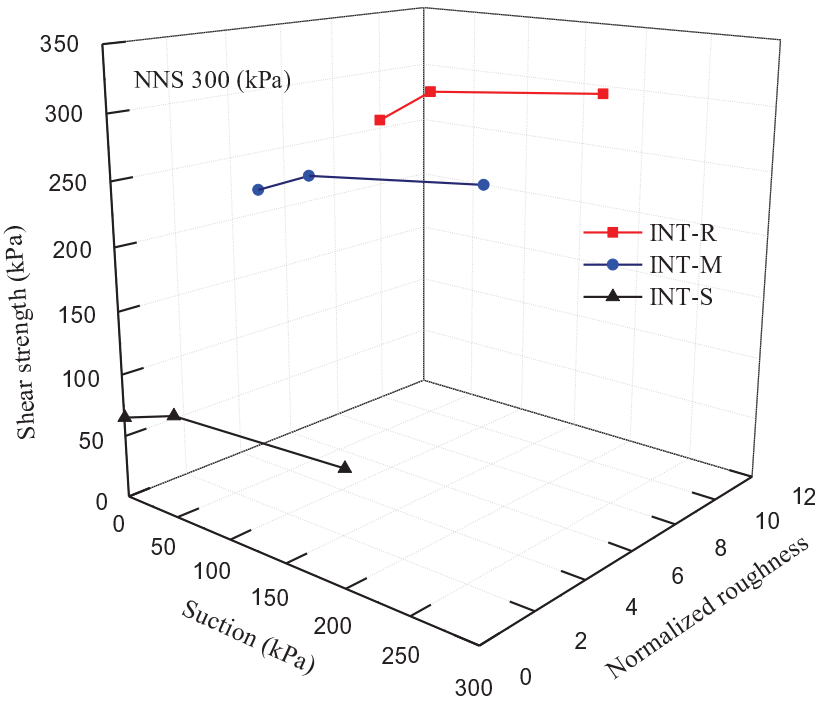

Figure 6.34 Variation of interface shear strength with respect to matric suction and normalized counterface roughness at constant net normal stress of 300 kPa.

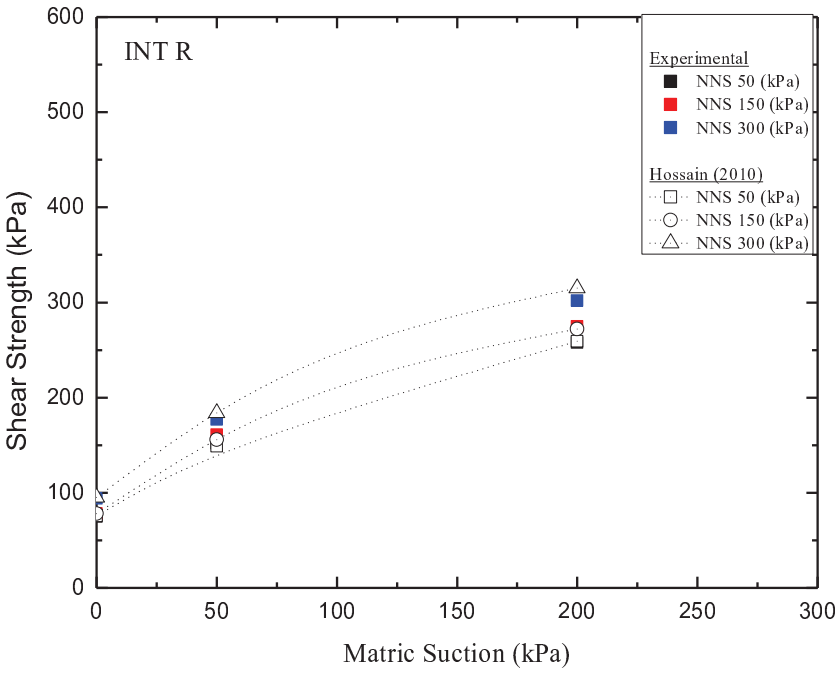

Figure 6.35 Comparison between experimental interface shear strength data for INT-R and analytical results obtained from the Hossain (2010) model.

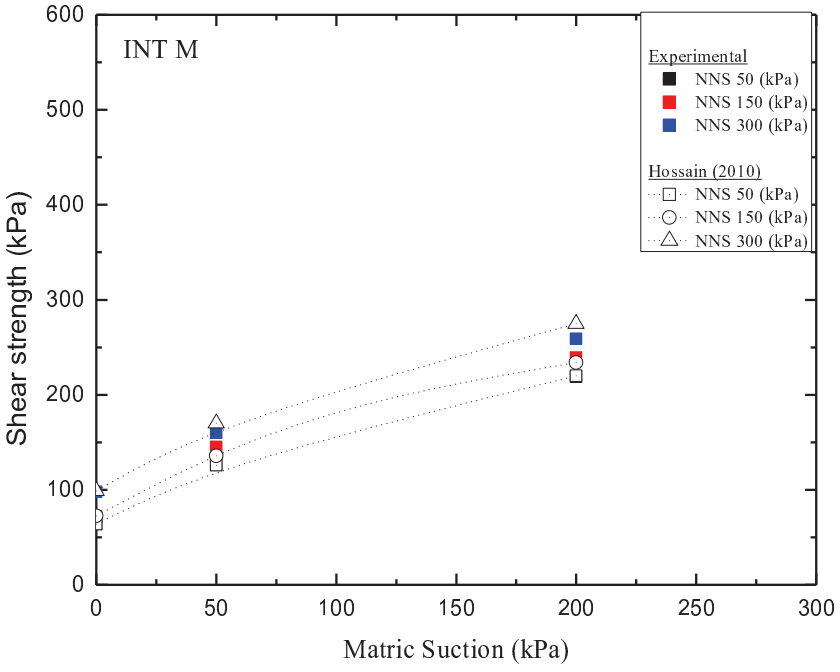

Figure 6.36 Comparison between experimental interface shear strength data for INT-M and analytical results obtained from the Hossain (2010) model.

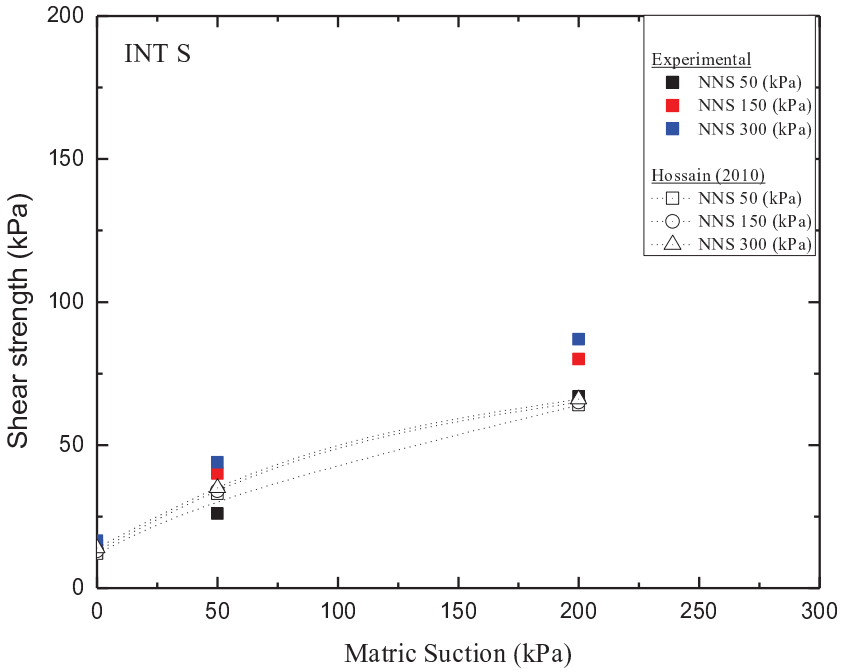

Figure 6.37 Comparison between experimental interface shear strength data for INT-S and analytical results obtained from the Hossain (2010) model.

Chapter 7

PULLOUT TEST RESULTS AND INTERPRETATIONS

7.1 INTRODUCTION

It is known that suction influences the soil behavior and may also have an influence on the interface behavior of pile foundations. The uplift resistance of the pile foundation depends on the side friction of the piles. Any uplift force acting on pile tends to induce tension in the pile. Pullout tests are frequently used to examine the interface behavior soil and a tension pile (or soil nail). As discussed in Chapter 2, two of the important factors that influence the interface behavior of piles include surface roughness and water content, and other being the mean particle size diameter. It is noted that pullout tests are not elementary tests and the data obtained from these test is indirect and needs careful interpretation. Unfortunately, there is a lack of literature regarding the interface behavior of tension piles in unsaturated soils. To investigate the influence of counterface roughness and degree of saturation several pullout test were performed on using two FBG sensored model piles (rough and smooth) at soil water content. Furthermore, to measure the skin friction and axial strain, FBG sensor were employed and uniformly mounted on the surface of each model pile in axial direction. The measured strain values are used to calculate the skin friction and axial strain of model piles. The experimental shear stress obtained by using the load cell is also presented and

discussed along with the shear stress obtained by FBG sensors for both the model piles (smooth and rough). Furthermore, the results and interpretation of the variation of average shear stress along section model pile obtained by using FBG are presented and discussed elaborately.

7.2 PULLOUT TEST RESULTS AND INTERPRETATIONS

The experiments concentrate on evaluating the effect of the water content of soil and the surface roughness of model piles on the shear strength of the model piles. A total of six pullout tests, for smooth and rough model piles, were performed in soils corresponding to different water contents. Table 7.1 lists the schedule of pullout test conducted using CDG soil. The test data obtained by FBG during the pullout period was used to calculate the axial strain and shear stress in the pile, can be expressed by Eq. (7.1) and Eq. (7.2). The test results obtained are presented and discussed in the following sections.

$$\varepsilon_{iavg} = \frac{\varepsilon_i + \varepsilon_i^{'}}{2} \tag{7.1}$$

$$S_i = \frac{\varepsilon_i - \varepsilon_i'}{2} \tag{7.2}$$

where, ε_{iavg} is the strain measured at *i*th point, $\varepsilon_i, \varepsilon_i'$ are strains measured by F1 and F4 (see Fig. 3.21) respectively, and S_i is the shear stress at *i*th point along the length of pile.

7.2.1 INFLUENCE OF WATER CONTENT ON THE PULL-OUT RESISTANCE OF SMOOTH AND ROUGH PILES

Figs. 7.1-7.3 show the variation of suction versus horizontal displacement for during the pullout test of model pile for rough and smooth piles at different water contents. It is noted that there is a slight increases in suction as the horizontal displacement increases. This might be due to any rupture or crack in the contractile skin during the pullout process which results in draining out of water from the ruptured areas. As the contractile skin ruptures water moves to adjoining areas as a result the suction near the interface increases marginally. Also, it is noted that suction change of rough model pile is greater than that of the smooth model pile. Fig. 7.4 presents the water of content of soil specimens before the start of the test and after the completion of the test. The change in water content of the soil is small (about 0.2-0.25%).

Fig. 7.5 and Fig. 7.6 depict the shear stress of the smooth and rough model pile respectively at different water contents, obtained by the loadcell during the pullout of the model piles. From the test results following important observations can be made:

- It is evident that the water content has significant influence over the pullout resistance of the model pile. The average shear stress decreases with an increase in soil water content. This shows that that as the soil tends to be unsaturated, the interface becomes stronger. This observation is in good agreement with the observation from the interface test results and the findings by Hamid & Miller (2009).

- From the curves of variation of shear stress with horizontal displacement for smooth pile, typical stick-slip phenomenon is evidenced for all the water contents after reaching the peak shear stress value. In other words, after reaching the peak

shear stress value no gain or loss in the shear stress is noted. This is a typical interface behavior, and exists particularly in interface having smooth counterface surface. It is mainly due to typical boundary conditions and reduced friction resistance prevailing the interface shearing plane. These results match very well with the findings reported in the literature (eg., Yoshimi and Kishida 1981)

- The post peak shear stress for higher degree of saturation (R_{15} and $R_{16.5}$) appears to be nearly constant and is not affected after achieving the peak shear stress. Whereas, at lower degree of saturation ($R_{13.5}$), the post peak shear stress seems to be influenced by water content and it decreases slightly after reaching the peak value. In other words, a partial softening behavior is observed at a lower degree of saturation (higher suction). This observation corroborates with the findings from the interface direct shear test results reported in previous chapter.

- The comparison of results for rough and smooth piles shows that the interface shear resistance is considerably influenced by the variation in counterface roughness at all the water contents. Interestingly it is noted that, the difference in gain or loss in the interface shear resistance of piles (smooth and rough) is more when the soil poses lower degree of saturation (higher soil suction). However the difference between the pull out resistance of smooth and rough pile reduces as the degree of saturation increases.

7.2.2 INFLUENCE OF SURFACE ROUGHNESS ON THE AXIAL STRAIN OF THE MODEL PILES

Fig. 7.7 and Fig. 7.8 show the comparisons of axial strains measured for smooth and rough piles respectively, using FBG sensors during the pullout test at a water content of

(a) 13.5 % (b) 15% and (c) 16.5 %. ε_1 , ε_2 and ε_3 indicates the average axial micro strains at different location obtained from the F1, F2 and F3, respectively (refer Fig. 3.21). Some important observations noted from the test results are presented and discussed as follows:

- The axial strain induced in the piles is noted to be significantly influenced by the counterface surface roughness. For constant water content, the axial strain induced in model pile having a rough counterface is noted to be greater than the smooth counterface. This difference in the axial deformation of the pile can be attributed to the counterface roughness.

- The soil water content affects the axial strain induced in the pile, irrespective of the counterface roughness. However, it is observed that as the degree of saturation increases the axial strain in the pile decreases and thereby possibly minimizing the influence of surface roughness in inducing axial strain in pile.

- The axial strain induced in the model pile (rough and smooth) is not uniform throughout the length of the pile. It is noted that the axial strain induced in FBG sensors is greatest for F1 and least for F3 , irrespective of the surface roughness and water content. It shows that radial stress acting on F1 is greater than F3. As the pile is pulled out the maximum load is transferred or resisted by the interface zone near F1 as compared to F3. In other words, the measured axial force at the upper part of model piles is greater that the measured axial force at lower part of the pile. Thereby the soil at the upper part of the model pile yields first and subsequently load is transferred to the base of the pile.

- It is noted that the difference of axial strains measured by the first FBG strain sensor and second FBG strain sensors, irrespective of counterface roughness, is much bigger than that between the second and third FBG sensors. In other words, this shows that variation of skin friction is not linear which is in good agreement with the test results from Pei et al. (2012a and 2012b).

7.2.3 COMPARISONS OF AVERAGE SHEAR STRESSES OBTAINED FROM FBG SENSORS

Fig 7.9 and Fig 7.10 depict the comparisons of average shear stress values, for smooth and rough piles respectively, obtained from axial strain values measured by FBG sensors at different water content of (a) 13.5 % (b) 15% and (c) 16.5 %. It must be noted that SC-1 represents the average shear stress between the F1 and F2 , while SC-2 represents the average shear stress between the F2 and F3. Generally, the curves of variation of average shear stress with horizontal displacement for smooth and rough piles are similar nature. It is noted that the average shear stress induced in the pile is dependent on the soil water content and the difference between SC-1 and SC-2 is inversely proportional to the soil water content. This reinstates the findings described earlier; that the axial strain induced in the piles is not uniform. Rough pile is noted to have a greater shear stress value as compared to the smooth pile. The results reaffirms that both soil water and roughness affects the interface behavior of tension piles. However, the axial strain and shear stress distribution in the pile is non-linear and is also dependent on the matric suction of the soil. Finally, it can be stated that it is worth to examine the interface behavior of piles in unsaturated by employing FBG sensors. However, further studies are recommended to ascertain the performance of FBG sensors in unsaturated soil to verify the non-linearity of axial strain, shear stress and skin friction in different types of pile.

7.3 SUMMARY

This chapter illustrates the influence of soil water content and surface roughness of model pile during the pullout test. The FBG sensors were used to measure skin friction and axial strain on the model piles in pullout tests. Based on the test results, the influences of water content and surface roughness on the skin friction of the model piles are presented and discussed. The next chapter will present and discuss the important findings and conclusion of soil, soil-interface direct shear test and pull out tests along with the recommendations for future study in this field.

Table 7.1 Parameter of steel bar and soil mass

Test	Type of model piles	Diameter (mm)	Water content (%)	Compaction Degree (%)
$S_{13.5}$	Smooth	20	13.5	95
S_{15}	Smooth	20	15	95
$S_{16.5}$	Smooth	20	16.5	95
R_{13}	Rough	20	13.5	95
R_{15}	Rough	20	15	95
$R_{16.5}$	Rough	20	16.5	95

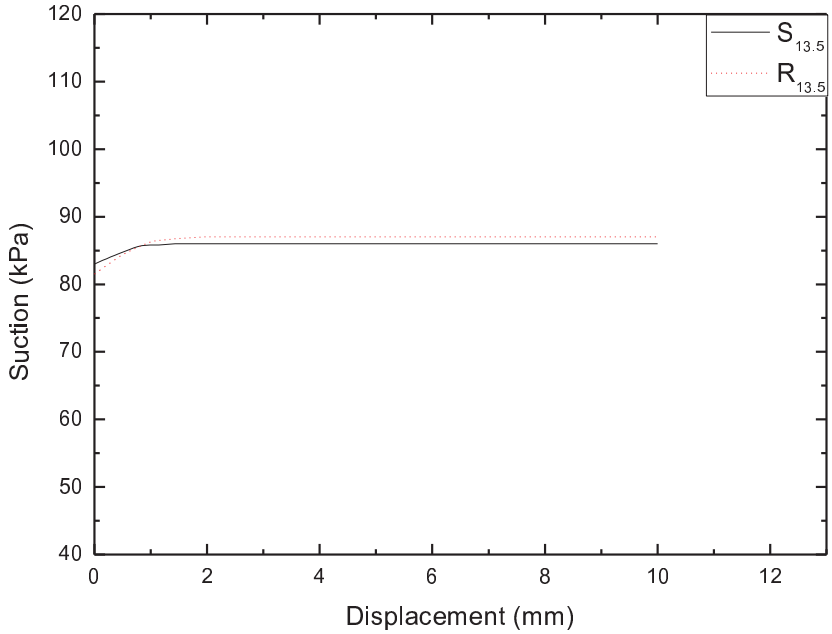

Figure 7.1 Curves for suction versus horizontal displacement for $S_{13.5}$ and $R_{13.5}$ during the pullout test of model pile

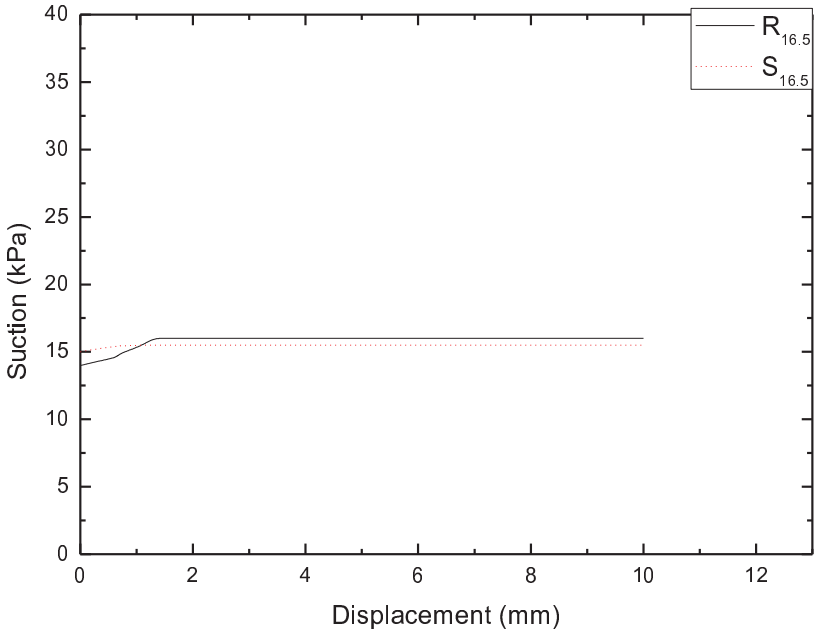

Figure 7.2 Curves for suction versus horizontal displacement for S_{15} and R_{15} during the pullout test of model pile

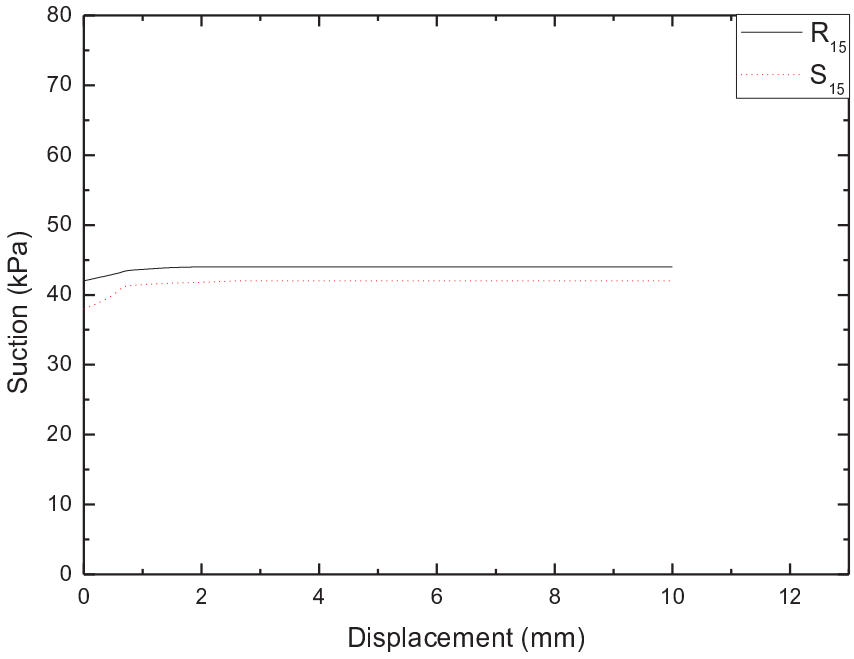

Figure 7.3 Curves for suction versus horizontal displacement for $S_{16.5}$ and $R_{16.5}$ during the pullout test of model pile

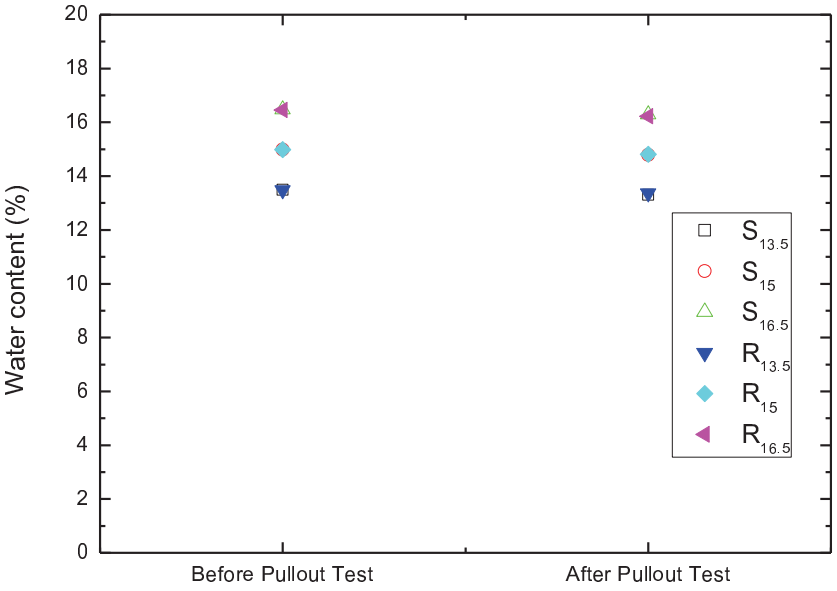

Figure 7.4 Water content of soil specimen before and after test

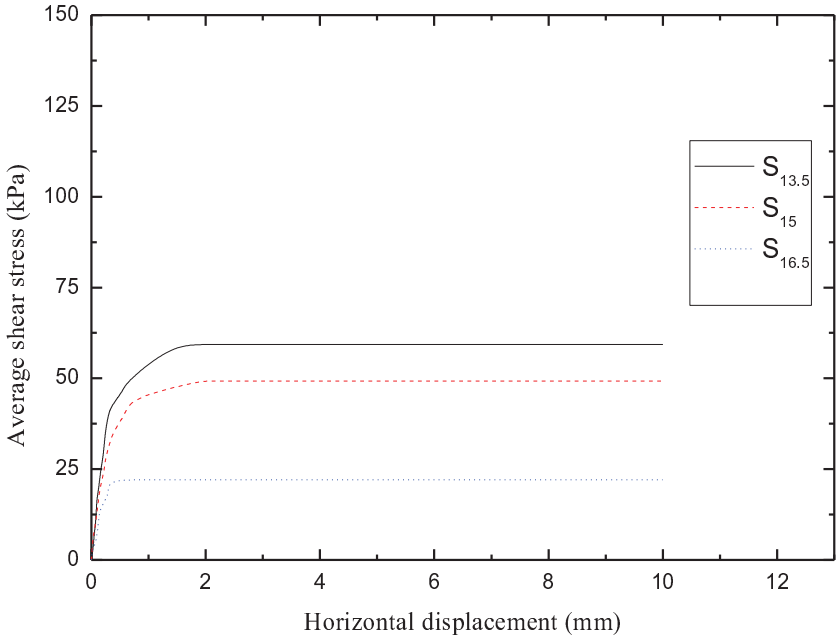

Figure 7.5 Shear stress of the smooth model pile regarding pullout displacement in soils at different water contents

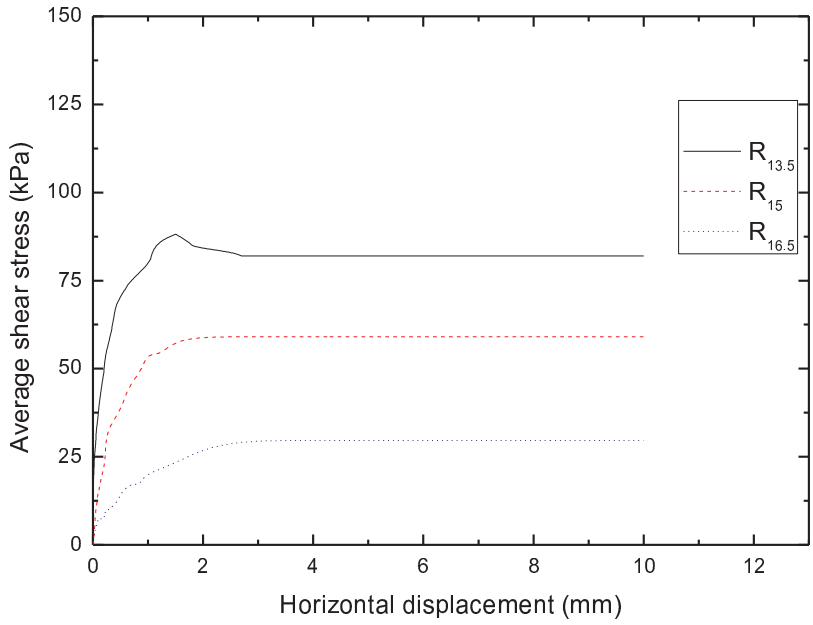

Figure 7.6 Average shear stress of rough model pile *vs.* displacement in soil mass with different water contents

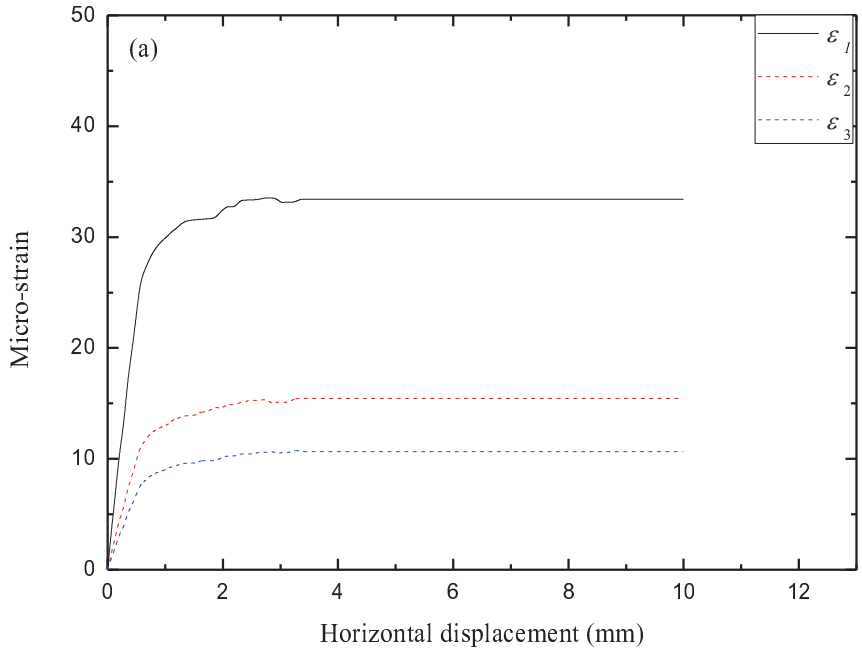

(a) Comparisons of axial strains measured by FBGs on the smooth model pile in soil at 13.5% water content

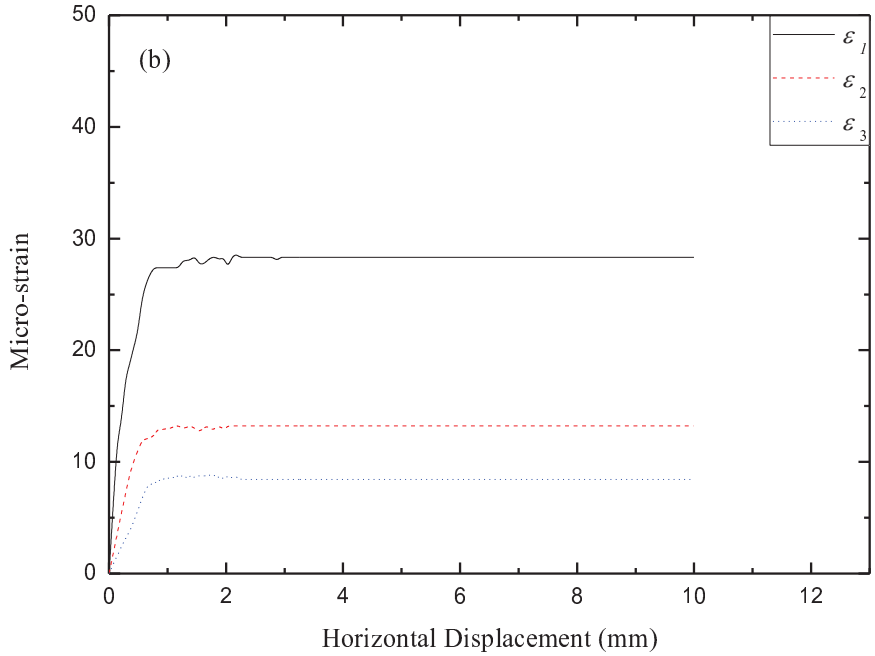

(b) Comparisons of axial strains measured by FBGs on the smooth model pile in soil at 15% water content

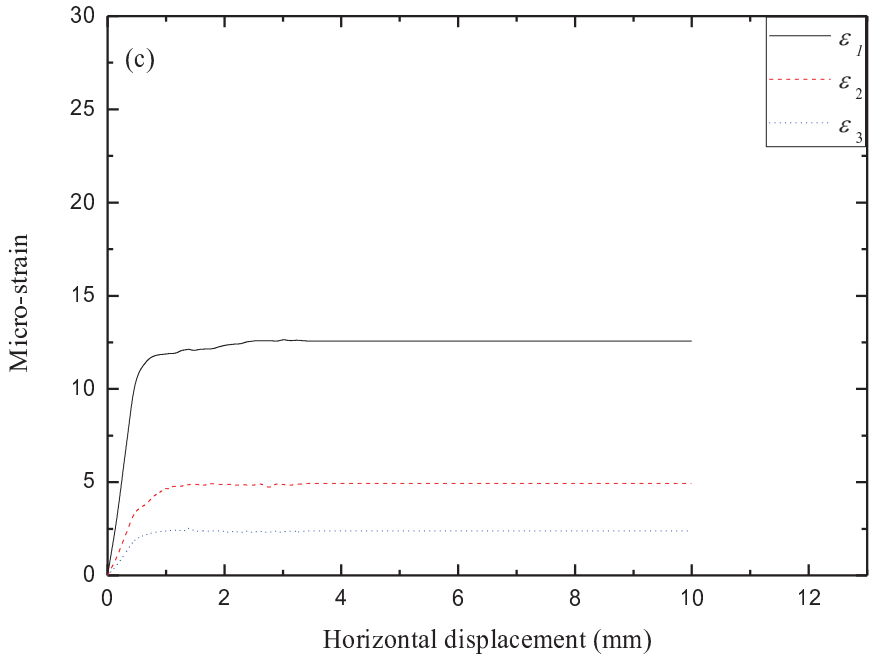

(c) Comparisons of axial strains measured by FBGs on the smooth model pile in soil at 16.5% water content

Figure 7.7 Comparisons of measured axial strains by FBG sensors for smooth model pile in soils at different water content

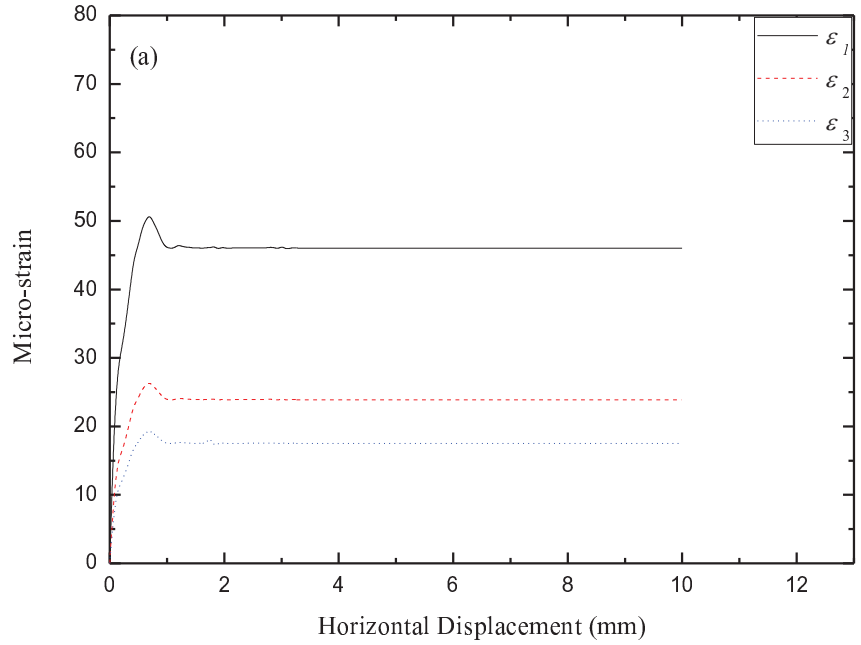

(a) Comparisons of axial strains measured by FBGs on the rough model pile for soil at 13.5% water content

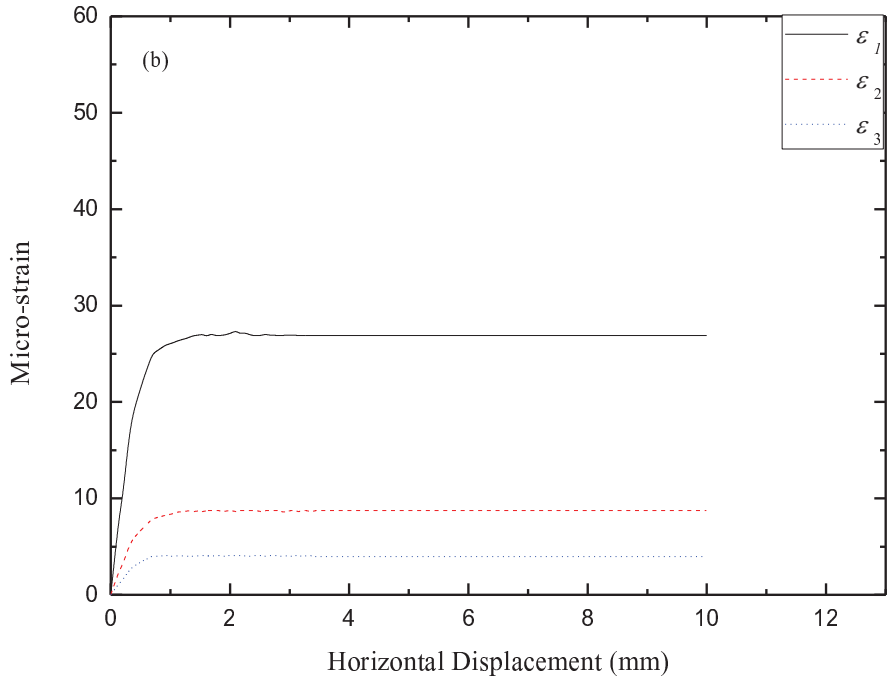

(b) Comparisons of axial strains measured by FBGs on the rough model pile for soil at 15% water content

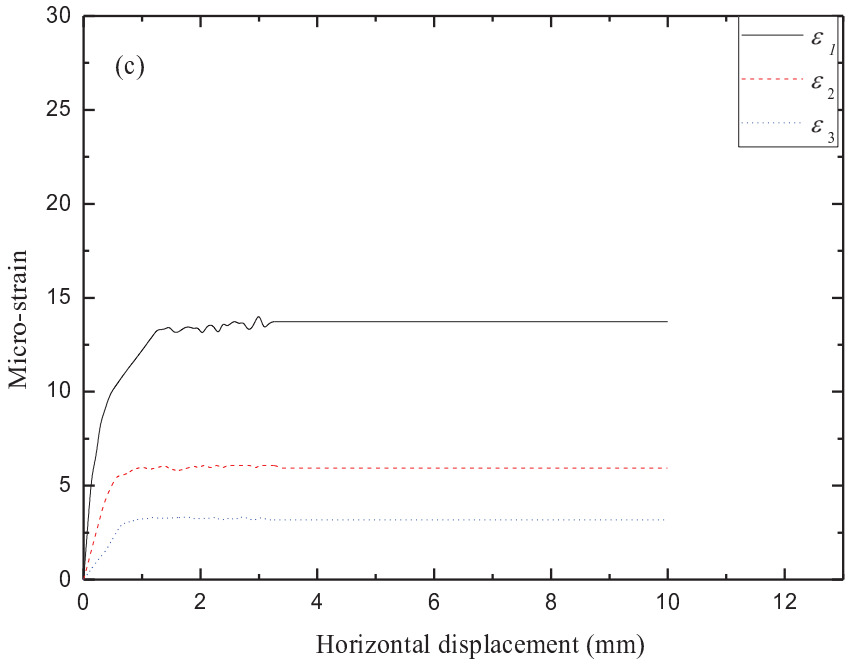

(c) Comparisons of axial strains measured by FBGs on the rough model pile for soil at 16.5% water content

Figure 7.8 Comparisons of measured axial strains by FBG sensors for rough model pile in soils at different water content

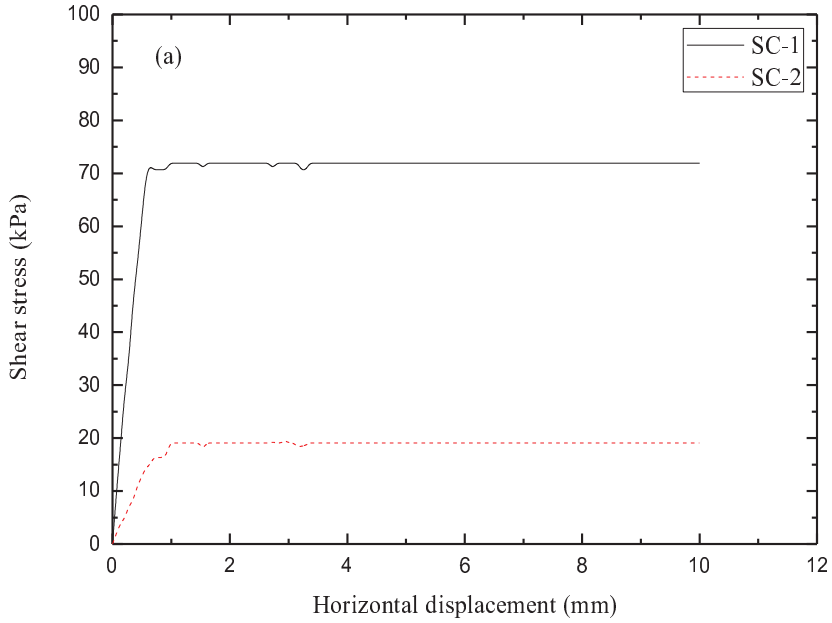

(a) at 13.5% water content

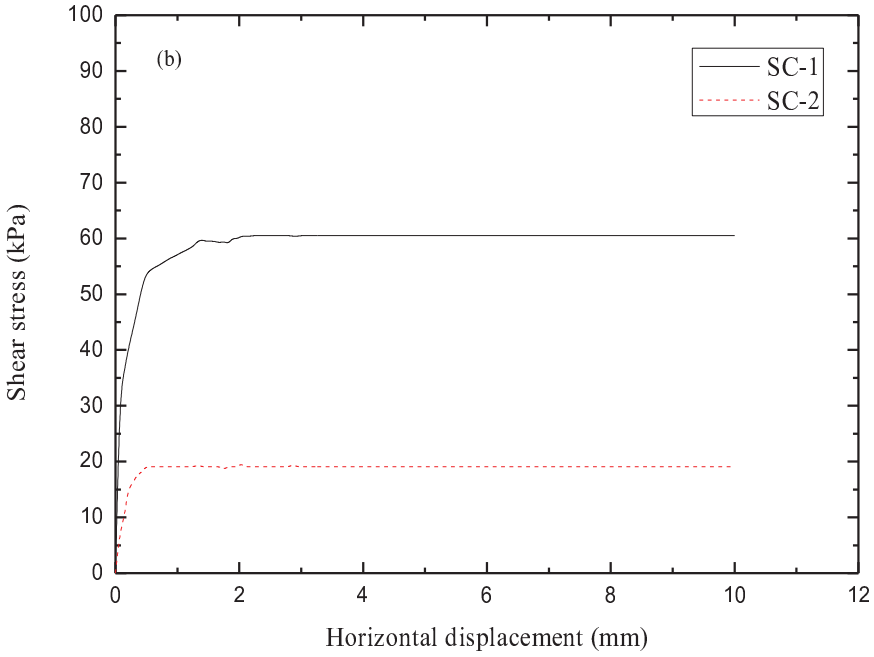

(b) at 15% water content

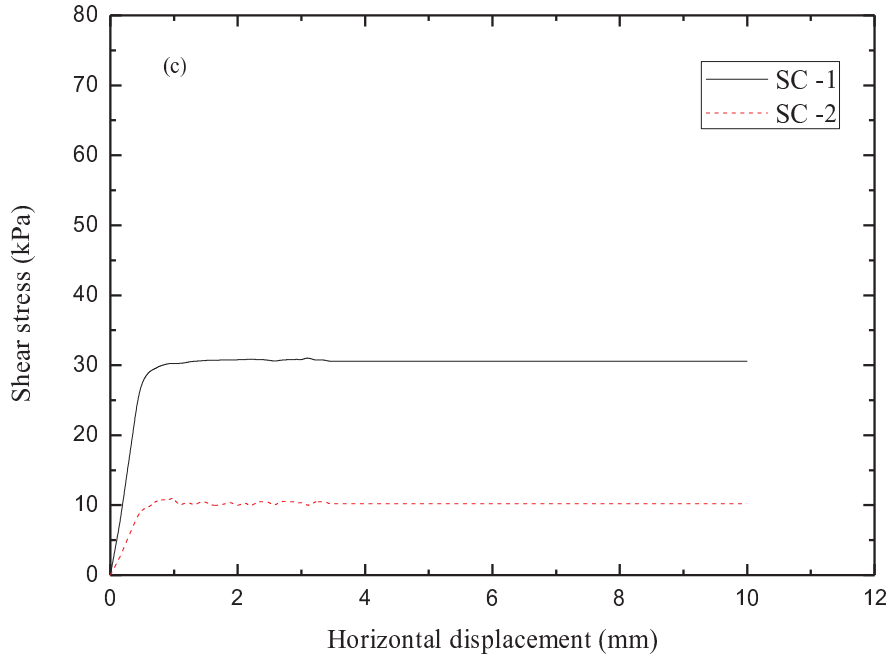

(c) at 16.5% water content

Figure 7.9 Comparisons of measured average shear stress calculated from strain values by FBGs on the smooth model pile in soils at different water contents

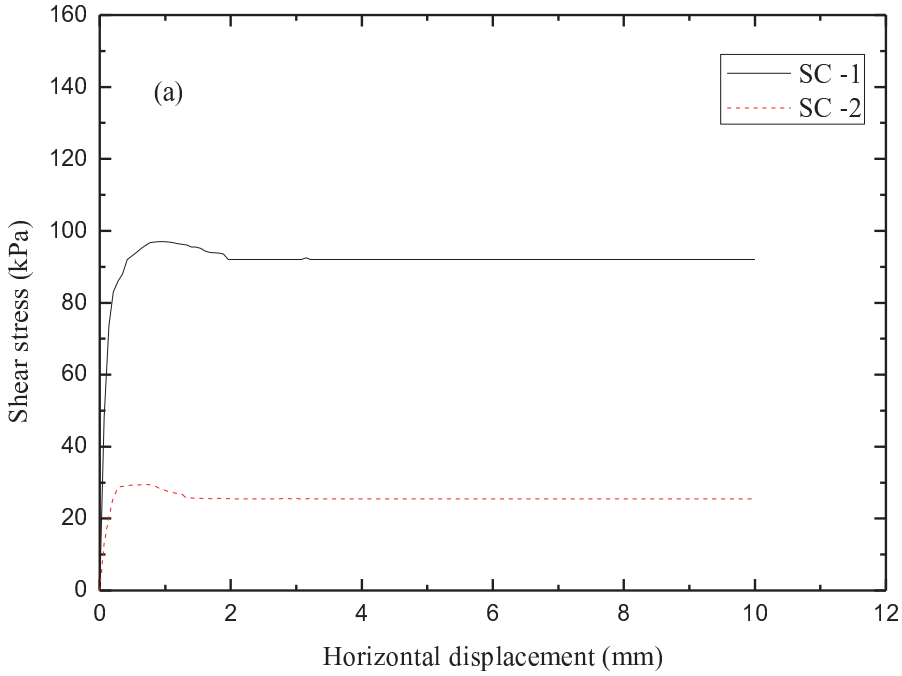

(a) at 13.5% water content

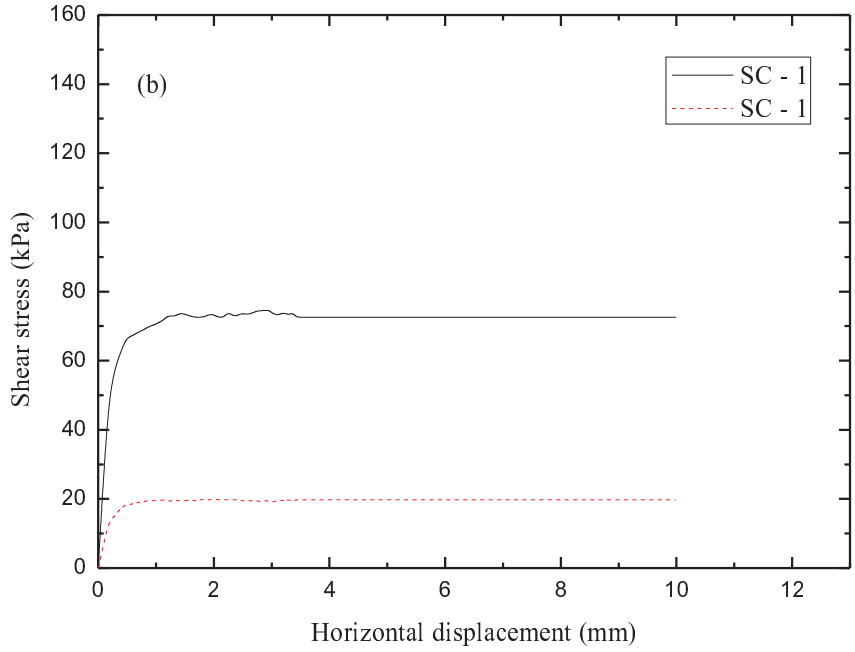

(b) at 15% water content

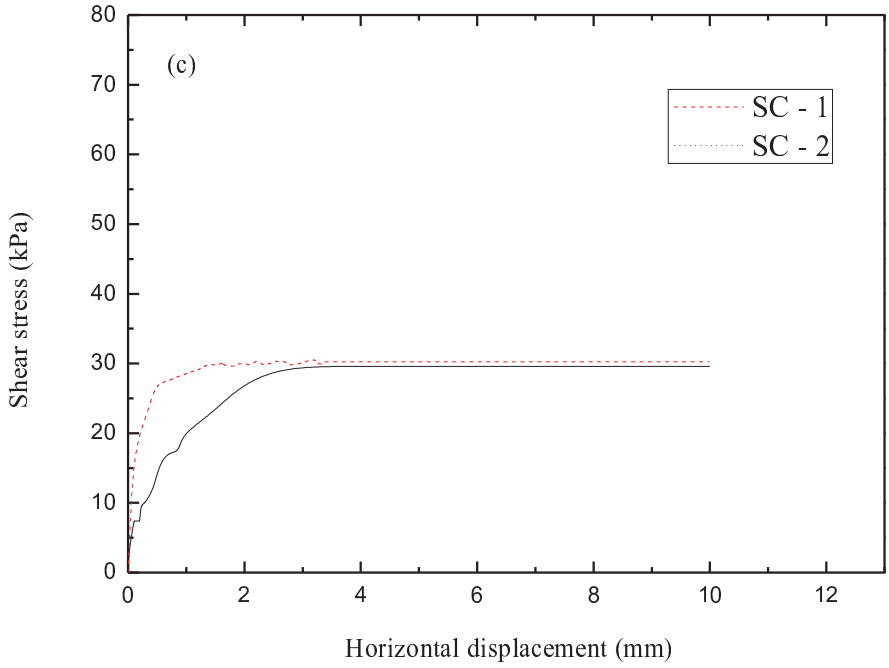

(c) at 16.5% water content

Figure 7.10 Comparisons of average shear stress calculated from strain values measured by FBGs on the rough model pile in soils at different water contents

Chapter 8

CONCLUSIONS AND RECOMMENDATIONS

A series of suction controlled single-staged consolidated drained direct shear tests have been conducted on completely decomposed granitic soil and soil-cement interface to investigate number of factors (viz, matric suction, net normal stress, shearing plane and counterface roughness) that may influence the behavior of soil and soil-steel interface. Also, the influence of counterface roughness and degree of saturation of the model pile was examined by conducting fibre bragg grating sensored model pile pullout test. The axial strain and skin friction model piles in a soil mass were determined by employing FBG sensors. Based on the experimental test results, their interpretation and discussion have been presented in the previous chapters. However, the main conclusions from this study are presented in the subsequent sections and followed by the recommendations for future research in the subject area.

8.1 CONCLUSIONS FROM INTERFACE SHEARING AT DIFFERENT SHEARING PLANES

A suction controlled direct shear device was suitably modified to include the provision of shearing soil-steel interface at different shearing planes. Cast in-situ interface was formed between soil and rough stainless steel counterface. The test data obtained from a series of suction controlled direct shear tests on completely decomposed granite (CDG)

soil and CDG soil-steel interface sheared at different planes and their interpretation are presented in Chapter 5. A special attention is paid to the influence of dilation on friction angle and shear strength under different suctions and net normal stresses. The experimental results are compared with an existing shear strength model that considers the influence of interface dilation on shear strength of unsaturated soils. Based on the discussion presented in Chapter 5 the following conclusions can be drawn:

- The shear strength characteristics of soil steel interface, sheared at different planes and soil, get significantly affected by the matric suction and net normal stress. Interface shear strength and soil shear strength are noted to increases with stress state variables. Matric suction play significant influencing role in determining the shear strength (both soil and interface) and any increase in the value of soil suction directly contribute to the increase in soil dilatancy. In other words, as the suction increases the capillary tension between soil grain particle increases which results the soil fabric to dilate and also contribute in change in shear strength. But the rate of change in shear strength with matric suction (or net normal stress) for all the three interfaces (INT-0, INT-1 and INT-2) and soil is non-linear.

- At lower suction and all the applied net normal stresses, a gentle hardening behavior is observed for the INT-0, INT1, INT-2 and the soil. Interface gains greater shear strength as compared to soil due to higher dilation in interface. At higher matric suction, it is noted that the net normal stress significantly influences the post peak shear strength. For all interfaces at net normal stress, considerable reduction in post peak shear strength is observed, while partial hardening stick-slip behavior is evidenced with an increase in net normal stress.

On the other hand, the soil gains higher peak shear strength value through dilation as compared to interface regardless of the applied net normal stress reaffirming that that net normal stress and matric suction significantly influences the shear behavior of interfaces and soil in a non linear way.

- The volume change behavior of all the interfaces and soil is also influenced by matric suction and net stress. A shear-compression is observed for soil under lower suction with higher net stress, and at saturated condition for all net stress. In contrast, a shear-dilation is observed for all the three interfaces with the increase of suction for particular net stresses. Apart from the stress state variables, the other important factor that influences the dilatancy potential of the interfaces is its plane of shearing. In other words the soil-steel interface dilatancy is directly proportional to the interface thickness.

- The critical shear failure plane that poses the minimum shear strength in noted to shift towards the counterface surface with an increase in matric suction increases. The interface with greater thickness (INT-2) gains higher strength as the suction increases reflecting that the critical shearing plane is dependent on the matric suction and gradually moves towards the counterface surface with an increase in suction.

- Interestingly, it is noted that the interface shear strength can be greater than the soil shear strength in saturated condition due to multiple factors, such as, interface counterface roughness, soil dilatancy, and different boundary conditions. In the case of soil shearing, the shearing plane is formed between soil-soil particle and the boundary conditions are in manner that the

rearrangement of particles is possible on either sides of the shearing plane. While for interface shearing, the shearing plane is formed between soil-steel counterfaces. During shearing the soil grain rolls over the counterface and rearrangement of soil particle takes place on soil side of the shearing plane resulting into greater dilatancy. As a result in saturated condition, the interface gains more shear strength as compared to soil (Hossain 2010).

- The shear strength envelope in the shear strength and the net normal stress space is almost linear. The apparent interface friction angle δ_{max} and adhesion intercept c_a increase with matric suction. The rate of increment of δ_{max} is greater in lower suction range (0 to 50 kPa) than higher suction range (200 kPa). A typical nonlinear suction envelope is observed for all the soil-steel interfaces and CDG soil within the applied suction range.

- The experimental shear strength data of soil and soil-steel interfaces matches well with the predicted shear strength values from the model proposed by Hossain (2010) using the SWRC at zero net normal stress considering the apparent friction angle.

8.2 CONCLUSIONS FROM INFLUENCE OF COUNTERFACE ROUGHNESS ON INTERFACE BEHAVIOR

The direct shear apparatus used for unsaturated soil and soil-steel interface shear test was employed for investigating the influence of counterface roughness on interface behavior. Cast in-situ interface was formed between the soil and steel counterface with different counterface roughness (i.e, INT-R, INT-M and INT-S). The experimental test

results and their interpretations are presented in Chapter 6. Similar to the interface test sheared at different planes and CDG soil tests, a special attention is paid on the influence of counterface roughness on the interface dilatancy and strength. The interface strength for different counterface roughness is compared with the strength of the CDG soil. The experimental results are compared with an existing shear strength model. The following conclusions can be drawn based on the discussion presented in the chapter 6:

- Matric suction and net normal stress significantly influence the hardening-softening behavior of soil-steel interfaces and soil. However, the degree of influence varies depending on the counterface roughness. At lower matric suction and all the applied net normal stresses, the three interfaces and the soil show a gentle hardening behavior. However, with an increase in net normal stress at lower suction, stick slip is observed for smooth interface. The shear compression is observed to increase with net normal stress for all the curves of interfaces and soil. As the suction increases and the soil tend to be unsaturated and the influence of net normal stress on the hardening softening behavior becomes more profound. For higher net normal stress value a stick slip behavior is observed for all the interfaces irrespective of the counterface roughness, whereas at lower net normal stresses the hardening softening behavior is evidenced.

- Counterface roughness significantly influences the shear behavior and interface shear strength for particular matric suction and net normal stress. The interface with greater counterface roughness (INT-R) gains a higher peak shear strength value due to larger soil dilation, whereas interface with smooth counterface (INT-S) gains less due to stick–slip phenomenon. The change in interface shear

strength for specific stress state variables and different counterface roughness is non linear.

- The interface shear strength envelope in the shear strength and the net normal stress space for all the three interfaces are almost linear and similar to that for CDG soil. The apparent interface friction angle $\delta_{\max}$ and adhesion intercept c_a increase with matric suction. As compared to the smooth interface, the apparent interface friction angles for rough interfaces at different suctions are closer to the values of apparent friction angles of soil for the particular suctions. The variation of δ^b angle is inversely proportional to the matric suction. Similar to CDG soil, a typical nonlinear suction envelope is observed soil–steel interface within the applied suction range of 0 to 200 kPa.

- The interface dilatancy increases with matric suction and counterface roughness. The peak dilatancy for interfaces is observed under higher suctions and lower net normal stress. The dilatancy decreases with an increase in the value of net normal stress. As compared to the INT-M and INT-S, greater interface dilation angle is obtained for INT-R at higher suction with lower net normal stress, and lower dilation is observed at higher net normal stress with lower suction, and at saturated condition. However, at higher suction levels, the interface dilation angle, irrespective of the counterface roughness, is lower compared to soil dilation angle.

- Hossain (2010) has proposed a modified model that to predict the unsaturated interface shear strength of the soil-cement grout. To testify and validate the suitability of the model in predicting the soil-steel interface shear strength, the

experimental interface shear strength data of the three counterfaces (INT-R, INT-M and INT-S) are compared with the prediction of the modified model. For a given matric suction and net normal stresses, the interface shear strength predicted from the modified model matches closely with the experimental shear strength data for rough interfaces (INT-R and INT-M). Nonetheless, the analytical model agrees partially for smooth interface especially under lower net normal stress. This indicates that interface dilation especially in rough interfaces has significant influence on apparent friction angle, and thereby on interface shear strength.

8.3 CONCLUSIONS FROM PULLOUT TEST RESULTS AND INTERPRETATIONS

A series of pullout tests have been conducted to examine the pullout interface behavior soil and a tension pile (or soil nail). The experimental shear stress values obtained are presented and discussed in previous chapter. A special attention is paid to investigate the influence of pile counterface roughness and degree of soil saturation on the pullout behavior, skin friction and axial strain in pile using FBG sensors. The following conclusions can be drawn based on the discussion presented in the previous chapter:

- The water content has significant influence pullout resistance of the model pile. The average shear stress decreases with an increase in soil water content and as the soil renders to be unsaturated the interface gains shear strength. This observation correlates well with the experimental results from the interface direct shear test.

- Similar to the interface test for smooth counterface, after reaching the peak

shear stress value, a typical stick-slip phenomenon is observed for smooth pile under all soil water contents. This is a typical interface behavior is mainly due to typical boundary conditions at the interface shearing plane and reduced frictional resistance. Whereas, for rough pile a partial softening behavior is observed at a lower degree of saturation (higher suction) and is consistent with the findings from the interface direct shear test results reported in chapter 6.

- It is obvious that the pullout resistance of the model pile is greatly influenced by the variation in counterface roughness at all the water contents. However, the difference in variation of the interface shear resistance of piles (smooth and rough) is more when the soil poses lower degree of saturation (higher soil suction). The impact of counterface roughness on the pullout resistance and skin friction reduces as the soil tends to be saturated (low suction).

- The axial strain induced in the piles is noted be significantly influenced by the counterface surface roughness. The axial strain induced in the model pile increases with pile counterface roughness for a specific degree of saturation.

- The degree of soil saturation has a noteworthy influence on the axial strain induced in the pile. However, it is observed that as the degree of saturation increases the axial strain in the pile decreases and thereby possibly minimizing the influence of surface roughness in inducing axial strain in pile. Also, the axial strain induced in the model pile is not uniform throughout the length of the pile. The axial force at the upper end of model piles is greater as compared to the axial force at lower end indicates that the soil near the upper end of the

model pile yields first and subsequently load is transferred to the base of the pile .

- For any specific soil water content and pile counterface roughness, the difference of axial strains measured by the FBG strain sensor installed at different locations on the piles indicates that the variation of skin friction is non linear throughout the length of the pile.

- It is noted that the average shear stress induced in the pile is dependent on the soil water content and the difference between SC-1 and SC-2 is inversely proportional to the soil water content. This reaffirms the findings described earlier that during pullout non uniform axial strain is induced in the piles.

- The results show that it is convenient and worth to investigate the pullout behavior of tension piles in unsaturated soil by employing FBG sensors. Nonetheless, further research studies are recommended to ascertain its performance in unsaturated soil and also to verify the non-linearity of axial strain, shear stress and skin friction in different types of pile.

8.4 RECOMMENDATIONS FOR FUTURE RESEARCH

- In the present study, the maximum R_n value used for all the interface direct shear testing was below to or equal 10. It shall be valuable to investigate the behavior of unsaturated soil and interface by using maximum R_n above 10.

- The preselected counterface roughness for interface testing sheared at different planes was R_n =10 and the maximum interface thickness selected was 2 mm. Further, studies should be conducted to examine the critical shear plane behavior by varying the interface layer thickness above 2 mm.

- In this study, to form the cast in-situ and non degrading interface, steel was used to form the counterface for the soil. Other types of materials like precast concrete, wood and geosynthetics materials can be used to form an interface and study different geotechnical aspects of an interface.

- For the present study, CDG soil was compacted to a relative density of 95% of the maximum dry density. A range of different relative compactions and different type of soil can be used for future studies.

- Constant normal load concept was used in this study to investigate the interface behavior. It would be interesting to investigate the unsaturated interface behavior using constant normal stiffness approach.

- In the present study, the model pile pullout test was conducted by maintaining a constant the bulk water content of the soil in the testing apparatus. It would be quite prudent e to perform the model pile pullout test by controlling the soil suction soil.

- The pullout test was conducted by placing the cylindrical container horizontal to the ground surface and the gravitational force acting normal to the model pile. However, further studies can be conducted by keeping the cylinder vertical to the ground surface.

- Numerical simulation can be performed to investigate the behavior of CDG soil–steel interface and compared with the experimental data.

Appendix

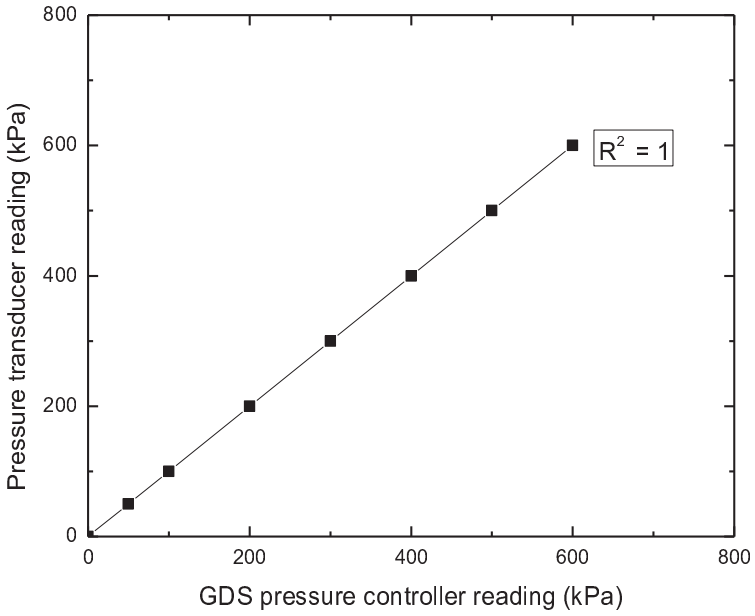

Figure 1 Calibration curve for the pore-water pressure transducer

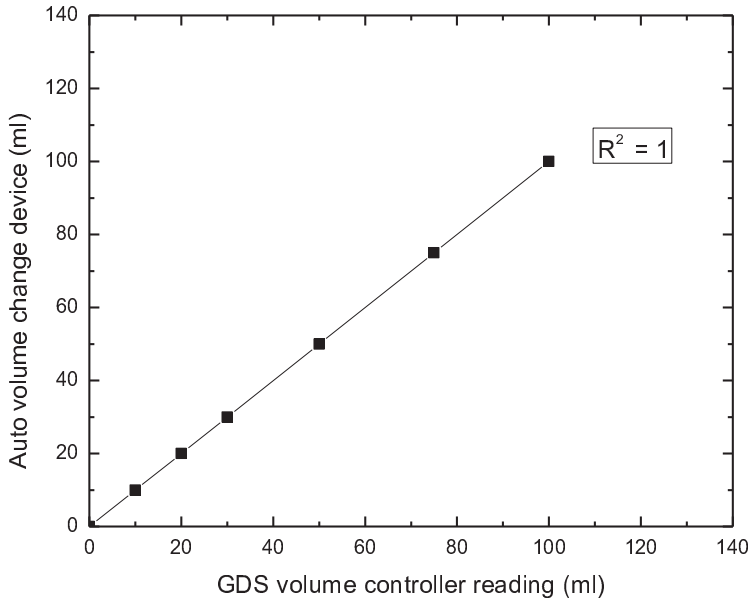

Figure 2 Calibration curve for the auto volume change (AVC) device

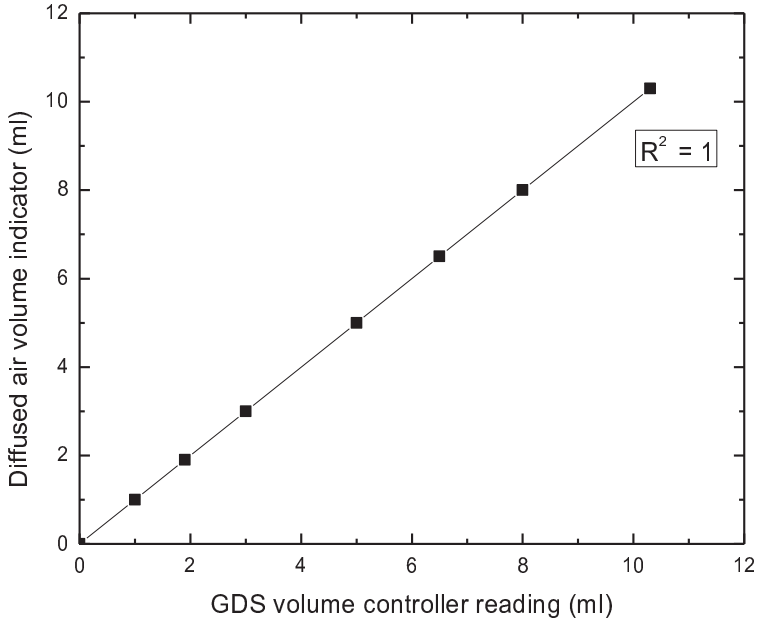

Figure 3 Calibration curve for the diffused air volume indicator (DAVI)

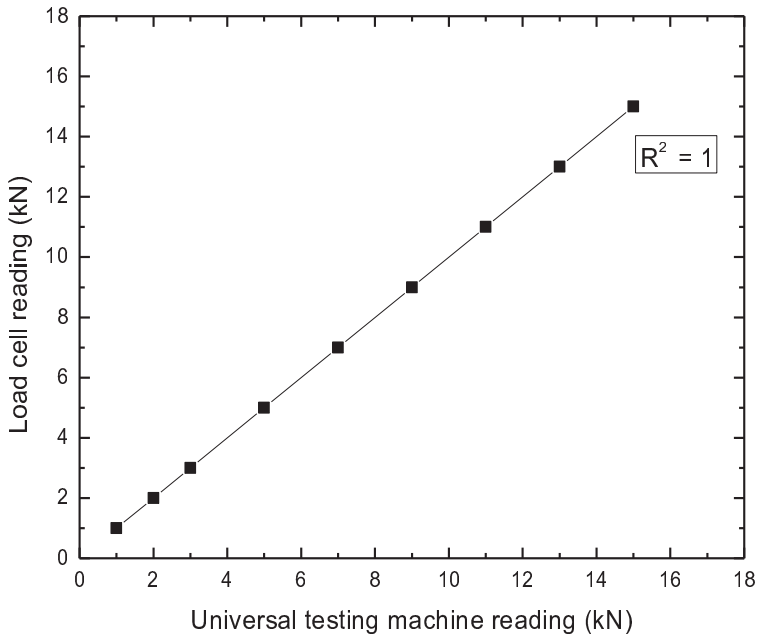

Figure 4 Calibration curve for the load cell for the MDSA

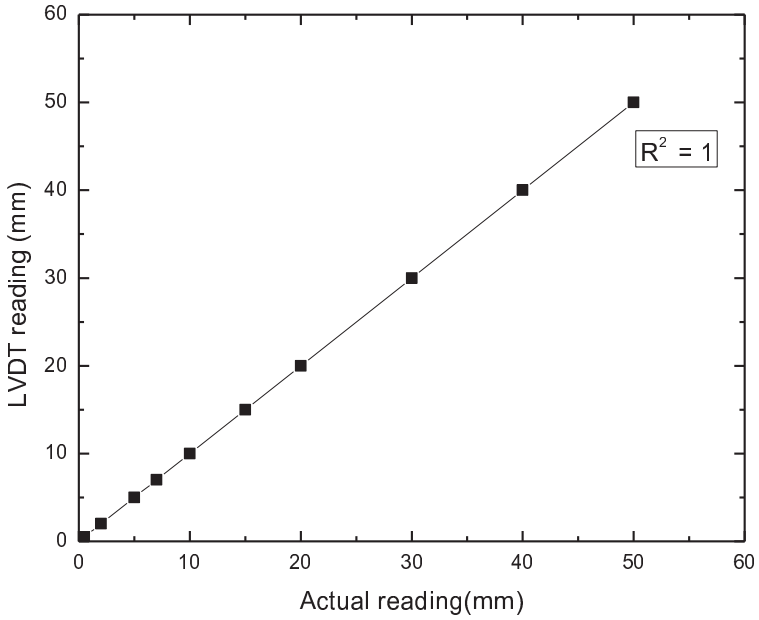

Figure 5 Calibration curve for the horizontal LVDT for the MDSA

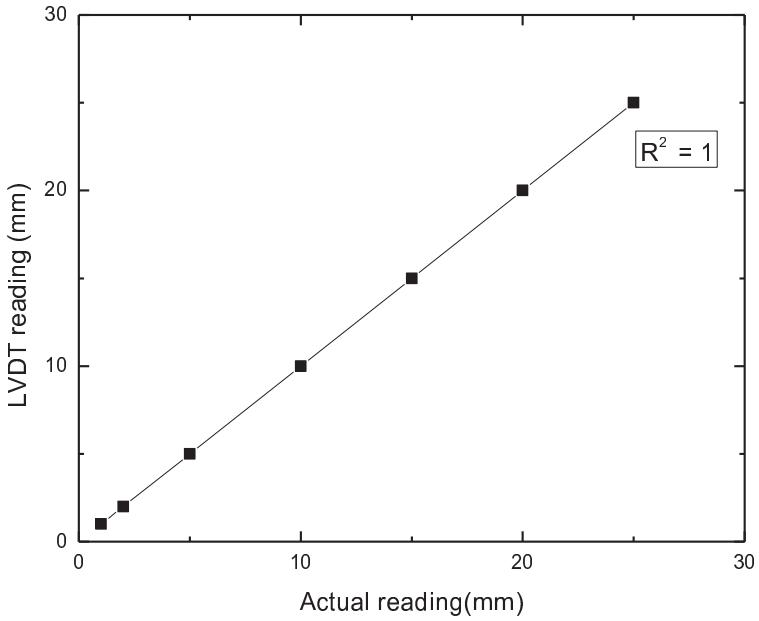

Figure 6 Calibration curve for the vertical LVDT for the MDSA

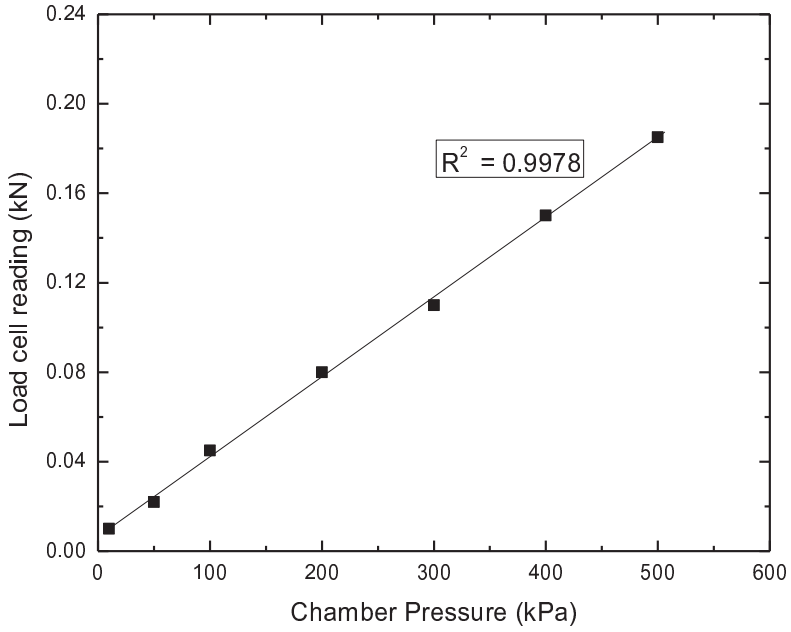

Figure 7 Correction on load cell reading for chamber pressure

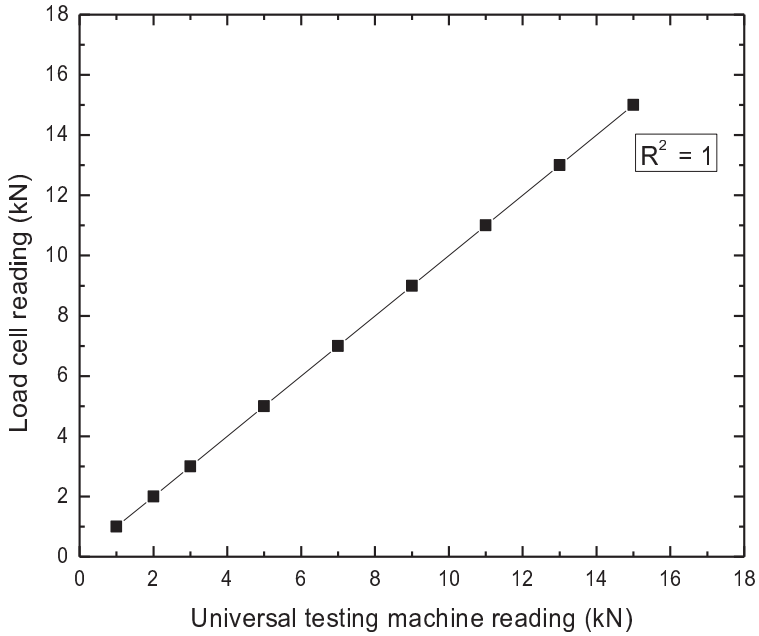

Figure 8 Calibration curve for load cell for the pullout test

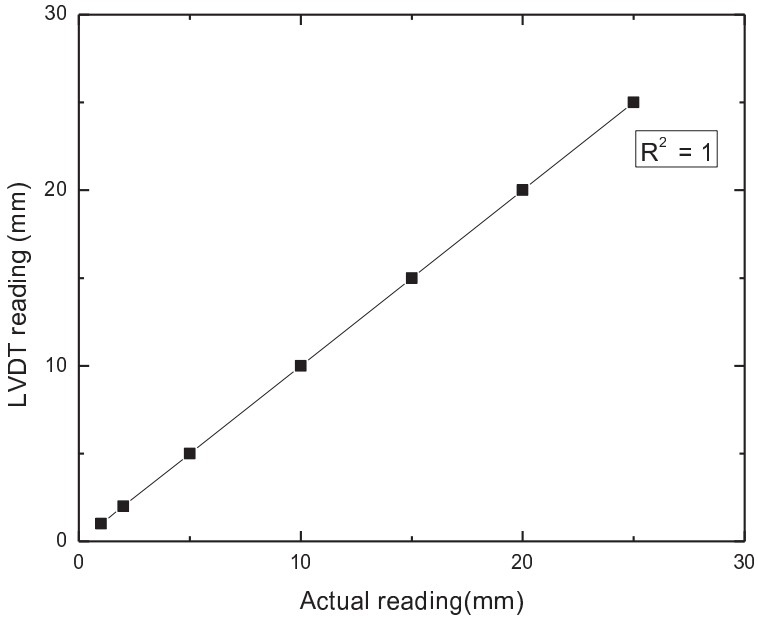

Figure 9 Calibration curve for LVDT for pullout test

REFERENCES

Acar, Y. B., Durgunoglu, H. T., and Tumay, M. T. (1982). Interface properties of sand. Journal of Geotechnical Engineering, 108(4): 648-654.

Aitchison, G. D., and Donald, I. B. (1956). Effective stresses in unsaturated soils. In Proceedings of the Australia-New Zealand Conf. on Soil Mechanics and Foundation Engineering, Technical Publications, Wellington, New Zealand. pp. 192–199.

Alonso, E. E., Gens, A., and Hight, D. W. (1987). Special problem soils: General report. In Proceedings of the 9th European Conference of Soil Mechanics and Foundation Engineering, Dublin. Vol.3, pp. 1087-1146.

Alonso, E. E., Gens, A., and Josa, A. (1990). A constitutive model for partially saturated soils. Geotechnique, 40(3): 405-430.

Bai, X., He, W., Jia, J., and Han, Y. (2006). Experimental study on the interaction mechanism of cap-pile group-soil. Marine Georesources and Geotechnology, 24(3):173–182.

Bao, C. G., Gong, B. W., and Zhan, L. T. (1998). Properties of unsaturated soils and slope stability for expansive soils. In proceedings of the 2nd International Conference on Unsaturated Soils, Beijing, China. Vol. 2, pp. 71-98.

Bernier, F., Volckaert, G., Alonso, E., and Villar, M. (1997). Suction-controlled experiments on Boom clay. Engineering Geology, 47: 325-338.

Bishop, A. W. (1959). The principle of effective stress. Lecture delivered in Oslo, Norway, in 1955. Tecknisk Ukeblad I Samarbeide Med Teknikk, 106(39): 859-863.

Bishop, A. W., Alpan, I., Blight, G. E., and Donald, I. B. (1960). Factors controlling the shear strength of partly saturated cohesive soil. ASCE Research Conference on Shear Strength of Cohesive Soils, Boulder, Colorado. pp. 505-532.

Bishop, A. W., and Henkel, D. J. (1962). The measurement of soil properties in the triaxial test. 2nd edition, London, Edward Arnold (Publisher) Ltd., UK. pp. 180-211.

Bishop, A. W., and Blight, G. E. (1963). Some aspects of effective stress in saturated and partly saturated soils. Geotechnique, 13(3): 177-196.

Borana, L., Xu, D.S., and Yin, J.H. (2012). A study on measurement of local small strain by FBG sensor, Proceedings of 65th Canadian Geotechnical Conference, GeoManitoba, Manitoba, Canada, Paper No. 414.

Borana, L., Yin, J.H., Singh, D.N., and Shukla, S. K. (2013). A modified suction controlled direct shear device for testing unsaturated soil and steel plate interface. Marine Georesources and Geotechnology. DOI:10.1080/1064119X.2013.843045

Bosscher, P. J., and Ortiz, G. C. (1987). Frictional properties between sand and various construction materials. Journal of Geotechnical Engineering, ASCE, 113(9): 1035-1039.

Boulon, M. (1989). Basic features of soil structure interface behaviour. Computer Geotechnics, 7: 115-131.

Boulon, M., Garnica, P., and Vermeer, P. A. (1995). Soil structure interaction: FEM computations. Mechanics of Geomaterial Interfaces, Elsevier Science, pp. 147-171.

Brabour, S. L. (1998). The soil-water characteristic curve: a historical perspective. Canadian Geotechnical Journal, 35: 873-894.

British Standards Institution (BSI). (1999). Code of practice for site investigations. BS 5930, BSI, London.

British Standards Institution (BSI). (1990). Methods of test for soils for civil engineering purposes. BS 1377, BSI, London.

Brooks, R. H., and Corey, A. T. (1964). Hydraulic properties of porous medium. Colorado State University, Fort Collins, Hydrology Paper No. 3.

Brumund, W. F., and Leonards, G. A. (1973). Experimental study of static and dynamic friction between sand and typical construction materials. Journal of Testing Evaluation, JTEVA, 1(2): 162-165.

Burland, J. B., and Ridley, A. K. (1996). The importance of suction in soil mechanics. In Proceedings of the 12th Geotechnical Southeast Asian Conference, Kuala-lumpur, Malaysia. Vol-2, pp. 27-49.

Campos, T. M. P., and Carrillo, C. W. (1995). Direct shear testing on an unsaturated soil from Rio de Janeiro. In Proceedings of the 1st International Conference on Unsaturated Soils, Paris, France. pp. 31-38.

Chan, D., Yi, C.T. and Scott, J. D. (1993). An interpretation of pull-out test. In Proceedings of the Geosynthetics Conference, Vancouver, Canada. Pp. 593-605.

Chandler, R.J. (1968). The shaft friction of piles in cohesive soils in terms of effective stress. Civ. Eng. and Pub. Wks. Review, 63, pp. 48-51.

Chiu, C. F., and Ng, C. W. W. (2003). A state-dependent elasto-plastic model for saturated and unsaturated soils. Geotechnique, 53(9): 809-829.

Chu, L. M., and Yin, J. H. (2005). Comparison of interface shear strength of soil nails measured by both direct shear box tests and pullout tests. Journal of Geotechnical and Geoenvironmental Engineering, 131(9): 1097-1107.

Chu, L. M., and Yin, J. H. (2006). Study on soil-cement grout interface shear strength of soil nailing by direct shear box testing method. Geomechanics and Geoengineering: An International Journal, 1(4): 259-273.

Cui, Y. J., and Delage, P. (1996). Yielding and plastic behaviour of an unsaturated compacted silt. Geotechnique, 46(2): 291-311.

Desai, C. S., Drumm, E. C., and Zaman, M. M. (1985). Cyclic testing and modeling of interface. Journal of Geotechnical Engineering, ASCE, 111(6): 793-815.

Donald, I. B. (1956). Shear strength measurements in unsaturated non-cohesive soils with negative pore pressures. In Proceedings of the 2nd Australia–New Zealand Conference on Soil Mechanics and Foundation Engineering. Christchurch, New Zealand. pp. 200-204.

Elzeftawy, A., and Cartwright, K. (1981). Evaluating the saturated and unsaturated hydraulic conductivity in soils. In Permeability and Groundwater Contaminant Transport, ASTM, STP 746: 168-181.

Escario, V. (1980). Suction controlled penetration and shear tests. In Proceeding of the 4th International Conference on Expansive soils. Denver, ASCE, Vol-2, pp. 781-797.

Escario, V., and Saez, J. (1986). The shear strength of partly saturated soils. Geotechnique, 36 (3): 453-456.

Estabragh, A. R., Javadi, A. A., and Boot, J. C. (2004). Effect of compaction pressure on consolidation behaviour of unsaturated silty soil. Canadian Geotechnical Journal, 41: 540-550.

Esteban, V., and Saez, J. (1988). A device to measure the swelling characteristics of rock samples with control of the suction up to very high values. ISRM Symposium on Rock Mechanics and Power Plants. Madrid, Vol-2, pp. 195-200.

Fakharian, K., and Evgin, E. (1996). An automated apparatus for three-dimensional monotonic and cyclic testing of interfaces. Geotechnical Testing Journal, 19(1): 22-31.

Feuerharmel, C., Pereira, A., Gehling, W. Y. Y., and Bica, A. V. D. (2006). Determination of the shear strength parameters of two unsaturated colluvium soils using the direct shear test. In Proceeding of the Unsaturated Soils, ASCE, pp. 1181-1190.

Fleming, I., Sharma, J.S., and Jogi, M.B. (2006). Shear strength of geomembrane-soil interface under unsaturated conditions., Geotextiles and Geomembranes, 24(5): 274-284.

Fredlund, D. G., and Morgenstern, N. R. (1977). Stress state variables for unsaturated soils. Journal of the Geotechnical Engineering Division, ASCE, 103(GT5): 447-466.

Fredlund, D. G., Morgenstern, N. R., and Widger, R.A. (1978). The shear strength of unsaturated soils. Canadian Geotechnical Journal, 15(3): 313-321.

Fredlund, D. G., Rahardjo, H., and Gan, J. K. (1987). Nonlinearity of the strength envelope for unsaturated soils. In Proceeding of the 6th International Conference on Expansive Soils. New Delhi, pp. 49-54.

Fredlund, D. G., and Rahardjo, H. (1993). Soil mechanics for unsaturated soils. John Wiley and Sons, Inc., New York.

Fredlund, D. G., and Xing, A. (1994). Equations for the soil-water characteristic curve. Canadian Geotechnical Journal, 31(3): 521-532.

Fredlund, D. G., Xing, A., Fredlund, M. D., and Barbour S. L. (1996). The relationship of the unsaturated soil shear strength to the soil-water characteristic curve. Canadian Geotechnical Journal, 33: 440-448.

Fredlund, D.G. (1998). Bringing unsaturated soil mechanics into engineering practice. In Proceedings of the 2nd International Conference on Unsaturated soils, Beijing, Vol- 2, pp. 1-36.

Frost, J. D., and Han, J. (1999). Behavior of interfaces between fiber-reinforced polymers and sands. Journal of Geotechnical and Geoenvironmental Engineering, ASCE, 125(8): 633-640.

Gallipoli, D., Gens, A., Sharma, R., and Vaunat, J. (2003). An elasto-plastic model for unsaturated soil incorporating the effects of suction and degree of saturation on mechanical behavior. Geotechnique, 53 (1): 123-135.

Gan, J. K. M. (1986). Direct shear testing of unsaturated soils. MS Thesis, University of Saskatchewan, Saskatoon, Canada.

Gan, J. K. M., and Fredlund, D. G. (1988). Multistage direct shear testing of unsaturated soils. Geotechnical Testing Journal, ASTM, 11(2): 132-138.

Gan, J. K. M., and Fredlund, D. G. (1992). Direct shear testing of a Hong Kong soil under various applied matric suction. GEO Report No. 11, Geotechnical Engineering Office, Hong Kong, China.

Gan, J. K. M., and Fredlund, D. G. (1994). Direct shear and triaxial testing of a Hong Kong soil under saturated and unsaturated condition. GEO Report No. 46, Geotechnical Engineering Office, Hong Kong, China.

Gan, J. K. M., and Fredlund, D. G. (1996). Shear strength characteristics of two saprolitic soils. Canadian Geotechnical Journal, 33(4): 595-609.

Gan, J. K., Fredlund, D. G., and Rahardjo, H. (1988). Determination of the shear strength parameters of an unsaturated soil using the direct shear test. Canadian Geotechnical Journal, 25(8): 500-510.

Gens, A., and Alonso, E. E. (1992). A framework for the behavior of unsaturated expansive clays. Canadian Geotechnical Journal, 29(6): 1013-1032.

Giuseppe, M., Mangiola, A., and Ghionna, V.N. (2007). Cyclic shear stress degradation and post-cyclic behaviour from sand–steel interface direct shear tests. Canadian Geotechnical Journal, 44 (7): 739–752.

Glisic, B., and Claire-Nan, I. D. (2002). Piles monitoring during the axial compression, pullout and flexure test using fiber optic sensors. In Proceedings of the Eighty first Annual Meeting of the Transportation Research Board, 2701-2710.

Gulhati, S. K., and Satija, B. S. (1981). Shear strength of partly saturated soils. In Proceedings of the 10th International Conference on Soil Mechanics and Foundation Engineering, Stockholm, Sweden. Vol-1, pp. 609-6612.

Hamid, T.B. (2005). Testing and modeling of unsaturated interfaces. Ph.D. Dissertation, School of Civil Engineering and Environmental Science, University of Oklahoma, Norman, Oklahoma.

Hamid, T. B., and Miller, G. A. (2008). A constitutive model for unsaturated soil interfaces. International Journal for Numerical and Analytical Methods in Geomechanics, 32(13): 1693-1714.

Hamid, T. B., and Miller, G. A. (2009). Shear strength of unsaturated soil interfaces. Canadian Geotechnical Journal, 46(5): 595-606.

Han, K. K. (1997). Effect of hysteresis, infiltration and tensile stress on the strength of unsaturated soil. Ph.D. Thesis, School of Civil and Structural Engineering, Nanyang Technological University, Singapore.

Heymann, G., Rhode, A.W., Schwartz, K., and Friedlaender, E. (1992). Soil nail pullout resistance in residual soils. In Proceedings of the International Symposium on Earth Reinforcement Practice, Kyushu, Japan. Vol-1, pp. 487-492.

Hilf, J. W. (1956). An investigation of pore water pressure in compacted cohesive soils. Technical Memo 654, Denver, Bureau of Reclamation.

Hill, K. O., Fujii F., Johnson, D. C., and Kawasaki, B. S. (1978). Photosensitivity on optical fiber waveguides: application to reflection filter fabrication. Applied Physics Letter. 32(10): 647-649.

Ho, D. Y. F., and Fredlund, D. G. (1982). Increase in strength due to suction for two Hong Kong soils. Engineering and Construction in Tropical Soils, ASCE, Honolulu, Hawaii, pp. 263-293.

Hossain, M. A. (2010). Experimental study on the interface behavior between unsaturated completely decomposed granite soil and cement grout. Ph.D. Thesis, The Hong Kong Polytechnic University, Hong Kong.

Hossain, M. A., and Yin, J. H. (2010a). Shear strength and dilative characteristics of an unsaturated compacted completely decomposed granite soil. Canadian Geotechnical Journal, 47(10): 1112-1126.

Hossain, M. A., and Yin, J. H. (2010b). Behavior of a compacted completely decomposed granite soil from suction controlled direct shear tests. Journal of Geotechnical and Geoenvironmental Engineering, ASCE, 136(1): 189-198.

Hossain, M. A., and Yin, J. H. (2012). Influence of grouting pressure on the behavior of an unsaturated soil-cement interface. Journal of Geotechnical and Geoenvironmental Engineering, ASCE, 138(2):193-202.

Hossain, M. A., and Yin, J. H. (2013). Behavior of a pressure grouted soil-cement interface in direct shear tests. International Journal of Geomechanics. (in press).

Inaudi, D. (1997). Fiber optic sensor network for the monitoring of civil engineering structures. Ph.D. Thesis, Swiss Federal Institute of Technology in Lausanne (EPFL), Lausanne, Switzerland.

Jewell, R. A., and Wroth, C. P. (1987). Direct shear tests on reinforced sand. Geotechnique, 37(1): 53-68.

Junaideen, S. M., Tham, L. G., Law, K. T., Lee, C. F., and Yue, Z. Q. (2004). Laboratory study of soil nail interaction in loose, completely decomposed granite. Canadian Geotechnical Journal, 41: 274-286.

Juran, I., Shaffiee, S., Schlosser, F., Humbert, P., and Guenot, A. (1982). Study of soil-bar interaction in the technique of soil nailing. In Proceedings of the 8th European Conference on Soil Mechanics and Foundation Engineering, pp. 513-516.

Karube, D. (1988). New concept of effective stress in unsaturated soil and its proving test. In Advanced triaxial testing of soil and rock. American Society for Testing and Materials, Philadelphia, ASTM, STP 977: 539-552.

Kayadelen, C., Tekinsoy, M.A., and Taskiran, T. (2007). Influence of matric suction on shear strength behavior of a residual clayey soil. Environmental Geology, 53(4): 891-901.

Kersey, A. D., Davis, M.A., Patrick, H. J, LeBlanc, M., Koo, K. P., Askins, C. G., Putnam, M. A., and Friebele, E. J. (1997). Fiber grating sensors. Journal of Light wave Technology. 15(8): 1442-1463.

Khalili, N., and Khabbaz, M. H. (1998). A unique relationship for χ for the determination of the shear strength of unsaturated soils. Geotechnique, 48(5): 681-687.

Khoury, C. N., Miller, G. A., and Hatami, K. (2010). Unsaturated soil geotextile interface behavior. Journal of Geotextile and Geomembrane, 29(1): 613-624.

Kim, M. H., and O'Neill, M. W. (1998). Side shear induced in drilled shaft by suction change. Journal of Geotechnical and Geoenvironmental Engineering, ASCE, 124(8): 771–780.

Kishida, H., and Uesugi, M. (1987). Tests of the interface between sand and steel in the simple shear apparatus. Geotechnique, 37(1): 45-52.

Kulhawy, F. H., and Peterson, M. S. (1979). Behavior of sand-concrete interfaces. In Proceedings of the 6th Pan-American Conference on Soil mechanics and Foundation Engineering, pp. 225-236.

Lamborn, M. J. (1986). A micromechanical approach to modeling partly saturated soils. M.Sc. Thesis, Texas A and M University, College Station, Texas.

Lee, I. M., Sung, S. G., and Cho, G. C. (2005). Effect of stress state on the unsaturated shear strength of a weathered granite. Canadian Geotechnical Journal, 42: 624-631.

Lee, Y. J., and Bassett, R. H. (2006). Application of a photogrammetric technique to a model tunnel. Tunnelling and Underground Space Technology, 21(1): 79-95.

Leong, E. C., and Rahardjo, H. (1997). Review of soil-water characteristic curve equation. Journal of Geotechnical and Geoenvironmental Engineering, ASCE, 123(12): 1106-1117.

Levachar, D. R. and Sieffert, J. G. (1984). Test on model tension piles. Journal of Geotechnical and Geoenvironmental Engineering, ASCE, 110 (12): 1735-1748.

Liu, H. L., Ng, C. W. W., and Fei, K. (2007a). Performance of a geogrid - reinforced and pile supported highway embankment over soft clay: Case Study. Journal of Geotechnical and Geoenvironmental Engineering, ASCE, 133(12): 1483-1493.

Liu, Y., Chiang, K. S., Rao, Y. J., Ran, Z. L., and Zhu, T. (2007b). Light coupling between two parallel CO_2-laser written long-period fiber gratings, Optics Express, 15: 17645-17651.

Mancuso, C., Vassallo, R., and D'Onofrio, A. (2002). Small strain behavior of a silty sand in controlled-suction resonant column-torsional shear tests. Canadian Geotechnical Journal, 39(1): 22-31.

Mashhour, M. M., Ibrahim, M. I., and El-Emam, M. M. (1996). Variation of unsaturated soil shear strength parameters with suction. In Proceedings of the First International Conference on Unsaturated Soils, France. pp. 1487-1493.

McKee, C. R., and Bumb, A. C. (1987). Flow-testing coal-bed methane production wells in the presence of water gas. SPE Formation Evaluation, pp. 50-58.

Meltz, G., Morey, W. W., and Glenn, W. H. (1989). Formation of bragg gratings in optical fibers by a transverse holographic method. Optics Letters, 14(15): 823-825.

Miller, G. A., and Hamid, T. B. (2007). Interface direct shear testing of unsaturated soil. Geotechnical Testing Journal, 30(3): 182-191.

Milligan, G. W. E., and Tei, K. (1998). The pull-out resistance of model soil nails. Journal of Soils and Foundations, 38(2): 179-190.

Morey, W. W., Meltz, G., and Glenn, W. H. G. (1989). Fiber optic bragg grating sensors. Proceedings of SPIE, Boston, 1169, 98-107.

Mroueh, I. and Shahrour, I. (2012). Response of piles to inclined uplift loads influence of the soil-pile interface. European Journal of Computational Mechanics. 16(3): 419-435.

Ng, C.W.W., and Menzies, B. (2007). Advanced unsaturated soil mechanics. Taylor and Francis, Abingdon, UK.

Ng, C. W. W., and Pang, Y. W. (2000). Influence of stress state on soil-water characteristics and slope stability. Journal of Geotechnical and Geoenvironmental Engineering, ASCE, 126(2): 157-166.

Ng, C. W. W., and Zhou, R. Z. B. (2005). Effects of soil suction on dilatancy of an unsaturated soil. In Proceedings of the 16th ICSMGE, Osaka, Japan. Vol-2, pp. 559-562.

Ng, C. W. W., and Yung, S. Y. (2008). Determination of the anisotropic shear stiffness of an unsaturated decomposed soil. Geotechnique, 58(1): 23-35.

Noorany, I. (1985). Side friction of piles in calcareous sands. In Proceedings of the 11th International Conference on Soil mechanics and Foundation Engineering, San Francisco. Vol-3, pp. 1611-1614.

Oloo, S. Y., and Fredlund, D. G. (1996). A method for determination of ϕ^b for statically compacted soils, Canadian Geotechnical Journal, 33(2): 272-280

O'Rourke, T. D., Druschel, S. J., and Netravali, A. N. (1990). Shear strength characteristics of sand-polymer interfaces. Journal of Geotechnical and Geoenvironmental Engineering, ASCE, 116(3): 451-469.

Othonos, A. and Kalli, K. (1999). Fiber bragg gratings: fundamentals and applications in telecommunications and sensing. London: Artech House.

Padilla, J.M., Perera, Y. Y., Housteon, W. N., Perez, N., and Fredlund, D. G. (2006). Quantification of air diffusion through high air entry ceramic disks. In Proceedings of the, Unsaturated Soils, ASCE, 147 (GSP), pp. 1852-1863.

Palmeira, E. M., and Milligan, G. W. E. (1989). Scale and other factors affecting the results of pull-out tests of grids buried in sand. Geotechnique, 39(3): 511-524.

Panchanathan, S., and Ramaswamy, S. V. (1964). Skin friction between sand and construction materials. Indian National Society of Soil Mechanics and Foundation Engineering, 3(4): 325-336.

Pei, H. F., Yin, J. H., Jin, W., Hong, C.Y., and Zhu, H. H. (2012a). Monitoring of lateral displacements of a slope using a series of special FBG based in-place inclinometers. Measurement Science and Technology. 23(2):DOI:10.1088/0957-0233/23/2/025007.

Pei, H. F., Yin, J. H., Zhu, H. H., and Hong, C. Y. (2012b). Monitoring performance of a glass fiber reinforced polymer soil nail during laboratory pullout test using FBG sensing technique. International Journal of Geomechanics, ASCE, DOI:10.1061/(ASCE)GM.1943-5622.0000226.

Peterson, R.F.W. (1988). Interpretation of Triaxial Compression Test Results on Partially Saturated Soils. Advanced Triaxial Testing of Soil and Rock. ASTM, STP 977: 512-538.

Potyondy, J. G. (1961). Skin friction between various soils and construction materials. Geotechnique, 11(4): 339-353.

Pradhan, B. (2003). Study of pullout behaviour of soil nails in completely decomposed granite fill. Master's Thesis, The University of Hong Kong, Hong Kong, China.

Rahardjo, H., and Leong, E. C. (1997). Soil-water characteristic curves and flux boundary problems. In Proceedings of the Unsaturated Soil Engineering Practice, New York, ASCE, pp. 88-112.

Rao, K. S., Allam, M. M., and Robinson, R. G. (2000). Drained shear strength of fine-grained soil-solid surface interfaces. In Proceedings of ICE - Geotechnical Engineering, 143(2): 75-81.

Rassam, D. W., and Williams, D. J. (1999). A relationship describing the shear strength of unsaturated soils. Canadian Geotechnical Journal, 36(2): 363-368.

Satija, B.S. (1978). Shear behaviour of partly saturated soils. Ph.D. Thesis, Indian Institute of Technology Delhi, India.

Schlosser, F., and Guilloux, A. (1981). Le frottement dans les sols. Revue Francaise de Geotechnique, 16: 65-77.

Schmidt-Hattenberger, C., and Borm, G. (1998). Bragg grating extensometer rods (BGX) for geotechnical strain measurements. In Proceedings of the SPIE, European Workshop on Optical Fibre Sensors, pp. 214-217.

Schofield, R. (1935). The pF of the water in soil. In proceedings of the 3rd Trans. International Congress on Soil Science, Vol-2, pp. 37-48.

Sharma, J. S., Fleming, I. R., and Jogi, M. B. (2007). Measurement of unsaturated soil-geomembrane interface shear-strength parameters. Canadian Geotechnical Journal, 44(1): 78-88.

Sharma, R. S. (1998). Mechanical behavior of unsaturated highly expansive clays. Ph.D. Thesis, Oxford University.

Shibuya, S., Mitachi, T., and Tamate, S. (1997). Interpretation of direct shear box testing of sands as quasi-simple shear. Geotechnique, 47(4): 769-790.

Sillers, W. S., and Fredlund, D. G. (2001). Statistical assessment of soil-water characteristic curve models for geotechnical engineering. Canadian Geotechnical Journal, 38(6): 1297-1313.

Sivakumar, V. (1993). A critical state framework for unsaturated soils. Ph.D. Thesis, University of Sheffield, UK.

Su, L. J. (2006). Laboratory pull-out testing study on soil nails in compacted completely decomposed granite fill. Ph.D. Thesis, The Hong Kong Polytechnic University, Hong Kong.

Su, L. J., Chan, T. C. F., Shiu, Y. K., Cheung, T., and Yin, J. H. (2007). Influence of degree of saturation on soil nail pullout resistance in compacted completely decomposed granite fill. Canadian Geotechnical Journal, 44(11): 1314-1428.

Subbarao, K.S., Rao, S.M., and Gangadhara, S. (1998). Band width of vertical movement of expansive soil. In Proceedings of the Indian Geotechnical Conference. Vol-1, pp. 71-74.

Thakur, K. S., Sreedeep, S., and Singh, D.N. (2005). Parameters affecting soil–water characteristic curves of fine-grained soils. Journal of Geotechnical and Geoenvironmental Engineering, ASCE, 131(4): 521-524.

Toll, D. G. (1990). A framework for unsaturated soil behaviour. Geotechnique, 40(1); 31-44.

Tsubakihara, Y., Kishida, H., and Nishiyama, T., (1993). Friction between cohesive soils and steel, Soil and Foundation, 33(2), 145–156.

Uesugi, M., Kishida, H., and Uchikawa, Y. (1990). Friction between dry sand and concrete under monotonic and repeated loading. Soil and Foundations, 30(1): 115-128.

Van-Genutchen, M. T. (1980). A closed-form equation for predicting the hydraulic conductivity of unsaturated soils. Soil Science Society of American Journal, 44(5): 892-898.

Vanapalli, S. K. (1994). Simple test procedure and their interpretation in evaluating the shear strength of an unsaturated soil. Ph.D. Thesis, University of Saskatchewan, Saskatoon, Canada.

Vanapalli, S. K., Fredlund, D. G., Pufahl, D. E., and Clifton, A. W. (1996). Model for the prediction of shear strength with respect to soil suction. Canadian Geotechnical Journal, 33(3): 379-392.

Vanapalli, S. K., Fredlund, D. G., and Pufahl, D. E. (1999). The influence of soil structure and stress history on the soil-water characteristic of a compacted till. Geotechnique, 49(2): 143-159.

Vinayagam, T. (2004). Understanding the stress-strain behavior of unsaturated minco silt using laboratory testing and constitutive modeling. M.S. Thesis., University of Oklahoma, USA.

Wang, Y.H., and Leung, S.C. (2008). A particulate-scale investigation of cemented sand behavior. Canadian Geotechnical Journal, 45(1): 29-44.

Wang, Y. H., and Yan, W. M. (2006). Laboratory studies of two common saprolitic soils in Hong Kong. Journal of Geotechnical and Geoenvironmental Engineering, ASCE, 132(7): 923-930.

Wheeler, S. J., and Karube, D. (1996). Constitutive modelling. In Proceedings of the 1st International Conference on Unsaturated. Soils, Paris, Vol-3, pp. 1323-1356.

Wheeler, S. J., and Sivakumar, V. (1995). An elasto-plastic critical state framework for unsaturated soil. Geotechnique, 45: 35-53.

Wheeler, S. J., Sharma, R. J., and Buisson, M. S. R. (2003). Coupling of hydraulic hysteresis and stress–strain behaviour in unsaturated soils. Geotechnique, 53(1): 41–54.

Wong, H. Y. (1995). Soil nails design manual for slopes (with worked example), Architectural Services Department.

Xu, D. S., Borana, L., and Yin, J. H. (2013). Measurement of small strain behavior of a local soil by fiber Bragg grating-based local displacement transducers. Acta Geotechnica, DOI 10.1007/s11440-013-0267-y.

Yin, J. H., and Zhou, W. H. (2009). Influence of grouting pressure and overburden stress on the interface resistance of a soil nail. Journal of Geotechnical and Geoenvironmental Engineering, ASCE, 135(9): 1198-1208.

Yin, J. H., Zhu, H.H., Fung, K. W., Jin, W., Mak, L. M., and Kuo, K. (2008). Innovative optical fiber sensors for monitoring displacement of geotechnical structures. The HKIE Geotechnical Division 28th Annual Seminar, Hong Kong, 287-294.

Yin, Z. Z., Zhu, H., and Xu, G. H. (1995). A study of deformation in the interface between soil and concrete. Computers and Geotechnics, 17: 75-92.

Ying, J., Liao, H., and Yin, J. H. (2006). An experimental study on the shear strength of undisturbed loess. Unsaturated Soil, Seepage and Environmental Geotechnics, ASCE, 148 (GSP): 127-135.

Yoshida, Y., Kashiwai, Y., Murakami, E., Ishida, S., and Hashiguchi, N. (2002). Development of the monitoring system for slope deformations with fiber bragg grating arrays. In Proceedings of SPIE 4694, pp. 296-303.

Yoshimi, Y., and Kishida, T. (1981). Friction between sand and metal surface. In Proceedings of the 10th International Conference on Soil Mechanics and Foundation Engineering, Vol-1, pp. 831-834.

Zhan, L. T., and Ng, C. W. W. (2006). Shear strength characteristics of an unsaturated expansive clay. Canadian Geotechnical Journal, 43(7): 751-763.

Zhang, X., and Lytton, R. (2006). Stress state variables for saturated and unsaturated soils. In Proceedings of UNSAT 2006, pp. 2380-2391.

Zhou, W. H. (2008). Experimental and theoretical study on pullout resistance of grouted soil nails. Ph.D. Thesis, The Hong Kong Polytechnic University, Hong Kong.

Zhu, H. H. (2009). Fiber optic monitoring and performance evaluation of geotechnical structures, Ph.D. Thesis, The Hong Kong Polytechnic University, Hong Kong.

Zhu, H. H., Ho, A. N. L., Yin, J. H., Sun, H. W., Pei, H. F., and Hong, C. Y. (2012). An optical fibre monitoring system for evaluating the performance of a soil nailed slope. Smart Structures and Systems, 9(5): 393-410.

Zhu, H. H., Yin, J. H., Jin, W., and Zhou, W. H. (2007). Soil nail monitoring using fiber Bragg grating sensors during pullout tests. The Joint 60th Canadian Geotechnical and 8th IAH-CNC Conferences, Canada. pp. 821-828.

Zhu, H. H., Yin, J. H., Zhang, L., Jin, W., and Dong, J. H. (2010a). Monitoring internal displacements of a model dam using FBG sensing bars. Advances in Structural Engineering, 13(2): 249-262.

Zhu, W. S., Zhang, Q. B., Zhu, H. H., Li, Y., Yin, J. H., Li, S. C., Sun, L. F., and Zhang, L. (2010b). Large-scale geomechanical model testing of an underground cavern group in a true three-dimensional (3-D) stress state. Canadian Geotechnical Journal, 47(9):935-946.

Zur, B. (1966). Osmotic control of the matric soil-water potential. Soil Science, 102(6): 394-398.